

Chapter 3

Gas Separation Membrane Materials and Structures

A membrane is a layer of material which serves as a selective barrier between two phases and is impermeable to specific particles, molecules, or substances when exposed to the action of a driving force. Some components are allowed passage by the membrane into a permeate stream, whereas others are retained by it and accumulate in the retentate stream. Membranes can be of various thicknesses, with homogeneous or heterogeneous structures. Membrane can also be classified according to their pore diameter. There are three different types of pore sizes based on the IUPAC (International Union of Pure and Applied Chemistry) classification: microporous ($d_p < 2$ nm), mesoporous ($2 \text{ nm} < d_p < 50$ nm), and macroporous ($d_p > 50$ nm) [1, 2]. Membranes can be neutral or charged, and the transport through a membrane can be active or passive. The latter can be facilitated by pressure, concentration, chemical or electrical gradients. Membranes can be generally classified into synthetic membranes and biological membranes.

The chemistry and the structure of membranes play an important role in their separation characteristics. Ideally, membranes should be defect-free in large scale, exhibiting high thermal, chemical, and mechanical stabilities, selectivity, and permeability. Another way of classifying membranes is by the type of material used: inorganic and polymeric. Inorganic membranes include metal, metallic oxide, glass, silicate and zeolite/zeolitic type materials, and so on. Compared with polymeric membranes, inorganic membranes have many advantages: such as high thermal, chemical, and mechanical stabilities, less plasticization, and better control of pore size and pore size distribution, which allows better control of selectivity and permeability. For example, molecular sieve membranes are inorganic membranes developed in recent years with unique properties such as uniform micropores, ion exchange, tunable-Si/Al ratios, high temperature stability, solvent resistance, a wide range of hydrophilicity–hydrophobicity, catalytic activities, and so on. Hence, molecular sieves have excellent membrane material to achieve separation and catalytic reaction, simultaneously. For this reason, they have been widely used as membrane separators, membrane reactors, and as sensors.

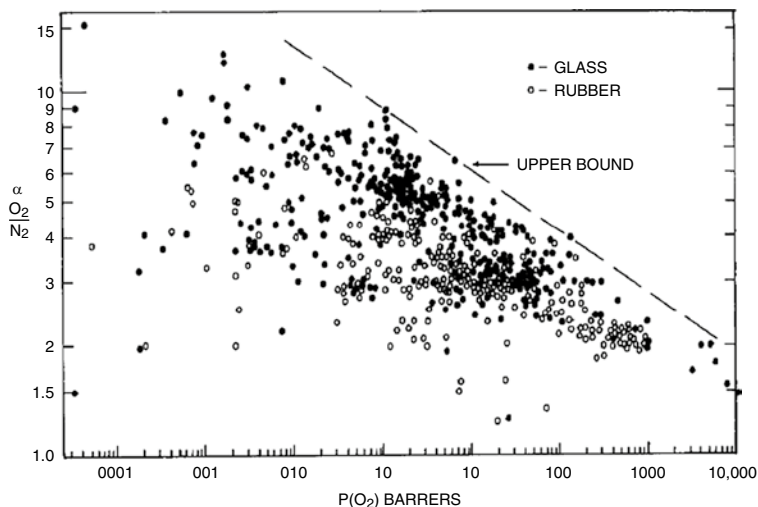


Fig. 3.1 Literature data for O_2/N_2 separation factor versus O_2 permeability [3]

For polymeric membrane materials, there is a trade-off between selectivity and permeability. Robeson [3] has suggested that this trade-off is represented as an upper boundary to the selectivity vs. permeability plot of many polymeric materials. This upper boundary can clearly be seen in Fig. 3.1 for a range of polymeric membrane materials involved in O_2/N_2 separations. Overcoming this upper boundary is the focus of many recently awarded patents in polymeric membranes, because achieving both high oxygen permeability and selectivity is desirable (Fig. 3.1).

As stated earlier, high permeability and selectivity are not the only properties that are desired. For membrane materials to be viable, they need to be thermally and chemically robust, resistant to plasticization and aging to ensure continual performance over long time periods, and at the same time they need to be cost-effective to be manufactured for industrial applications.

3.1 Membrane Materials for Gas Separation

The selection of membrane materials is one of the most important tasks in membrane separation technology. One way to choose membrane material for gas separation is based on its chemical properties. Chemical interactions between membrane materials and gaseous penetrants determine the separation efficiency between the components of gas mixtures [3, 4].

Despite the many advantageous characteristics of inorganic membranes, organic polymeric membranes are first surveyed here, since most of the industrial membranes are currently manufactured from polymeric materials.

3.1.1 Polymeric Membranes

Polymeric membranes take the form of polymeric interphases, which can selectively transfer certain chemical species over others. There are several mechanisms that could be deployed in their functioning. Knudsen diffusion and solution diffusion are prominent mechanisms (see Chap. 2). Polymeric membranes are of particular importance in gas separation applications. Polymeric membrane materials are generally characterized by their transport properties such as permeability and selectivity. Permeability is a measure of the productivity of the membrane and selectivity is a measure of separation efficiency.

Usually nonporous polymeric membranes are used for gas separation. The vapors and gases are separated due to their different solubility and diffusivity in the polymers. The permeability or permeation coefficient of such nonporous membranes can generally be expressed as the solubility, S , of the gas in the membrane polymer multiplied by the diffusivity, D , of the gas in the polymer, i.e., $P=D \cdot S$. In such cases, permeation is said to occur by a “solution-diffusion” model. Polymers in the glassy state are generally more effective for separation, and predominantly differentiate gases based on their different diffusivities. Small molecules of penetrants move among polymer chains according to the formation of local gaps by thermal motion of polymer segments. In a polymeric membrane, pores and channels have a wide range of sizes and topologies. Free volume, the fraction of the volume not occupied by the electronic clouds of the macromolecule, plays a significant role in the transport properties of low molecular weight species and gases. In other words, this is the volume that is not occupied by polymer chains due to conformational constraints. Within this free volume, transient gaps are formed which can accommodate gas molecules. According to the driving force, the gas molecules have to be transported by successive movement between transient gaps close to the feed side to those close to the permeate side. Thus, movement necessary for the transport of the gas molecules between the microvoids is possible due to thermal motion of segments of the polymer chains. Moreover, the distribution of the effective micropore size, if the free-volume elements are interconnected, is likely to have a significant influence on the properties of the membrane. Some experimental techniques (probe methods such as Positron Annihilation Lifetime Spectroscopy, Inverse Gas Chromatography, Xe NMR, and small angle neutron diffraction) can be used to determine the average radius (1–10 Å) and the distribution of the free volume elements. Free volume pockets or voids are crucial for a variety of dynamic processes in membranes. The diffusivity of a penetrant gas depends mainly on its molecular size.

Porous membranes can also be utilized for the gas separation. The pore diameter must be smaller than the mean free path of gas molecules. Under normal conditions (100 kPa, 300 K), this is about 50 nm. In this case, the gas flux through the pore is proportional to the molecule’s velocity, i.e., inversely proportional to the square root of the molecule’s mass. This is known as Knudsen diffusion. Gas flux through a porous membrane is much higher than through a nonporous one by 3–5 orders of magnitude. The separation efficiency is moderate; hydrogen diffuses four times

Table 3.1 Comparison of glassy polymers in CO₂/CH₄ separation

Polymer	Selectivity A = {P(CO ₂)/P(CH ₄)}	Permeability P(CO ₂) {Barrer}
Cellulose derivatives	3	4,550
Polycarbonate	11–33	75–15
Polyimides	15–25	110–65

faster than oxygen. Porous polymeric or ceramic membranes for ultrafiltration serve the purpose. Note that when the pores are larger than the limit viscous flow occurs, and hence no separation will take place.

Polymeric membrane materials can be divided into rubbery and glassy polymers. Rubber is an example of an elastomer type polymer, which has the ability to return to its original shape after being stretched or deformed. The rubbery polymer is coiled when in the resting state. The elastic properties arise from its ability to stretch the chains apart, but when the tension is released the chains snap back to the original position. Long range motions of chains in rubbery polymers are not possible in glassy polymers. In other words, the chains of glassy polymers are rigid. On increasing the temperature glassy polymers will soften and become rubbery. Glassy polymers are not elastomer type polymers.

Glassy polymers show very attractive separation characteristics, e.g., high selectivity combined with medium/low permeability. On the other hand, rubbery polymers show comparatively low selectivity and high permeability for common gas pairs such as O₂/N₂, H₂/CH₄, and CO₂/CH₄ [5]. The correlation for the CO₂/CH₄ separation is shown in Table 3.1 [5].

The high selectivity of a glassy polymer is due to its lower free volume, a narrower distribution of the free volume, as well as lower flexibility of the polymer chains compared to those of rubbery polymers. Rubbery polymers present high permeabilities and their selectivities are mainly influenced by differences in the condensability of the gas species. When applied to separate an organic vapor from nitrogen, rubbery membranes are preferentially permeable to the organic molecules. An amorphous polymer will behave as a rubbery state when above its glass transition temperature (T_g). It will present a relatively large amount of free volume, owing to transient voids between the highly mobile polymer chains. At below its T_g , the polymer will behave as a rigid glass, which will result in a reduction of the fractional free volume. Thus, there will be an insufficient space for the large-scale cooperative movements of the polymer's backbone.

Many polymers have been investigated as gas separation membrane materials, but up to now only a handful have found commercial success. These include rubbery polymers, such as poly(dimethylsiloxane), and glassy polymers, such as polysulfone, poly(phenylene oxide), cellulose acetate, and polyimides. For gas separation membranes, materials are required to offer high permeability as well as good selectivity for a desired separation.

For a given polymer, how to make a high separation performance membrane by studying the membrane formation protocol is an important topic in research.

Higher permeability decreases the amount of membrane area to treat a given amount of gas, thereby decreasing the capital cost of membrane units. Higher selectivity results in higher purity product gas. A polymer that exhibits good selectivity generally has low permeability and vice versa. For glassy polymers, the gas transport properties depend on the amount and distribution of free volume and on chain mobility. The most highly permeable polymers have rigid, twisted macromolecular backbones that give rise to microvoids [6]. Examples include substituted polyacetylene, perfluoropolymers, addition-type polynorbornene, polymers of intrinsic microporosity (PIMs), and some polyimides. High permeability membranes may also be produced by thermal rearrangement of precursor polymers.

Although thousands of polymers exhibit permselective properties for gas mixtures, only a few glassy polymers are useful in making asymmetric gas separation membranes, particularly polysulfone (PSf), polyether sulfone (PES), polyimide (PI) and polyetherimide (PEI). For example, PSf is one of the most promising polymers for separating oxygen and nitrogen with respect to its permeability and selectivity, even though other polymers such as polyacetylenes, polyaniline, poly(acrylene ethers), polyacrylates, polycarbonates, polyetherimides, poly(ethylene oxide), poly(phenylene oxide), poly(pyrrolone) [7], and cellulose acetate [8] can also be used for gas separation membranes.

Examples of structures of polymers used in fabrication of gas separation membranes are displayed in Fig. 3.2.

Though a large number of polymeric materials have been developed for gas separations, the number of polymers used in commercial systems is still limited [9]. Rubbery membranes reject lighter gases such as nitrogen, methane, and hydrogen, and permeate heavier hydrocarbon components. The main rubbery and glassy polymers employed for gas separation are listed in Table 3.2 [10].

Further to discussions in Chap. 2, the chemical structures of high free volume polymers are elaborated upon below in Fig. 3.3 [6]. Membrane permeability and selectivity data for those polymers are plotted in Fig. 3.4 for the O_2/N_2 and CO_2/CH_4 gas pairs.

Table 3.3 shows the polymers used for gas separation membranes. It should be noted that new polymers have been further developed on the basis of these polymers.

3.1.1.1 Silicone Rubber

Silicone rubber is an elastomer (rubber-like material) composed of polysiloxane that contains silicon together with carbon, hydrogen, and oxygen. Silicone rubbers are often one- or two-part polymers, and may contain fillers to improve properties or reduce cost. Silicone rubber is generally non-reactive, stable, and resistant to extreme environments and temperatures from $-55\text{ }^\circ\text{C}$ to $+300\text{ }^\circ\text{C}$ while still maintaining its useful properties. Compared to organic rubbers, however, silicone rubber has a very low tensile strength. For this reason, care is needed in designing products to withstand even low imposed loads. The material is also very sensitive to fatigue from cyclic loading.

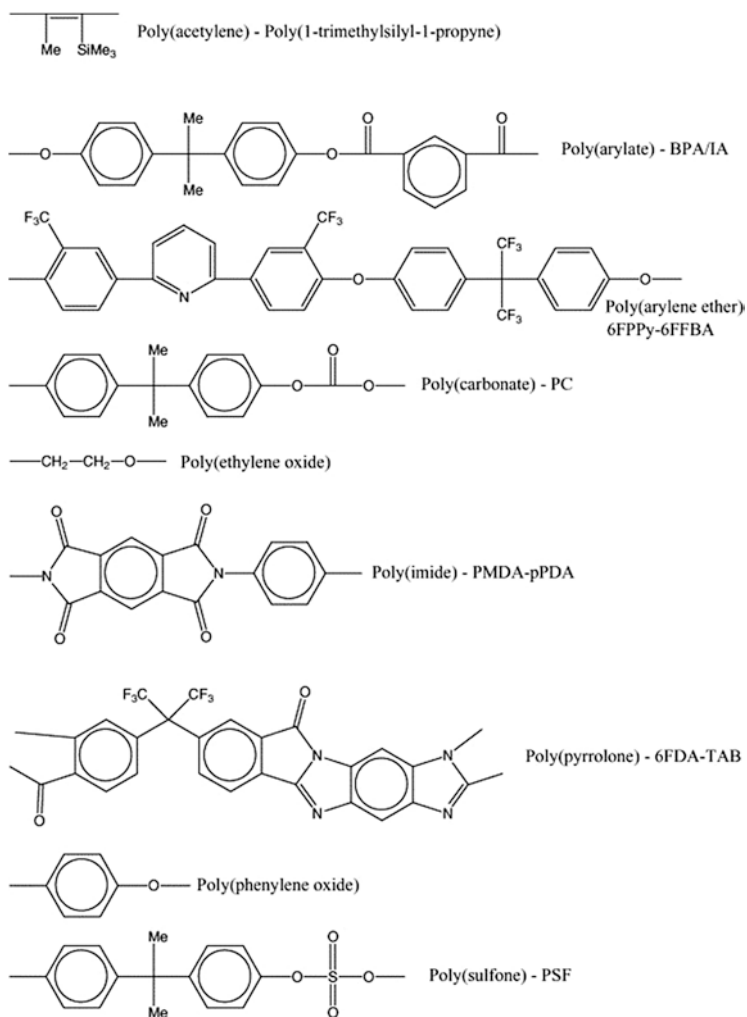


Fig. 3.2 Example of polymeric structures [7]

Table 3.2 Most important glassy and rubbery polymers used in industrial membrane gas separation

Rubbery polymers	Glassy polymers
Poly(dimethylsiloxane)	Cellulose acetate
Ethylene oxide/pyrrolone oxide-amide copolymers	Polycarbonates
	Polyperfluorodioxoles
	Polyimides
	Poly(phenylene oxide)
	Polysulfone

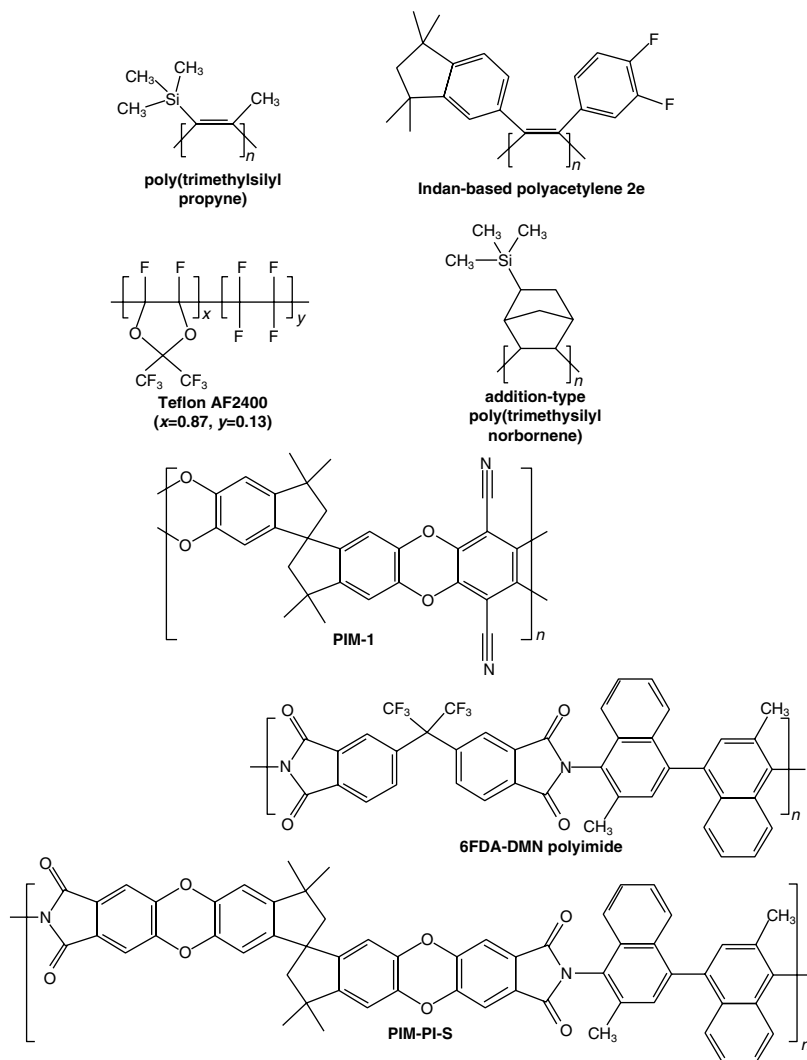
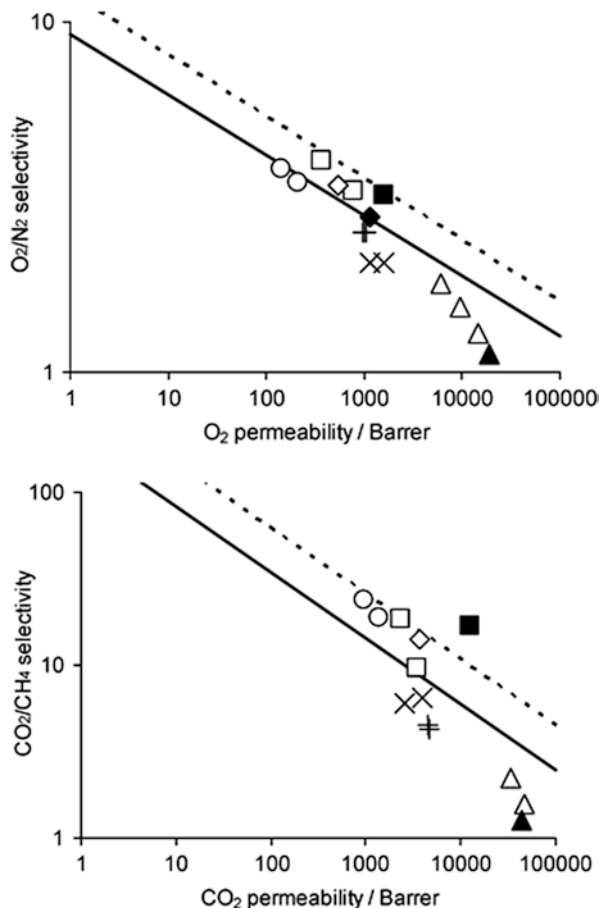


Fig. 3.3 Chemical structures of important high free volume polymers

Polysiloxanes (Fig. 3.5) differ from other polymers in that their backbones consist of Si–O–Si units unlike many other polymers that contain carbon backbones. The C–C backbone unit has a bond length of 1.54 Å and a bond angle of 112°, whereas the siloxane backbone unit Si–O has a bond length of 1.63 Å and a bond angle of 130°. Polysiloxane is very flexible due to large bond angles and bond lengths when compared to those found in more basic polymers such as polyethylene.

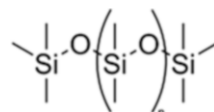
Fig. 3.4 Double logarithmic plots of selectivity versus permeability for (top) O_2/N_2 and (bottom) CO_2/CH_4 . (Solid line) Robeson's 1991 upper bound and (dashed line) 2008 upper bound, and data for (open triangle) poly(trimethylsilyl propyne) (PTMSP), (filled triangle) indan-based polyacetylene 2e, (times) Teflon AF2400, (plus) addition-type poly(trimethylsilyl norbornene), (open square) PIM-1, (filled square) PIM-1 after methanol treatment, (open circle) 6FDA-DMN polyimide, (open diamond) PIM-PI-8, and (filled diamond) PIM-PI-8 after methanol treatment [6]



Polysiloxanes also tend to be chemically inert, due to the strength of the silicon-oxygen bond. The application of silicone rubber in synthetic membranes for gas separation is of special interest due to its intrinsic high permeation rate. The high permeability of silicone rubber has been attributed to the flexibility of the siloxane linkages in the polymer. This is accompanied by a low permselectivity. Silicone rubber coated composite membranes are commonly utilized in industrial membranes for gas separation [11], removal of organic vapors from air, pervaporation of various organic species, olefin separation, etc. [12]. Silicone rubber has also been used as a gutter layer as well as sealing layer to make thin film composite (TFC) membranes of potentially high-performance materials, if formation of defect-free ultrathin membranes for such types of polymers is difficult. The substitution of polysiloxane with different groups has been reported to improve the intrinsic selectivity, which was usually accompanied by a general decrease in penetrant solubility and

Table 3.3 Polymers used for gas-separation membranes

Polymer
Silicon rubber
Cellulose acetate
Polyether sulfone
Polyimides and polyetherimides
Polypropylene
Polyetherketone
Poly(norbornene)s
Poly(2,6-dimethyl-1,4-diphenyl oxide) (PPO)
Perfluoropolymers
Polycarbonates
Polysulfone
Polyperfluorodioxoles
Polyacetylenes
Polyaniline
Polyalkynes
Polybenzimidazole
Polysaccharides
Polyvinylidene fluoride PVDF

Fig. 3.5 Silicone rubber (polysiloxane)

permeability. Effects of various alkyl group substitutions on gas permeability of the resulting polysiloxanes were studied by Stern et al. [13]. Effects of the incorporation of amide in multiblock copolymers with poly(dimethylsiloxane) (PDMS) are well documented by Furuzono et al. [14].

The use of silicone rubber (SR) based thin film composite (TFC) membranes is increasing significantly in various industries due to the rubber's thermal and chemical stability. Achalpurkar et al. [12] studied the gas permeation properties of dense and thin film composite membranes (TFC) based on amine substituted silicone rubber (ASR) and unsubstituted silicone rubber (SR). The ASR dense membrane exhibited higher CO₂ (15 %) as well as CH₄ (12 %) permeability as compared to the SR dense membrane, while the permeability for other gases (He, H₂, N₂, and O₂) was decreased up to 15 %. Accordingly, CO₂-based selectivities in the ASR dense membrane increased by 22–34 %. The permeance of TFC membranes based on different UF supports decreased in the order of decreasing porosity and increasing solution concentration (ASR). It was also noted that the gas permeance of TFC membranes based on SR and ASR remained unaffected with increasing pressure (up to 4.2 kg/cm²), except for a nominal increase in CO₂ permeance.

3.1.1.2 Cellulose Acetate

Cellulose acetate membrane, initially developed for reverse osmosis [15], is the most widely used and tested for natural gas sweetening (Table 3.4), as in UOP's membrane systems [16].

Gantzel and Merten [8] applied a cellulose acetate membrane, used for desalination by RO, for the permeation of different gases. They reported the permeances in units of GPU = 10^{-10} cm³ (STP)/cm²-s-cm of Hg for He, 10.6; Ne, 1.9; O₂, 0.71; Ar, 0.37; CH₄, 0.34, and N₂, 0.31; all at 22 °C. Cynara-NATCO produces hollow fiber modules with cellulose triacetate for natural gas sweetening in an offshore platform in the Thailand gulf (830,000 Nm³ h⁻¹, which is the biggest membrane system for CO₂ removal) [10].

Cellulose acetate based membranes for CO₂ separation from CH₄ have been commercialized since the mid-1980s, and arose directly from the use of cellulose acetate reverse osmosis membranes [17]. A critical factor in the performance of cellulose acetate membranes is the degree of acetylation, which is the substitution of the hydroxyl groups on the glucoside repeating unit with acetyl groups. The size difference between the hydroxyl and acetyl group reduces the efficiency of chain packing, as the degree of acetylation increases, and improves chain flexibility and mobility because of reduced internal molecular hydrogen bonding between chains. This improves the intrinsic gas permeability, as shown in Fig. 3.6, with little change in the selectivity.

Table 3.4 Intrinsic permeation properties of cellulose acetate [10]

Permeability (Barrer)	Separation factor (<i>i</i> /CH ₄) (-)				
	H ₂ O	CO ₂	H ₂ S	N ₂	C ₂ H ₆
8.9	500	20–25	50	1	0.42
8.9	500	21	19	1	0.42

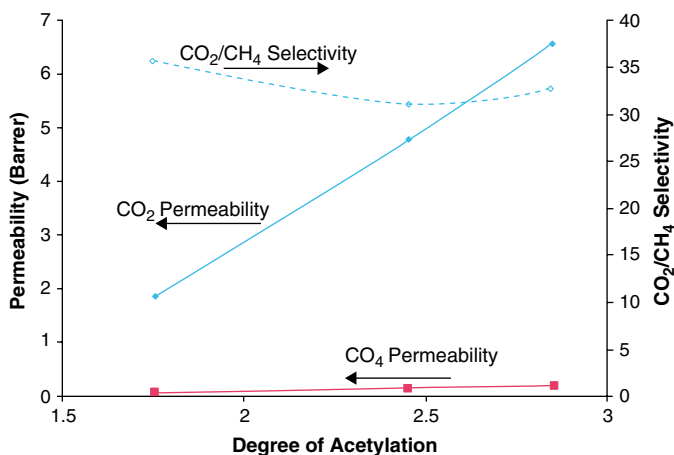


Fig. 3.6 Cellulose acetate membrane permeability (Barrer) and CO₂/CH₄ selectivity as a result of different degrees of acetylation, at 35 °C and 1 atm [18]

Table 3.5 Cellulose acetate membrane performance dried from different solvent exchange, at 60 °C and 300 psi [19]

Drying solvent	Surface tension (mN/m)	CO ₂ permeance (GPU)	CO ₂ /CH ₄ selectivity
Heptane	20.1	18	24
Octane	21.6	144	27
Nonane	22.9	174	33
Decane	23.9	156	36
Undecane	24.7	216	28
Cycloheptane	27.1	23	19
Toluene	28.4	57	22
Xylene	30.1	113	30

The other critical factor is fabrication of the membrane, and importantly the approach taken to achieve a dry film. During drying of water wet membranes, evaporation of water leads to capillary forces collapsing the microporous structure, creating a denser active layer. In the case of solvent exchange, water—a high surface tension solvent—is gradually replaced by a low surface tension solvent that has less impact on the membrane structure when evaporated. The effect of different solvents in the exchange on the membrane performance is shown in Table 3.5 [19].

The evaporation temperature for the preparation of wet reverse osmosis membranes is also critical for gas membrane performance. Minhas et al. [20] reported around 80 °C provided the best morphology for selectivity, but generally with low permeability, depending on the combination of solvents used for solvent exchange.

In natural gas processing via CA membranes, plasticization occurs in the membrane, either by CO₂ or heavy hydrocarbon components in feed gas. Plasticization increases the flexibility of the polymer chains and alters the separation performance as well as reduces the mechanical strength and speeds up aging effects. These effects are the cause of catastrophic membrane failure. Houde et al. [21] noticed that CO₂ plasticization pressure at around 10 atm for a dense membrane of 76 μm thickness, while Donohue et al. [22] observed the plasticization at <5 atm for asymmetric cellulose acetate membranes.

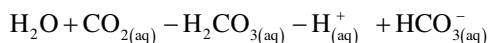
To achieve better separation and performances, some research work on cellulose acetate polymer derivatives has been reported. Some examples in the literature incorporate zeolites, transition metal complexes, and silicon species into the membrane or form composites with poly(methyl methacrylate) or poly(ethylene glycol) [20]. Another approach has been to cross-link cellulose acetate, which produces a more resistant structure that reduces the influence of plasticization [23–26]. Rahman et al. [27] also reported that the structure and separation properties of the asymmetric CA membranes depend on the variation in casting shear rate. Cellulose acetate membranes can also be used for the separation of ammonia from ammonia–nitrogen and ammonia–hydrogen systems [28].

Tanioka et al. [29] synthesized a freeze-dried CA membrane with high permeability and high separation factor. It was reported that the gas permeabilities for such a membrane were inversely proportional to the square root of molecular weight,

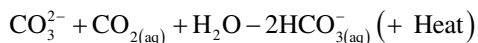
suggesting that the mechanism of gas flow through this membrane was Knudsen flow. Separation factors for H₂-He, Ar-Kr, N₂-Kr, He-Ne, H₂-Ne, He-Ar, Ar-H₂, He-Kr, Ar-He, and He-H₂ were measured. Separation efficiency largely depended upon the combinations of mixed gases.

Kim et al. [30] fabricated composite membranes with cellulose acetate and 2–6 wt% AMH-3 flakes and studied the CO₂/CH₄ gas separation. It was reported that performance of the CA membrane was significantly increased by incorporating only 2–6 wt% of silicate SAMH-3 flakes. There was a large increase in CO₂ permeability with maintenance of selectivity.

The first facilitated transport membranes fabricated from cellulose acetate (patent awarded to General Electric in 1967) [31] were related to CA films swollen by the inclusion of an aqueous carbonate solution. Carbon dioxide readily dissolves and reacts with water to form the bicarbonate anion.



Carbonate acts as a carrier by increasing the amount of carbon dioxide absorbed:

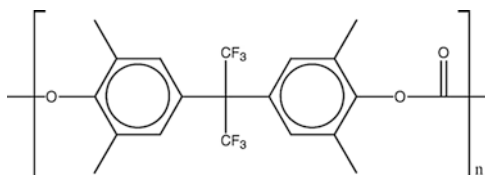


Hence, this reaction occurs on the feed side of the membrane and the bicarbonate anion transports through to the permeate side, where the reverse reaction occurs and carbon dioxide is released.

3.1.1.3 Polycarbonate (PC)

Polycarbonate membranes possess good mechanical properties and are able to operate under extreme conditions of temperature and pressure. However, polycarbonate membranes sometimes possess lower gas flux or permeability, or gas selectivity than desired for certain applications. A number of polycarbonates (PCs) have been synthesized and their carbon dioxide/nitrogen gas transport properties studied. Polycarbonates are generally synthesized by reaction between a diol and phosgene under a variety of conditions. Like many polymers used for gas separation membrane materials, the ready availability of structural variants of bisphenol A has led to a large number of different PCs. Most PCs tend to have a carbon dioxide permeability of under 40 Barrer, and selectivity ranges from 15 to over 25. One notable exception to this is the polycarbonate TMHFPC, which has a carbon dioxide permeability of 111 Barrer and a carbon dioxide selectivity of 15.0 [7]. The structure of this polymer is given in Fig. 3.7.

Fig. 3.7 TMHFPC



Ward et al. [32] reported that uniform and defect-free ultrathin polycarbonate membrane can produce 30 % oxygen-enriched air, which enables on-board generation of nitrogen-rich air to inert fuel tank vapor spaces and vent lines. Acharya et al. [33] reported that the permeability of hydrogen was greater than that of carbon dioxide through the polycarbonate (Bisphenol-A polycarbonate) membrane. They suggested that it could be due to the more diffusion energy required for carbon dioxide (linear shape of molecules) than hydrogen (spherical shape). In another study Vijay et al. [34] reported that the permeability of both gases, i.e., H₂ and CO₂, increased rapidly after etching PC membranes by α particles. The etched samples, which received a higher dose of particles showed better selectivity than the lower dose etched samples. Fu et al. [35] demonstrated that the permeability of gases in polycarbonate membranes was related to the forming of pores on the membrane surface.

Hacarlioglu et al. [36] reported that the gas separation properties of the polycarbonate-polypyrrole MMMs systems were highly dependent on the synthesis method (electrochemical or chemical) and also membrane casting conditions (casting solvent type). The MMM of electrochemically synthesized polypyrrole-polycarbonate (ECPY-PC) showed considerably higher permeabilities compared with both pure PC and the chemically synthesized polypyrrole-polycarbonate (CPPY-PC) films, with a loss in selectivities, whereas the CPPY-PC membranes had good separation properties. A mixed matrix membrane structure, which can be cast as permselective gas separation membranes with attractive gas separation performances, could be obtained with polycarbonate as matrix and zeolite 4A filler [37].

López-González et al. [38] measured the transport of pure oxygen, nitrogen, and carbon monoxide through the membranes prepared from poly[bisphenol A carbonate-co-4,4'-(3,3,5-trimethylcyclohexylidene) diphenol carbonate]. The permeabilities of oxygen, nitrogen and carbon monoxide at 35 °C and $p_0=1$ atm were 8.75, 1.87, and 2.91 Barrer, respectively. The values of the diffusion coefficient in 10⁻⁸ cm²/s, measured in the same conditions, were 8.26, 2.81, and 3.08, respectively. By replacing the two methyl groups of bisphenol A by other molecular groups, higher permeability was achieved without a substantial diminution of permselectivity. The permeability and the diffusion coefficients followed Arrhenius behavior.

3.1.1.4 Poly(norbornene)s

Norbornenes are important monomers in ring-opening metathesis polymerizations (ROMP). Polynorbornenes are polymers with high glass transition temperatures. Norbornene derivatives may be polymerized either by ring-opening metathesis polymerization (ROMP) or by addition polymerization at the double bond. Most ROMP polynorbornenes show modest permeabilities; however, addition-type poly(trimethylsilyl norbornene), prepared with nickel as catalyst and methyl aluminumoxane as co-catalyst, exhibited high free volume and high permeability [6].

Yampol'skii et al. [39] studied the two fluorine-containing glassy polynorbornenes (permeabilities, diffusion, and solubility coefficients, etc.). It was observed that these studied polymers had very high free volumes, and thus high permeabilities.

Addition-type poly(norbornene)s with siloxane substituents were synthesized using the $n^3(\text{allyl})(n^5\text{-cyclopentadienyl})\text{palladium}$, (Cp)Pd(ally) system [40, 41]. These synthesized polymers had very high T_g of up to 255 °C, and their films displayed high flexibility and optical clarity. The gas permeabilities of the polymer films varied with the content and structure of the siloxane substituents, and the films for the polymers with branched side groups showed high oxygen permeability ($P(\text{O}_2)=66\text{--}360$ Barrer). The films obtained for the polymers in the three arm-siloxane group ($-\text{Si}(\text{OSiMe}_3)_3$) displayed high oxygen permeability in the range of 39–239 Barrer. Asymmetric poly(norbornene) membranes were first prepared by a dry/wet-phase inversion technique. The membranes consisted of the thin skin layer supported by the porous substructure, and the surface skin layer had a unique nanoporous structure related to the nature of the side groups. The findings of this study suggest that the structure of the side group linked to the chain is an important factor for the regulation of the material properties and presents a new possibility for the application of poly(norbornene) materials.

Dorkenoo et al. [42] studied the permeation of gases in polynorbornenes and concluded that for noncondensable gases such as H_2 and He, the selectivity over N_2 decreased when the length of the pendant group increased, but remained relatively stable for the more condensable gases (O_2 and CO_2). The permeability correlates well to the inverse of the fractional free volume of the polymers.

3.1.1.5 Poly(2,6-Dimethyl-1,4-Diphenyl Oxide) (PPO)

Poly(2,6-dimethyl-1,4-diphenyl oxide) (PPO) exhibits excellent film formation and gas separation properties, and is resistant against a number of chemical agents, strong acids and bases. It belongs to the thermally stable glassy polymers having high glass transition temperatures. PPO is an example of a fairly permeable polymer having alternating aromatic cycles and C–O linkage in the main chain. Among the many aromatic polymers that possess high glass transition temperatures (T_g), PPO shows the highest permeability to gases. It is not evident why this polymer is much more permeable than polysulfone or bisphenol A polycarbonate, having similar structures of repeating units. A possible reason could be the absence of polar groups attached to the main chain. Whatever the reason for its properties, PPO drew attention as a permeable and rather permselective material.

The main application of modified and unmodified PPO membranes is directed to gas separation because of PPO's high permeability to gases. A number of electrophilic substitution reactions have been conducted on PPO to improve its gas permeation characteristics, such as bromination, carboxylation, methyl esterified carboxylation, sulfonylation, acylation, and silylation, introduction of trialkyl-silyl, hydroxyethylene, and ethyleneoxytrialkyl-silyl groups to be polymer backbone [43]. Permeability of PPOs as high as 100–200 Barrer have been reported for gases such as H_2 and CO_2 [44, 45]. Membranes from PPO are also known to be moderately permselective and it ranks among the hydrophobic polymers. Table 3.6 shows the permeability data of PPO for CO_2 , CH_4 , O_2 , and N_2 gases [46].

Table 3.6 Permeability data of PPO for CO₂, CH₄, O₂, and N₂

Gas permeability (Barrer) ^a				Perm selectivity	
CO ₂	CH ₄	O ₂	N ₂	CO ₂ /CH ₄	O ₂ /N ₂
90.0	5.4	16.7	3.7	16.7	4.5

^aPermeabilities at permeate pressure (absolute) \approx 100.0 kPa

Khulbe et al. [47] studied a PPO dense membrane prepared at different temperatures (22, 4 and -10 °C) via ESR, AFM and gas permeation. It was reported that the morphology of the surfaces of the membrane, the shape of its spin, and the selectivity of gases depend on the temperature of the evaporation of solvent used. The permeation rate of CO₂ increased with the decrease in the temperature used in the preparation of the membrane. However, methane permeation rate increased in the membrane prepared at -10 °C. It was suggested that Langmuir sites could be favorable for the CH₄ permeation.

Hamad et al. [48] reported that a brominated high molecular weight PPO membrane showed higher permeability of CO₂, CH₄, O₂, and N₂ gases when compared with non-brominated PPO. However, the permeability ratios for CO₂/CH₄ and O₂/N₂ changed only a little. Solubility of gases increased on increasing the bromination level. The trends in the gas permeability data and IR spectra obtained in this study both conform with and support the mechanism proposed in the literature that a higher degree of bromination is needed to enhance the permeability of gases by stiffening the PPO backbone, which increases the rate of diffusional jumps. It was also reported by Hamad and Matsuura [46] that the main effect of simultaneous sulfonation and bromination of PPO was: (1) to increase the gas permeability, and decrease the gas permeability ratio, in comparison to sulfonated PPO (SPPO), while on the other hand, (2) to decrease the gas permeability, and increase the gas permeability ratio, in comparison to brominated PPO (PPOBr). The observed trend in sulfonated brominated PPO membranes, when the degree of bromination was increased while the same degree of sulfonation was maintained, was the occurrence of a minimum in both gas permeability and diffusivity at 37.4 % degree of bromination. All these effects due to sulfonation of PPO, or bromination of PPO, or simultaneous sulfonation and bromination of PPO, were believed to be the direct result of the manipulation in polymer backbone stiffness, the packing density, and the free volume fraction.

Yu et al. [49] reported that sulfonated poly(2,6-diphenyl-1,4-phenylene oxide) (BSPPO_{dp}) as a new material for CO₂/N₂ separation. Compared with PPO membrane, the CO₂ permeability (58 Barrer) and CO₂/N₂ permselectivity (36) of the BSPPO_{dp} membrane were higher by 1.2 and 2.5 times, respectively, than the PPO membrane. The addition of silica nano particles in the BSSPO_{dp} membrane resulted in an increase in CO₂ permeability while maintaining CO₂/N₂ selectivity. The CO₂ permeability increased as a function of the silica content in the membrane. The separation mechanism for CO₂/N₂ in the membranes was attributed to the gas solubility effect rather than the gas diffusivity.

3.1.1.6 Polyimides (PI)

An extensive review of the gas separation properties of polyimides was published in 1996 [50]. Aromatic polyimides, usually obtained from bifunctional carboxylic acid dianhydrides and primary diamines, are widely used in different branches of industry such as electronics, insulators, high-temperature adhesives, and photoresistance. The successful applications of such high-performance polyimides are mainly due to excellent physicochemical properties such as high temperature stability, exceptional mechanical strength, low thermal expansion coefficient, dimensional stability, superior insulation properties, and radiation and chemical resistance. In the field of membrane science and technology, polyimide membranes have been extensively studied because of their excellent separation performances, particularly for gas separation [51].

Many polyimides exhibit good selectivity, but at the expense of permeability. Polyimides are a class of polymers that display high permeability for CO_2 and good selectivity against CH_4 . They are supposed to be an alternative to cellulose acetate because they are also easy to prepare as asymmetric membranes while demonstrating good thermal and chemical stability. PIs are rigid, have high melting point and high T_g , and are thermally stable polymers obtained by polycondensation reactions of dianhydrides and diamines. A wide range of polyimides exist with good gas separation properties based on varying both the diamine and dianhydride. Some polyimides, particularly those incorporating the group 6FDA (2,2-bis(3,4-dicarboxyphenyl) hexafluoropropane dianhydride), possess both high selectivities and high permeabilities due to following reasons:

1. The CF_3 group considerably increases the stiffness of the chain, allowing the membrane to more effectively separate molecules on the basis of steric bulk.
2. Effective chain packing is reduced by the large CF_3 groups, which leads to an increase in the permeability.

6FDA-based polyimide membranes for gas separation have been studied mainly with dense membrane containing various diamine moieties [52]. Kim et al. [52] synthesized 6FDA-based polyimides with polar hydroxyl or carboxyl group in diamine, such as 6FDA-BAPAF, 6FDA-DAP, and 6FDA-DABA by the thermal imidization method. The corresponding composite membranes were then prepared by the dip-coating technique using a poly(ether sulfone) (PES) membrane as the supporting layer. Chemical structures of the 6FDA-based polyimides synthesized by Kim et al. are shown in Fig. 3.8. 6FDA-TrMPD polyimide was used for the preparation of a reference membrane material to compare solubility.

Table 3.7 shows the gas permeation characteristics of the composite membranes with different 6FDA-based polyimides.

The 6FDA-DAP polyimide membrane exhibited higher permeance and selectivity than other polyimides. CH_4 permeance for the 6FDA-BAPAF membrane was obtained at a much higher level than expected; hence, CO_2/CH_4 selectivity for the 6FDA-BAPAF polyimide membrane was low. CO_2/N_2 selectivities for the composite membranes prepared using different polyimides above were equal to those for

Fig. 3.8 Chemical structure of 6FDA-based polyimides

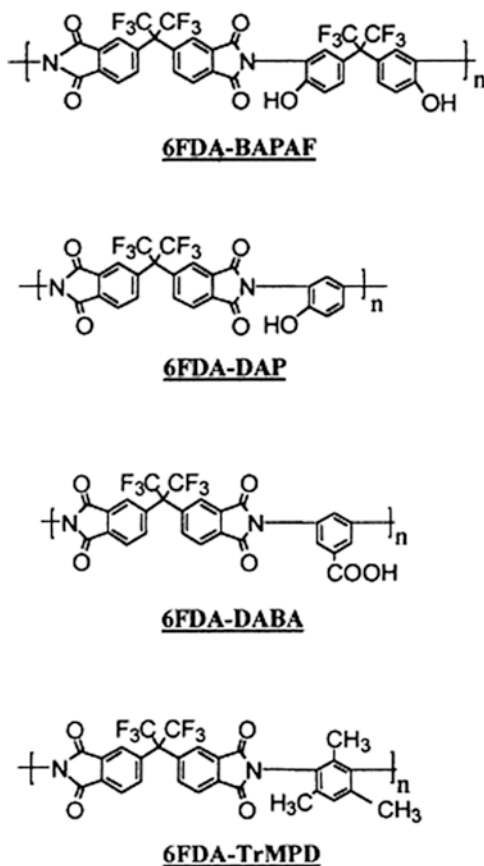


Table 3.7 Gas permeation characteristics of the composite membranes with different 6FDA-based polyimides

Polyimides	Permeance (GPU)					α^a	
	CO ₂	N ₂	CH ₄	H ₂	O ₂	CO ₂ /N ₂	CO ₂ /CH ₄
6FDA-BAPAF	24.60	1.23	1.10	46.93	4.86	20.11	22.78
6FDA-DAP	38.57	1.32	0.49	73.80	6.52	29.26	78.82
6FDA-DABA	26.30	0.93	0.56	52.85	4.85	28.28	46.96

^a α : ideal selectivity. Coating solvent: 2-methoxyethanol. Coating polymer concentration: 1 %. GPU = 10⁻⁶ cm³(STP)cm⁻² s⁻¹ cmHg⁻¹

other dense or asymmetric 6FDA-based polyimide membranes in the literature, as shown in Table 3.8 [52].

Li et al. [53] developed a delamination-free, dual layer, asymmetric composite hollow fiber membrane. 6FDA-durene-1,3-phenylenediamine (mPDA) (50:50) copolyimide was used to form the outer asymmetric separating layer, while PES was employed to yield the inner interpenetrated porous supporting layer.

Table 3.8 Gas selectivity of 6FDA-based polyimide membranes in the literature [52]

Polyimide	Membrane type	α (selectivity)	
		CO ₂ /N ₂	CO ₂ /CH ₄
6FDA-3BDAF	Dense	27	48
6FDA-IPDA	Dense	23	43
6FDA-DAFO	Dense	22	60
6FDA-APPS	Asymmetric	29	39

Pure gas permeance test results revealed that the O₂/N₂ selectivity of the dual layer asymmetric hollow fiber was about 4.6, which is very close to the intrinsic value of the outer-layer material (4.7) with an O₂ permeance of around 28 GPU at room temperature.

The insertion of bulky substituents into the peripheral polymer backbones should disrupt efficient packing of the polymeric chains, leading to an increase in the permeabilities and a loss of selectivities. A number of different polymers have been investigated for this effect. Some bulky novel polyimides structures are given in Fig. 3.9.

A range of polyimide membranes are given in Table 3.9. Among these, Matrimid 5218 is the most often reported in the literature. The chemical structure of Matrimid is given in Fig. 3.10.

Figure 3.11 displays the carbon dioxide permeability and carbon dioxide/nitrogen selectivities of a variety of polyimides [7] and Table 3.10 provides permeability and selectivity data of pure and mixed gas for Matrimid 5218 [54].

Like cellulose acetate, polyimides are known to be susceptible to plasticization by CO₂. For asymmetric Matrimid, the plasticization pressure is <4 bar, while dense 6FDA-DAD at 35 °C is plasticized by 14 bar CO₂ [55]. However, plasticization pressure is dependent on the thickness of the membrane. Polyimides are more sensitive to plasticization than cellulose acetate. This could be due to the more ordered structure in the polyimide film compared to cellulose acetate, which makes it more susceptible to, structural changes. White [17] observed that hexane plasticized polyimide membranes and that naphthalene fouled the polyimide membrane surface. Various approaches have been made to improve polyimide performance in terms of gas separation properties, as well as resistance to plasticization by CO₂ and other components in natural gas. Approaches, such as hyper-branching and cross-linking, preparation of mixed matrix membranes, and blending with other polymers such as polysulfone and polyethersulfone have been studied. Bos et al. [56] observed an increase in the plasticization pressure of Matrimid when blended with Therrmid FA-700 from around 10 bar to around 20 bar.

Faiz and Li [57] concluded that of all the investigated polyimide and copolyimide membranes, 6FDA-based membranes showed the best performances for olefin/paraffin separation due to loose polymer chain packing. However, the membrane performances seemed to deteriorate with time since the glassy state of the polymer was not in an equilibrium state initially, and shifted to a denser packing state with aging time.

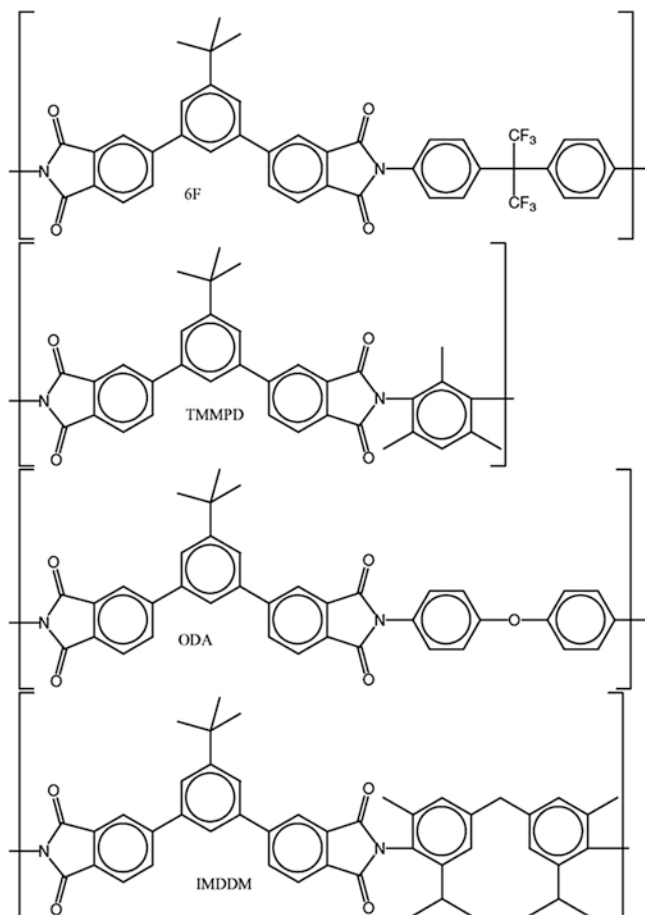
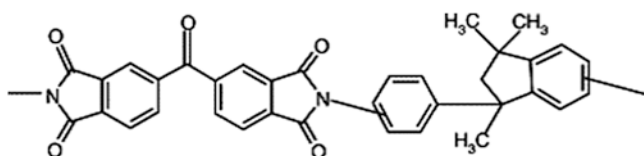
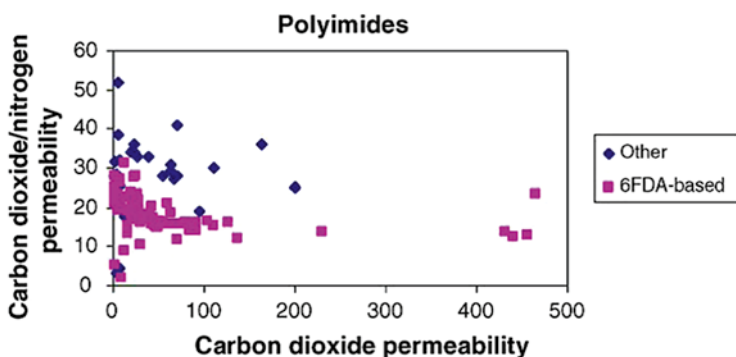


Fig. 3.9 Structure of some bulky novel polyimide [7]

Tin et al. [54] modified the Matrimid® 5218 membrane by cross-linking. A room temperature cross-linking modification of Matrimid® 5218 has been done by immersing the films in a 10 % (w/v) of *p*-xylenediamine in methanol solution for a certain period of time. The chemical structure changes during the cross-linking process, i.e., after cross-linking, imide functional groups of Matrimid were converted to the amide functional groups. The gas permeabilities and ideal selectivities of He, O₂, N₂, CH₄, and CO₂ through cross-linked Matrimid films are summarized in Table 3.11. The table depicts the behaviors of pure gas permeabilities with immersion time. The gas permeabilities are found to attain the maximum values for 1-day cross-linking, followed by subsequent decrease with immersion time. It seems that the degree of cross-linking governs the gas transport properties. The selectivity of CO₂/CH₄ for cross-linked film is higher than the film without cross-linking. It was

Table 3.9 CO₂ permeability and CO₂/CH₄ selectivity for a range of polyimide membranes at 35 °C [19]

Polymer	CO ₂ permeability (Barrer)	CH ₄ permeability (Barrer)	CO ₂ /CH ₄	Temp. (°C)	Press.
Matrimid 5218	6.5	0.19	34	35	10 bar
Matrimid 5218	5.39	0.15	36	35	2 bar
6FDA-TAPOB	7.4	0.098	75	25	1 bar
ODPA-TAPOB	0.63	0.0064	98	25	1 bar
PMDA-TAPOB	3.3	0.66	50	35	1 bar
6FDA-DATPA	23	0.68	34	35	10 bar
ODPA-IPDA	0301	0.0064	47	35	10 bar
6FDA-6FpDA	63.9	1.5	39.9	35	10 bar
6FDA-6FmDA	5.1	0.08	63.8	35	10 bar
DAD-6FDA	381	15.24	25	25	300 psi
DAM-6FDA	691	48.7	14.2	25	300 psi
DDBT-BPDA	8.20	0.24	34.2	50	10 bar

**Fig. 3.10** Chemical structure of Matrimid**Fig. 3.11** Carbon dioxide permeability vs. selectivity for polyimides

also observed that Matrimid membranes undergo the plasticization phenomenon at 15 atm; however, plasticization is effectively suppressed by the cross-linking modification.

Asymmetric hollow fibers fabricated from commercially available polyimide material Matrimid[®] gave high CO₂/CH₄ separation factors (ranging up to 67), which were among the highest reported for purely polymeric hollow fibers without post-treatments and exceeded the commonly reported bulk values of Matrimid[®] [58].

Table 3.10 CO₂ and CH₄ permeability (Barrer) and CO₂/CH₄ selectivity in Matrimid 5218 under mixed gas conditions (10 % CO₂ in CH₄) at 7.5 bar and 35 °C in comparison with pure gas [19]

	CO ₂ permeability (Barrer)	CH ₄ permeability (Barrer)	CO ₂ /CH ₄
Pure gas	11.5	0.23	49
Mixed gas	9.0	0.22	41

Table 3.11 Gas separation properties of original and cross-linked Matrimid dense films^a

Immersion time (days)	Permeability (Barrer)					Selectivity			
	He	O ₂	N ₂	CH ₄	CO ₂	He/N ₂	O ₂ /N ₂	CO ₂ /CH ₄	CO ₂ /N ₂
0	22.2	1.7	0.25	0.19	6.5	87	6.6	34	25.6
1	26.2	1.9	0.29	0.20	7.4	91	6.5	36	25.6
3	25.0	1.6	0.24	0.18	6.0	105	6.9	34	25.2
7	22.1	1.5	0.21	0.15	5.1	107	7	33	24.6
14	21.7	1.4	0.19	0.14	4.7	112	7	34	24.1
21	19.4	1.1	0.15	0.10	3.4	128	7.4	32	22.2
32	17.5	0.9	0.13	0.07	1.9	140	6.9	38	15

^a1 Barrer = 1×10^{-10} cm³ (STP) cm cm⁻² s⁻¹ cmHg

Peng and Chung [59] spun a defect free as-spun Torlon® hollow fiber membrane with an ultrathin dense layer of around 540 Å from only a one polymer/one solvent binary system at reasonable take-up speeds of 10–50 m/min. The best O₂/N₂ permselectivity achieved was much higher than the intrinsic value of Torlon® 4000TF poly(amide imide) dense film, which was about 8.

Polyimide membranes were modified by immersing the films in the diamine/methanol solution for a stipulated period of time (cross-linking). A series of linear aliphatic cross-linking diamines reagents (ethylenediamine, propane-1,3-diamine, and butane-1,4-diamine) were used. This study demonstrated that diamine cross-linked membranes possess high separation performance and provide impressive separation efficiency for H₂/CO₂ separation. Both pure gas and mixed gas data were better than other polymeric membranes and above the Robeson's upper boundary curve (Fig. 3.12) [60].

It was suggested that this modification can alter the physiochemical structure of polyimide membranes with superior performances for H₂ and CO₂ separation. Liu et al. [61] developed an extremely simple room temperature chemical cross-linking technology for the modification of polyimide films for gas separation of He/N₂ and O₂/N₂. Using 6FDA-durene as an example, chemical modification was performed by immersing the dense 6FDA-durene films in a *p*-xylenediamine methanol solution for a certain period of time followed by washing with fresh methanol and drying at ambient temperature. Gas permeation properties of modified polyimides for He, O₂, N₂, and CO₂ were measured at 35 °C and 10 atm. The gas permeabilities of the cross-linked 6FDA-durene dense films are summarized in Table 3.12.

Table 3.12 indicates that the gas permeability decreased significantly in the order of CO₂ > N₂ > O₂ with an increase in the degree of cross-linking, which was mainly

Fig 3.12 Both pure gas and mixed gas separation properties of H₂/CO₂ separation membrane derived from 6-FDA-durene with respect to the *upper bound curve* [60]

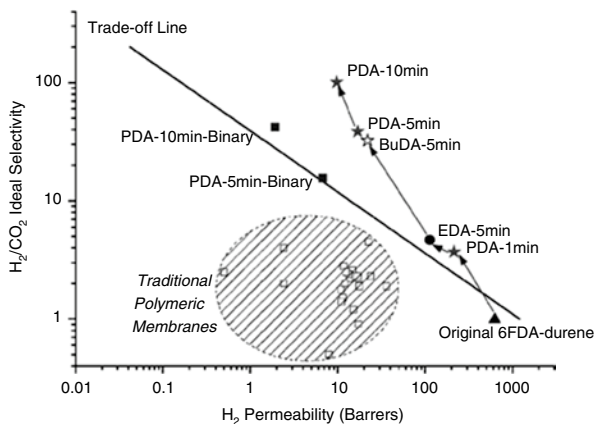


Table 3.12 Gas permeabilities of the cross-linked 6FDA-durene dense films

Immersion time (min)	<i>P</i> (Barrer)			
	He	O ₂	N ₂	CO ₂
0	362	125	33.5	456
5	204	45.2	11.1	136
10	168	28.9	6.53	91.8
15	157	26.5	6.05	70.0
30	109	13.7	2.87	30.3
60	34.4	2.34	0.40	2.14

attributed to the significant decreases in diffusion coefficients, but CO₂/N₂ decreased from 12 to 5.4, which suggested that this cross-linking approach was most useful for the application of He/N₂ and O₂/N₂ separation.

Wang et al. [62] synthesized a series of novel fluorinated copolyimides and studied the permeation of pure and mixed gases through these membranes. The basic formula of copolyimides was 2,2'-bis(3,4'-dicarboxyphenyl)hexafluoropropane dianhydride (6FDA)-2,6-diamine toluene (2,6-DAT)/1,3-phenylenediamine (mPDA). The permeability decreased with increasing mPDA content; however, the permselectivity of gas pairs such as H₂/N₂, O₂/N₂, and CO₂/CH₄ was enhanced with the incorporation of mPDA moiety. The permeabilities of H₂, O₂, N₂, CO₂, and CH₄ were found to decrease with increasing order of kinetic diameters of the penetrant gases. 6FDA-2,6-DAT/mPDA (3:1) copolyimide and 6FDA-2,6-DAT polyimide had high separation properties for H₂/N₂, O₂/N₂, and CO₂/CH₄. Their H₂, O₂, and CO₂ permeabilities were 64.99, 5.22, and 23.87 Barrer for 6FDA-2,6-DAT/mPDA (3:1) copolyimide, respectively, while for 6FDA-2,6-DAT polyimide they were 81.96, 8.83, and 39.59 Barrer, respectively. All copolyimides exhibited similar performances, lying on or above the existing upper boundary trade-off lines between permselectivity and permeability.

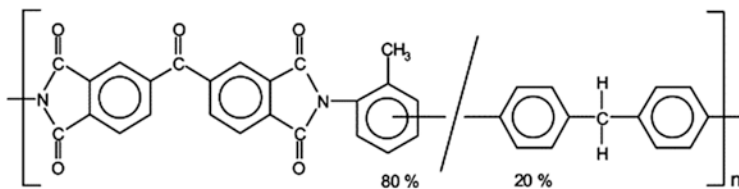


Fig. 3.13 Chemical structure of BTDA-TDI/MDI (P84) co-polyimide

Co-polyimide BTDA-TDI/MDI is a commercial polymer produced by Lenzing with the trade name P84. The chemical structure of this polymer is shown in Fig. 3.13. This material is known as non-plasticizable and its glass transition temperature is 315 °C.

Barsema et al. [63] prepared dense flat sheets as well as asymmetric hollow fiber membranes based on BTDA-TDI/MDI (P84) and used both for the separation of a CO₂-N₂ (80/20) mixture and permeation rates of pure gases. The permeation rates of He, CO₂, O₂, and N₂ were measured by the variable pressure method at different feed pressures and temperatures. It was revealed that P84 co-polyimide is one of the most selective glassy polymers. It is a promising material for the preparation of gas separation membranes with high selectivities such as 285–300 for He/N₂, 45–50 for CO₂/N₂, and 8.3–10 for O₂/N₂. The permeability of CO₂ was relatively low (1 Barrer at 25 °C). The permeation of CO₂ through the asymmetric hollow fiber membranes increased with pressure indicating that the plasticization behavior of asymmetric membranes differs from the respective dense ones. However, no evidence of plasticization was observed when a CO₂/N₂ (80/20) mixture was fed to the hollow fiber membranes at a pressure up to 30 bar. In all cases, CO₂ permeance decreased with pressure while that of N₂ remained constant.

3.1.1.7 Polyetherimide

Polyetherimide (PEI) is an amorphous, amber-to-transparent thermoplastic with characteristics similar to the related plastic PEEK. Relative to PEEK, PEI is cheaper and lower in impact strength, but has a higher use temperature. The repeating unit of PEI is shown in Fig. 3.14.

The molecular formula of the repeating unit of PEI is C₃₇H₂₄O₆N₂ and the molecular weight is 592 g/mol. The glass transition temperature of PEI is 216 °C. Its amorphous density at 25 °C is 1.27 g/cm³. It is prone to stress cracking in chlorinated solvents.

Ultem is a family of PEI products manufactured by SABIC as a result of acquiring the General Electric Plastics Division in 2007. Ultem 1000 (standard, unfilled polyetherimide) has a high dielectric strength, natural flame resistance, and extremely low smoke generation. Ultem has high mechanical properties and performs in continuous use to 340 °F (170 °C). Ultem 1000 has a thermal conductivity of 0.122 W/m K.

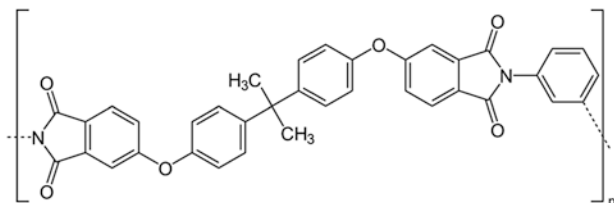


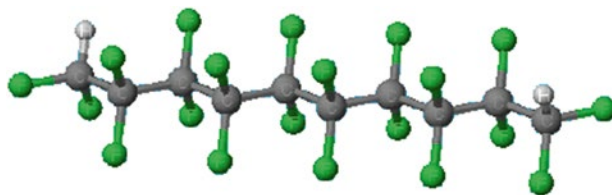
Fig. 3.14 Repeating unit formula of PEI

Kneifel and Peinemann [64] developed asymmetric PEI (Ultem[®] 1000) hollow fiber membranes both with a microporous skin and with a dense skin on the bore side of the fibers. The effect of the composition of the polymer solution, the spinning conditions and the post-treatment on the porosity of the skin, and on the shape and morphology of the fiber wall was investigated. Silicone composite membranes with an oxygen permeance up to $5.3 \times 10^{-9} \text{ m}^3(\text{N}) \text{ m}^{-2} \text{ s}^{-1} \text{ Pa}^{-1}$ and dense membranes with a helium/nitrogen selectivity of about 170, at a helium permeance up to $5.6 \times 10^{-10} \text{ m}^3(\text{N}) \text{ m}^{-2} \text{ s}^{-1} \text{ Pa}^{-1}$ were obtained.

Gas permselection properties for N_2 , CH_4 , Ar, CO_2 , O_2 , H_2 , and He through the PEI membranes were investigated in some detail as a function of pressure and temperature. Wang et al. [65, 66] studied the permeation properties of pure H_2 , N_2 , CH_4 , C_2H_6 and C_3H_8 through asymmetric PEI hollow fiber membranes. The PEI asymmetric hollow-fiber membrane was spun from an *N*-methyl-2-pyrrolidone/ethanol system via a dry-wet phase-inversion method, with water as the external coagulant and 50 wt% ethanol in water as the internal coagulant. The prepared asymmetric membrane exhibited sufficiently high selectivity (H_2/N_2 selectivity > 50) at 25 °C. The apparent separating layer thickness determined by the gas permeation was in the range of 370–500 Å. It was also reported by Wang et al. that on adding volatile organic compounds as additives into the dope solutions for the preparation of PEI hollow fiber, the hollow fiber membrane showed high selectivity for He/ N_2 separation [67].

It has been reported that homogeneous and ultrathin (60 nm) uniform films of polyetherimide polymer (Ultem) can be fabricated on a smooth support, like a clean glass by spin coating. The thin Ultem film can be laminated and removed from the support without any damage using an in situ cast support film of PPO over an Ultem film. The films of Ultem and PPO have shown good adhesion without any interpenetrating regions. It has also been reported that the oxygen and nitrogen permeability was independent of the Ultem film thickness down to 60 nm. The helium permeability for the 150 and 60 nm films were about 20 % higher than 500 and 815 nm thick films [68].

Bruma et al. [69] synthesized a series of polyetherimides by polycondensation reactions of 2,2-bis[4,4-(3,4-dicarboxyphenoxy)phenyl]propane dianhydride with various aromatic diamines at high temperature. Polymer solutions in chloroform were processed into thin films, which were tested as gas separation membranes. Transport parameters for light gases were measured. The dependence of glass



Teflon, $-(CF_2CF_2)-$

Fig. 3.15 Chemical structure of Teflon

transition and decomposition temperature on conformational rigidity parameters was calculated. All these properties, associated with easy processability, make these polymers potential candidates for practical applications as gas separation membranes.

3.1.1.8 Perfluoropolymers

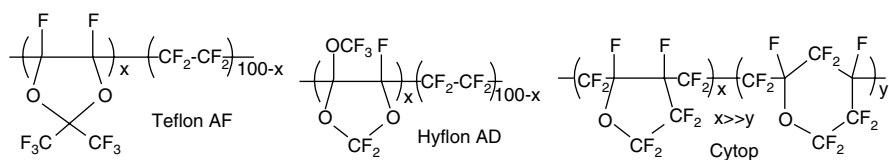
Perfluoropolymers are a class of polymers that display unique resistance to hostile chemical and thermal environments, and in particular resistance to plasticization from both CO_2 and hydrocarbons. The reason for their unique properties is the high energy of the C–F bonds that exist in the substituent groups of the polymer backbone. The most common perfluoropolymer is poly(tetrafluoroethylene) (PTFE). PTFE and similar polymers, such as poly(hexafluoropropylene-tetrafluoroethylene), have poor gas separation properties because of a high degree of crystallinity when cast as a film. The discovery in the 1980s of amorphous perfluoro polymers, in particular Cytop[®], Teflon AF[®], and Hyflon AD[®] [70, 71] that utilize bulky fluorine substituent groups to inhibit chain packing has enabled efficient gas separation membranes to be fabricated. Teflon is one brand name for a number of fluorinated polymers (Fig. 3.15) and its chemical name is polytetrafluoroethylene (PTFE). This is a polymer with repeating chains of $-(CF_2-CF_2)-$ in it. Teflon was first discovered accidentally by Roy J. Plunkett (1910–1994) in 1938 at the DuPont research laboratories in N.J. and introduced as a commercial product in 1946. Teflon resists many chemicals. This includes ozone, chlorine, acetic acid, ammonia, sulfuric acid, and hydrochloric acid. The only chemicals known to affect these coatings are molten alkali metals and highly reactive fluorinating agents.

There are a number of commercially available perfluoropolymers (Teflon AF, Hyflon AD, Cytop) that form amorphous and glassy films. Highest permeabilities were obtained for Teflon AF2400 and Teflon AF1600, which are copolymers of 2,2-bistrifluoromethyl-4,5-difluoro-1,3-dioxole and tetrafluoroethylene with dioxole mole fractions of 0.87 and 0.65, respectively [72, 73].

The permeability and selectivity performance of some common perfluoropolymers are listed in Table 3.13 [19].

Table 3.13 Permeability and selectivity of perfluorinated glassy polymers for natural gas separation [20]

Membrane	CO ₂ permeability (Barrer)	CH ₄ permeability (Barrer)	CO ₂ /CH ₄	Temp. (°C)	Press. (bar)	Refs.
Teflon AF2400	2,200	390	5.7	35	27	[71]
Teflon AF1600	520	80	6.5	–	–	[71]
Hyflon AD80	150	12	13	–	–	[71]
Hyflon AD60	130	10	13	–	–	[71]
Cytop	35	2.0	18	–	–	[71]
Poly-(perfluoro (2-methylene-4-methyl-1,3-dioxolane)	67	2	33.5	25	7.8	[74]
Cyclic perfluorodimethylene-bis(perfluorovinyl ether)	8.2	0.21	39	–	–	[75]
PDD-CTFE	70.4 (GPU)	0.88 (GPU)	80.0	60	–	[76]
Pdd-TFE-MA	18.6 (GPU)	0.69 (GPU)	27.0	60	–	[76]

**Fig. 3.16** Repeat units of glassy and amorphous perfluoropolymers used in the preparation of gas separation membranes. Teflon AF2400: $x=87$, $T_g=240$ °C. Teflon AF1600: $x=65$, $T_g=160$ °C. Hyflon AD80X: $x=80$, $T_g=134$ °C. Hyflon AD60X: $x=60$, $T_g=130$ °C. Cytop, $T_g=108$ °C [10]

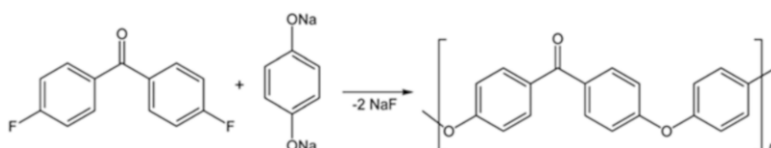
Amorphous Teflon AF2400 possesses many advantages as a membrane material, including good film forming properties, extremely high chemical stability, low susceptibility to swelling, and—unlike other high permeability polymers—no detectable aging. Beside this, AF2400 is insoluble in common organic solvents but shows good solubility in perfluorinated solvents, which are used in preparation of composite membranes [77]. Teflon AF2400 and Teflon AF1600 (DuPont) are the most permeable among perfluoropolymers (Fig. 3.16 and Table 3.14), a family with excellent thermal and chemical resistance, melt stability, good mechanical properties, and usable at broad temperature range. Hyflon AD60X is a compromise of a moderately high selectivity and still interesting permeability, in comparison with the more permeable but less selective Teflon AF. It is particularly suitable for use in dense GS membranes.

In perfluoropolymers the solubility selectivity substantially changes; therefore, they represent materials suited for challenging separations (e.g., olefin/paraffin or natural gas treatment).

Table 3.14 Permeation properties of glassy and amorphous perfluoropolymer membranes

Polymer	Permeability (Barrer)						Selectivity
	O ₂	N ₂	CH ₄	CO ₂	C ₂ H ₆	C ₃ H ₈	CO ₂ /CH ₄
Teflon AF2400 ^a	1600	780	600	3,900	370	200	6.5
Teflon AF1600	270	110	80	520			6.5
Hyflon AD80	67	34	12	150			13
Hyflon AD60	57	20	10	130			13
Cytop	16	5.0	2.0	35			18

^aPure gases, feed pressure, 3.5 bar; thickness, 20 μm

**Fig. 3.17** Polyether ether ketone formation

3.1.1.9 Poly(Ether Ether Ketone) (PEEK)

Polyether ether ketone (PEEK) is a colorless organic thermoplastic polymer in the polyaryletherketone (PAEK) family. PEEK polymers are obtained by step-growth polymerization by the dialkylation of bisphenolate salts (Fig. 3.17). Typical is the reaction of 4,4'-difluorobenzophenone with the disodium salt of hydroquinone, which is generated in situ by deprotonation with sodium carbonate. The reaction is conducted at around 300 °C in polar aprotic solvents—such as diphenyl sulfone.

Poly(ether ether ketone)-WC is a phenolphthalein-based poly(ether ether ketone), having a lactone group sticking out of the backbone. PEEK polymer is amorphous and soluble in chlorohydrocarbons, amides, and ethers; therefore, it is well suited for the preparation of polymeric membranes by phase separation techniques. CO₂/N₂ and O₂/N₂ selectivity of asymmetric PEEK-WC membranes prepared by the dry phase inversion technique are 33 and 6, respectively, which are comparable to typical commercial membranes, such as composite polyimide membranes. On the other hand, CO₂ and O₂ permeance are $2.3 \times 10^{-11} \text{ m}^3 \text{ m}^{-2} \text{ s}^{-1} \text{ Pa}^{-1}$ and $4.3 \times 10^{-12} \text{ m}^3 \text{ m}^{-2} \text{ s}^{-1} \text{ Pa}^{-1}$, respectively, which are slightly lower than the typical commercial membranes [78].

3.1.1.10 Polyurethane (PU)

Polyurethane (PUR and PU) is a polymer composed of a chain of organic units joined by carbamate (urethane) links. While most polyurethanes are thermosetting polymers that do not melt when heated, thermoplastic polyurethanes are also available. The properties of polyurethane are greatly influenced by the types of isocyanates and polyols. Figure 3.18 shows the PU synthesis.

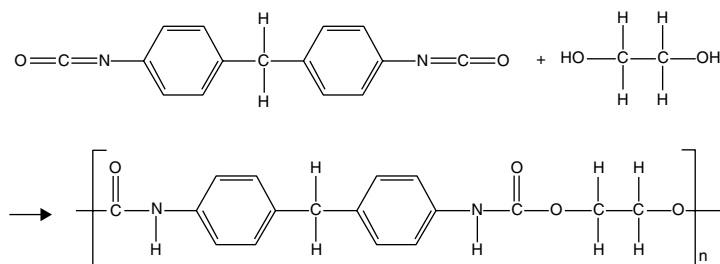


Fig. 3.18 Polyurethane synthesis, wherein the urethane groups -NH-(C=O)-O- link is the molecular units

Polyurethane (PU) membranes own high gas permeability but low selectivity. Some efforts were made to increase gas selectivity by modifying the polymer structure of these membranes but the effort was unsuccessful. It was reported that increasing the amount of oxygen carrier salt (cosalen) into a polycarbonate membrane increase the selectivity of oxygen to nitrogen, especially at low temperature [79].

Chen et al. [80] also reported the effects of oxygen carrier salt, namely cosalen. The dual mode analysis showed that the gas separations in PU membranes were dominated by gas diffusion rather than gas sorption. The selectivity of O_2/N_2 was 8.6 and the oxygen permeability was 1.1 Barrer for the PU membrane with 5 wt% cosalen at 5 °C. The key issue for improving the gas separation performance of a polyurethane membrane is to increase the diffusivity ratio but not the solubility ratio.

Sadeghi et al. [81] fabricated polyurethane-silica membranes by a solution blending and casting method. It was reported that CO_2/N_2 , CO_2/CH_4 , and O_2/N_2 permselectivities increased from 24.96, 9.56, and 2.17 for pure polyurethane to 41.26, 13.43, and 2.58 for polyurethane-silica (20 wt%). The gas permeation properties of prepared nano-composite membranes showed the decrease in gas permeability of membranes with silica content, but an increase in CO_2/N_2 and CO_2/CH_4 selectivities. The permeation of gases was also modeled by the modified Higuchi model. New constants for the Higuchi model were obtained for studied gases. The experimental data and modified model showed good agreement.

Talakesh et al. [82] studied the effect of the structure of polyether-based polyurethane (PU) membranes on their gas separation properties. In this regard, a series of polyurethanes were synthesized based on hexamethylene diisocyanate (HDI) and 1,4-butanediol as hard segments and different soft segments such as poly(tetramethylene glycol) (PTMG, 2,000 g/mol), poly(ethylene glycol) (PEG, 2,000 g/mol), and PTMG/PEG mixture. The results of gas permeation experiments showed that by increasing the ether group content in the polymer structure, permeability of the pure gases decreased, while CO_2/N_2 ideal selectivity increased. The obtained results also indicated that the permeability of CO_2 decreased from 132.52 Barrer in PU0 (PU containing 100 wt% of PTMG in soft segment) to 20 Barrer in PU100 (the PU containing 100 wt% of PEG in soft segment), respectively. CO_2/N_2 selectivity increased from 28 to 90. Trade-off evaluation also showed

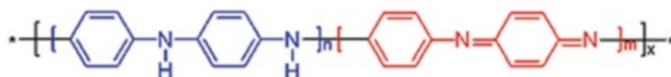


Fig. 3.19 Main polyaniline structures $n + m = 1$, $x =$ degree of polymerization

that the commercialization potential of the studied membranes for CO_2/N_2 and even CO_2/CH_4 separation increased with the PEG content in the polymer. In particular, the PU membrane which contained 75/25 wt% ratio of PEG/PTMG had the highest potential for commercialization.

3.1.1.11 Polyaniline (PANi)

Polyaniline (PANi) ($\{[\text{C}_6\text{H}_4\text{NH}]_{2n}[\text{C}_6\text{H}_4\text{N}]_{2m}\}_x$) is a conducting polymer of the semi-flexible rod polymer family. Its structural formula is shown in Fig. 3.19.

Polymerized from the inexpensive aniline monomer, polyaniline can be found in one of three idealized oxidation states.

1. Leucoemeraldine—white/clear and colorless ($\text{C}_6\text{H}_4\text{NH}$)_n.
2. Emeraldine—green for the emeraldine salt, blue for the emeraldine base ($\{[\text{C}_6\text{H}_4\text{NH}]_2[\text{C}_6\text{H}_4\text{N}]_2\}_n$).
3. (Per)nigraniline—blue/violet ($\text{C}_6\text{H}_4\text{N}$)_n.

PANi, which belongs to an important member of the family of electrically conducting polymers, has been studied extensively as a membrane due to its distinct electrochemical properties and environmental stability. The Martin group [83, 84] and the Anderson group [85] showed that electronically conductive polymers (example PANi) are promising membrane materials for industrial gas separation. Adding dopants to PANi leads to a decrease in gas permeability, while removal of these dopants would produce extremely high permeability [86]. Polypropylene-supported polyaniline membranes—photografted with 2-hydroxyethyl methacrylate and glycidyl methacrylate to produce hydrophilicity and reactivity and then reacted with diamines to provide basicity—have been prepared and used for the separation of carbon dioxide and methane. After solvation with water, these membranes exhibit a permeability of around 3,400 Barrer and a separation factor up to 490 [87]. Kuwabata and Martin [88] recommended that polyaniline must be regarded as a promising material for O_2/N_2 separation because its combination of $\alpha_{\text{O}_2/\text{N}_2} = 15$ and $P_{\text{O}_2} = 0.16$ Barrer places it above Robeson's upper bound [3].

Gas permeation experiments of O_2 and N_2 were performed with conducting polyaniline (PANi) composite membranes prepared by using a porous nylon membrane as a support. Lee et al. [89] reported that PANi composite membranes can be easily obtained by a novel solvent welding process. Doping, dedoping, and redoping kinetics of PANi composite membranes were studied by calculating the [Cl]/[N] content using elemental analysis. After doping and dedoping processes, the permeability of a dedoped PANi membrane decreased while selectivity slightly increased, probably

because the changes in morphology of PANi. d -Spacing of the PANi film decreased from 4.89 to 3.67 Å. As redoping continued, the d spacing decreased, resulting in a dramatic increase in selectivity of the PANi membrane. The highest O₂/N₂ selectivity and permeability obtained from PANi redoped was 28 and 0.13 Barrer, respectively.

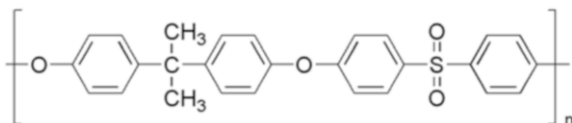
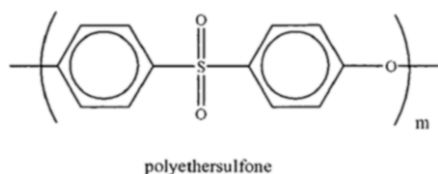
Illing et al. [90] reported transport rates (permeability) and ideal separation factors for several gas pairs through dense polyaniline membranes. PANi membranes were modified by doping into hydrochloric acid (4 M), dedoped by similar treatment with ammonia liquor (1 M) and slightly redoped with HCl solution. The ideal separation factors for all gas pairs tested were found to be independent of the polyaniline membrane thickness whereas the permeability of the single gases showed significant variations. The highest selectivities $\alpha_{(A/B)}$ found were 7.6 for the gas pair H₂/CO₂ (in the case of the dedoped membrane) and 10 for the gas pair H₂/CO₂, 6 for O₂/N₂ and 200 for H₂/N₂ (in the case of the redoped membrane). Hasbullah et al. [91] further developed an emeraldine base (EB) PANi integrally skinned asymmetric hollow fiber membrane for gas separation application. The macromolecular orientation was formed by the synergistic effect due to spin-line stresses, which improved the performance of the PANi hollow fiber for gas separation. The gas flux was significantly decreased while the selectivity was increased with increase in air gap from 2.5 to 50 cm. Membranes with longer air gaps (50 cm) showed promising ideal gas separation properties for H₂/N₂ (105.6), O₂/N₂ (10.2), CO₂/N₂ (13.3), and H₂/CO₂ (7.9) and the H₂ and O₂ permeance of about 5.0 and 0.49×10^{-6} cm³ (STP) cm⁻² s⁻¹ cmHg, respectively.

3.1.1.12 Polysulfone (PSf) and Polyethersulfone (PES)

Polysulfone (PSf) and polyether sulfone (PES) are widely used for preparation of gas separation membranes. Polysulfone describes a family of thermoplastic polymers. These polymers are known for their toughness and stability at high temperatures. They contain the subunit aryl-SO₂-aryl, the defining feature of which is the sulfone group. Polysulfones were introduced in 1965 by Union Carbide. Figure 3.19 shows the repeating unit of polysulfone.

Polyethersulfone (PES) is a similar polymer having the structure of a repeating unit as shown in Fig. 3.20. The greatest characteristic of PES is that it has by far better high-temperature properties than conventional engineering plastics. Specifically, PES remains in satisfactory condition in long-term continuous use without causing any dimensional change or physical deterioration at temperatures as high as 200 °C. Hence, both PSf and PES are high performance engineering polymers. They have good stability, permeability, selectivity, high critical pressure of plasticization, and low cost (Fig. 3.21).

One of the most widely investigated glassy polymer membrane materials for CO₂/CH₄ separation is PSf. Its Polysulfone pure- and mixed-gas permeation properties have been extensively explored for gas separation due to PSf's low price, chemical stability, and mechanical strength. Compared to CA, PSf has lower CO₂

Fig. 3.20 Polysulfone repeating unit**Fig. 3.21** Polyether sulfone

permeability and CO_2/CH_4 selectivity, but higher plasticization pressure [92]. There are three types of PSf membrane that can be used for CO_2/CH_4 separation: dense, asymmetric, and composite. Dense and asymmetric membranes consist of PSf only while composite membranes consist of PSf and other polymers in different layer. Manufacturing processes of these types of membranes are different and versatile. For dense and asymmetric membranes there are three major process: dry, wet, and dry/wet. The most extensively studied polysulfone is PSf formed using bisphenol A. Most other polysulfones are structurally related to this polymer. Two routes for the synthesis of PSf are displayed in Fig. 3.22.

The chemical structure and physical properties of the membrane material influence the permeability and permselectivity. For example, substitution of bulky groups in the side chains appears to have a greater influence on diffusivity than substitution of these groups in the polymer back bone.

To functionalize PSf bromination is an effective route for increasing the reactivity of the polymer, leading to the potential for more structural variation. A number of polysulfones have been modified by reaction with butyl-lithium followed by addition of a pendent group [93, 94].

By substitution of bisphenol A with a different diol, a large number of PSf derivatives have been synthesized. These display a wide range permeabilities and selectivities of carbon dioxide or other gases. The structures of these polymers are displayed in Figs. 3.23 and 3.24.

McHattie et al. [95] reported that replacing phenylene hydrogens of polysulfone with a methyl group had a significant effect on gas transport as well as other properties. It was revealed that the effect of the substituent on chain mobility and chain packing was related to the gas transport properties. Permeability measurements were made for He, H_2 , O_2 , N_2 , CH_4 , and CO_2 at 35°C over a range of pressures up to 20 atm. Sorption experiments were also done for N_2 , CH_4 , and CO_2 under the same conditions. The permeability coefficients of these polymers for all of the gases rank in order: TMPSF (tetramethyl bisphenol A polysulfone) \gg PSF (unsubstituted bisphenol A polysulfone) \gg DMPSF (dimethyl bisphenol A polysulfone) \gg DMPSF (dimethyl bisphenol Z polysulfone).

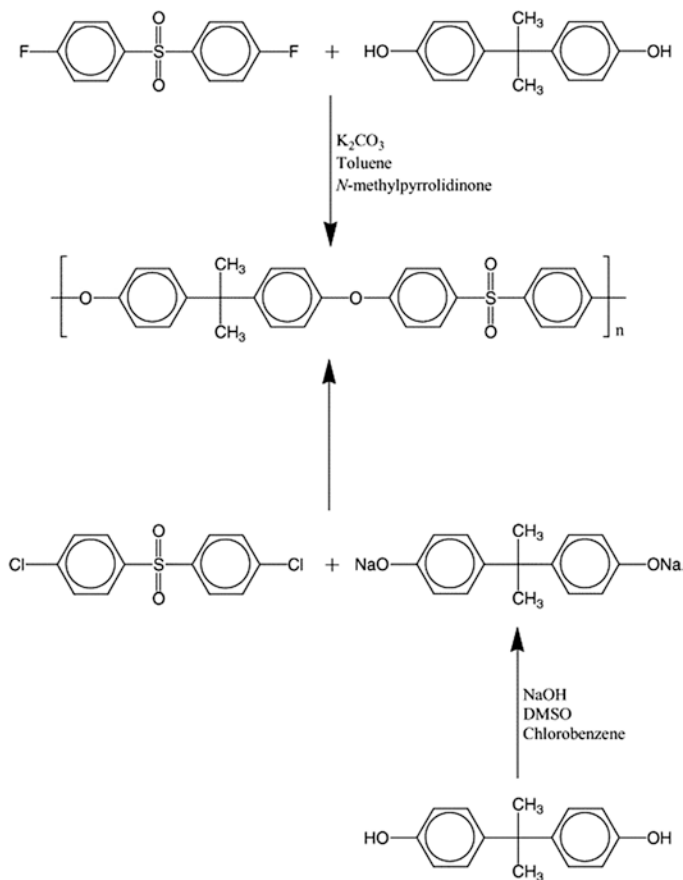


Fig. 3.22 Synthesis of PSf

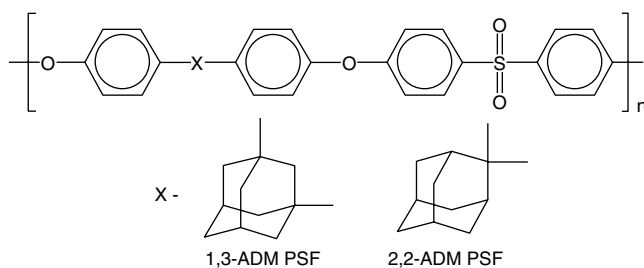


Fig. 3.23 Adamantane-based polysulfone membrane

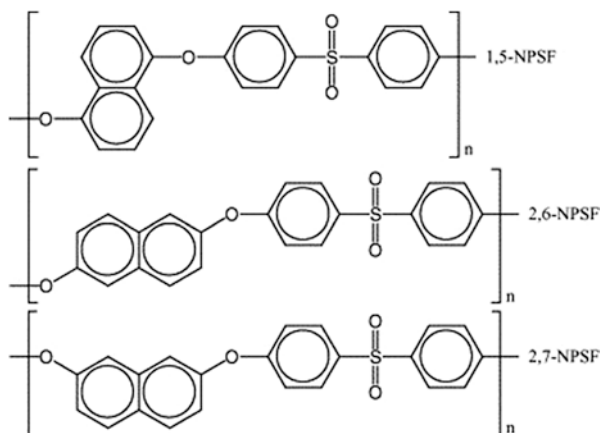


Fig. 3.24 Naphthalene-based polysulfone membrane

Marchese et al. [96] showed that composite membranes with appropriate H₂ separation performance can be obtained by flooding for a short time (1 min) the surface of an asymmetric polysulfone membrane with a solution of 6 % Sylgard 182 in cyclohexane. They achieved the ideal separation factors of 43.24 and 34.04 for H₂/N₂ and H₂/CH₄, respectively.

Wang et al. [97] introduced polysulfone (PSf) hollow fiber membranes with high gas separation performance from *N*-methyl-2-pyrrolidone(NMP)/H₂O and NMP/ethanol solvent systems. Water was used as the external coagulant. The internal coagulants used included water, ethanol, 2-propanol, a mixture of water and ethanol and of water and 2-propanol. The separation performance of the membranes prepared from the NMP/water solvent system was better than that of the membranes spun from a NMP/EtOH system. The O₂ permeance of the membranes prepared was in the range of 20–30 GPU with the O₂/N₂ selectivity of 5–6.5 at 25 °C. The air gap had significant influence on the hollow fiber separation performance. The selectivity decreased with a decrease of coagulation bath temperature.

Ahn et al. [98] used PSf/silica nanoparticle MMMs to study gas permeabilities as well as diffusion and solubility coefficients of hydrogen, helium, oxygen, nitrogen, methane, and carbon dioxide as a function of silica volume fraction via a time-lag method. The effect of silica nanoparticles in PSf membranes on gas permeability was compared with a prediction using the Maxwell model. The O₂ permeability was approximately four times higher and CH₄ permeability was over five times greater than the pure PSf membrane. The performance, comprising permeability versus selectivity of PSf/silica MMMs for O₂/N₂ and CO₂/CH₄, followed a similar slope to that of the trade-off upper bound with increasing silica content.

Weng et al. [99] prepared nanocomposite membranes using MWCNTs with poly(A-co-4-nitrophthalic anhydride-co-1,3-phenylene diamine), and (PBNPI) as the polymer matrix. They extended this approach and demonstrated that at high MWCNTs concentrations, the permeabilities of H₂ and CH₄ improved significantly

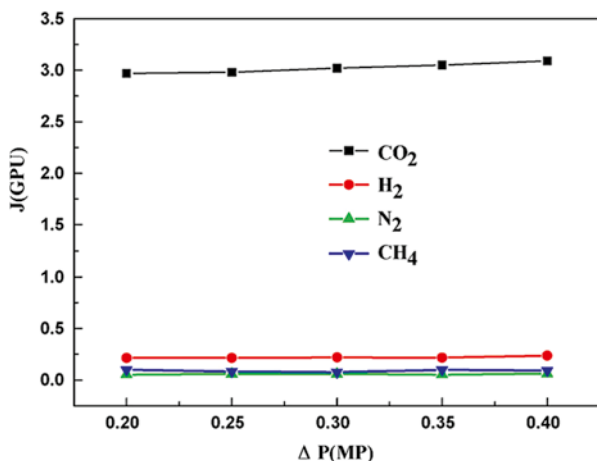


Fig. 3.25 Pressure difference dependence of permeability of various gases for the “water-swollen” dual layer cellulose/PSf hollow fiber

from 4.71 to 14.31 and 0.7 to 1.78 Barrer, respectively. They also cited that the selectivity of H_2/CH_4 reached 8.04.

Dual-layer cellulose/PSf hollow fiber membranes were used for the dehydration of isopropanol and CO_2 separation [100]. The water swollen dual-layer cellulose/PSf hollow fiber membrane showed a much higher gas permeation rate and comparable selectivities of CO_2/H_2 , CO_2/N_2 , and CO_2/CH_4 when compared with a dry membrane. The CO_2 permeance of a dual layer cellulose/PDf hollow fiber membrane was about 3 GPU, which was five times higher than that of a single-layer cellulose hollow fiber membrane. Thus, the performance, especially the permeation rate of a newly developed dual layer cellulose/PSf hollow fiber membrane, was greatly improved by its reduced separation layer (layer of cellulose). Figure 3.25 shows the permeance and permselectivity of CO_2 , H_2 , N_2 , and CH_4 in the “water-swollen” dual layer cellulose/PSf hollow fiber membrane. Table 3.15 also compares the permeance and selectivity between a single-layer cellulose hollow fiber membrane and a dual layer cellulose/PSf hollow fiber membrane. The CO_2 permeance of the dual-layer cellulose/PSf hollow fiber membrane was five times higher than that of the single-layer cellulose hollow fiber membrane. The increase in permeance was mainly because of the large decrease of cellulose layer thickness, which was 10–15 μm compared with the single layer symmetric dense cellulose membrane (almost 160 μm).

Arahman et al. [101] studied the effect of the addition of hydrophilic polymeric surfactant Pluronic F127, polyvinylpyrrolidone (PVP) and Tetricon 1307 on the performance of the PES hollow fiber membrane. The addition of 5 wt% polymeric surfactant on the polymer solution resulted in a membrane with improved length and macrovoid structure. All membranes had a skin layer on the surface and finger like macrovoid structure inside the hollow fiber. The Sponge formation both near

Table 3.15 Comparison of permeance and selectivity between single-layer cellulose hollow fiber membrane and cellulose/PSf dual layer hollow fiber membrane [100]

Membrane	Permeance (GPU)				Separation factor		
	CO ₂	N ₂	CH ₄	H ₂	CO ₂ /N ₂	CO ₂ /CH ₄	CO ₂ /H ₂
Dual-layer	3.05	0.058	0.08	0.178	53	38.7	17.1
Single-layer	0.6	0.013	0.02	0.038	45.4	30	15.8

the inner and outer surfaces of the hollow fiber membrane was another impact caused by the addition of polymeric additives.

Studies on gas permeation properties of isotropic polyethersulfone (PES) dense films have shown that PES exhibits better selectivity for the commercially important gas pairs (CO₂/CH₄, He/CH₄, H₂/N₂, O₂/N₂) compared to bisphenol-A polysulfone and cellulose acetate [102]. Studies have revealed that this polymer has only a moderate permeability. In order to use this polymer to prepare commercially attractive gas separation membranes, fabrication of ultrathin-skinned asymmetric hollow fiber membranes was studied. However, these studies are limited.

Researchers from the University of Twente have studied preparation of PES asymmetric hollow fiber membranes from NMP alone and a NMP/glycerol solvent mixture under different spinning conditions [103–106]. The PES hollow fibers prepared at various spinning conditions exhibited very low gas permeation. The observed CO₂ permeance was less than 12 GPU at 24 °C.

In the late 1980s, PES hollow fiber membranes with good permeance and selectivity were prepared from a spinning solution containing 1:1 molar mixtures of propionic acid and NMP and high polymer concentration (more than 35 wt%) [107]. The oxygen permeance was reported to be 13.1 GPU with a O₂/N₂ selectivity of 5.1 at 50 °C. The skin layer structure of the membrane was examined by Fritzsche et al. [108].

Systematic studies on the preparation and characterization of PES hollow fiber membranes spun from moderate polymer concentrations (25–30 wt%) and solvent systems containing various alcohols as non-solvent additives (NSA) have been done by Wang et al. [109, 110]. These studies show that NSA plays a dominant role in determining membrane structure and gas separation properties. The PES hollow fiber membranes with the best combination of gas permeability and selectivity were prepared using ethanol as an additive. The studies also demonstrated that good NSAs should possess good affinity and diffusivity with the coagulant. Wang et al. [109] fabricated ultrathin silicone-coated PES asymmetric hollow fiber membranes with high permeances and ideal selectivities for gas pairs of He/N₂, CO₂/N₂, and O₂/N₂, from NMP/H₂O solvent systems with a mass ratio of 8.4:1. The observed permeance and selectivity were higher than those of the PES hollow fibers spun from NMP/alcohols and NMP/propionic acid solvent systems reported in the literature. The macrovoids on the membrane wall could be reduced significantly by choosing a suitable internal coagulant with a moderate non-solvent strength, such as a mixture of alcohol and water.

Kim et al. [111] used PESf hollow fiber membrane to recover sulfur hexafluoride (SF_6) from a N_2/SF_6 binary mixture gas. The highest SF_6 purity in recovered gas was 50.4 vol% when the pressure difference, temperature, and stage cut was highest in experimental conditions, but the recovery ratio marked the lowest value.

Jiang et al. [112] fabricated almost defect-free Matrimid/PES dual-layer hollow fibers with an ultrathin outer layer of about 10×10^{-6} m (10 μm). These dual-layer membranes showed impressive CO_2/CH_4 selectivity of around 40 in tests using a gas mixture.

Defect-free high performances for O_2/N_2 separation PES membranes were reported by Ismail et al. [113]. Membranes were prepared by coating the porous PES membrane of a hyperthin-skin layer with silicon rubber. The combined effects of fabrication parameters in a dry/wet phase inversion process and a casting dope rheology, enabled improvement of membrane performance in O_2 and N_2 separation. The thinnest skin layer was 538 ± 95.6 Å.

3.1.1.13 Polybenzimidazole (PBI)

PBI is a heterocyclic polymer and is well known for its many excellent properties such as high thermal stability (over 550 °C), excellent mechanical properties and chemical stability, making it an outstanding candidate over common polymers. Because it has a rigid structure ($T_g = 420$ °C) and stability at high temperatures, PBI could be best suited for $\text{H}_2\text{-CO}_2$ separation applications at high temperature. Its extremely rigid structure, as evident from its high T_g , should show resistance towards CO_2 plasticization and—unlike other polymers—may not lose its separation performance even at elevated temperatures. It has been studied for gas permeability at 200–270 °C and selectivity for H_2/CO_2 of about 20 was noted [114]. PBI-based composite membranes can function at significantly higher temperatures (>350 °C) than commercially available polymeric membranes (<150 °C). The membranes can maintain commercially attractive selectivity between H_2 and CO_2 even at 400 °C [115].

Composite membranes of PBI with proton exchanged AMH-3 (silicate) and swollen AMH-3 were characterized by electron microscopy and X-ray scattering, and tested for hydrogen/carbon dioxide ideal selectivity [116]. Proton-exchanged AMH-3 was prepared under mild conditions by the ion exchange of Sr and Na cations in the original AMH-3 using aqueous solution of DL-histidine. Swollen AMH-3 was fabricated by sequential interaction of dodecylamine following ion exchange in the presence of DL-histidine. Both silicate materials were introduced into a continuous phase of PBI as a selective phase. Mixed matrix nanocomposite membranes, prepared under certain casting conditions with only 3 wt% of swollen AMH-3, resulted in substantial increase of hydrogen/carbon dioxide ideal selectivity at 35 °C, i.e., by a factor of more than 2 compared to pure PBI membranes (40 vs. 15). Similar ideal selectivity was noted using higher loading (14 wt%) proton exchanged AMH-3 particles, suggesting that transport of hydrogen was faster than carbon dioxide in AMH-3 derived silicates. However, the ideal selectivity of MMMs approaches that of pure polymer as the operating temperature increases to 100 °C

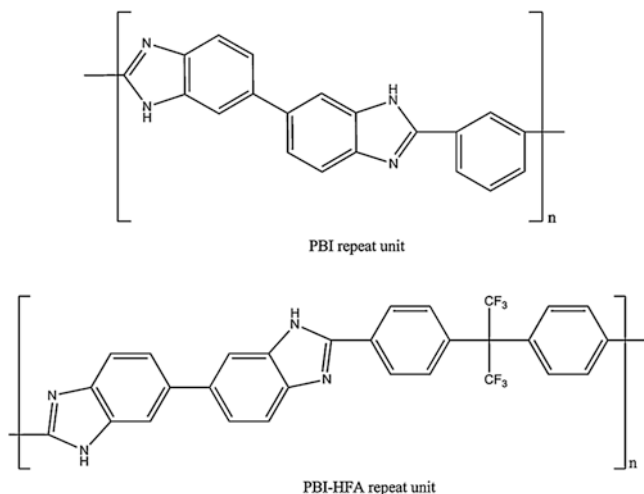


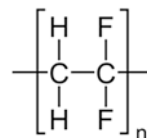
Fig. 3.26 Structure of repeat unit of PBI and PBI-HFA

and 200 °C. Dual layer hollow fiber prepared from PBI and Matrimid® after silicon rubber coating showed a H₂/CO₂ selectivity of about 11 [117].

Kumbharkar et al. [118] demonstrated the development of a polybenzimidazole (PBI)-based asymmetric hollow fiber membrane for H₂/CO₂ separation at high temperatures. High molecular weight PBI was synthesized in-house by a solution polycondensation method using polyphosphoric acid (PPA) as catalyst. Two different PBI, viz., PBI (based on isophthalic acid) and PBI-HFA [based on 4,4'-(hexafluoroisopropylidene)bis(benzoic acid)] were prepared. The chemical structures of the repeat unit of these PBIs are shown in Fig. 3.26. Defect free asymmetric hollow fiber membranes were successfully produced, which eliminated the step of silicon rubber coating, and the membranes were tested in the high temperature range of 100–400 °C. With an increase in temperature these membranes showed a relatively larger increase in H₂ permeance than CO₂ permeance, thereby enhancing the H₂/CO₂ selectivity. This was due to the high rigidity of PBI and smaller kinetic diameter of H₂ than CO₂, which led to relatively higher diffusion of the former than the later with an increase in temperature. The H₂ permeability at 400 °C was increased to 2.6 GPU by around eightfold over its permeability at 100 °C. The CO₂ permeability was increased by only around twofold at 400 °C as compared to its permeability at 100 °C. This significant improvement in permeance of H₂ led to H₂/CO₂ of 27.3, about 3.5 times higher than at 100 °C.

Young et al. [119] patented their invention as cross-linked polybenzimidazole membranes for gas separation. A cross-linked, supported polybenzimidazole membrane for gas separation was prepared by reacting polybenzimidazole (PBI) with sulfone-containing cross-linking agent 3,4-dichloro-tetrahydro-thiophene-1-1 dioxide. The cross-linking reaction product exhibited enhanced gas permeability to H₂, CO₂, N₂, and methane as compared to the unmodified analog, without significant loss of selectivity, at temperatures from about 20 °C to about 400 °C.

Fig. 3.27 Chemical structure of PVDF



3.1.1.14 Polyvinylidene Fluoride (PVDF)

Polyvinylidene fluoride or polyvinylidene difluoride (PVDF) (Fig. 3.27) is a highly non-reactive and pure thermoplastic fluoropolymer produced by the polymerization of vinylidene difluoride.

PVDF has a glass transition temperature (T_g) of about $-35\text{ }^\circ\text{C}$ and is typically 50–60 % crystalline. PVDF exists in several forms: alpha (TG₂GTG'), beta (TTTT), and gamma (TTTGTTTG') phases, depending on the chain conformations. PVDF is widely used as a basic polymer for the formation of hollow fibers. PVDF is a semicrystalline polymer containing a crystalline phase and an amorphous and/or rubbery phase. The crystalline phase provides thermal stability and the amorphous phase flexibility towards membranes. PVDF is stable while it is attacked by most of the corrosive chemicals and organic compounds including acids, alkaline, strong oxidants and halogens. In addition, the hydrophobicity of this polymer provides a potential application in membrane-based gas absorption and oil/water separation.

Porous PVDF hollow-fiber membranes with high porosity were fabricated using the immersion precipitation method [120]. Shen and Lua [121] fabricated three types of inorganic fillers, i.e., SiO₂, MCM-41, and zeolite 4A were incorporated into a PVDF matrix to prepare MMMs. The single gas (He, CO₂, O₂, and N₂) permeabilities of the resulting membranes were measured. The gas permeabilities of the three MMMs exhibited similar behaviors, especially at lower inorganic filler loadings, although the inorganic fillers had different pore structures and particle sizes. The highest permeabilities for CO₂ and O₂ were obtained by the PVDF/zeolite-4A 32 % composite membrane—3.26 and 0.41 Barrer, respectively—and the highest permeabilities for He and N₂ were obtained by the PVDF/MCM-41 32 % composite membrane—10.2 and 0.14 Barrer, respectively. These permeabilities are much higher than those of a pure PVDF membrane. The highest selectivities of 120.7, 33.1, and 4.6 for He/N₂, CO₂/N₂, and O₂/N₂, were obtained by three different membranes—PVDF/SiO₂ 4 %, PVDF/SiO₂ 32 %, and PVDF/SiO₂ 24 %, respectively. These selectivities are also higher than those achieved by the pure PVDF membrane. However, the selectivities of the composite membranes showed differences and were dependent on the inorganic filler content and the specific gas pairs.

3.1.1.15 Poly(1-Trimethylsilyl-1-Propyne) (PTMSP)

Poly(1-trimethylsilyl-1-propyne) (PTMSP) is a glassy polymer. The chemical structure of 1-trimethylsilyl-1-propyne is illustrated in Fig. 3.28. PTMSP has one of the highest permeabilities recorded for glassy polymers for several permeants, including H₂, O₂, and CO₂. Poly[(1-trimethylsilyl)-1-propyne] (PTMSP) showed

Fig. 3.28 Chemical structure of 1-trimethylsilyl-1-propyne monomer

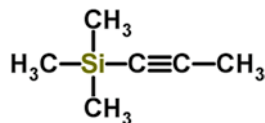


Table 3.16 Fractional free volume (FFV) and permeation properties of “very high free volume” polymers

Polymer	FFV (%)	O ₂ permeability (Barrer)	O ₂ /N ₂ selectivity	
			(–)	References
PTMSP	32–34	6,100	1.8	[126]
PMP	28	2,700	2.0	[127]
PIM-1	22–44	370	4.0	[122]
PIM-7		190	4.5	[122]

the highest permeability to gases— 3.4×10^{-7} for nitrogen and 6.1×10^{-7} for oxygen—expressed by $\text{cm}^3(\text{STP}) \text{cm s}^{-1} \text{cmHg cm}^{-2}$, at room temperature [122].

PTMSP was first reported by Masuda et al. [123]. It is a glassy polymer that resembles rubber in its properties. Beyond PTMSP, other highly permeable polyacetylenes have been reported, including poly(4-methylpentyne) PMP and poly{1-phenyl-2-(*p*-trimethylsilylphenyl)acetylene}. However, PTMSP remained the champion until 2008, when certain indan-containing poly(diphenylacetylene) derivatives were shown to exhibit even higher oxygen permeabilities [6]. The common feature of highly permeable acetylene-based polymers (polyalkynes) is the presence of bulky side groups that inhibit conformational change and force the backbone into a twisted shape. When these rigid, randomly coiled macromolecules are packed in solid state, the free volume distribution includes both small disconnected elements, as in conventional glassy polymers, and larger continuous microvoids. These results were discussed by molecular modeling as well as by positron annihilation lifetime spectroscopy (PALS).

These polyalkynes are known to be “very high free volume” polymers. Table 3.16 shows fractional free volume (FFV) and permeation properties of PTMSP and PIMs (polymers of intrinsic microporosity); the details of PIMs are discussed separately later. The polymer’s high permeability stems from its large free volume, which is the space within the material that is not occupied by the polymer atoms. Due to its outstanding gas permeability and also vapor/gas selectivity PTMSP membranes became the focus by Nagai et al. [124] for gas separation. It was reported by Ichiraku et al. [125] that the permeability of PTMSP to light gases is higher than that of any other nonporous synthetic polymers at ambient temperature. Merkel et al. [126] reported an *n*-C₄H₁₀/CH₄ mixed gas selectivity of 35 in PTMSP membranes, which is the highest value reported for this gas-pair. However, practical utility of PTMSP is limited by a fast *physical aging* (gradual relaxation of non-equilibrium excess free volume in glassy polymers) and also by its solubility in many organic compounds, which results in membrane potential dissolution in process streams.

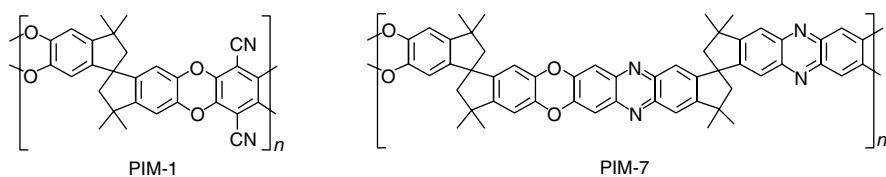


Fig. 3.29 Structure of PIM-1 and PIM-7

PTMSP has been shown much interest in the last 20 years because it has the highest known permeability of any polymer to gases and vapors [127]. This has been attributed to fast diffusion through the microvoids and the large excess free volume within the polymer matrix. However, the high permeability is coupled with low ideal selectivity (the ratio of the single gas permeabilities of two permeants), and numerous attempts have been made to overcome this trade-off. By using additives (organic or inorganic) the performances of the membrane can be changed. Permeability and positron annihilation measurements were carried out on PTMSP membranes, in pristine structure, as well as in the modified polymer after chlorination. It was found that permeability decreases in the chlorinated films; this can be due to the microscopic free volume decrease as probed by positronium [122].

The structure of PIM-1 and PIM-7 is given in Fig. 3.29.

Qui et al. [128] added a small organic filler trimethylsilylglucose (TMSG) to PTMSP and showed reduced permeabilities with increased selectivities, owing to the filling of the larger free volume elements in the polymer by TMSG and blocking the transport of gases through the microvoids. Merkel et al. [126] found that the mixed-gas *n*-butane/methane selectivity decreased with increasing filler concentration while the permeability of the two components increased.

Woo et al. [127] used PTMSP/MFI (silicalite-1) composite membranes for the separation of equimolar mixtures of *i*-butane and *n*-butane. The addition of 50 % MFI particles into PTMSP matrix showed increased permeability and simultaneously improved selectivity in the temperature range 25–200 °C. The best improvement was seen at 150 °C for the composites, giving almost threefold increase in permeability and 56 % higher *n*-butane/*i*-butane selectivity over the pure polymer. The composite membranes were also tested for separations of *n*-hexane/2,2-dimethylbutane and *p*-xylene/*o*-butane isomer separations.

Peter and Peinemann [129] developed a new multilayer composite membrane for gas separation, which consists of PTMSP as the gutter layer deposited on a poly(acrylonitrile) porous support and partially cross-linked Matrmid® 5218. The effect of PTMSP gutter layer on gas transport properties was compared with that of the PDMS sealing layer. It was observed that the gutter layer enhances both gas permeance and selectivities, whereas the sealing layer increases selectivities but with a small gas permeance decrease.

Vopiča et al. [130] developed a novel measuring procedure for mixed gas sorption tests on the *n*-C₄/CH₄ and CO₂/CH₄ mixtures in films of PTMSP. It was observed that the presence of CH₄ does not alter significantly the sorption of CO₂ and of *n*-C₄

in PTMSP, while the mixed gas solubility of CH₄ is lower than the pure gas value at the same CH₄ fugacity. The real CO₂/CH₄ solubility-selectivity of PTMS is similar to the ideal value at low CO₂ fugacity, but it becomes significantly higher, up to 4.5 times, at 25 bar of CO₂ fugacity. A quantitative rule can be drawn from this study, using data of several binary gas mixtures in glassy polymers. The ratio between actual mixed gas and pure ideal solubility selectivity of CO₂ over CH₄ is a single, monotonously increasing function of the ratio between the concentration of the two components, $c(\text{CO}_2)/c(\text{CH}_4)$, and becomes higher than unity as $c(\text{CO}_2) > c(\text{CH}_4)$. In other words, the competition effects depress the less abundant penetrant in the polymer, which is usually CH₄.

3.1.1.16 Polysaccharide

Polysaccharides are long carbohydrate molecules of monosaccharide units joined together by glycosidic bonds. They range in structure from linear to highly branched. Polysaccharides are often quite heterogeneous, containing slight modifications of the repeating unit. Depending on the structure, these macromolecules can have distinct properties from their monosaccharide building blocks. They may be amorphous or even insoluble in water. When all the monosaccharides in a polysaccharide are the same type, the polysaccharide is called a *homopolysaccharide* or *homoglycan*, but when more than one type of monosaccharide is present they are called *heteropolysaccharides* or *heteroglycans*.

Polysaccharides are an important class of biological polymers. Their function in living organisms is usually either structure- or storage-related. Starch (a polymer of glucose) is used as a storage polysaccharide in plants, being found in the form of both amylose and the branched amylopectin. In animals, the structurally similar glucose polymer is the more densely branched glycogen, sometimes called “animal starch.” Glycogen’s properties allow it to be metabolized more quickly, which suits the active lives of moving animals. Cellulose and chitin are examples of structural polysaccharides. Cellulose is used in the cell walls of plants and other organisms, and is said to be the most abundant organic molecule on earth. It has many uses such as a significant role in the paper and textile industries, and is used as a feedstock for the production of rayon (via the viscose process), cellulose acetate, celluloid, and nitrocellulose. Chitin has a similar structure, but has nitrogen-containing side branches, increasing its strength. It is found in arthropod exoskeletons and in the cell walls of some fungi. It also has multiple uses, including surgical threads.

Cellulose

In cellulose membranes the strong intermolecular and intramolecular H-bonding can lead to the dense packing of polymer chains. The dry cellulose membrane appears to be rigid. Within the cellulose matrix, water acts as a plasticizer, and decreases the T_g of the cellulose network. It is reported in the literature that the gas

permeability of the dry cellulose membranes is low, but the “water-swollen” cellulose membrane shows a high permeation rate to CO₂ and excellent separation factors of CO₂ over N₂, CH₄, and H₂ [100].

Chitosan

Chitosan, poly[β(1→4)-2-amino-2-deoxy-D-glucopyranose] is a linear polysaccharide obtained by deacetylation of chitin, poly[β(1→4)-2-acetamido-2-deoxy-D-glucopyranose]. Chitosan has proved to be a good biomedical material based on the properties of biocompatibility and biodegradability, and has also seen increased use as a functional polymer material in industries, especially in membrane technologies [131]. Non-porous chitosan membranes are applied in gas separation and pervaporation. The gas permeation properties of chitosan membranes have been reported in the literature; however, these references are few in number.

Chitosan membranes are dense and rigid in their fully dry state, and they show very low permeability to gases. However, higher permeation rates can be achieved after they are swollen by water. Xiao et al. [131] prepared cross-linked chitosan membranes via interfacial cross-linking in trimesoyl chloride (TMC)/hexane. The membrane with a higher degree of cross-linking showed a higher degree of swelling in water, and the degree of swelling decreased after gas separation and pervaporation. The TMC moieties changed the thermal properties of the chitosan membranes. Pure gas permeation was performed with CO₂ and N₂ at room temperature. The amino groups and transient gaps in the chitosan matrix, which influenced the permeation of CO₂ and N₂, were affected by TMC moieties from the cross-linking reaction. Chitosan-TMC membrane, which formed with a cross-linking time of 40 min (dry thickness was 145 μm) showed the best performance for the separation of CO₂/N₂, with a CO₂ permeability of around 163 Barrer and an ideal separation factor of around 42.

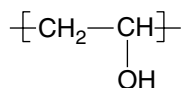
3.1.1.17 Polyvinyl Alcohol (PVA)

PVA is unique among polymers in that it is not built up in polymerization reactions of vinyl alcohol (Fig. 3.30). Instead, PVA is made by dissolving polyvinyl acetate (PVAc), in an alcohol such as methanol and treating it with an alkaline catalyst such as sodium hydroxide. The resulting hydrolysis, or “alcoholysis,” reaction removes the acetate groups from the PVAc molecules without disrupting their long-chain structure. The chemical structure of the resulting vinyl alcohol repeating units is shown in Fig. 3.28.

When the reaction is allowed to proceed to completion, the product is highly soluble in water and insoluble in practically all organic solvents. Incomplete removal of the acetate groups yields resins less soluble in water and more soluble in certain organic liquids.

The applications of PVA-based membranes for catalysts or membranes for gas separation have been discussed by Papanecaa et al. [132]. Polyvinyl alcohol has

Fig. 3.30 Repeat unit of PVA



excellent film-forming, emulsifying and adhesive properties. It is also resistant to oil, grease and solvents. Zou and Ho [133] synthesized cross-linked PVA (containing amines) and reported that it was a good CO₂-selective membrane. The PVA membrane showed good selectivities for CO₂/N₂ and CO₂/CO separation. The membrane also showed good CO₂ permeabilities and CO₂/H₂ selectivities up to 170 °C. At 120 °C, the CO₂ permeability and CO₂/H₂ selectivity reached 8,200 Barrer (1 Barrer = 10⁻¹⁰ cm³ (STP) cm cm⁻² s⁻¹ cmHg) and 450, respectively.

Matsuyama et al. [134] studied PEI/PVA blend membranes for the facilitated transport of CO₂. The CO₂ permeance decreased with the increase in the CO₂ partial pressure, whereas the N₂ permeance was nearly constant. This suggested that only CO₂ was transported by the facilitated transport mechanism and also that PEI functioned efficiently as the carrier of CO₂.

Water-swollen hydrogel (WSH) membranes for gas separation were prepared by dip-coating asymmetric porous PEI supports with PVA-GA (glutaraldehyde) solution, followed by the cross-linking of the coated layer by a solution method, by Park and Lee [135]. It was observed that the behavior of gas permeation through a WSH membrane was parallel to the swelling behavior of the PVA/GA film in water. The permeance of carbon dioxide through the WSH membranes was 10⁻⁵ (cm³ cm⁻² s⁻¹ cmHg) and a CO₂/N₂ separation factor was about 80 at room temperature.

3.1.2 Copolymers and Polymer Blends

A heteropolymer, also called a copolymer, is a polymer formed when two (or more) types of monomer are linked in the same polymer chain, as opposed to a homopolymer where only one monomer is used. If exactly three monomers are used, it is called a terpolymer. Copolymerization refers to methods used to chemically synthesize a copolymer.

Since a copolymer consists of at least two types of constituent units (called also structural units), copolymers can be classified based on how these units are arranged along the chain. These include (also, see Fig. 3.29):

- Alternating copolymers with regular alternating A and B units (see 2 in Fig. 3.29).
- Periodic copolymers with A and B units arranged in a repeating sequence (e.g., (A-B-A-B-B-A-A-A-A-B-B-B)_n).
- Statistical copolymers, which are copolymers where the sequence of monomer residues follows a statistical rule. If the probability of finding a given type monomer residue at a particular point in the chain is equal to the mole fraction of that monomer residue in the chain, then the polymer may be referred to as a truly random copolymer (see 3 in Fig. 3.29).

Fig. 3.31 Different types of copolymers



- Block copolymers comprise two or more homopolymer subunits linked by covalent bonds (see 4 in Fig. 3.29). The union of the homopolymer subunits may require an intermediate non-repeating subunit, known as a junction block. Block copolymers with two or three distinct blocks are called diblock copolymers and triblock copolymers, respectively [136].
- Graft copolymers are a special type of branched copolymer in which the side chains are structurally distinct from the main chain. Number 5 in Fig. 3.31 depicts a special case where the main chain and side chains are composed of distinct homopolymers. However, the individual chains of a graft copolymer may be homopolymers or copolymers. Note that different copolymer sequencing is sufficient to define a structural difference, and thus, an A-B diblock copolymer with A-B alternating copolymer side chains is properly called a graft copolymer.

Copolymers may also be described in terms of the existence or arrangement of branches in the polymer structure. Linear copolymers consist of a single main chain whereas branched copolymers consist of a single main chain with one or more polymeric side chains. Copolymers offer the potential to fine tune permeabilities. A copolymer will tend to have permeabilities which are intermediate compared with the homopolymers which make it up.

Polymer blends are an inexpensive route to the modification of polymer properties. Examples of the properties that may be altered upon blending are impact resistance, fatigue behavior, heat distortion, and improved processability [137]. In some blend systems, the effective property modification is dependent upon the miscibility or compatibility (i.e., the ability to form a homogeneous mixture) of the two homopolymers. Compatibility of polymers in a blend has been defined in a number of ways. The simplest definition of polymer compatibility in a blend is optical clarity upon preparation. Another definition of blend compatibility involves the glass transition temperature of the homogeneous polymers and the blend. Compatible blends must exhibit a single glass transition temperature (T_g) between the T_g 's of the homopolymers, while incompatible blends will have two T_g 's that correspond to those of the homopolymers [138]. A third definition of compatibility involves the use of infrared spectroscopy. Coleman and Painter [139] have proposed that if two polymers are compatible, then the IR spectra obtained from the blend should include band shifts and broadening when compared to the scaled addition of the infrared spectra of the homopolymers.

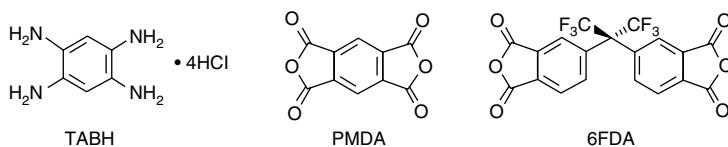


Fig. 3.32 Structure of monomers

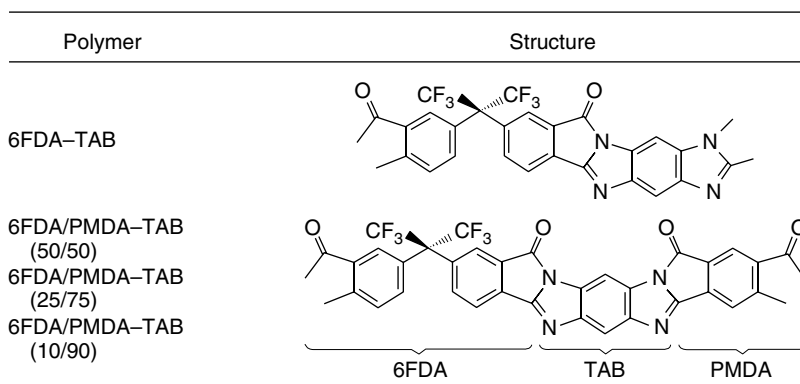


Fig. 3.33 Structures and compositions of 6FDA-TAB and the 6FDA/PMDA-TAB copolymers

The CO_2/N_2 gas separation properties of a large series of poly(ethylene oxide) (PEO) segmented copolymers with polyurethanes, polyamides and polyimides was studied by Yoshino et al. [140]. It was observed that the CO_2/N_2 separation properties depend on the hard-segment polymer. The contents of the hard and soft segments in the soft and hard domains, W_{HS} and W_{SH} respectively, were estimated from glass-transition temperatures with the FOX equation. The phase separation of the PEO domain depended on the kind of hard-segment polymer, that is, W_{SH} was in the order $\text{PU} > \text{PA} \gg \text{PI}$ for PEO block length (n) of 45–52.

Zimmermann and Koros synthesized polypyrrolone copolymers comprising various compositions of 6FDA, PMDA and TAB for O_2/N_2 gas separation. The structure of monomers used to synthesize the polymers is shown in Fig. 3.32 [141].

Structures and compositions of 6FDA-TAB and the 6FDA/PMDA-TAB copolymers used in the gas transport study are shown in Fig. 3.33.

It was reported by Zeeman and Koros [148], on varying the fractions of 6FDA (bulky group) and PMDA (flat, packable group), that a *molecular jack* was created which altered the average interchain spacing and gas transport properties of these materials. All of the materials showed O_2/N_2 gas separation properties lying on or above the upper bound trade-off limit, indicating they possess superior transport properties to most polymers.

In another study Zimmerman and Koros [142] reported activation energies for permeation and diffusion as well as heat of sorption for He, CO_2 , O_2 , N_2 , and CH_4 in the 6FDA/PMDA-TAB copolymer series. These gas transport properties were

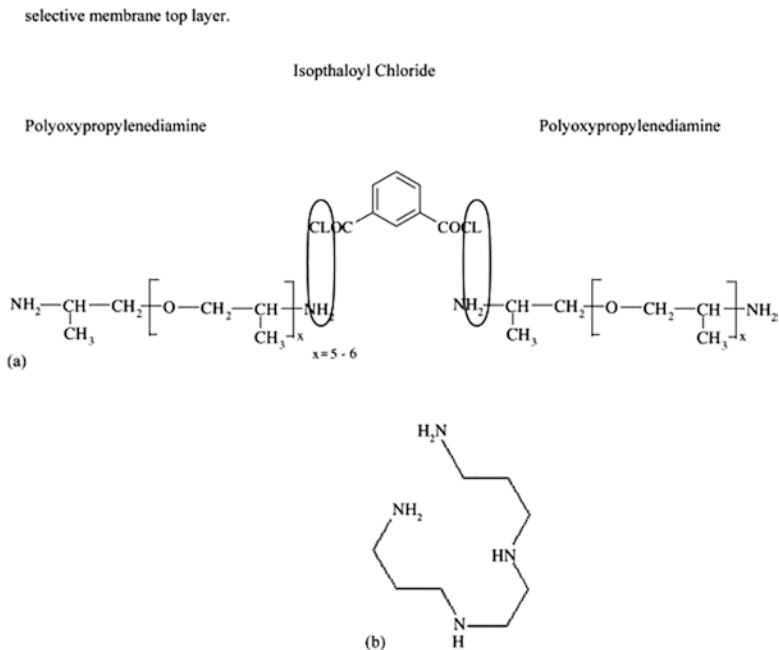


Fig. 3.34 (a) Interfacial polymerization reaction scheme for forming the polyamide (IPC) selective membrane top layer. (b) Cross-linking agent 1,5,8,12-tetraazadodecane (N_4) [143]

interpreted in terms of their polypyrrolone structures, which possess different average interchain spacing. It was also reported that the activation energy for diffusion was dominant in influencing the activation energy for permeation.

Patil et al. [143] studied the permeation of CO_2 for two types of composite polymeric hollow fiber membranes. The membrane consists of a polyamide copolymer (IPC) layer or a polyvinyl alcohol (PVA) layer on top of a polyethersulfone (PES) support membrane. The reaction scheme of the interfacial polymerization process is shown in Fig. 3.34.

As well, two polyamide top layers were fabricated with a different degree of cross-linking. The crosslinked layers were obtained by the addition of 1,5,8,12-tetraazadodecane (N_4) as the cross-linking agent. It was noted that permeance of CO_2 for both membranes had a maximum as a function of feed pressure at about 8 MPa. Both membranes showed an increase in the carbon dioxide permeance as a function of the exposure time to supercritical carbon dioxide. The stability of the IPC membrane was improved by cross-linking of the selective layer.

Wang et al. [144] developed PEI-PVA blend membranes for the removal of CO_2 from natural gas. The blend of a PEI-PVA composite membrane was used as a separation layer and PS (polysulfone) UF membrane as substrate. The permselectivity of the membrane was measured with CO_2/CH_4 mixed gases. The permeances of both CO_2 and CH_4 decreased with the increase of temperature, and the permeances decreased more quickly under low pressure than those under high pressure.

Semsarzadeh and Ghalei [145] fabricated blend membranes of polyurethane (PU) and polyvinyl acetate (PVAc) in the presence of various polyethylene oxide-polyethylene oxide triblock polymer (Pluronic) contents by solution casting technique. The blends with 5 wt% PVAc showed higher CO₂ permeability (~73 Barrer) compared to the PU membrane. A comparative increase in permselectivity of pair gases was shown with an increase in CO₂/N₂ and O₂/N₂ (in the membrane 15 wt% PVAc) by up to 417 % and 200 %, respectively. CO₂/CH₄ (in the membrane with 5 wt% PVAc) increased by up to 220 %.

The addition of polyethylene glycol (PEG) to the poly(amide-*b*-ethylene oxide) copolymer (Pebax) demonstrated that CO₂ permeability and selectivity over H₂ can be simultaneously increased [146]. The enhancement was attributed to the high CO₂ solubility in PEG, but a free volume increase was also taken into consideration because a decrease in density and glass transition temperature (T_g) was observed. Later, the increase in total free volume was demonstrated for the Pebax/PEG blend [147].

Yave et al. developed a nanostructured and CO₂-philic polymer membrane for CO₂ separation [148]. The authors demonstrated that poly(ethylene oxide)-poly(butylene-terephthalate) (PEO-PBT) is a material with high CO₂ separation. The membranes presented outstanding performance for CO₂ separation, and the measured CO₂ flux was extremely high (>2 m³ m⁻² h⁻¹ bar⁻¹) with selectivity over H₂ and N₂ of 10 and 40, respectively, making them attractive for CO₂ capture.

Madaeni et al. [149] fabricated pyromellitic dianhydride-co-4,4'-oxy dianiline (PMDA/ODA) polyimide membranes using polyamic acid (PAA) as precursor materials. On adding PVDF as an additive in the preparation of PMDA/ODA polyimide membrane, the gas separation performance of the membrane was improved for pure N₂ and C₂H₄ gases. The ideal selectivity of 100 % was achieved for ethylene by PMDA/ODA polyimide membranes with 1 wt% PVDF at the feed pressure of 1 bar.

Based on PES and polyimide Matrimid 5218 (PI) blends, hollow fibers were spun for CO₂/N₂ separation by Kapantaidakis et al. [150]. The developed membranes exhibited a typical asymmetric structure and remained miscible for each blend composition. PDMS coated hollow fibers had CO₂ permeances varying from 30 to 60 GPU and CO₂/N₂ selectivities varying from 30 to 40. Hollow fibers, rich in PES, showed a pronounced plasticization behavior but the reduction of CO₂/N₂ selectivity was totally reversible after a short period of time. It was also demonstrated that the air-gap distance in the dry/wet spinning processes affected both membrane structure and permeation properties [151]. In another study for gas separation using PES/PI blend hollow fibers, Kapantaidakis et al. [152] reported that by adjusting major process parameters, such as polymer concentration, air-gap distance, bore liquid composition, and take-up velocity, highly permeable, selective, and ultrathin fibers could be produced. Suitable selection of the spinning conditions resulted in gas separation hollow fibers with a thin skin layer (0.1 μm), macrovoid-free structure, high permeation rate (CO₂: 40–60 GPU) and selectivity coefficient (CO₂/N₂: 40).

Koros and Wood [153] studied the effect of elevated temperatures on three asymmetric hollow fiber membranes (polyaramide, polyimide, and composite polyimide on a polyimide/polyetherimide blend support). Polyaramide membranes were shown to exhibit good stability at elevated temperatures and good separation properties after silicon rubber post-treatment. The hydrogen permeance of 300 GPU at 175 °C is acceptable for industrial application. The polyimide-containing membranes had superior room-temperature properties; however, the thin skin aged at elevated temperatures. This aging effect decreased the permeance of the membranes approximately 40 % at 175 °C and slightly increased the permselectivity; however, the effects of aging leveled out over 200–250 h at 175 °C and the membrane properties became constant. At this level, the polyimide membranes exhibited around 400 GPU of hydrogen permeance with 660 selectivity to *n*-butane.

Seo et al. [154] demonstrated a novel concept of a (universal) “organic molecular sieve” and experimentally proved its possibility by showing that organic polymer molecules at the interface between the permeable phase and the impermeable phase play the role of molecular sieves. The authors prepared polymeric composite film by using a semicrystalline polymer (Nylon 6) as a barrier component dispersed in an amorphous matrix polymer (poly(2,6-dimethyl-1,4-phenylene oxide), PPO) and a compatibilizer (poly(styrene-co-maleic anhydride), PSMA). A mixture of Ny6, PPO, and PSMA was extruded at a process temperature of 240 °C in a Brabender twin screw extruder. A film with an even thickness of 100 μm having 3 % error limits was used for the gas separation. They reported that there was a significantly improved selectivity in gas separation, going over the so called “upper-boundary.” The performance of the composite film is shown in Fig. 3.35. This study showed that compatibilizer works like a molecular sieve to separate one gas molecule from

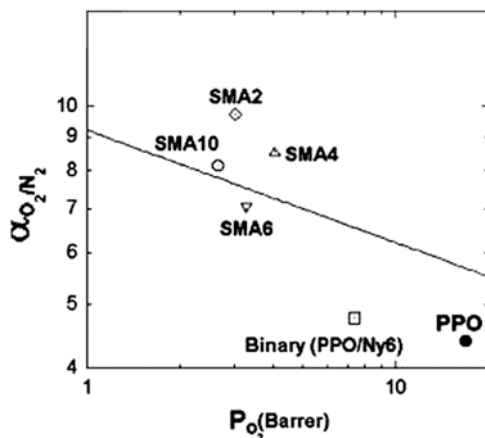


Fig. 3.35 The relationship between the oxygen permeability and the O_2/N_2 selectivity for PPO and Ny6 blended films. (filled circle) PPO, (open square) a binary blend, (open diamond) a ternary blend with 2 wt% PSMA, (triangle) a ternary blend with 4 wt% PSMA, (inverse triangle) a ternary blend with 6 wt% PSMA, and (open circle) a ternary blend with 10 wt% PSMA. The solid line is an empirical upper-bound relation. Since the size of error bars was smaller than the size of symbols, the error bars were deleted

the other. Hence, this strategy can be easily used to make extraordinary polymeric gas-separation membranes for all different gas pairs. The film can be used for oxygen gas enrichment or CO₂ gas removal as well as other gas separation. They also claimed that this strategy would be applicable to various separation processes for many chemicals.

3.1.3 Other Polymers

A range of other polymers showed potential for gas separation; however, none has been commercialized. Among others, polybenzoxazoles (PBOs) are a class of polymers with good gas permeation and selectivity properties that show promise [155].

3.1.3.1 Polymers of Intrinsic Microporosity (PIMS)

The idea of PIMs started from the work of McKeown in 1998 [156]. Intrinsic microporosity in polymers is defined as “a continuous network of interconnected intermolecular voids, which forms as a direct consequence of the shape and rigidity of the component macromolecules” [157, 158]. Intrinsic microporosity can arise simply from a polymer whose molecular structure is highly rigid and contorted so that space-efficient packing in the solid state is prohibited (Fig. 3.36). The lack of rotational freedom along the polymer backbone ensures that the macromolecules cannot rearrange their conformation to collapse the open structure of the material.

These polymers (PIMs) can exhibit analogous behavior to that of conventional microporous materials, but, in addition, may be processed into convenient forms for use as membranes. These membranes have excellent performance for gas separation and evaporation [159]. In general, due to maximum attractive interactions between the constituent macromolecules, the pack space in the polymer minimizes the void space. Most polymers have sufficient conformational flexibility to allow them to rearrange their shape so as to maximize intermolecular cohesive interactions and pack space efficiently. Due to fused ring structures, PIMS do not possess rotational freedom along the polymer backbone, which ensures that the macromolecular components cannot rearrange their conformation. Thus, during synthesis, their contorted shape does not change [160].

PIMs are prepared by a polymerization reaction based on a double-aromatic nucleophilic substitution mechanism to form the dibenzodioxin linkage. This reaction is one of the few capable of forming two covalent bonds simultaneously, with sufficient efficiency to provide a linking group composed of fused rings and, thus, able to form ladder polymers of high average molecular mass [160]. Generally, aromatic nucleophilic substitutions are known to proceed readily, especially if the halide-containing monomer is activated by an electron-withdrawing substituent (e.g., -CN, F) [161]. This reaction was used previously by Makhseed et al. [168] to prepare phthalocyanine oligomers and extended to planar molecules and oligomers for discotic liquid crystals [162]. Du et al. developed,

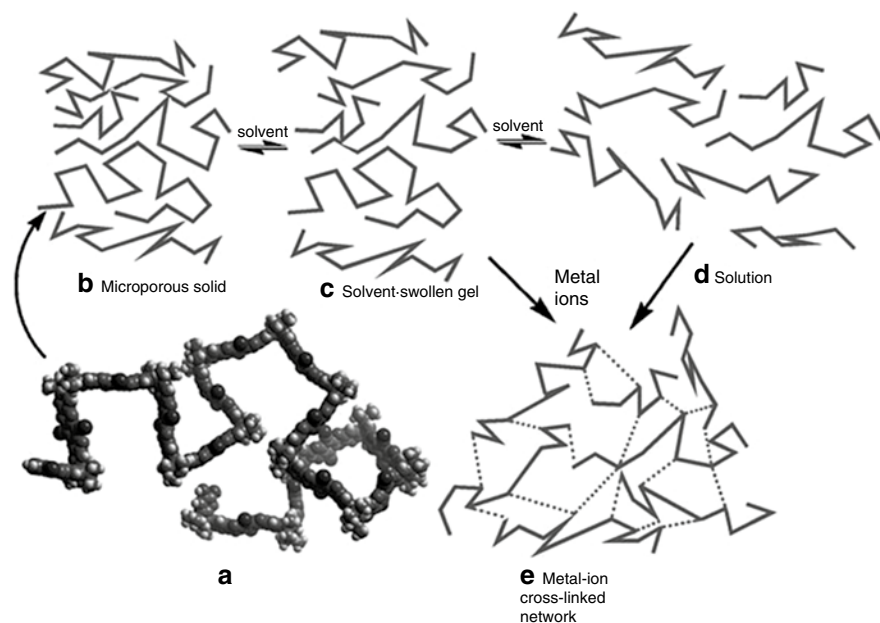


Fig. 3.36 PIMS representation. (a) Model of a molecular fragment of PIM-1 showing its randomly contorted structure together with cartoon representation of the various states that can be obtained from a PIM including: (b) a microporous solid due to the inability of the polymer molecules to pack efficiently; (c) a solvent-swollen gel, (d) solution and (e) a metal ion cross linked microporous net work [159]

what is called a “high temperature method” [163], in which a high-speed stirring of the mixture in dimethyl acetamide at 155 °C is performed for only 8 min with the addition of toluene to enable the continuation of stirring.

Du et al. introduced azide-based cross-linking of polymers of intrinsic microporosity (PIM) membranes for condensable gas separation [164]. Membranes were prepared by a nitrene reaction from a representative PIM in the presence of two different diazide cross-linkers. These cross-linked polymeric membranes showed excellent gas separation performance and can be used for O₂/N₂ and CO₂/N₂ gas pairs and for the separation of condensable gases such as CO₂/CH₄ and propylene/propane. These membranes were different from typical gas separation membranes derived from glassy polymers as the cross-linked PIMs showed no obvious CO₂ plasticization up to 20 atm pressures of pure CO₂ and CO₂/CH₄ mixtures. Du et al. also discussed these membranes for CO₂ [165].

Incorporation of tetrazoles (TZPIM) into the microporous polymeric framework of PIM, has been shown to create a very high permeability for CO₂ and excellent CO₂/N₂ mixed gas separation, even under plasticization conditions (Fig. 3.37).

The presence of the tetrazole groups leads to favorable sorption and selective pore blocking by presorbed CO₂ molecules, thus limiting access by other light gas molecules such as nitrogen. The introduction of tetrazoles into PIM is the first

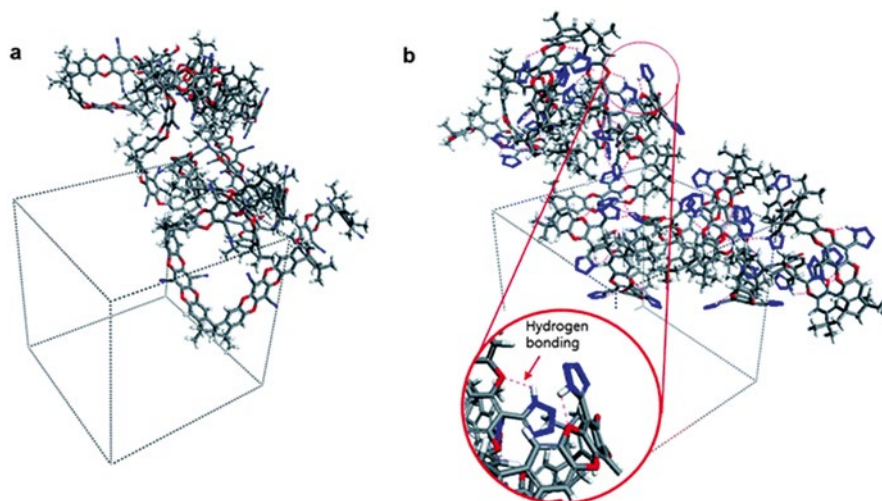


Fig. 3.37 Incorporation of tetrazoles in PIM. (a) Three-dimensional view of PIM-1 in an amorphous periodic cell (the number of repeat units in PIM-1 is 20), and (b) a three-dimensional view of TZPIM-3 containing tetrazole in an amorphous periodic cell (the number of repeat units in TZPIM is 20; 100 % full conversion from nitrile groups to tetrazole groups; the blue dotted lines indicate possible hydrogen bonding modes) [161]

example of a {2+3} cycloaddition of a polymer containing aromatic nitrile groups with an azide. This strategy of incorporating nitrogen heterocycles into PIMs provides new directions in the design of other polymeric membrane materials for important CO₂ separation process. PIMs also undergo some degree of physical aging and plasticization.

3.1.3.2 Cross-linking of Polymers and Other Techniques for Modification

Cross-linking offers the potential to improve the mechanical and thermal properties of membranes. Koros and Mahajan have suggested that cross-linking can be used to increase membrane stability in the presence of aggressive feed gases and to simultaneously reduce plasticization of the membrane [166].

A plasma polymerization process is a technique that allows for obtaining highly cross-linked polymers from nonfunctional monomers that are not utilized in conventional polymer synthesis. Plasma surface modification can improve biocompatibility and biofunctionality. When membrane surfaces are brought into contact with gas plasmas by energetic species such as ions, electrons, radicals, metastables, and photons in the short wave ultraviolet range, their energy is transferred from the plasma to the solid. As a result, the surface of the membrane is etched forming many reactive sites (mostly radicals) on the surface. Polymerization takes place at the reactive sites of the membrane when an organic vapor or a monomer is introduced into the plasma reactor.

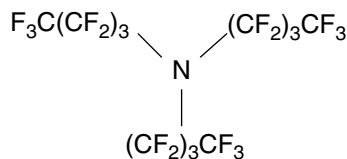
Plasma polymers were prepared from three different organosilicon: diethoxydimethyl silane, hexamethyldisiloxane (HMDSO), and octamethyltrisiloxane (OMTSO). Films were deposited upon silicon wafers and on different porous substrates. Silicon-containing polymers are well known as polymers excelling in gas permeation. When they are synthesized by the plasma process, they also exhibit high selectivities because of high cross-linking compared with conventional polymers. Roualdes et al. studied the gas (N_2 , H_2 , O_2 , CO_2 , and CH_4) separation properties of organosilicon plasma polymerized membranes [167]. Surfaces of polyimide and PSf membranes were modified by Won et al. [168] by using an ion-beam carbonization technique. To control the structure of membrane skin and to improve gas-transport properties, the irradiation conditions, such as the dosage and the source of ion beam, have been varied. The ideal separation factor of CO_2 over N_2 through the surface modified PI and PSf membranes increased threefold compared with those of the untreated, pristine membranes, whereas the permeability decreased by almost two orders of magnitude. This could be due to the fact the structure of the membrane skin had changed to a barrier layer.

Maya et al. [169] noted that thermally treated copolyimides consisting of flexible PEO segments and rigid polyimide segments are very attractive as CO_2/N_2 separation membranes. After thermal treatment of these membranes under an inert atmosphere, a large improvement in CO_2 permeability was observed, yielding a more productive membrane.

By using a coextrusion and dry jet wet spinning phase-inversion technique with the aid of heat treatment at $75^\circ C$, Li et al. [170] fabricated dual-layer PES hollow fiber membranes with an ultrathin dense-selective layer of 407 \AA . The dual-layer hollow fibers had an O_2 permeance of 10.8 GPU and O_2/N_2 selectivity of 6.0 at $25^\circ C$. It was observed that heat treatment at $75^\circ C$ improved the gas permeation and ideal selectivity, whereas heat treatment at $150^\circ C$ resulted in a significant reduction in both permeation and selectivity due to enhanced substructure resistance. SEM pictures confirmed that higher heat-treatment temperature can significantly reduce pore sizes and the amount of pores in substructure immediately underneath the dense-selective layer.

Castro-Domínguez et al. [171] reported the implementation of perfluorotributylamine (PFTBA) (Fig. 3.38) imbued in porous alumina tubes as a supported liquid membrane to carry out the separation of O_2 and N_2 at $40^\circ C$ and 1 atm. The membrane had an average O_2/N_2 separation factor of around 60 with an O_2 permeance of $8 \times 10^{-10} \text{ mol m}^{-2} \text{ s}^{-1} \text{ Pa}^{-1}$, an average H_2/N_2 separation factor of 100, and a H_2 permeance of $1 \times 10^{-9} \text{ mol m}^{-2} \text{ s}^{-1} \text{ Pa}^{-1}$. The O_2/N_2 selectivity was higher as the temperature increased, but the lifetime of the membrane was reduced.

Fig. 3.38 Chemical structure of PFTBA



3.2 Inorganic Membranes

In most cases, gas separation membranes are based on amorphous glassy polymers (polysulfones, polycarbonates, polyimide). Although glassy polymeric membranes exhibit a good combination of gas permeability and selectivity properties, their performance in the separation of gaseous mixtures may decline with time due to aging or plasticization at specific feed conditions. Moreover, the maximum operating conditions of polymeric membranes is about 100 °C, whereas the temperatures encountered in numerous industrial processes are considerably higher. Thus, researchers started to develop other routes or materials for the separation of gases at high temperatures, e.g., inorganic material. Inorganic membranes can be classified in three categories; (1) zeolites, (2) sol–gel based microporous membranes, and (3) Pd-based and Perovskite-like dense membranes. Table 3.17 shows the inorganic materials for gas separation.

There are basically two types of inorganic membranes: (1) dense (nonporous) and (2) porous. Examples of commercial porous inorganic membranes are ceramic membranes, such as alumina, silica, titanium, and glass and porous metals, such as stainless steel and silver. These membranes are characterized by high permeabilities and low selectivities. Dense inorganic membranes are very specific in their separation behaviors; for example, Pd–metal based membranes are hydrogen specific and metal oxide membranes are oxygen specific. Dense membranes prepared from palladium or perovskites only allow certain gases (such as H₂ or O₂) to permeate via mechanisms such as solution-diffusion or solid-state ionic conduction. Such nonporous systems exhibit extremely high selectivities but have limited permeabilities, although substantial research efforts during the last decade have produced fluxes within reach of targets. These membranes further require high capital investment due to the use of precious metals and/or extreme synthesis and operating conditions; the membranes may be mechanically unstable. In contrast, microporous silica membranes have proven to be promising for molecular sieving applications. Precise pore size control (0.3–0.4 nm in diameter) to allow for separation on the basis of size by molecular filtration or “sieving” has, however, not yet been achieved for amorphous inorganic membranes and they are also chemically, mechanically and thermally less robust than zeolite membranes [172].

Table 3.17 Inorganic materials for gas separation membranes

Zeolites/zeolitic materials
Carbon molecular sieves
Nanoporous carbon
Carbon nanotubes
Ultramicroporous amorphous silica or glass
Palladium alloys (metals)
Mixed conducting perovskites
Graphene

Several natural gas resources around the world contain large amounts of CO₂. Economic recovery of the CH₄ from streams having CO₂ as a major component presents numerous technical challenges. One potential separation option is based on inorganic membranes. With the recent advent of commercial ceramic membranes, inorganic membranes are receiving much attention as unique separators and reactors due to their excellent thermal and chemical stabilities. Microporous inorganic membranes ($r_{\text{pore}} < 1$ nm) have great potential for gas separation. Compared to polymeric membranes, microporous inorganic membranes with molecular sieve-like properties have relatively high gas permeances and stability in higher temperatures and corrosive atmospheres. Moreover, inorganic membranes can be used in membrane reactors for conversion enhancement such as in dehydrogenation reactions. State-of-the-art microporous silica membranes consist of a microporous top layer on top of a supported mesoporous ($1 \text{ nm} < r_{\text{pore}} < 25 \text{ nm}$) γ -Al₂O₃ membrane. The support of the γ -Al₂O₃ layer provides mechanical strength to the selective silica top layer.

3.2.1 Ceramic Membranes

In general, a ceramic membrane can be a permselective barrier or a fine sieve. Ceramic membranes are usually composite, consisting of several layers of one or more different ceramic materials. They generally have a macroporous support, one or two mesoporous intermediate layers and a microporous (or a dense) top layer. The bottom layer provides mechanical support, while the middle layers bridge the pore size differences between the support layer and the top layer where the actual separation takes place. Membrane properties such as permeation and selectivity depend on the microstructures of the membrane/support composite such as pore size and distribution, porosity, and affinity between permeating species and the pore walls. Separation of a gas mixture can take place based on differences in molecular mass, size or shape, or on differences in the affinity of the gas molecules to the membrane material.

Numerous theories for describing transport in microporous media have been presented in the literature [173, 174]. These theories become increasingly complex when the microporous medium is less uniform and when more mobile species are present. For the assessment of membrane quality, a simple phenomenological approach is sufficient [175].

For single gas permeation through amorphous microporous silica membranes, at sufficiently high temperatures and low pressures, transport is activated and permeance is independent of pressure [176–178]. Hence, permeance is described by:

$$P = N / \Delta p = (H_0 D_0) \exp\left\{\frac{(Q - E_D)}{RT}\right\} \quad (3.1)$$

where N is the molar flux, H_0 and D_0 are pre-exponential factors related to the Henry and diffusion coefficients, respectively, and R and T have their usual meaning.

The overall thermally activated nature of transport arises from the simultaneous occurrence of diffusion (E_D) and sorption (Q).

Pohl and Heffelfinger [179] simulated pressure-driven gas permeation of gases in a porous silica model using a dual control volume grand canonical molecular dynamics (DCV-GCMD) technique. The molecular sieving nature of microporous zeolites and amorphous silica made by sol-gel methods were discussed and compared. One mesoporous and one microporous membrane model were tested with Lennard-Jones gases corresponding to He, H₂, Ar, and CH₄. The mesoporous membrane model clearly followed a Knudsen diffusion mechanism, while the microporous model, having a hard-sphere cutoff pore diameter of ~ 3.4 Å, demonstrated molecular sieving of CH₄ ($\sigma = 3.8$ Å) but anomalous behavior for Ar ($\sigma = 3.4$ Å).

Perovskite oxide-type ceramic membranes are used for gas separation etc. The general formula of the perovskite is ABO₃ and the properties are determined by cations occupying its A-site and B-site lattice. The A-site cations are mainly composed of alkaline earth, as well as alkaline and lanthanide ions, while B-site cations are mainly composed of transitional metal ions. These perovskite-type ceramic membranes can be used for oxygen production or gas separation. Oxygen transport through such membranes can occur only via hopping oxygen ions to neighboring vacant sites in the crystal lattice of mixed conductors, whereas the transport of any other species is excluded. Owing to this, gas-tight mixed-conductive membranes possess an infinite permselectivity. Several reviews on mixed conducting membranes (perovskite) for oxygen separation are available, which provide the main understanding on the material composition, structure, preparation as well as the transport mechanism of oxygen permeable membranes [180]. While many perovskite oxide materials have been explored over the past two decades, there are hardly any materials with sufficient practical economic value and performance for large scale applications; the search for new materials is justified and should continue.

Oxygen permeability of a number of dense oxide membranes with perovskite-type structure was studied by Kharton et al. [181]. The cubic perovskite solid membranes derived from SrCoO_{3- δ} by partial substitution of cobalt with higher valency transition metal cations (Fe, Cr, Ti) exhibited higher permeation fluxes in comparison with other mixed-conducting ceramics. The highest permeation fluxes were observed for the SrCo_{1-x}Ti_xO_{3- δ} ($x = 0.05-0.20$) and SrCo_{0.90-x}Fe_{0.10}Cr_xO_{3- δ} ($x = 0.01-0.20$) ceramic membranes.

3.2.2 Silica Glass Membranes

Silica (SiO₂) shows unique properties related to the ability of its elemental bricks, i.e., SiO₄ tetrahedra, to be connected together, forming a large numbers of different amorphous or crystallized solids that can be microporous, mesoporous or macroporous. Silica is also known as a chemical compound that contains an oxide of silicon with the chemical formula SiO₂. Silica is most commonly found in nature as sand or

quartz. Glass is a hard, brittle substance, typically transparent or translucent, made by fusing sand (silica) with soda lime and some other ingredients.

Homogeneous and defect free amorphous films of silica can be deposited on porous substrate using sol–gel routes or chemical vapor deposition (CVD) methods to produce asymmetric membranes. With sol–gel routes, the starting solutions generally are based on tetramethoxysilane, $\text{Si}(\text{OCH}_3)_4$, or tetraethoxysilane $\text{Si}(\text{OC}_2\text{H}_5)_4$, diluted in methanol or ethanol, respectively. The formation of the oxide network results from the polymerization of the molecular precursor [182]. The hydrolysis of the alkoxide (a) produces activated species and their condensation by alcoxolation (b) or oxolation (c) leads to a reticulation by formation of siloxane bridge $\equiv\text{Si}-\text{O}-\text{Si}\equiv$.

- $\text{Si}(\text{OR})_4 + \text{H}_2\text{O} \Rightarrow \text{Si}(\text{OR})_3\text{OH} + \text{ROH}$ (a)
- $\equiv\text{Si}-\text{OH} + \text{RO}-\text{Si}\equiv \Rightarrow \equiv\text{Si}-\text{O}-\text{Si}\equiv + \text{ROH}$ (b)
- $\equiv\text{Si}-\text{OH} + \text{HO}-\text{Si}\equiv \Rightarrow \equiv\text{Si}-\text{O}-\text{Si}\equiv + \text{H}_2\text{O}$ (c)

The hydrolysis and condensation reactions are catalyzed in acidic and basic media respectively.

CVD Routes: Conventional CVD techniques (atmospheric pressure AP or low pressure LP) at high temperature (400–700 °C) or Plasma Enhanced CVD methods (PECVD) at low temperatures (room temperature—400 °C) can also be easily used to prepare silica layers. The usual silica precursors are SiH_4 or tetraethoxysilane (TEOS). They are mixed with O_2 , N_2O , or O_3 as oxidizing reactants. A large number of other organosilanes or alkoxy silanes can also be used.

Highly selective microporous silica membranes with high fluxes can be prepared by sol–gel dip-coating processes. The structure of the thin silica layer mainly depends on the size and shape of the silicalite polymers and their packing behavior during drying and heat treatment. Design of the pore networks is of great importance in deciding the transport properties through the membrane since permeation and permselectivity are mainly determined by the microstructure of the membrane, such as pore size, pore size distribution, porosity, and the interaction of permeating species with the pore walls [178, 183]. The use of mono-dispersed silica spheres of a size smaller than 10 nm, with narrow particle size distribution, make it possible to prepare microporous silica membranes with controllable pore structures for specific applications in gas separation [184].

The gas permeation properties of He, H_2 , CO_2 , O_2 , N_2 , and CH_4 in microporous silica membranes were studied as a function of temperature and pressure by Shelekhin et al. [185]. Selectivities were found to be a function of differences in the gas kinetic diameters. The ideal selectivity for He/ CH_4 was more than 10,000 at 30 °C. Selectivity decreased with increasing temperature.

Naskar et al. [186] prepared silicate-1 zeolite membranes hydrothermally on the porous ceramic supports, both unmodified and modified with 3-aminopropyl triethoxysilane (APTES) as coupling agents, following ex situ (secondary) crystal growth process. The membrane developed on surface-modified support rendered

a lower permeance value, i.e., $9 \times 10^{-7} \text{ mol m}^{-2} \text{ s}^{-1} \text{ Pa}^{-1}$ of N_2 compared to that formed on the unmodified support, which gave a permeance value of $20 \times 10^{-7} \text{ mol m}^{-2} \text{ s}^{-1} \text{ Pa}^{-1}$ of N_2 .

Glass membranes are actually not very important for hydrogen separation. One of the reasons is their low selectivity. Glass membranes are porous. Depending on the pore size, they can be subdivided into micro porous (pores below 2 nm) and mesoporous (pores 2–5 nm). Microporous membranes have higher selectivity yet lower fluxes. Both membrane types are usually produced from silica using the leaching manufacturing process. The temperature range where they can be used has an upper limit of 400–500 °C. Vycor glass membranes are commercially available. Porous glass membranes are characterized by a wide range of pore sizes and a good accessibility to the active sites. Porous glasses possess, in comparison with other porous inorganic solids, high thermal stability, chemical resistance, high optical transparency, and good accessibility to eventually available active side inside the porous structure. They can be prepared in different geometrical forms. Due to their large surface areas, molecular sieving ability and controlled host–sorbate interactions, microporous and mesoporous glass membranes can be applied as a medium for gas separation.

Marković et al. [187] demonstrated the preparation and quantitative investigation of gas transport and equilibrium properties of porous glass membranes with pore diameters in a relatively narrow range between 2.3 and 4.2 nm. Original glass for the membranes consisted of 70 % SiO_2 , 23 % B_2O_3 , and 7 % Na_2O . This composition assured the absence of stresses during the cooling process of glass melt. The authors used three mesoporous glass membranes with pore diameters around 2.3 nm (membrane M1), 3.1 nm (membrane M2), and 4.2 nm (membrane M3) as determined by low-temperature nitrogen adsorption. To change surface affinities of the membranes, the surface of membrane M1 was modified with trimethylsilyl groups (membrane M1-mod). As a result, the surface properties of the modified membranes favored interaction with nonpolar gases. During this modification procedure the pore diameter of the membrane was only slightly reduced. Figure 3.39 demonstrates that the permeabilities decrease for all investigated membranes, and for all tested gases, with increasing temperature.

Permeabilities of all examined gases are presented in Fig. 3.40 as a function of the membrane pore diameters at two different temperatures (293 K: Fig. 3.37a, and 433 K: Fig. 3.38b). The same curve shapes were obtained for inert gases for both temperatures. At higher temperatures (Fig. 3.37b) the permeabilities of the adsorbable gases are increasing with increasing pore diameters, but at lower temperature (Fig. 3.38a) they are obviously affected more by the differences in adsorption affinity. The curves of CO_2 and C_3H_8 pass through a maximum observed at 2.3 nm (membrane M1) due to the largest adsorption contribution. Similar trends, as in Fig. 3.38b (where adsorption effects are negligible), were predicted by Bhatia and Nicholson [187] using molecular dynamic simulations for single gas transport in the same range of nanopore sizes.

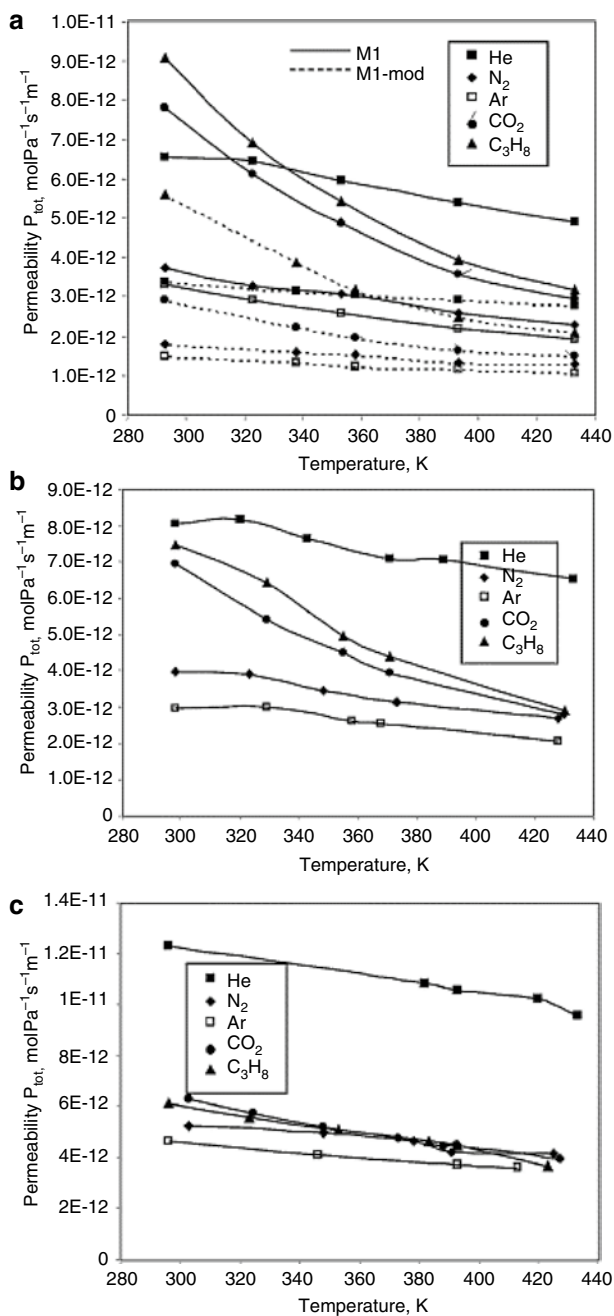


Fig. 3.39 Experimentally observed permeability data of different gases as a function of temperature for: (a) membrane M1 and M1-mod, (b) membrane M2 and (c) membrane M3 [187]

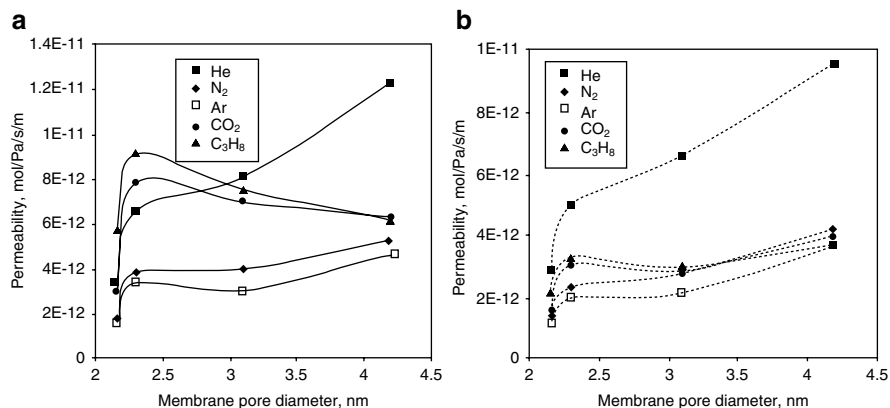


Fig. 3.40 Experimentally observed permeability as a function of pore diameters for all examined membranes presented at two different temperatures: (a) 293 K and (b) 433 K. M1-mod: 2.18 nm, M1: 2.3 nm, M2: 3.1 nm, and M3: 4.2 nm

3.2.3 Zeolites

Zeolite is a crystalline aluminosilicate made up of a 3D framework that forms uniformly sized pores of molecular dimensions (2–20 Å). Zeotype is any crystalline material (e.g., aluminophosphates, titanosilicates) with a 3D framework in which one of the tetrahedral sites occupied by Si is replaced with another element. Many zeotypes have the same structure as known zeolites. Molecules with different sizes and shapes can be discriminated or separated by zeolites through their channels. Like most silicates, the zeolites are based on TO_4 tetrahedra, where T is an aluminum or silicon atom (phosphorus in aluminophosphates). The vast three-dimensional networks are a result of all four corners for the tetrahedra being shared, producing low density microporous materials [188]. Zeolite structures are made of finite or infinite (chains, layers, etc.) component units. The finite units that have been found to occur are shown in Fig. 3.41.

In Fig. 3.41 the T atom of the TO_4 tetrahedron is located at each of the corners, and the oxygens are located towards the mid-points of the lines joining each T atom (*the oxygens are not shown to aid clarity*). These secondary building units (SBUs)—the primary building units being the TO_4 tetrahedra—can contain up to 16 T atoms. SBUs are non-chiral (neither left nor right “handed”). A unit cell always contains the same number of SBUs, and although rare, some materials can have different combinations of SBUs within the zeolite framework [188].

The exact definition of the term “Zeolite” is still the subject of discussion. The naming of zeolites in the literature seldom follows a scientific system such as defined by the *The Atlas of Zeolite Structure Types* published and frequently updated by the IZA (International Zeolite Association) Structure Commission. The maximum size of the molecular or ionic species that can enter the pores of a zeolite is

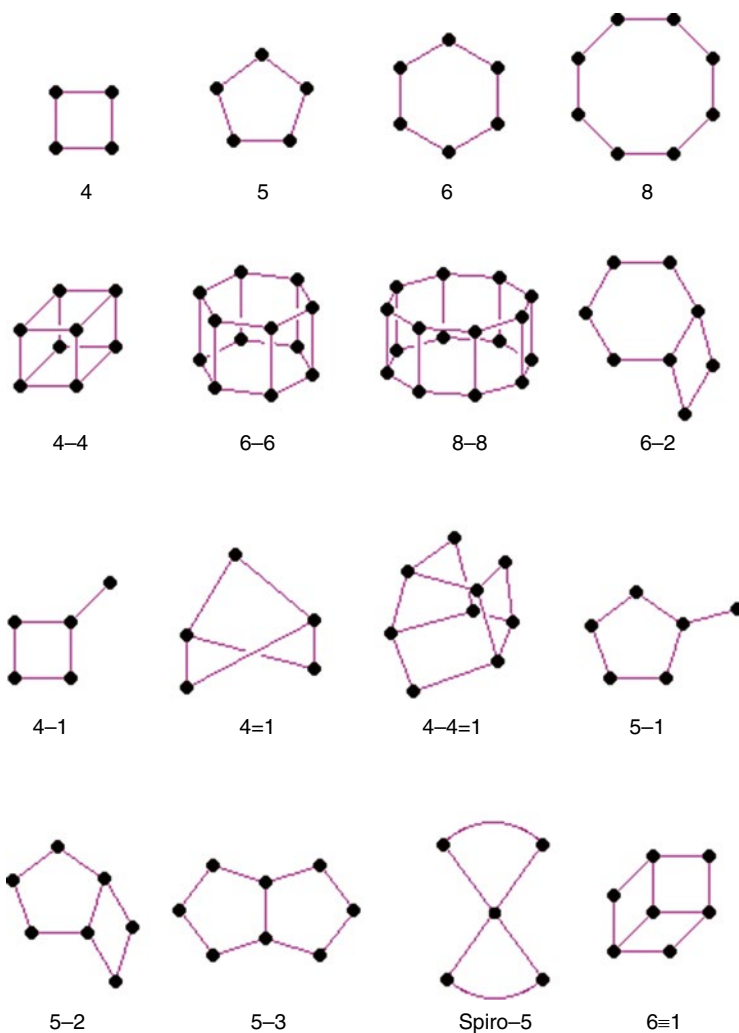


Fig. 3.41 Secondary Building Units (SBUs) in zeolites. (The corners of the polyhedra represent tetrahedral atoms)

controlled by the dimensions of the channels. These are conventionally defined by the ring size of the aperture, where, for example, the term “8-ring” refers to a closed loop that is built from eight tetrahedrally coordinated silicon (or aluminum) atoms and eight oxygen atoms. These rings are not always perfectly symmetrical due to a variety of effects, including strain induced by the bonding between units that are needed to produce the overall structure, or coordination of some of the oxygen atoms of the rings to cations within the structure. Therefore, the pores in many zeolites are not cylindrical.

Zeolites have a porous structure that can accommodate a wide variety of cations, such as Na^+ , K^+ , Ca^{2+} , Mg^{2+} , and others. These positive ions are rather loosely held

and can readily be exchanged for others in contact with solution. Some of the more common mineral (natural) zeolites are analcime, chabazite, clinoptilolite, heulandite, natrolite, phillipsite, and stilbite. An example zeolite mineral formula is $\text{Na}_2\text{Al}_2\text{Si}_3\text{O}_{10}\cdot 2\text{H}_2\text{O}$, the formula for natrolite. There are two types of zeolites, natural and synthetic and some of the differences between the two include:

1. Synthetics are manufactured from energy-consuming chemicals and naturals are processed from natural ore bodies.
2. Synthetic zeolites have a silica-to-alumina ratio of 1-to-1 and natural clinoptilolite (clino) zeolites have a 5-to-1 ratio.
3. Clino natural zeolites do not break down in a mildly acid environment, whereas synthetic zeolites do. The natural zeolite structure has more acid resistant silica to hold its structure together.

Membranes made from zeolites are promising to achieve high selectivities based on molecular recognition by the membrane pores. As well, zeolite membranes show selective adsorption properties and catalytic abilities.

The preparation of a “defect free” zeolite layer for gas separation was and is still a matter of study. Therefore, the aim of zeolite membrane design is to tune the size of zeolite pores and/or to decrease the number of defects. For example, the intercrystal pores formed inherently in polycrystalline zeolite films should be minimized, because the existence of intercrystal pores is the major cause for decline in molecular separation efficiency [189].

The framework of the zeolite can be modified by synthesizing them with metal cations other than aluminum and silicon in the framework. There are many propriety methods to modify zeolites that impart unique characteristics to them. However, zeolite membranes have been too expensive to replace competing polymeric membranes.

Synthetic zeolites hold some key advantages over their natural analogs. The synthetics can, of course, be manufactured in a uniform, phase-pure state. It is also possible to manufacture desirable zeolite structures which do not appear in nature. Zeolite A is a well-known example. Since the principal raw materials used to manufacture zeolites are silica and alumina, which are among the most abundant mineral components on earth, the potential to supply zeolites is virtually unlimited.

As of October 2012, 206 unique zeolite frameworks have been identified, and over 40 naturally occurring zeolite frameworks are known [188, 190, 191]. There are more than 200 different zeolites with different structures that have been reported by the International Zeolite Association (IZA). Among them, only 15 structures have been tried to fabricate membranes [192, 193]. Table 3.18 provides a brief description of structure and pore sizes for the few different zeolites used for membranes.

3.2.3.1 Preparation of Zeolite Membrane by Crystallization and Seeding

In order to achieve a better separation performance, zeolite membranes should be preferably made of pure zeolite crystals with uniform and small particle sizes. Zeolitic nucleation is affected by the surface composition and chemistry of the support material [194].

Table 3.18 Brief description of structure and pore sizes of different zeolites used for membranes etc

Zeolite/zeotype	Brief description of structure	Nanopore size
T	Intergrowth type zeolite of erionite and offretite	0.36 nm × 0.51 nm
FAU (faujasite), A (LTA)	12-membered ring (NaX, Si/Al:1/1.5), pore 4 Å (NaY, Si/Al:>1.5)	~0.74 nm (pd) (NaA zeolite—pore size 0.41 nm)
MOR	12-membered ring	
MFI ZSM-5	Ten-membered ring	0.56 nm (pd), pore size ~6 Å
MEL		
MER (merlinoite)	Comprises double-eight-rings and γ cage	pd. 0.27–0.51 nm
W	Same framework topology as the mineral merlinoite (MER), eight membered ring	Channel dimension 0.31 nm × 0.35 nm
FER	Eight-membered ring	
L	Si/Al:3/1	Cavity, 0.48 × 1.24 × 1.07 nm
DDR	Comprises silicon and oxygen atoms, eight membered ring	0.36 × 0.44 nm
Boron substituted ZSM-5	Boron substituted into the framework for silicon	0.53–0.56 nm pores
SUZ-4	Composition $K_5Al_5Si_31O_{72}$; framework topology is related to zeolites ferrierite and ZSM-5 and contains straight channels having apertures defined by rings of ten (Si,Al)–O species. A novel cage may serve as the site for non-exchangeable potassium ions.	97 nm pd
Imidazolates (ZIFs)	A subclass of metal–organic frameworks (MOFs)	ZIF-8, 11.6 Å Cell dimension 16.32 Å
ZIF-8	Sodalite (SOD) type	11.6 Å
AIPOs	3D framework, AlO_4^- and PO_4^- tetrahedral building units	3.8 Å
ITQ	Similar to Zeolite A, but a much higher Si/Al ratio (up to infinity, i.e., pure silica)	Hydrophobic smaller pore size than Zeolite A
SAPO-34	Micropore, similar to chabazite	Internal cages ~1.4 nm in diameter and each cage has six pores. XRD pore diameter of 0.38 nm
SAPO-44	Micro pore, similar to chabazite	~0.43 nm
A-Type zeolite	Hydrophilic	0.4–0.43 nm
UZM	16 cages per unit cell	6–8 Å

pd means pore diameter

There are several types of synthetic zeolites that form by a process of slow crystallization of a silica–alumina gel in the presence of alkalis and organic templates. One of the important processes used to carry out zeolite synthesis is sol–gel processing. The product properties depend on reaction mixture composition, pH of the system, operating temperature, pre-reaction “seeding” time, reaction time, and the

templates used. In the sol–gel process, other elements (metals, metal oxides) can be easily incorporated. The silicalite sol formed by the hydrothermal method is very stable. The ease of scaling up this process makes it a favorite route for zeolite synthesis.

A number of synthetic strategies have been applied to zeolite membrane synthesis, such as in situ (without seeding) hydrothermal synthesis (in situ crystallization), secondary (seeded) growth and post-treatments of zeolite membranes.

Zeolite membrane synthesis is more commonly carried out by the in situ crystallization technique which involves placing a porous support in contact with a synthesis solution or gel under hydrothermal conditions. For successful membrane formation, proper conditions are necessary to allow for preferential nucleation and growth of zeolite crystals on the support surface (possibly competing with solution events) in an interlocking fashion with minimal non-selective interzeolitic porosity.

The other approach for zeolite membrane formation is a technique called secondary (seeded) growth, which involves attaching a closely packed layer of zeolite seed crystals on the surface of a support. The first seeding was demonstrated by Horii et al. [195]. The use of seed crystals facilitates the formation of zeolite membranes since a seeded support grows to a pure-phase zeolite membrane more easily, even when the crystallization conditions and the chemical batch compositions are not optimum. Seeded growth has significant advantages such as better control over membrane microstructure (thickness, orientation), higher reproducibility, and a wider range of hydrothermal synthesis conditions leading to continuous film formation. Elimination of the constraints imposed by the need for crystal nucleation, due to the preexistence of nuclei on the support surface, renders crystal growth as the main film formation mechanism and, thus, adds improved flexibility in zeolite film and membrane preparation [196].

There are four main ways to attach the seeds to the support [197].

1. Charging the support surface by pH control such that seeds and support have opposite surface charges for an electrostatic attachment.
2. Charging the support surface by adsorption of positively charged cationic polymers like poly-DADMAC (diallyl dimethyl ammonium chloride) or Redifloc (Trade name of EKA Chemicals, a polyamine) to adjust different zeta potentials between the ceramic support and the zeolite nanocrystals to be attached as seeds. The counter ions of the ammonium polymer are usually chlorides which go in the solution, and negatively charged silica nanoparticles are attached. The use of seeded supports usually results in a c-orientation of the MFI (Mordenite Framework Inverted, example ZSM-5, medium pores 5.3 Å) layer but under certain conditions also for secondary growth the desired b-orientation can be obtained.
3. Electrophoretic deposition of nanosized seeds on solid supports.
4. Immersion of the dried support into a seed solution followed by thermal treatment of the seeded support to burn helping organic additives and to fix the seeds via de-hydroxylation to the support.

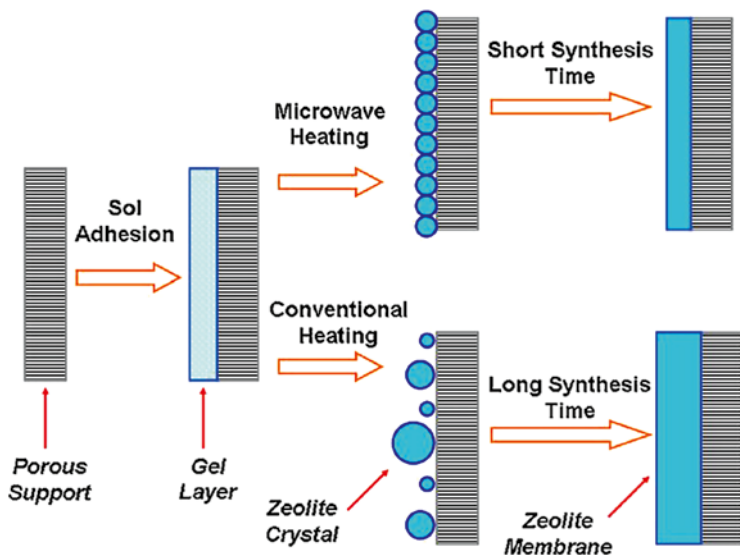


Fig. 3.42 Comparative synthesis model of zeolite membrane by microwave heating and conventional heating

Microwave synthesis of zeolite can be much faster than conventional heating and create a more selective membrane product. Microwave synthesis has often proven to create more uniform (defect-free) products than from conventional hydrothermal synthesis. As compared with conventional hydrothermal synthesis, microwave synthesis of zeolites has the advantages of a very short time, small zeolite particle size, narrow particle size distribution and high purity. All these characteristics make it a promising method for rapid preparation of high performance zeolite membranes. However, microwave synthesis is in the early stages of development, and further research is required [198]. Articles written by Li and Yang [199], Cundy [200], and Li et al. [201] are recommended for more general information on the subject of synthesis of microwave zeolites and microwave chemistry. Figure 3.42 illustrates a comparative synthesis of zeolite membrane by microwave heating and conventional heating [201].

Li et al. [201] developed a method called, “in situ aging–microwave synthesis” of zeolitic membranes without seeding. It decouples two successive steps in the formation of zeolite membranes. The first step is the rearrangements of synthesis mixture and formation of germ nuclei on the support surface obtained by in situ aging. The second step is the nucleation and crystal growth on the support achieved by in situ crystallization under fast and homogeneous heating. Choi et al. [202] demonstrated that rapid thermal processing in the preparation of zeolitic membranes can improve the separation performance of thick columnar films of a certain zeolite (silicate-1) by eliminating grain boundary defects, possibly by strengthening grain bonding at grain boundaries.

Varoon et al. [203] demonstrated the synthesis and structure determination of highly crystalline nanosheets of zeolite frameworks MWW. MWW structured zeolites such as MCM-22 possess two independent pore systems. One system consists of two-dimensional sinusoidal 10-member ring (MR) channels with an elliptical ring cross section of $4.1 \text{ \AA} \times 5.1 \text{ \AA}$. The other is composed of a large 12-MR supercage connected by 10-MR windows [204] and MFI (mordenite framework inverted). The purity and morphological integrity of those nanosheets allow them to pack well on porous supports, facilitating the fabrication of molecular sieve membranes.

3.2.3.2 LTA Zeolite

Zeolite A exhibits the LTA (Linde Type A) structure. It has a three-dimensional pore structure with pores running perpendicular to each other in the x , y , and z planes, and is made of secondary building units 4, 6, 8, and 4-4. The pore diameter is defined by an eight member oxygen ring and is as small as 4.2 \AA . This leads to a larger cavity of minimum free diameter 11.4 \AA . The cavity is surrounded by eight sodalite cages (truncated octahedra) connected by their square faces in a cubic structure. The zeolite LTA membrane, with a relatively small pore size of about 0.4 nm , is a candidate for the separation of small sized molecules such as H_2 and CO_2 , while zeolite FAU (faujasite) membrane with larger pore size will not reduce the permeation flux like the narrower LTA layer. Further, the composition difference between the zeolite LTA and FAU layers is relatively small and both of them have strong hydrophilicity due to their low Si/Al ratio. Therefore, sandwich-structured composite LTA-FAU membranes will be formed and show higher gas separation performances corresponding to single-phase zeolite membranes.

Huang et al. [205] reported that sandwich-structured zeolite membranes enhanced hydrogen selectivity. Sandwich-structured LTA-FAU composite membranes were prepared by using 3-aminopropyltriethoxysilane (APTES) as an interlayer between the LTA and FAU layers as well as between the alumina support and the zeolite LTA layer, as shown in Fig. 3.43.

Figure 3.44 shows the permeances of the single gases through the LTA-FAU composite membrane as well as the single zeolite LTA and FAU membranes at $100 \text{ }^\circ\text{C}$ and 1 bar pressure difference as a function of the gas kinetic diameters of the permeating molecules.

H_2 has the highest permeance for all membranes due to its smallest kinetic diameter of 0.29 nm . At $100 \text{ }^\circ\text{C}$ for the LTA-FAU composite membrane, the ideal separation factors of H_2 from CO_2 , N_2 , CH_4 , and C_3H_8 are 10.6, 8.6, 7.1, and 24.3, respectively, which not only exceed the corresponding Knudsen coefficients (4.7, 3.7, 2.8, and 4.7, respectively) but are also higher than the corresponding ideal separation factors of the single phase zeolite LTA (7.0, 5.8, 4.9, and 6.8) and FAU (8.0, 7.2, 5.6, and 18.6) membranes. This data suggests that the LTA-FAU composite membrane displays higher hydrogen selectivities. The enhancement of the separation performance could be due to the novel sandwich structure of zeolite membranes by using APTES as an interlayer.

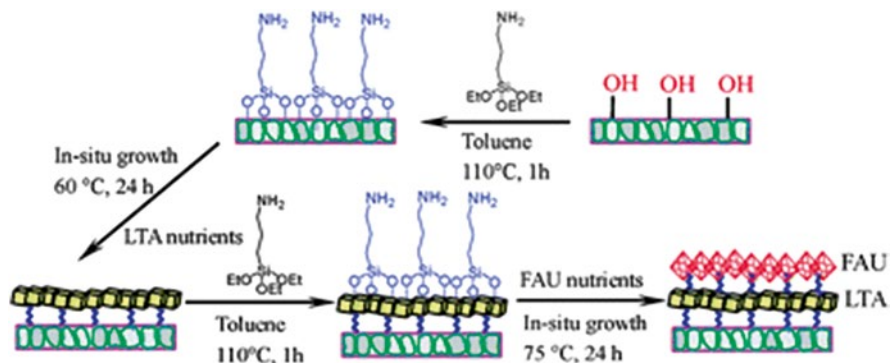


Fig. 3.43 Schematic diagram for stepwise synthesis of a sandwich-structured zeolite LTA-FAU composite membrane by using APTES as an interlayer [205]

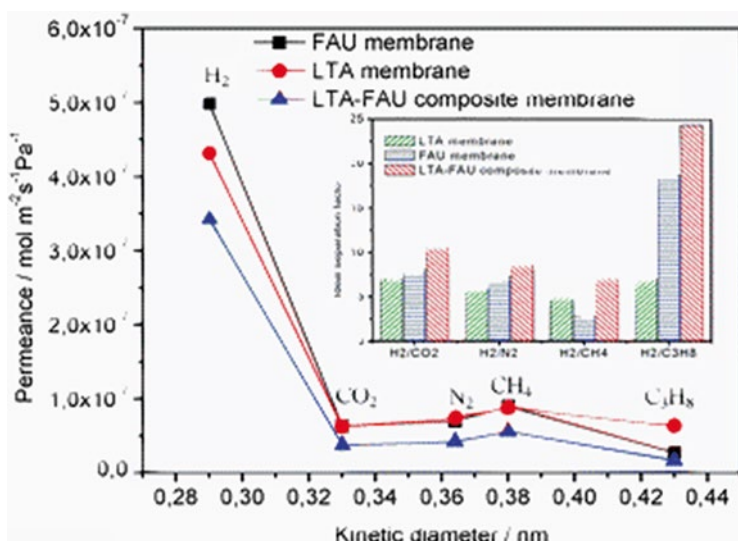


Fig. 3.44 Single gas permeances of different gases through the LTA-FAU composite membrane as well as the single zeolite LTA and FAU membranes, at 100 °C and 1 bar pressure difference as a function of the gas kinetic diameter. (The inset shows the ideal separation factors of the membranes for H₂ over other gases [205])

Cheng et al. [206] synthesized NaA zeolite using microwave heating. The method involved two steps: prior seeding of 120 nm of LTA crystals on substrate and then employing a secondary hydrothermal synthesis. The effects of seeding time and synthesis time on performance were studied. The ideal H₂/N₂ selectivity increased from 1.90 of the substrate to 6.37 of the three-stage synthesized membrane, which was distinctly higher than the corresponding Knudsen diffusion selectivity of 3.74.

3.2.3.3 NaA Zeolite

NaA zeolite is one of the microporous crystalline aluminosilicate zeolites, which has a channel opening size of 0.41 nm. The pore size of NaA zeolite is close to many molecular diameters. As it has strong hydrophilicity, the synthesized NaA zeolite membrane has great potential in many fields, such as gas separation. For example, the molecular kinetic diameters of O₂ and N₂ are 0.346 nm and 0.364 nm, respectively. Due to configurational diffusion, the slight difference in molecular diameter between O₂ and N₂ leads to a big difference in the rate of diffusion through the NaA zeolite channels, with the diffusion rate of O₂ being faster than that of N₂. Thus, nitrogen–oxygen mixtures can be separated effectively by the NaA zeolite membrane. Moreover, NaA zeolite membranes can be used for separating many different mixtures of small gases [207]. The permeation of *n*-C₄H₁₀ via a high quality NaA zeolite membrane reveals that the NaA zeolite membrane has intercrystalline pores larger than those of the NaA zeolite channels [208]. Though the NaA type zeolite membrane shows excellent performance, the acid stability of the membrane is poor. The surface of A-type zeolite is hydrophilic due to the low Si/Al ratio in the framework. Few papers have been published on the small gas permeation characteristics for A-type zeolite membrane [209, 210]. Aoki et al. [209] suggested that the behavior of the NaA zeolite (*d_p* = 0.41 nm) membrane is dominated by the molecular sieving mechanism, despite the presence of defects larger than the structural pores. Another consequence of the low Si/Al ratio found in A-type zeolite is a lack of thermal stability, which is why there have been no reports on its gas permeation characteristics at high temperatures (>300 °C).

Dey et al. [211] synthesized NaA-zeolite membrane hydrothermally by a secondary crystallization process at different temperatures (55–75 °C) on porous alpha-alumina support tubes (inner side) precoated with a poly(ethyleneimine) (PEI) buffer layer. The application of PEI as a buffer layer was found to be very effective for proper attachment of NaA crystals with the support. Adsorption/interaction of CO₂ in the NaA zeolite channel was stronger than the other gases, which is reflected in their permeation behaviors. The permance values of different gases through PEI-modified membranes were in the order of CO₂ < N₂ < H₂. The order of permselectivity was (H₂/CO₂) > (H₂/N₂) > (N₂/CO₂). Thus, the PEI-modified NaA membrane could be very effective in separation of CO₂ from other gases.

3.2.3.4 DDR Type Zeolite

Recently, DDR type zeolites have been widely used for gas separation. The all-silica zeolite deca-dodecasil 3R (DD3R) is a clathrasil (8-ring) first synthesized by Gies [212]. Its crystal structure consists of a three-dimensional arrangement of building units. The highly siliceous DDR (Deca-Dodecasil 3R)-type zeolite contains pores formed by a polyhedron with an oxygen eight-membered ring. DDR type zeolite particles have an aperture of 0.36 × 0.44 nm. This zeolite has a high thermal stability allowing for the study of gas permeation (or diffusion) at high

temperatures where adsorption is negligible. This stability avoids the necessity to measure the equilibrium of gas adsorption in supported, thin zeolite film. Furthermore, this zeolite has small pore opening ($0.36 \times 0.44 \text{ nm}^2$) making it an ideal candidate to study the effects of size or molecular weight of gases on permeation or diffusion properties for zeolites and zeolite membranes. The DDR critical diameter with eight-membered-ring windows closely matches the diameters of light hydrocarbons and carbon dioxide.

Nakayama et al. [213] patented the method for the preparation of DDR zeolites. They reported that the DDR type zeolite membrane separates at least one type of a gas component from a mixed gas containing at least t from a group consisting of carbon dioxide, hydrogen, oxygen, nitrogen, methane, propane, propylene, carbon monoxide, and nitrogen oxide. Single gas permeances were different both at room temperature and 100°C , enabling the separation of at least one selected gas component from the mixed gas.

Bergh et al. [214] measured the equilibrium adsorption data of pure CO_2 , N_2 , and CH_4 and their mixtures in pure silica DDR membranes at a temperature range of $200\text{--}400 \text{ K}$ and at pressures up to $1,500 \text{ kPa}$. From the measured equilibrium data of these gases, the membrane's transport parameters were derived by using the unary permeation. A model based on the generalized Maxwell–Stefan equations was used to simulate the component fluxes and separation factors of the binary mixtures as a function of temperature and total feed pressure. It was concluded that DDR membranes have very high selectivities for CO_2/CH_4 separations with good permeances. At a total pressure of 101 kPa and at 225 K , the CO_2 selectivity of an equimolar CO_2/CH_4 mixture was found to be $>3,000$ and for N_2 over CH_4 selectivity was 40 with a 50/50 feed. The N_2/CH_4 selectivity was constant with pressure, while the selectivity for CO_2/CH_4 decreased. Figure 3.45 shows the selectivities of equimolar mixtures through the DDR membrane as a function of the temperature at constant total feed pressure of 101 kPa , using sweep gas He at 101 kPa [215].

Figure 3.46 shows the CO_2 selectivity of a DDR membrane for an equimolar CO_2/CH_4 mixture as a function of permeation temperature.

Tomita et al. [216] coated molecular-sieve type zeolite (DDR) with an aperture of $0.36 \times 0.44 \text{ nm}$ on a porous alumina substrate using a hydrothermal process. The permeation through the membrane in the single gas feed of helium, hydrogen, carbon dioxide, oxygen, nitrogen, methane, *n*-butane, *i*-butane, and sulfur hexafluoride was measured at 301 and 373 K up to 0.5 MPa . Figure 3.47 shows the permeance plotted against the kinetic diameter of various gases. The permeance decreased by more than three orders of magnitude between 0.35 and 0.40 nm of the kinetic diameter of permeated gas at both 301 and 373 K . The separation factor of CO_2 to CH_4 in $50\% \text{ CO}_2$ and $50\% \text{ CH}_4$ mixed gas feed was 220 and 100, at 301 and 373 K , respectively. Total gas feed pressure was 0.5 MPa . The DDR type membranes were found to have few defects and worked as molecular-sieving membranes. It was suggested that DDR type zeolite membranes are not perfectly hydrophobic.

Kanezashi et al. [217] prepared DDR type zeolite membranes by the secondary growth method on a porous $\alpha\text{-Al}_2\text{O}_3$ disc. To eliminate the crystalline micropores, the surface was modified by an on-stream counter diffusion chemical vapor deposition (CVD) technique. Table 3.19 shows the permeance for four gases for the

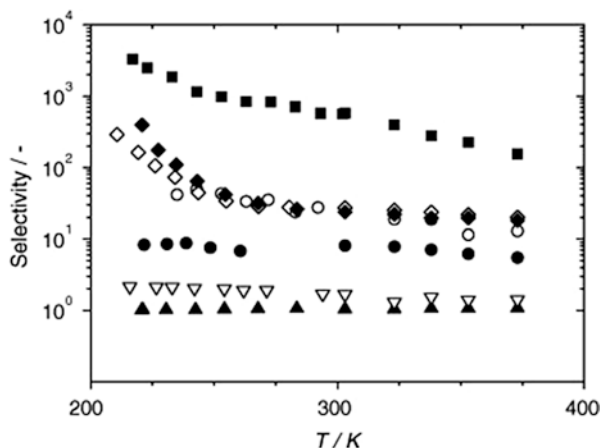


Fig. 3.45 Selectivities of equimolar mixtures through the DDR membrane as a function of the temperature constant total feed pressure of 101 kPa, sweep gas He at 101 kPa. CO_2/CH_4 (filled square), N_2/CH_4 (open circle), CO_2/Air (filled diamond), $\text{N}_2\text{O}/\text{Air}$ (open diamond), Air/Kr (filled circle), O_2/N_2 (inverse triangle), $\text{N}_2\text{O}/\text{CO}_2$ (filled triangle) [215]

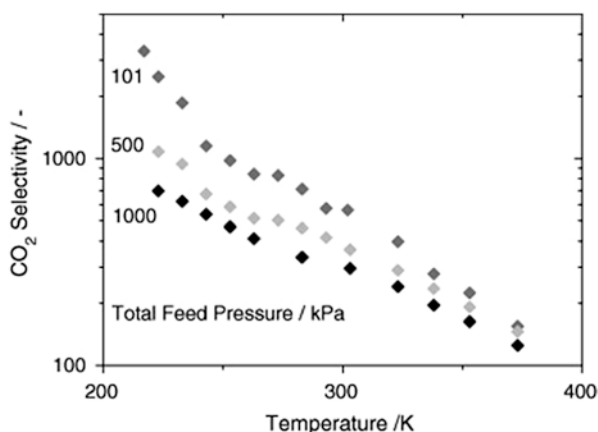


Fig. 3.46 CO_2 selectivity of a DDR membrane for an equimolar CO_2/CH_4 mixture as function of permeation temperature [214]

CVD-modified DDR type zeolite membranes before and after exposure to steam at 500 °C. The table clearly shows that there is negligible change in gas permeation before and after exposure to steam. Similar results were also observed for activation energy. It proved that CVD-modified DDR type membranes are hydrothermally stable, and that single gas permeance decreases as $\text{H}_2 > \text{He} > \text{CO}$. This order is determined by both molecular size and weight of permeating gases. This permeance indicates the presence of intercrystalline pores in the as-synthesized DDR-type zeolite membranes.

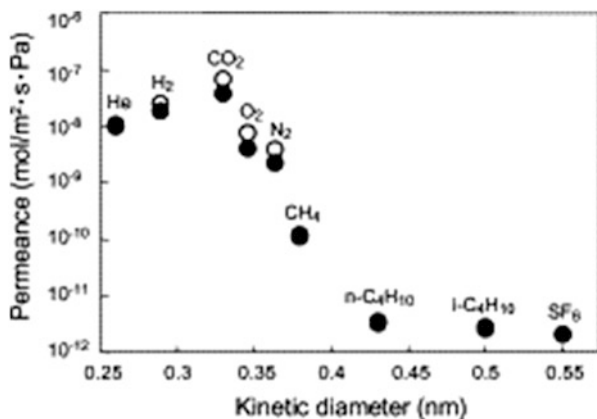


Fig. 3.47 Single gas permeance versus kinetic diameter of gas for DDR type zeolite membrane at 301 K (open circle) and 373 K (filled circle) [216]

Table 3.19 Permeance of gases for CVD-modified DDR-type zeolite membrane before and after exposure to steam at 500 °C (partial pressure of steam: 50 kPa)

Gases	Permeance at 500 °C ($10^{-8} \text{ mol m}^{-2} \text{ s}^{-1} \text{ Pa}^{-1}$)	
	Before exposure to steam	After exposure to steam
He	2.79	2.74
H ₂	2.34	2.18
CO ₂	0.38	0.39
CO	0.20	0.18

Kanezashi et al. [217] suggest that high temperature diffusion data for the small gases in the DDR type zeolites measured by the macroscopic membrane permeation method are consistent with the theory of translation gas diffusion in zeolites as proposed by Xiao and Wei [218].

Himeno et al. [219] coated the outer surface of a porous α -alumina tube with highly hydrophobic DDR zeolite membrane. Single gas permeance for CO₂, CH₄, He, H₂, O₂, and N₂, and CO₂/CH₄ binary gas were measured. The permeances were in the following order: CO₂>H₂>He>O₂>N₂>CH₄. Single-gas permeance was dependent on the relative molecular size of the DDR to the pore diameter; however, CO₂ permeance was dominated by the adsorption affinity to the pore wall of DDR zeolite. The respective single-gas permeances of CO₂ and CH₄ at 298 K at a feed pressure of 0.2 MPa and a permeate pressure of 0.1 MPa were 4.2×10^{-7} and $1.2 \times 10^{-9} \text{ mol m}^{-2} \text{ s}^{-1} \text{ Pa}^{-1}$; the ideal selectivity for CO₂/CH₄ was 340. These CO₂/CH₄ selectivities and CO₂ permeance are better than other zeolite membranes. Himeno et al. [220] developed a membrane separation process for biogas using a DDR-type zeolite membrane with high CO₂/CH₄ selectivities. Biogas produced in a sewage plant was separated by using a DDR-type zeolite membrane, and the performance and durability of the membrane was estimated. Himeno et al. reported that

the developed membrane separation process was fully applicable to the separation and purification of biogas; however, the membrane performance was reduced by long periods of ventilation and by exposure to compounds of high boiling points such as higher hydrocarbons and siloxane, which are present as impurities in the biogas.

3.2.3.5 SAPO-34

The molecular sieve SAPO-34 has the composition $(\text{Si}_x\text{Al}_y\text{P}_z)\text{O}_2$, where $x=0.01-0.98$, $y=0.01-0.60$, and $z=0.01-0.52$. A SAPO-34 membrane removed CO_2 from CO_2/H_2 mixtures because CO_2 adsorbed more strongly than H_2 ; the fluxes of H_2 at low temperatures were orders of magnitude lower in the presence of CO_2 . At low temperatures and high pressures, the CO_2/H_2 selectivity was greater than 100, and thus, SAPO-34 membranes may have a significant potential for application in separation of CO_2 from CO_2/H_2 mixtures for the purification of hydrogen [221].

Li et al. [222] synthesized powerful SAPO-34 membranes by in situ crystallization on a porous tubular stainless steel support. For a SAPO-34 membrane with a Si/Al gel ratio of 0.1, a CO_2/CH_4 mixture selectivity of $\alpha=170$ with a CO_2 permeance of $P=1.2\times 10^{-7}$ mol m^{-2} s^{-1} Pa^{-1} was achieved at 22 °C. With decreasing temperature the selectivity increases, and at -21 °C a CO_2/CH_4 separation factor $\alpha=560$ was achieved. Membranes of SAPO-34 prepared with the higher Si/Al ratio of 0.15 showed slightly lower selectivity ($\alpha=115$), but a higher permeance for CO_2 (4×10^{-7} mol m^{-2} s^{-1} Pa^{-1}) at 35 °C. At 7 MPa, the SAPO-34 membrane had a $\alpha=100$ for a 50/50 feed of CO_2/CH_4 mixture at room temperature.

In another study, Li et al. [223] also reported that SAPO-34 membrane can separate CO_2 from CO_2/CH_4 mixtures best at low temperatures with a selectivity of $\alpha=270$ at -20 °C. Another study noted that SAPO-34 on porous alumina support can be used for the separation of light gases at both low and high temperature [224]. Zhou et al. [225] made a SAPO-34 membrane which showed high permeances (maximum of 1.2×10^{-6} mol m^{-2} s^{-1} Pa^{-1}) and high CO_2/CH_4 selectivities (70) at 46 bar of feed pressure.

In an additional study, Li et al. [226] fabricated high flux SAPO-34 membranes on porous, tubular stainless steel supports with CO_2/CH_4 separation selectivities greater than 200. Monolith-supported SAPO-34 also was used for the separation of a CO_2/CH_4 mixture. Monoliths increased the membrane surface area per volume and, thus, had the potential to decrease membrane module cost; however, CO_2 permeances and CO_2/CH_4 selectivities at 4.6 MPa feed pressure were similar to SAPO-34 membranes on single channel supports [227]. Humidity has a strong effect on permeation of gases through SAPO-34 membranes, and the effect depends on the fraction of permeation through non-SAPO pores in the membrane. For high quality membranes, water almost completely blocks the SAPO pores and dramatically decreases the permeances of gases that can enter the pores. The degradation accelerates with prolonged exposure until the membranes have low CO_2/CH_4 selectivities and exhibit viscous flow [228].

3.2.3.6 AIPO-18

Microporous aluminophosphates (AIPOs) are a class of zeolites with framework structures built of AlO_4^- and PO_4^- tetrahedral building units. In particular, AIPO-18 is an appealing zeolite composition for membrane preparation. The AEI framework topology of this aluminophosphate is characterized by a three-dimensional framework possessing eight-membered intersecting channels with a diameter of 3.8 Å. Due to its pore size, this membrane was used for the separation of CO_2 (kinetic diameter 3.3 Å). The membrane can be synthesized mainly via a hydrothermal approach and under microwave irradiation [237]. The separation performances of these membranes for equimolar CO_2/CH_4 gas mixtures was studied by Carreon et al. [229] and they reported that the AIPO-18 membranes displayed CO_2 permeances as high as $\sim 6.6 \times 10^{-8} \text{ mol m}^{-2} \text{ s}^{-1} \text{ Pa}^{-1}$ with CO_2/CH_4 selectivities in the ~ 52 –60 range at 295 K and 138 kPa.

3.2.3.7 Beta Zeolite or ZSM Zeolite (MFI Zeolite Membranes (ZSM-5))

Beta zeolite is an old zeolite discovered before Mobil began the “ZSM” naming sequence. As the name implies, it was the second in an earlier sequence. The very complex structure of beta zeolite was only recently determined because interest was not high enough until the material became important for some dewaxing operations. Beta zeolite consists of an intergrowth of two distinct structures termed Polymorphs A and B. The polymorphs grow as two-dimensional sheets and the sheets randomly alternate between the two. Both polymorphs have a three-dimensional network of 12-ring pores.

Among the different types of zeolites available, zeolite MFI (ZSM-5 and its Al-free analog, silicate-1) has been more commonly used in zeolite membrane synthesis because of its pore size (~ 5.5 Å) suitable for several industrially important separations, and the relatively easy synthesis from a variety of silica sources and structure directing agents. ZSM-5 is composed of several pentasil units linked together by oxygen bridges to form pentasil chains. A pentasil unit consists of eight 5-membered rings. In these rings, the vertices are Al or Si and an O is assumed to be bonded between the vertices. The pentasil chains are interconnected by oxygen bridges corrugated with 10-ring holes. Its chemical formula is $\text{Na}_n\text{Al}_n\text{Si}_{96-n}\text{O}_{192} \cdot 16\text{H}_2\text{O}$ ($0 < n < 27$) [230].

Poshusta et al. [231] measured the effect of pressure on the CO_2 permeance of three different MFI membranes chosen to represent membranes with small, medium and large amounts of non-zeolite pores. A model expressing the flux as the sum of surface diffusion, Knudsen diffusion, and viscous flow showed that the differences in the pressure behavior of the membranes were due to different relative amounts of zeolite and non-zeolite pores.

Membranes with the largest permeation through non-zeolite pores had the lowest CO_2/CH_4 mixture selectivity. The highest CO_2/CH_4 mixture selectivity was 5.5 at room temperature, and for all membranes, the selectivity decreased with temperature

because of a decrease in competitive adsorption. The separation performance decreased with pressure despite an increase in the selectivity.

MFI zeolite membranes were prepared by Takata et al. [232] via secondary growth on α -alumina microfiltration membranes. Colloidal silicate (size around 100 nm) was used as a seed crystal. An MFI membrane in which the zeolite layer was oriented to the (1 0 1) plane, showed a n -C₄H₁₀ permeance of 1.5×10^{-5} m³ (STP) m⁻² s⁻¹ kPa⁻¹ and a n -C₄H₁₀/*iso*-C₄H₁₀ selectivity of 15 at 150 °C. N₂ permeated faster than He at temperatures lower than 150 °C. The authors reported that at high temperatures (300 °C) the permeation mechanism obeys the Knudsen mechanism, irrespective of molecular size in the experimental range.

ZSM-5 membrane was prepared by Kwon et al. [233] on the porous alumina support using in situ seeding techniques in hydrothermal conditions. The packed density of zeolite membrane was controlled by the hydrothermal time and temperature. The sample packed at 100 °C was densely packed with ZSM-5 seeds on the top of the alumina substrate. The prepared zeolite films were characterized with SEM and thin film XRD. The hydrogen permeance and selectivity toward carbon dioxide gas were 0.6×10^{-6} mol m⁻² s⁻¹ Pa⁻¹ and 3.16, respectively. The hydrogen selective zeolite membranes show promising application in hydrogen separation from coal gasification such as Integrated Gasification Combined Cycle (IGCC).

Welk and Nenoff [234] studied the permeance and selectivity of both ZSM-5 and silicate-1 zeolite membranes under the flow of gas mixtures, two chosen as benchmarks (50/50 mol% H₂/CH₄ and 50/50 mol% H₂/CO₂) and one chosen to simulate an industrial methane reformat stream. Permeation experiments of mixed gases through both ZSM-5 and silicate-1 zeolite membranes revealed the extraordinary selectivities of these membranes for H₂. The ZSM-5 membrane had the following H₂ selectivities for the 50/50 H₂/CH₄ mixture, the 50/50 H₂/CO₂ mixture and the reformat mixture: 39.4, 60.1 and 58.8, respectively.

Richter et al. [235] coated ZSM-5 zeolite membrane on the inner surface of ceramic tubes and capillaries to get useful membrane shapes with a high membrane area/module volume ratio for industrial application. On flat discs and by a two-step-crystallization of ZSM-5 membranes of 20 μ m thickness, a very low H₂ permeance of only 30 l/(m² h bar) and a high H₂/SF₆ single gas permselectivity of 51 were achieved (Fig. 3.48).

The coated membranes were tested by H₂ and SF₆ single gas permeation at 110 °C. The results are given in Table 3.20.

In Table 3.20, all tubular membranes had a much higher H₂ permeance and a lower H₂/SF₆ permselectivity compared with flat discs because of the simpler one-step crystallization. The preparation in a resting synthesis solution causes very low H₂/SF₆ permselectivities of 10–14. By using nano-sized MFI seeds and by pumping the synthesis solution through the support tubes, a homogeneous ZSM-5 membranes of 30 μ m thickness, a high permeance of 4,500 l/(m² h bar), and an H₂/SF₆ single gas permselectivity above the Knudsen factor were achieved.

Bernal et al. [196] have grown zeolite MFI membranes (thickness 15–20 μ m) on the surface of macroporous α -alumina and stainless steel support tubes (pore size 200 and 500 nm respectively) by the secondary (seeded) growth technique.

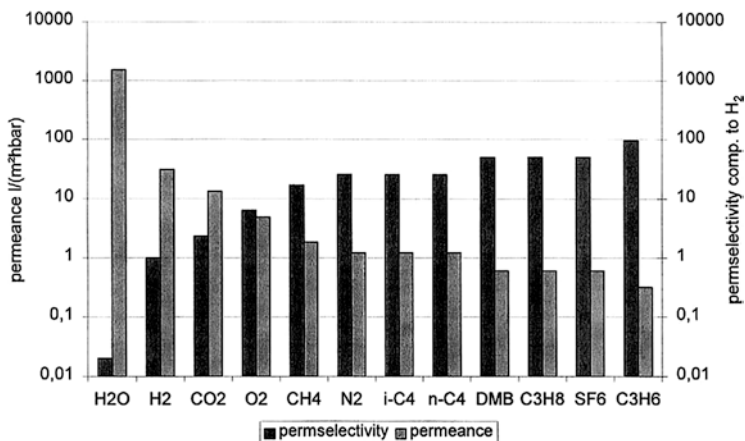


Fig. 3.48 Single gas permeance of ZSM-5 membrane on flat support at 105 °C, prepared by two-step-crystallization

Table 3.20 Single gas permeation of ZSM-5 membranes at 110 °C

Support	Seeding	H ₂ permeance (l/m ² h bar)	SF ₆ permeance (l/m ² h bar)	H ₂ /SF ₆ permselectivity
<i>Two-step-crystallization, resting synthesis solution</i>				
Flat disc	MFI powder	30 ^a	0.6 ^a	51 ^a
<i>One-step-crystallization, resting synthesis solution</i>				
Tube	MFI powder	6,300	460	14
Small tube	MFI powder	–	–	–
Capillary	MFI powder	–	–	–
Tube	Nano seeds	18,040	1,520	12
Small tube	Nano seeds	8,580	610	14
Capillary	Nano seeds	3,140	660	5
<i>One step-crystallization, moved synthesis solution</i>				
Tube	Nano seeds	9,540	480	20
Small tube	Nano seeds	5,310	170	31
Capillary	Nano seeds	4,550	210	22

^aMeasurement at 105 °C

The tubular supports were dipped vertically in an aqueous suspension of colloidal silicate-1 seed crystals (particle size 100 nm) and withdrawn at a speed of 1–2 cm/h to allow the uniform formation of seed layers on the outer (for stainless steel) or inner (for α -alumina) cylindrical surface of the support tubes. The seeded tubes were treated hydrothermally with clear solution of different compositions given in Table 3.21.

Aoki et al. [236] hydrothermally synthesized ZSM-5 zeolite (Si/Al=2,525 and 600). These membranes were ion exchanged with H⁺, Na⁺, K⁺, Cs⁺, Ca²⁺, and Ba²⁺.

Table 3.21 Molar compositions of clear solutions for secondary growth

Code	KOH	TPABr	TPAOH	SiO ₂	H ₂ O
A ^a	1.0	1.0	–	4.5	1,000
B ^a	–	–	3.0	25	1,500
C ^a	1.0	1.0	–	9.0	1,000
D ^b	1.6	2.0	–	40	1,000

^aSilica source is TEOS

^bSilica source is Ludox AS-40

Their gas permeation properties were measured over the temperature range of 323–523 K. Both the Si/Al ratio and the exchanged ion size affected the separation performance. For the membrane with a Si/Al ratio of 600, ion exchange only changed the single gas permeation of *i*-C₄H₁₀, because the number of exchange sites was small. For the membrane with Si/Al=25, single gas permeances increased for the exchanged forms in the order: K⁺ < Ba²⁺ ~ Ca²⁺ < Cs⁺ < Na⁺ ~ H⁺, which coincides with the decrease in ion size and only the Cs ion does not fit this trend. It was concluded that zeolite membranes can be ion exchanged without irreversibly damaging the membrane performance.

Tuan et al. [237] prepared boron-substituted ZSM-5 membranes on porous stainless-steel and α -alumina support. These membranes had higher *n*-C₄H₁₀/*i*-C₄H₁₀ separation selectivities, and effectively separated these isomer mixtures at higher temperatures than membranes with aluminum substituted into the framework. Membranes were prepared with Si/B ratios as low as 12, and the best membranes were prepared from alkali-free gels. The highest *n*-C₄H₁₀/*i*-C₄H₁₀ permselectivity was 60 at 473 K, and 24 at 527 K. It was also reported that B-ZSM-5 membrane preparation was reproducible and the membranes were stable at elevated temperatures.

Wang and Lin [238] fabricated a thin, high quality ZSM-5 top layer on a thick silicalite layer (bottom) to form a ZSM-5/silicalite bilayer membrane. The ZSM-5/silicalite bilayer membrane was supported on a porous alpha alumina support coated with an yttria stabilized zirconia (YSZ) intermediate barrier layer for membrane stability improvement. Both membranes were CCD (catalytic cracking deposition) modified using methyldiethoxysilane (MDES) as the precursor to reduce the zeolitic pore size for improving the H₂/CO₂ separation factor. Compared with the ZSM-5 zeolite membrane, the ZSM-5/silicalite bilayer membrane showed more improvement in H₂/CO₂ separation and less reduction in H₂ permeance by CCD modification. The CCD modified ZSM-5/silicalite bilayer zeolite membrane exhibited good stability and hydrogen separation performance.

Cheng et al. [239] studied the effects of synthesis parameters on the properties of a Ce-ZSM-5 zeolite membrane grown onto porous α -alumina supports. Under optimum synthesis conditions, the permeances for H₂, N₂, CH₄, and CO₂ were 4.73×10^{-6} , 1.56×10^{-6} , 1.51×10^{-6} , and 1.36×10^{-6} mol m⁻² s⁻¹ Pa⁻¹, respectively; the ideal selectivity of the membrane at room temperature for H₂/CO₂, H₂/N₂, and H₂/CH₄ were 3.13, 3.03, 3.48, respectively.

3.2.3.8 FAU-Type Zeolite

The FAU-type zeolite has relatively large pores, which are composed of 12-membered oxygen rings of approximately 0.74 nm in diameter. Thus, FAU-type zeolite membranes do not show strict molecular-sieving properties unlike the MFI-types, and separation by FAU-type zeolite membranes is usually achieved by differences in the adsorptivities of permeates. The larger pores of FAU-type zeolite membranes are, however, beneficial for higher permeation rates compared to the MFI- and LTA-type zeolite.

The FAU-type zeolite includes X- and Y-types, Si/Al ratios of which are 1–1.15 and 1.5–3.0, respectively; the number of cations that can be coordinated in the X-type structure is larger than that in the Y-type structure. It has been reported that the CO_2/N_2 reaches a maximum of approximately 100 for the NaY-type zeolite membrane on porous alumina at a permeation temperature of 308 K [240]. Hasegawa et al. [240] fabricated hydrothermally FAU-type zeolite membranes with different Si/Al ratios on the outer surface of a porous α -alumina support tube. The membranes were ion-exchanged with Rb^+ and K^+ ions, and their permeation properties were investigated by using equimolar mixtures of CO_2/CH_4 and CO_2/N_2 at 308 K. Permeances for single component system at a temperature of 308 K were in the order of $\text{CO}_2 > \text{N}_2 > \text{CH}_4$, and decreased with decreasing Si/Al ratio. Permeances and selectivities of CO_2 for the CO_2/CH_4 system were approximately half the values for the CO_2/N_2 system. The NaX-type zeolite containing Si/Al ratio 1.26 showed the maximum CO_2 selectivities, which were 28 for the CO_2/CH_4 system and 78 for CO_2/N_2 system, respectively. The effect of the ion-exchange was the highest for the NaY-type zeolite membrane. The CO_2 separation ability of the NaY-type zeolite membrane was further improved by ion exchange with K^+ . The CO_2/CH_4 selectivity of the KY-type zeolite membrane was in the range of 25–40, and CO_2 permeance was in the range of $(7.5\text{--}9.0) \times 10^{-7} \text{ mol m}^{-2} \text{ s}^{-1} \text{ Pa}^{-1}$.

Gu et al. [241] studied the effects of seeding methods, synthesis gel chemistry, and conditions of hydrothermal treatment on the FAU membrane quality in terms of the crystal phase purity and CO_2/N_2 separation performance. The membrane exhibited a CO_2 separation factor of 31.2 at room temperature for the equimolecular CO_2/N_2 dry mixture. The addition of water vapor to the mixture was found to significantly increase the selectivity for CO_2 above 110 °C, but decreased the CO_2 permeance. Kumar et al. [242] reported the removal of H_2S from mixtures containing N_2 , CO_2 , and CO by using zeolite X and Y in sodium form and ion-exchanged with silver and copper cations. Ag and Cu exchanged zeolite demonstrated very high H_2S adsorption capacities at room temperatures and in H_2S –He mixtures at 150 °C.

3.2.3.9 Hydroxy-Sodalite Zeolite Membrane (HDS-zeolite)

Hydroxy-sodalite has the same framework structure as sodalite and consists of the cubic array of beta-cages. It has a six-membered ring aperture with a pore size of 2.8 Å. Its pore size is smaller than that of the zeolites with an eight-membered ring

aperture, e.g., NaA zeolite. Only small molecules, such as helium and hydrogen, can enter into the pore of HDS-zeolite. Thus, HDS-zeolite membrane has a better performance on the separation of small molecules from gas mixtures than the zeolite membranes with a bigger pore size. Julbe et al. [243] synthesized a sodalite/ α -Al₂O₃ composite membrane by microwave heating (MAHS), which has a low He/N₂ permselectivity of 6.2 at 115 °C. Xu et al. [244] further explored the MAHS method for the synthesis of HDS membranes. They synthesized a high-quality pure HDS-zeolite membrane on an alpha-alumina support by a novel MAHS method. The pure HDS zeolite membrane was found to be well inter-grown and the thickness of the membrane was 6–7 μ m. Gas permeation results showed that the hydrogen/*n*-butane permselectivity of the HDS membrane was larger than 1,000. The authors claimed that the HDS zeolite membrane is a promising candidate for the separation of hydrogen from gas mixtures and important for the emerging hydrogen energy fuel system.

3.2.3.10 Zeolite T

Zeolite T with a Si/Al ratio of 3–4 is less hydrophilic than zeolite Y with a Si/Al ratio of less than 3. Zeolite T is an intergrowth-type zeolite of erionite and offretite, of which the pore sizes are 0.36 \times 0.51 nm and 0.67 \times 0.68 nm, respectively [245]. Zeolite T has both hydrophilic and fairly high acid resistant properties because of their proper Si/Al ratio. Chen et al. [246] described a new seeding method, namely, varying temperature hot-dip coating (VTHDC) for synthesis of zeolite T membrane. The authors revealed that the method was flexible and effective for combined control over the seed suspension concentration, seed size, and coating temperature, leading to better control of the seed layer over the seed size, thickness, and coverage defect.

Cui et al. [245] synthesized the T-zeolite membrane by hydrothermal synthesis on porous mullite tubes seeded with zeolite T crystals. Single gas and mixed-gas permeation experiments through zeolite-T membranes were carried out by a vacuum method at 303–473 K using He, H₂, CO₂, O₂, N₂, CH₄, C₂H₆, and C₃H₈ single component gases and CO₂/N₂, CO₂/CH₄, and other CO₂/hydrocarbon mixtures, respectively. In single-gas permeation experiments, with increasing kinetic diameters from 0.33 nm of CO₂ to 0.43 nm of C₃H₈, the gas permeation rate decreased by four orders. Permeance of CO₂ was much higher than those of N₂ and CH₄ and the ideal selectivities for CO₂/N₂ and CO₂/CH₄ were 31 and 266 at 343 K, respectively. In mixed-gas permeation, zeolite T membranes showed high selectivities for CO₂/N₂ and CO₂/CH₄ pairs of 107 and 400, respectively, at 308 K. The selectivity α decreased with an increase in temperature, but even at 473 K w still at high levels of 20 and 52 for CO₂/N₂ and CO₂/CH₄, respectively. This is due to the synergetic effects of competitive adsorption of CO₂ and molecular sieving of zeolitic pores. Because of the increasing effect of single file diffusion, the selectivities for CO₂/C₂H₆ (α =61) and CO₂/C₃H₈ (α =17) were rather low. Zeolite T showed excellent CO₂ separation performance for CO₂/N₂, and CO₂/CH₄ systems even at a high temperature of 473 K, mainly due to the molecular sieving effect.

3.2.3.11 Zeolite L

The crystal structure of the synthetic zeolite, Linde L, $K_6Na_3Al_9Si_{127}O_{72} \cdot 21H_2O$, was determined by Barrer and Villger [247]. The zeolite L is hexagonal with uni-cell dimensions $a = 18.4 \text{ \AA}$ and $c = 7.5 \text{ \AA}$. The minimum constricting aperture is defined by a ring of 12 tetrahedral atoms (T atoms, e.g., Si, Al) that forms an opening of 0.71 nm [248]. Zeolite L crystals contain a one-dimensional pore with an opening of 0.71 nm, which runs along its c -axis. The channel contains cationic sites, which can strongly interact with negatively charged or polarized molecules. Zeolite L can separate gas species by selective adsorption in addition to size discrimination. Zeolite L can be synthesized without the aid of an organic template, eliminating the strong agglomeration of the nano-sized zeolite particles at high temperature calcinations, which is beneficial to the homogeneous distribution of zeolite particles in the carbon matrix [249]. Yin et al. [249] fabricated thin zeolite L/carbon nanocomposite membranes. The results of CO_2 adsorption isotherms indicated that the zeolite L/carbon composite materials had greater CO_2 sorption ability than the pure carbon materials; therefore, the composite membranes can exhibit higher gas permeance and selectivities of CO_2/CH_4 and CO_2/N_2 than the pure carbon membranes. At 298 K, CO_2/CH_4 and CO_2/N_2 separation factors reached 43.59 and 27.21, respectively in experiments with gas mixtures; these results are higher than the 35.75 and 20.43 attained in the single gas permeation experiments.

3.2.3.12 ITQ-29 zeolite

Corma et al. [250] first introduced ITQ-29 as a zeolite with the same topological structure as zeolite A, but a much higher Si/Al ratio (up to infinity, i.e., pure silica), using a bulky organic template obtained from the self-assembly of two identical organic cationic moieties through π - π type interactions. Casado-Coterillo et al. [251] prepared ITQ-29 crystals and used in ITQ-29/polysulfone mixed-matrix-membranes for gas separation. The molar composition of the synthesis gels was:

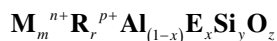
$(1-x)SiO_2:xGeO_2:0.25 \text{ ROH (4-methyl-2,3,6,7-tetrahydro-1H,5H-pyrido(3.2.1-ij) quinolium hydroxide):0.25 TMAOH (tetramethylammonium hydroxide):0.5 HF:yH}_2O$, where $x = 0-0.05$ and $y = 3-12$.

These membranes were used for the gas separation of H_2/CH_4 mixtures and showed promising results (highest H_2 permeability of 21.9 Barrer and a separation factor of 118 for the 4 wt% ITQ-29/polysulfone membrane) were obtained.

Pure-silica ITQ-29 is a hydrophobic small pore zeolite, which gives ITQ-29 the possibility of sieving and processing small organic molecules with high precision, even in the presence of water or other polar molecules. Al-free ITQ-29 was tested for N_2 , CH_4 , and propane, but the selectivity and the permeability were not very high [252]. ITQ-29 membranes prepared by using Kryptofix 222 as SDA (structure directing agent) and activated in situ in presence of oxygen at 300 °C, gave a separation factor of 127 for H_2/C_3H_8 separation [253].

3.2.3.13 UZM Zeolites

Moiscoso et al. [254] and Blackwell et al. [255] introduced a new family of crystalline alumino-silicate zeolites, named UZM. These zeolites are represented by the following empirical formula:



where M is an alkali or alkaline earth metal such as lithium and strontium, R is nitrogen containing organic cation such as tetramethyl ammonium, and E is a framework element such as gallium.

Recently Liu et al. [256] patented two methods for the preparation of small pore microporous UZM-5 zeolite membrane: (1) in situ crystallization of one or more layers of UZM-5 zeolite crystals on a porous membrane support; and (2) a seeding method by in situ crystallization of a continuous second layer of UZM-5 zeolite crystals on a seed layer supported on a porous membrane support. The membrane in the form of discs, tubes, or hollow fibers had superior thermal and chemical stability, good erosion resistance, high CO₂ plasticization resistance, and significantly improved selectivity over polymer membranes for gas, vapor, and liquid separation. Liu et al. [256] claimed that the microporous UZM-5 zeolite membranes are useful for liquid separation such as deep desulfurization of gasoline and diesel fuels, ethanol/water separation, and pervaporation dehydration of aqueous/organic mixtures; these membranes are also useful for a variety of gas and vapor separations such as CO₂/CH₄, CO₂/N₂, H₂/CH₄, and O₂/N₂. They can also be used for separating olefin/paraffins such as propylene/propane and iso/normal paraffins, polar molecules such as H₂O, and H₂S, and NH₃ mixtures with CH₄, N₂, H₂, and other light gases.

3.2.3.14 Zeolite W

Zeolite W is a synthetic zeolite that has the same framework topology as the mineral merlinoite (MER). It has an eight-membered ring (8MR); the channel dimensions are 0.31 × 0.35 nm, 0.27 × 0.36 nm, and 0.51 × 0.34 nm [257]. Membranes consisting of W-type zeolite have a unique nanopore structure which is stable at low pH. Mohammdi and Maghsoodloorad [258] fabricated W-type zeolite membranes on the surface of α-alumina (porous) via grown hydrothermally. Studies showed that maximum gas permeation flux (minimum ideal selectivity for O₂/SF₆ gas separation) was obtained for single layer membranes synthesized at 200 °C for 6 h. With changing synthesis temperature, synthesis time and number of layers, and keeping other effective parameters constant, maximum ideal selectivity of 20.1 for O₂/SF₆ gas separation was achieved using double layer zeolite membrane synthesized via Al₂O₃:SiO₂:K₂O:H₂O = 1.0:6.4:5.6:164.6 gel formula over the flat support at 185 °C for 18 h.

3.2.3.15 Zeolitic Imidazole Frameworks (ZIFs)

Zeolitic imidazolate frameworks (ZIFs) are three-dimensional structures consisting of rigid MN_4 tetrahedra (M =metal ion), linked through bridging imidazolate (Im) $C_3H_3N_2^-$ anions. Among numerous MOFs, zeolitic imidazole frameworks have drawn significant attention due to their superior chemical and thermal stability. They are very promising material to be used in gas storage and separation processes. This zeolite has sodalite topology with a six-member ring and is constructed by connecting zinc metal clusters with benzimidazole linker. The size of ZIF-7 pore openings is estimated to be 0.30 nm. Several ZIFs can be synthesized easily and fast and at low cost, such as ZIF-8, ZIF-90, and ZIF-7.

Several studies have investigated ZIFs, such as ZIF-8, ZIF-90, and ZIF-7, as porous fillers with various polymers, including polysulfone, Matrimid, PBI, and polyimide for MMMs for gas separation and pervaporation. Almost every report showed improved permeability, sometimes coupled with enhanced selectivity for gas separation [259]. Bae et al. [260] synthesized ZIF-90 particles and used them to fabricate nanocomposite membranes with three different poly(imide)s (Ultem, Matrimid, and 6FDA-DAM). The imidazole linker in ZIF-90 contains a carbonyl group which has a favorable chemical noncovalent interaction with CO_2 . The ZIF-90 crystals showed excellent adhesion with the poly(imide)s without any surface-compatibilization procedures. Interfacial voids were absent, and the MOF crystals were well dispersed. Figure 3.46 shows the pure-component CO_2 and CH_4 gas-transport properties of MMMs containing 15 wt% of ZIF-90 crystals. Ultem and Matrimid MMMs showed significantly enhanced CO_2 permeability without any loss of CO_2 - CH_4 selectivity. MMMs fabricated with 6FDA-DAM (a highly permeable polymer) showed substantial enhancement in both CO_2 permeability and CO_2/CH_4 selectivity, suggesting that the membrane is defect free and that permeabilities of the MOF and the polymer are well matched (Fig. 3.49).

Bux et al. [261] fabricated gas separating ZIF membranes, selective for H_2 over other gases via a novel microwave-assisted solvothermal process. The membrane achieved a fine balance between flux and selectivity compared to other MOF membranes. The hydrogen permeance of the novel MOF membrane with a relatively thick ZIF-8 layer was around 50 % of the hydrogen permeances of zeolite membranes of the same selectivity. Caro's group [262] fabricated an ultramicroporous imidazolate framework, ZIF-7 molecular sieve membrane on porous alumina support and tested for H_2 gas separation. ZIF-7 has many advantages for hydrogen separation: (1) its pore dimension approaches the size of H_2 , and therefore, a high H_2 selectivity could be obtained without any sophisticated pore-size engineering as is essential for zeolite membranes targeting H_2/CO_2 separation; (2) it is thermally stable for use at elevated temperatures (ZIF-7 is stable at least up to 500 °C in air); and (3) its hydrophobic property endows it with very high hydrothermal stability.

ZIF-69 membranes were also used for the separation of gases. Liu et al. [263] studied single gas permeation through ZIF-69 membranes by a vacuum method at room temperature using H_2 , CH_4 , CO , CO_2 , and SF_6 . The permeances were in the order of $H_2 > CO_2 > CH_4 > CO > SF_6$. The permselectivity of the CO_2/CO gas mixture

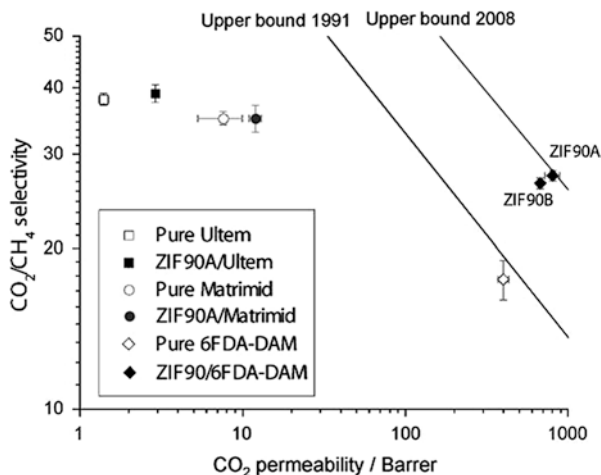


Fig. 3.49 Gas-permeation properties of mixed-matrix membranes containing 15 wt% of ZIF-90 crystals obtained from experiments with pure gases. (Measurements were performed at 35 °C and 4.5 atm upstream pressure for Ultem and Matrimid membranes, and at 25 °C and 2 atm upstream pressure for 6FDA-DAM membranes. The data for pure Ultem and Matrimid are averaged values from the literature. The upper bounds for polymer membrane performance as defined in 1991 and 2008 are shown [260])

at room temperature was 3.5 ± 0.1 with CO₂ permeance of $3.6 \pm 0.3 \times 10^{-8}$ mol m⁻² s⁻¹ Pa⁻¹. Venna and Carreon [264] synthesized thin ZIF-8 membranes with around 5–9 μm thicknesses by secondary seeded growth on tubular α-Al₂O₃ porous supports. The separation performance of these membranes for equimolecular CO₂/CH₄ gas mixtures was demonstrated. The membrane displayed unprecedented CO₂ permeance as high as $\sim 2.4 \times 10^{-5}$ mol m⁻² s⁻¹ Pa⁻¹ with CO₂/CH₄ selectivities of ~ 4 – 7 and separation indexes $\pi \left\{ \pi = (P_{\text{CO}_2} \times (\text{selectivity} - 1)) \times \text{Permeation pressure} \right\}$ in the ~ 6.5 – 10 range at 295 K, and a feed pressure of 139.5 KPa.

3.2.3.16 Other Zeolitic Type or Ceramic/Inorganic Membranes

Sandström et al. [265] used an MFI membrane comprising an approximately 0.7 μm silicate-film on a fully open and graded porous alumina support to separate CO₂/H₂, CO₂/CO/H₂, and CO₂/CH₄ mixtures at high pressures. CO₂ fluxes up to 657 kg m⁻² h⁻¹ were observed, which are many times larger than those previously reported for any zeolite membrane. The very high fluxes were a result of low film thickness, open support, high pressure, relatively high diffusivity, molecular weight and pressure drop. The maximum CO₂/H₂ ideal selectivity was 32.1, which was observed at 1,000 kPa feed pressure, a permeate pressure of 200 kPa and a temperature of 275 K. The highest measured CO₂ permeance for the binary CO₂/H₂ mixture was 93×10^{-7} mol m⁻² s⁻¹ Pa⁻¹. The membrane was also CO₂ selective for a CO₂/CO/H₂ mixture. However, both the

CO₂ flux and the CO₂/H₂ separation factor were reduced slightly in the presence of CO, probably as a result of competing adsorption between CO and CO₂. The highest measured CO₂/CH₄ separation factor was 4.5.

Nair et al. [266] discussed the results on the separation of close boiling point hydrocarbon mixtures by means of zeolite membranes. In the case of silicate membranes (MFI), the selectivity was found to depend on the microstructure. Permeation of xylene isomers through the silicate membranes occurred through both zeolitic and non-zeolitic (intercrystalline) nanopores. The faujasite membranes were found to have high selectivities (40–150) for the separation of binary mixtures containing one aromatic component, and modest selectivities (4–9) for the separation of unsaturates from saturated low-molecular-weight hydrocarbons.

Choi et al. [116] synthesized composites of polybenzimidazole (PBI) with proton-exchanged AMH-3 (a silicate with three-dimensional microporous layers) and swollen AMH-3. Proton-exchanged AMH-3 was prepared under mild conditions by the ion exchange of Sr and Na cations in the original AMH-3 using aqueous solution of DL-histidine. Swollen AMH-3 was prepared by sequential intercalation of dodecylamine following the ion exchange in the presence of DL-histidine. Both silicate materials were introduced into a continuous phase of PBI as a selective phase. Mixed matrix nano-composite membranes, prepared under certain casting conditions, with only 3 wt% of swollen AMH-3 presented a substantial increase of hydrogen/carbon dioxide ideal selectivity at 35 °C, i.e., by a factor of more than 2 compared to pure PBI membranes (40 vs. 15). Similar ideal selectivity was observed using higher loadings (e.g., 14 %) of proton-exchanged AMH-3 particles, suggesting that transport of hydrogen is faster than carbon dioxide in AMH-3-derived silicates. However, the ideal selectivity of MMMs approaches that of a pure polymer as the operating temperature increases to 100 °C and 200 °C.

By using the stepwise deposition method, Bétard et al. [267] fabricated membranes from MOF **1** and **2**, using macroporous alumina and titania as supports. SEM images (Fig. 3.50) reveal that the MOF crystallites have grown on the support surface and also up to 30 μm deep inside the support pores, where they form a foam-like, lamellar structure.

Figure 3.51 shows permeances from MOF **1** in the range of 10⁻⁸ mol m⁻² s⁻¹ Pa⁻¹ for both CO₂ and CH₄ which moderately increase with increasing pressure. Particularly at lower pressure, obvious reductions of mixed gas permeances occur compared to the pure gas.

Figure 3.52 shows the permeances of pure and equimolar mixed CO₂ and CH₄ measured for the [Cu₂(BME-bdc)₂(dabco)]_n.

The CO₂ and CH₄ permeance of the membrane **2** (Fig. 3.52) are of the same order of magnitude as the permeances of the membrane **1**. It should be noted that the selectivity is less than unity for membrane **1**, while it is more than unity for membrane **2**. Bennett et al. [268] studied the ZIF-4, a metal organic framework (MOF) with a zeolitic structure, and suggested an avenue for designing broad new families of amorphous and glasslike materials that exploit the chemical and structural diversity of MOFs. Microporous metal organic framework (MMOF) membranes on porous alumina supports, synthesized by the seeded growth method, showed moderate ideal selectivity for H₂/N₂ [269].

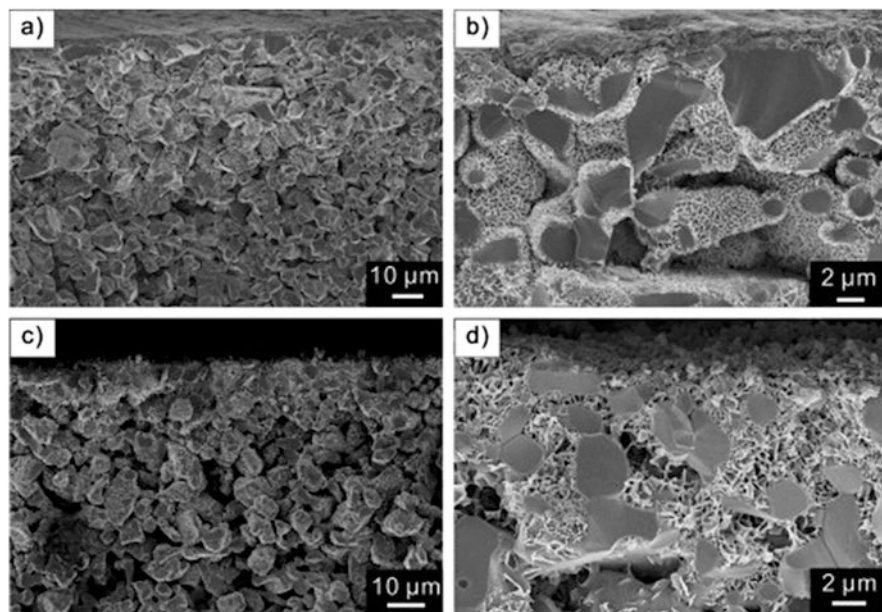


Fig. 3.50 Representative examples of SEM micrographs of the cross-sections of $[\text{Cu}_2(\text{ndc})_2(\text{dabco})]_n$. (1) On alumina (a, b) and $[\text{Cu}_2(\text{BME-bdc})_2(\text{dabco})]_n$ (2) on titania substrates (c, d) at different magnifications. (The morphology of the resulting MOF crystals seems to be independent of the support type)

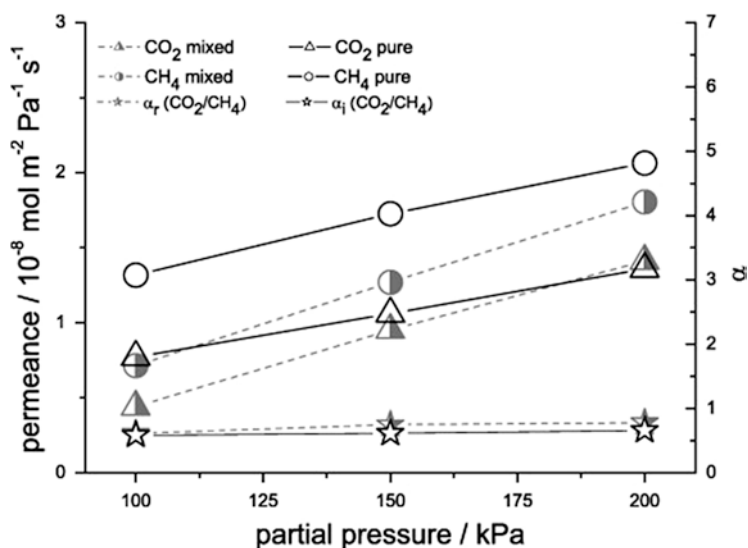


Fig. 3.51 Permeances of pure and equimolar mixed CO_2 and CH_4 measured for the $[\text{Cu}_2(\text{ndc})_2(\text{dabco})]_n$. (1) Membrane at room temperature ($T=298\text{ K}$) as function of pressures at the feed side (total pressures for pure gases, partial pressures for the gas mixture). The ideal and mixed gas separation factor α_i and α_T were calculated from the corresponding ratio of the CO_2/CH_4 permeances

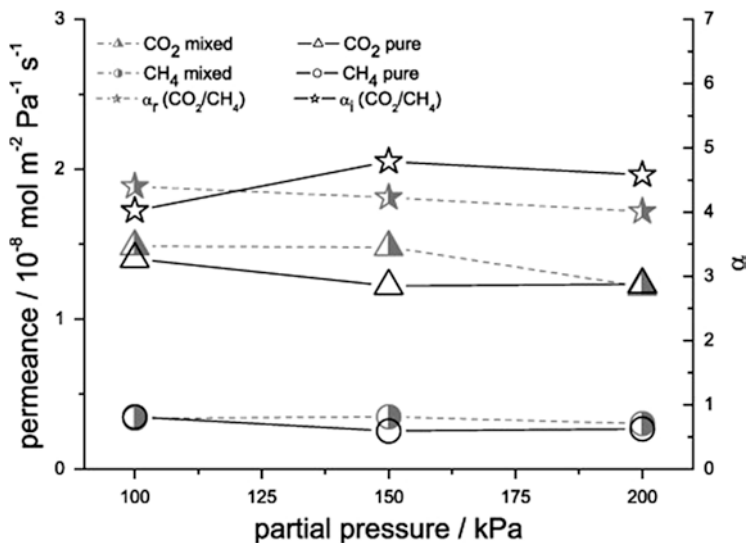


Fig. 3.52 Permeances of pure and equimolar mixed CO₂ and CH₄ measured for the [Cu₂(BME-bdc)₂(dabco)]_n. (2) Membrane at room temperature ($T=298$ K) as function of pressures at the feed side (total pressures for pure gases, partial pressures for the gas mixture). (The ideal and mixed gas separation factor α_i and α_r were calculated from the corresponding ratio of the CO₂/CH₄ permeances)

Bohrman and Carreon [270] used metal–adeninate biometal organic frameworks (Bio-MOFs) for the separation of a CO₂/CH₄ mixture. Bio-MOFs were introduced by Rosi's group [271, 272]. Bio-MOFs have permanent microporosity, high surface areas, chemical stability, and exceptional CO₂ adsorption capacities due to the presence of basic bio-molecule building units. In particular, Zn₈(ad)₄(BPDC)₆O·2Me₂NH₂ (where ad=adeninate, BPDC=biphenyldicarboxylate, denoted as Bio-MOF-1), a three-dimensional metal organic framework with infinite-adeninate columnar secondary building units (SBUs) which are interconnected via biphenyldicarboxylate linkers, is an attractive material with great potential for CO₂ separation if prepared in a membrane form. These membranes displayed high CO₂ permeances and separation ability for CO₂/CH₄ gas mixtures. The observed CO₂/CH₄ selectivities above the Knudsen selectivity indicated the separation was promoted by preferential CO₂ adsorption over CH₄. The preferential CO₂ adsorption was attributed to the presence of adeninate amino basic sites present in the Bio-MOF-1 structure. However, selectivity was slightly below in Robeson plot for CO₂/CH₄ mixtures [3]. Table 3.22 shows the CO₂/CH₄ separation performance of the stainless-supported Bio-MOF-1 membranes.

Xomeritakis et al. [273] demonstrated a novel and efficient method for molecular engineering of the pore size and porosity of microporous sol–gel silica membranes. The addition of a suitable organic template (e.g., tetraethyl- or tetrapropylammonium bromide) in polymeric silica sols resulted in pores in the range of 5–6 Å.

Table 3.22 CO₂/CH₄ separation performance of Bio-MOF-1 membranes at a pressure drop of 138 kPa and 298 K [271, 272]

Permeance mol m ⁻² s ⁻¹ Pa ⁻¹ (×10 ⁻⁷)			
Membrane ^a	CO ₂	CH ₄	CO ₂ /CH ₄ selectivity
M1 (3)	11.5	4.6	2.5
M2 (3)	11.9	4.6	2.1
M3 (4)	10.5	4.8	2.6
M4 (7)	5.8	4.7	–

^aNumber in parentheses indicate number of layers

In general, without any modification, the pore size of the synthetic zeolites will be in the range of 3–4 Å. With pore sizes of 5–6 Å, sol–gel silica membranes are useful for hydrocarbon isomer separations. The templated membranes exhibit as high as 10⁻⁷–10⁻⁶ mol m⁻² s⁻¹ Pa⁻¹ for molecules with $d_k < 4.0$ Å (e.g., CO₂, N₂, CH₄), coupled with single-component selectivities of 100–1,800 for N₂/SF₆, 20–40 for *n*-butane/*iso*-butane, and 10–20 for *para*-xylene/*ortho*-xylene. The unique features of this new approach include simple, fast and scalable processing under ambient conditions, and demonstrate the possibility to tune membrane pore size and porosity by proper choice of the type and amount of template.

Dual-layer polyethersulfone (PES)-zeolite beta/BTDA-TDI/MDI co-polyimide (P84) composite hollow fibers, were applied to fabricate dual layer nanocomposite hollow fiber membranes through pyrolysis by Li and Chung [274]. After pyrolysis at 800 °C, these nanocomposite hollow fibers exhibited a significantly enhanced O₂/N₂ and CO₂/CH₄ selectivity of 11.3 and 152, respectively in the pure gas measurement. It was also noticed a comparable CO₂/CH₄ selectivity of 140 in the mixed gas measurement. The authors claimed that these dual-layer hollow fibers are a potential type of excellent membrane material for oxygen enrichment and natural gas separation in industrial applications.

Zeolite membranes were synthesized by the dry gel method, using a tubular support of stainless steel by Alfaro and Valenzuela [275]. The composition of the precursor gel was 0.22Na₂O:10SiO₂:280H₂O:0.5TPABr (tetrapropylammonium bromide). It was observed that the amount of each hydrocarbon that permeated from the mixture of hydrocarbons was as follows: *n*-C₄H₁₀ > *i*-C₄H₁₀ > C₃H₈ > C₂H₆ > CH₄. The separation factor measured for the N₂/SF₆ ratio was five times higher than the theoretical one. This improved selectivity to N₂ was explained in terms of properties such as the pore size of the membrane, controlling Knudsen-type diffusion. In hydrocarbon separation of natural gas, *n*-butane showed the higher concentration in the permeated side of the membrane.

Kuznicki [276] synthesized a new class of molecular sieve materials, which are generally denoted as Engelhard titano-silicates (ETS). Unlike zeolites their frameworks are built by corner sharing SiO₄ tetrahedra and TiO₆ octahedra, resulting in new structures that cannot be built by connecting only tetrahedral units, the framework units of zeolites. The ETS materials contain a channel system like zeolites which, in principle, enables them to be used in similar molecular sieve and/or

adsorptive separations. Membranes consisting of thin intergrown layer of Na-ETS-4 on porous titania supports were highly water permselective with selectivities as high as 400 and a corresponding water flux of $0.01 \text{ mol m}^{-2} \text{ s}^{-1}$ in room temperature pervaporation experiments using 1:1 water/ethanol mixtures. With increasing water content in the feed solution (in the range of 10–90 %) the water flux was increasing linearly, while the selectivity did not vary significantly. The selectivity of the ETS-4 membranes was similar to the highest reported for Na-X and Na-Y membranes. These Na-ETS-4 membranes may find applications in pervaporation as well as separation of permanent gases.

Stoeger et al. [277] fabricated highly c-oriented, intergrown, continuous crystalline aluminophosphate $\text{AlPO}_4\text{-5}$ and $\text{CoAlPO}_4\text{-5}$ (both of the AFI framework type) films, grown on porous α -alumina by the seeded method. The membrane quality was inspected through pervaporation measurements consisting of a liquid hydrocarbon feed of *n*-heptane and 1,3,5-triisopropylbenzene. It was observed that the separation factor was 2.8 with a corresponding flux of $1.2 \text{ kg m}^{-2} \text{ h}^{-1}$. However, further investigation is needed, focusing on growth, calcination, and microstructure optimization.

MER type zeolite was investigated by Nagase et al. [278]. The micropore structure of MER-type zeolite comprises double-eight rings and γ -cage, and pore diameter is 0.27–0.51 nm. The MER (merlinoite) zeolite membranes are relatively acid tolerant in the low-silica 8MR zeolite group, and the low-SAR type. MER membranes exhibit high water selectivity for pervaporation of 90 % acetic acid solution. The separation factor of the membrane is as high as that of the LTA-type zeolite membrane (more than 5,000). However, the dehydration performance and permeation mechanism of the membrane are not clear. Hasegawa et al. [279] determined the stabilities and dehydration performances of MER-type zeolite membranes prepared on porous α -alumina tubes by the secondary growth of seed crystals ($\text{SiO}_2/\text{Al}_2\text{O}_3=4.7$). The membranes showed relatively high stability, permeability, and separation performances. The permeation flux and separation factors were $1.9 \text{ kg m}^{-2} \text{ h}^{-1}$ and 9,300, respectively, for an equimolar mixture of ethanol and water at 350 K. Membranes were also used for the dehydration of several organic solvents (methanol, *n*-propanol, *i*-propanol, and acetone) containing water. It was noticed that the separation factor increased with the molecular diameter of the organic solvents.

Kim et al. [280] investigated modified MFI-type zeolite membranes as high-temperature water-gas shift (WGS) membrane reactors (MRs) using nanocrystalline Fe/Ce WGS catalyst. The effects of the MR operating conditions and the membrane separation performance on the CO conversion (χ_{co}) were studied experimentally and by calculations using an ample one-dimensional plug-flow reactor (PFR) model. The model calculations indicated that the membrane had the potential to achieve high CO conversion of $\chi_{\text{co}} > 99 \%$ under practical operating conditions. Due to its excellent hydrothermal stability and chemical resistance, the modified MFI-type zeolite membranes are potentially useful for constructing MR for high temperature WGS reaction of coal-derived syngas.

Recently, UK researchers have developed a porous material named NOTT-202 that can soak up CO₂ from the atmosphere. NOTT-202 is a “metal–organic framework” that works like a sponge, absorbing a number of gases at high pressures. But as the pressure is reduced, CO₂ is retained as other gases are released [281]. Solvothermal reaction of H₄L (biphenyl-3,3',5,5'-tetra(phenyl-4-carboxylic acid)) (Fig. 3.50) with In(NO₃)₃ in an acidic (HNO₃) mixture of CH₃CN/DMF(dimethylformamide) (v/v = 1:2) at 90 °C affords the solvated framework complex Me₂(NH₂)_{1.75} [In(L)]_{1.75}(DMF)₁₂(H₂O)₁₀ (NOTT-202). The counter-cation Me₂NH₂⁺ is generated by in situ decomposition of the DMF solvent during the reaction.

The unique partially interpenetrated metal–organic framework (MOF) NOTT-202 represents a new class of dynamic material that undergoes pronounced framework phase transition on desolvation. NOTT-202 consists of two MOF networks attached to a central indium metal atom and overlaid in such a way as to leave gaps where the carbon dioxide is stored. This discovery holds promise for carbon dioxide capture and storage, or even for removing CO₂ from the exhaust gases of power plants and factories. However, there are some drawbacks to the material, i.e., its stability in the presence of high-temperature water vapor is questionable. Large-scale production of this type of material has long been considered a major challenge [282, 283]. Table 3.23 shows the gas permeation/separations by using different types of zeolites.

3.3 Metal–Organic Framework Membranes for Gas Separations

Metal–organic frameworks (MOFs) are a relatively new class of hybrid materials consisting of organic and inorganic moieties in crystalline lattice. Pore size tailorability combined with tunable sorption behavior provides promising avenues for applications of MOFs as membranes for gas separation applications. Synthesis conditions are less energy intensive as compared to zeolites. For instance, most MOFs do not require high-temperature/pressure conditions for their fabrications and can be synthesized using click chemistry. Also, unlike zeolites, structure-directing agents are not required; therefore, a subsequent calcination step is not necessary [284]. This new class of porous material is attracting attention due to demonstration of their large pore sizes, high apparent surface areas, and selective uptake of small molecules. Most important is that their synthesis from molecular building blocks holds the potential for directed tailoring of these properties [285]. MOFs consist of metal–oxygen polyhedral, interconnected with a variety of organic linker molecules, resulting in tailored nanoporous materials. With a judicious choice of organic linker groups, it is possible to fine-tune size, shape, and chemical functionality of the cavities and the internal surfaces. This unique structural feature offers unprecedented opportunities in small-molecule separation as well as chiral separations [286]. MOF membranes are polycrystalline in nature just like zeolite membranes.

Table 3.23 Gas permeation/separation by using different types of zeolites

Permeation/separation of gases	Reference
<i>LTA zeolite</i>	
H ₂ , CO ₂ , N ₂ , CH ₄ , C ₃ H ₈ , H ₂ /CO ₂	[205]
H ₂ , CO ₂ , N ₂ , CH ₄ , C ₃ H ₈	[206]
<i>Zeolite NaA, Faujasite</i>	
H ₂ , O ₂ , N ₂ , H ₂ / <i>n</i> -C ₄ H ₁₀	[207, 208]
He, H ₂ , CO ₂ , N ₂ , CH ₄ , O ₂ , C ₃ H ₈ , H ₂ /N ₂	[209, 210]
CO ₂ , N ₂ , H ₂	[211]
<i>DDR type zeolite</i>	
H ₂ , CO ₂ , N ₂ , CH ₄ , O ₂ , CO, propane, propylene	[213]
CO ₂ , N ₂ , and CH ₄ and their mixtures	[214, 215]
He, H ₂ , CO ₂ , N ₂ , CH ₄ , O ₂ , C ₃ H ₈ , <i>n</i> -butane, <i>i</i> -butane, and sulfur hexafluoride	[216]
He, H ₂ , CO, CO ₂	[217]
CO ₂ , CH ₄ , He, H ₂ , O ₂ , and N ₂ , and CO ₂ /CH ₄	[219]
<i>SAPO-34</i>	
CO ₂ /H ₂ , H ₂ /CH ₄	[223–228]
<i>AlPO-18</i>	
CO ₂ /CH ₄	[229]
<i>Beta zeolite or ZSM Zeolite (MFI Zeolite Membranes (ZSM-5))</i>	
CO ₂	[231]
He, N ₂ , <i>n</i> -C ₄ H ₁₀ / <i>iso</i> -C ₄ H ₁₀	[232]
H ₂ , CO ₂	[233]
H ₂ /CH ₄ , H ₂ /CO ₂	[234]
H ₂ /SF ₆	[236]
<i>i</i> -C ₄ H ₁₀	[236]
<i>n</i> -C ₄ H ₁₀ / <i>i</i> -C ₄ H ₁₀	[237]
H ₂ /CO ₂	[238]
H ₂ , N ₂ , CH ₄ , CO ₂	[239]
<i>FAU-type zeolite</i>	
CO ₂ /N ₂ , CO ₂ /CH ₄	[240]
CO ₂ /N ₂	[241]
N ₂ , CO ₂ , CO, H ₂ S/He	[242]
<i>Hydroxy-sodalite zeolite membrane (HDS-zeolite)</i>	
He, H ₂ , N ₂	[243]
H ₂ / <i>n</i> -butane	[244]
<i>T-Zeolite</i>	
He, H ₂ , CO ₂ , O ₂ , N ₂ , CH ₄ , C ₂ H ₆ , C ₃ H ₈ , CO ₂ /N ₂ , CO ₂ /CH ₄	[245]
<i>L Zeolite</i>	
CO ₂ /CH ₄ and CO ₂ /N ₂	[249]
<i>ITQ-29 Zeolite</i>	
H ₂ /CH ₄	[251]
N ₂ , CH ₄ , propane	[252]
H ₂ /C ₃ H ₈	[253]

(continued)

Table 3.23 (continued)

Permeation/separation of gases	Reference
<i>UZM Zeolites</i>	
CO ₂ /CH ₄ , CO ₂ /N ₂ , H ₂ /CH ₄ , O ₂ /N ₂ , olefin/paraffin such as propylene/propane, iso/normal paraffin, polar molecules such as H ₂ O, H ₂ S, and NH ₃ mixtures with CH ₄ , N ₂ , H ₂ , and other light gases	[256]
<i>W-Type zeolite</i>	
O ₂ /SF ₆	[258]
<i>Zeolitic imidazole frameworks (ZIFs)</i>	
CO ₂ , CO ₂ /CH ₄	[260]
H ₂ over other gases	[261, 262]
H ₂ , CH ₄ , CO, CO ₂ , SF ₆	[263]
CO ₂ /CH ₄	[264]
<i>Other zeolitic type or ceramic/inorganic membranes</i>	
CO ₂ /H ₂ , CO ₂ /CO/H ₂ , CO ₂ /CH ₄	[265, 267]
CO ₂ /CH ₄	[270]
CO ₂ , N ₂ , CH ₄	[273]
CO ₂ /CH ₄	[274]
CH ₄ , C ₂ H ₆ , C ₃ H ₈ , <i>n</i> -C ₄ H ₁₀	[275]

The first MOF membranes were reported in 2009 by the Lai and Jeong groups [286, 287]. Like zeolite, fabrication of thin films of crystalline framework materials follows one of two approaches, in situ growth and secondary or seeded growth [197]:

1. In situ growth: substrate is immersed in the growth solution without any crystals previously attached to the surface, and during the fabrication, nucleation, growth, and intergrowth of crystals on the substrate will happen.
2. Secondary or seeded growth: refers to film growth from preattached seed crystals. The advantage of this method is to make tailored membrane.

Other methods for the fabrication of MOF membranes have been reported, such as chemical modification of the support surfaces with self-assembled monolayers [197]. Klinowski et al. [288] discussed microwave heating for the preparation of MOF membranes. Macroscopic or microscopic cracks in polycrystalline films can form for a number of reasons and will likely ruin membrane performance for gas separation. In the preparation of MOF membranes the prevention of cracks is a subject of importance. Mixed matrix membranes (MMMs) with MOFs are a new class of membranes.

Hu et al. [289] developed a facile reactive seeding (RS) method for the preparation of continuous MOF membranes on alumina porous supports, in which the porous supports acted as the inorganic source reacting with the organic precursor to grow a seeding layer. Figure 3.53 shows the schematic of the RS method with the MIL-53 membrane as an example. In this technique, α -Al₂O₃ support itself acts as the aluminum precursor in place of Al(NO₃)₃·9H₂O, which reacts with 1,4-benzenedicarboxylic acid (H₂BDC) under mild hydrothermal conditions to

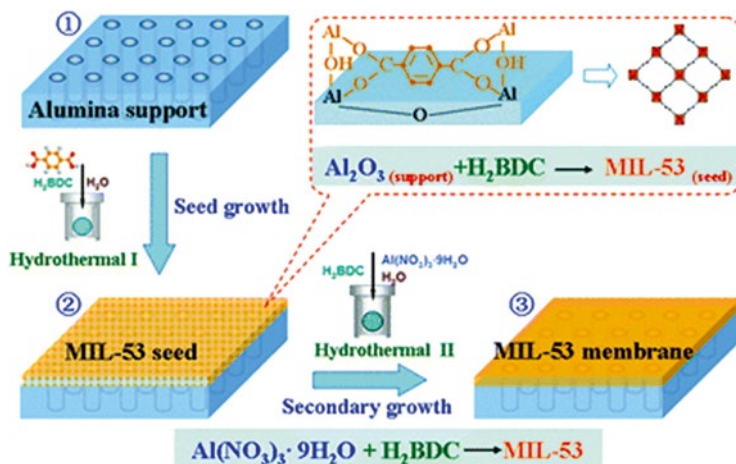


Fig. 3.53 Schematic diagram of preparation of the MIL-53 membrane on alumina support via the RS method

produce a seed layer. This is followed by a secondary growth process when $\text{Al}(\text{NO}_3)_3 \cdot 9\text{H}_2\text{O}$ and H_2BDC form the MIL-53 membrane under hydrothermal conditions (typical synthesis condition: 220 °C for 12 h).

Schoedel et al. [290] demonstrated that the gel-layer approach enables the synthesis of differently oriented MOF structures on functionalized gold surfaces at room temperature. Lu and Zhu [291] developed a method for MOF membrane preparation based on a liquid–liquid interfacial coordination mechanism. For example, MOF precursors, zinc nitrate and terephthalic acid (TPA or H_2BDC) as well as catalyst triethylamine (TEA), were dissolved in two immiscible solvents, dimethylformamide (DMF) and hexane. The reaction of $\text{Zn}(\text{NO}_3)_2$ and TPA in DMF was catalyzed by TEA in hexane at the solvent interface, thus forming a free-standing membrane. Ben et al. [292] reported a convenient and universal method to prepare MOF membranes. The polymer-supported and free-standing MOF membrane preparation is illustrated in Fig. 3.54.

In a typical procedure, preparations of the HKUST-1 membrane, polymethyl methacrylate (PMMA) are dissolved in chloroform and then spin-coated onto a silica wafer, which serves as a shape template substrate. When the solvent is evaporated, the PMMA-coated substrate is immersed into 12 M sulfuric acid for 20 s to hydrolyze the external PMMA into polymethacrylic acid (PMAA). After careful washing with deionized water, the PMMA–PMAA–silica substrate is introduced into a water/ethanol solution (1:1, v/v) of $\text{Cu}(\text{NO}_3)_2 \cdot 3\text{H}_2\text{O}$ and trimesic acid in a Teflon-lined autoclave where crystal intergrowth takes place at 120 °C for 3 days. Then, the membrane is washed several times with ethanol and dried at room temperature.

As shown in Fig. 3.55 polymer-inorganic nanocomposite membranes can be classified into two types according to their structure: (a) polymer and inorganic phases connected by covalent bonds and (b) polymer and inorganic phases connected by van der Waals force or hydrogen bonds [293].

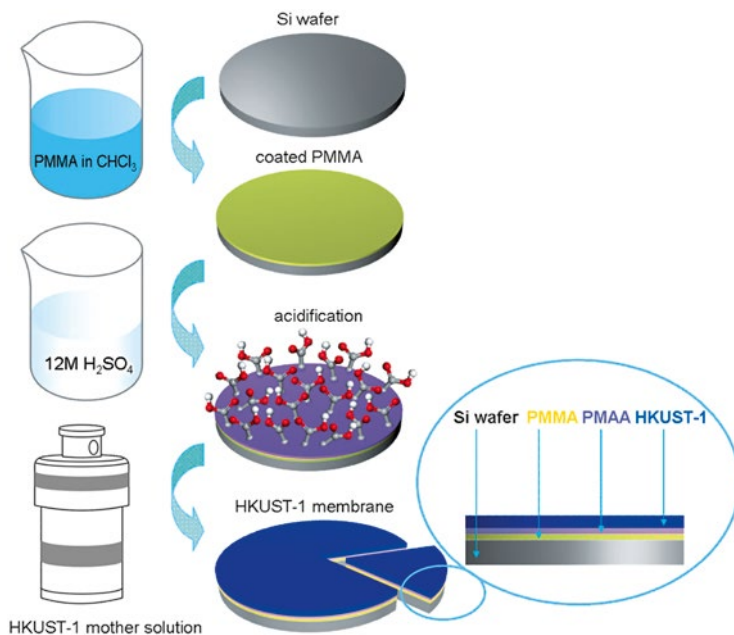


Fig. 3.54 Schematic illustration of the preparation procedure for the free-standing HKUST membrane

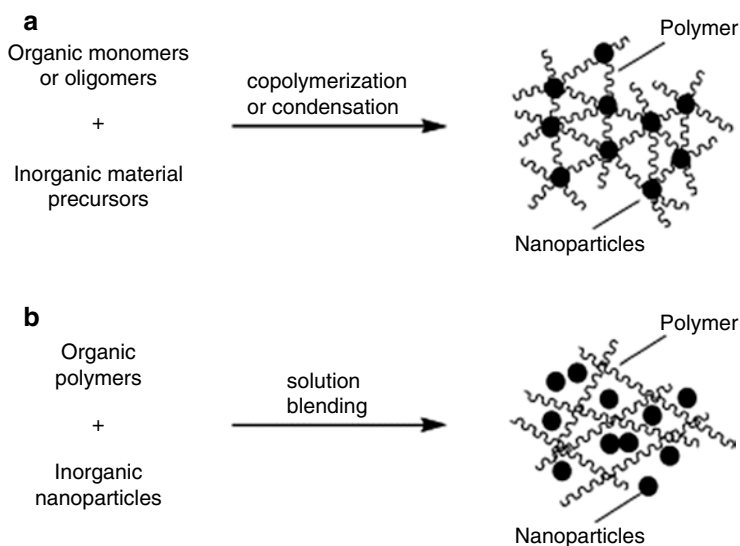
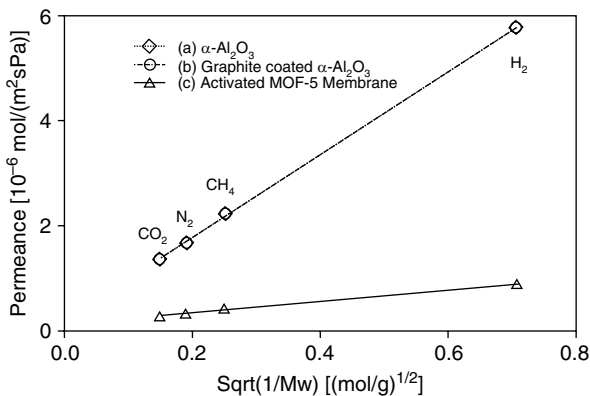


Fig. 3.55 Illustration of different types of polymer–inorganic nanocomposite membranes. (a) Polymer and inorganic phases connected by covalent bonds and (b) polymer and inorganic phases connected by van der Waals force or hydrogen bonds

Fig. 3.56 Permeation of various gas molecules. (a) α -Alumina support, (b) graphite-coated α -alumina support, and (c) activated randomly oriented MOF-5 membrane (note that three membrane samples were prepared under the same condition and their performance was tested and plotted) [286]



Yoo et al. [286] fabricated MOF-5, or IRMOF-1 (isoreticular metal–organic framework 1, consisting of four Zn_4O clusters in octahedral subunits interconnected with benzene dicarboxylate linkers to form a three-dimensionally porous open framework structure) membranes on porous α -alumina substrate by secondary growth method. Figure 3.56 [288] shows the permeance of gas molecules as a function of their molecular weight. First, the permeation through graphite coated α -alumina substrate is compared with that of bare α -alumina, confirming that there is no resistance to permeation of gas molecule due to the presence of thin graphite powders on the substrate surface. Both substrates show Knudsen diffusion behavior (i.e., the permeance is proportional to $1/\sqrt{Mwt}$). Permeation of gas molecules through the activated MOF-5 membranes indicates the behavior of the Knudsen diffusion process.

Bétard et al. [267] fabricated a metal–organic framework (MOF) membrane by stepwise deposition of reactants. Two pillared layered MOFs with the general formula $[Cu_2L_2P]_n$ (L =dicarboxylate linker, P =pillaring ligand) were selected. For this demonstration, they selected the nonpolar $[Cu_2(ndc)_2(dabco)]_n$ (**1**: ndc =1,4-naphthalene dicarboxylate; $dabco$ =1,4-diazabicyclo(2,2,2)octane) and the polar $[Cu_2(BME-bdc)_2(dabco)]_n$ (**2**: $BME-bdc$ =2,5-bis(2-methoxyethoxy)-1,4-benzene dicarboxylate). The framework structure of **1** is shown in Fig. 3.57.

The performances of both membranes were evaluated in gas separation experiments of CO_2/CH_4 (50:50) mixtures using a modified Wicke–Kallenbach technique. The separation-active MOF layer was located inside the macroporous support in a depth ranging in the μm scale. The microstructures of the MOF-based membranes resemble a foam with the inter-grown lamellae as transport-selective membrane. Proof of principle that the functionalization of linker can induce CO_2 membrane selectivity was found.

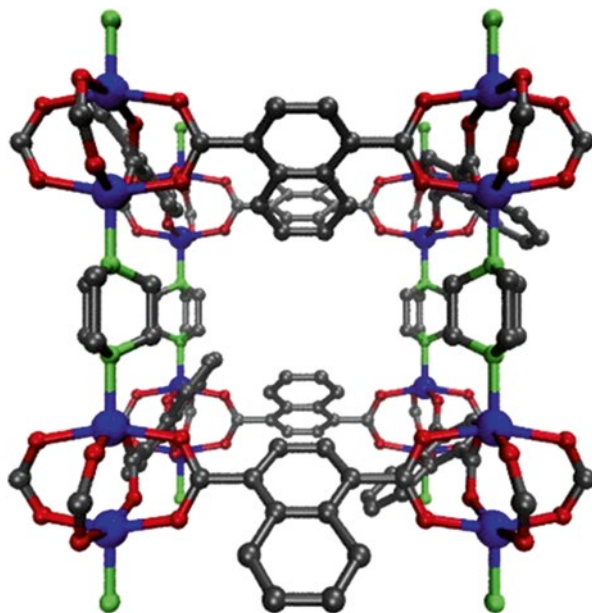


Fig. 3.57 Structure of $[\text{Cu}_2\text{L}_2\text{P}]_n$ MOFs (here $\{\text{Cu}_2(\text{ndc})_2(\text{dabco})\}_n$). (1) With linker $\text{L}=\text{ndc}$ (1,4-naphthalenedicarboxylate) and ligand $\text{P}=\text{dabco}$ (1,4-diazabicyclo(2,2,2)octane) seen in $[100]$ direction. (Structure 2 is quite similar to 1 by just replacing ndc by BME-bdc (see Fig. 3.58))

3.4 Mixed Matrix Membranes (MMMs)

Gas separation by selective transport through polymeric membranes is one of the fastest growing branches of membrane technology. However, the existing polymeric membrane materials are inadequate to fully exploit the application opportunities on an industrial scale: the improvement in permeability is at the expense of selectivity, and vice versa. New types of membrane material emerging, with the potential for future applications, are mixed-matrix materials composed of homogeneously interpenetrating polymeric and inorganic particle matrices.

Robeson [3] predicted the upper limits for the performance of polymeric membranes in gas separation. The performance of various materials available for the separation of O_2/N_2 is depicted in Fig. 3.59. The figure presents both the permeability of the fast gas oxygen on the abscissa and O_2/N_2 selectivity on the ordinate, on a logarithmic scale. For the polymeric materials, either rubbery or glassy, a rather general trade-off exists between permeability and selectivity, with an *upper bound line* shown in Fig. 3.59.

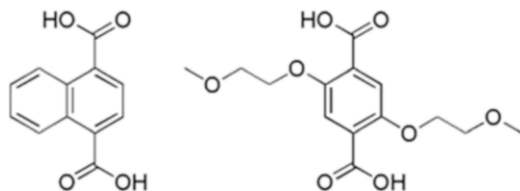
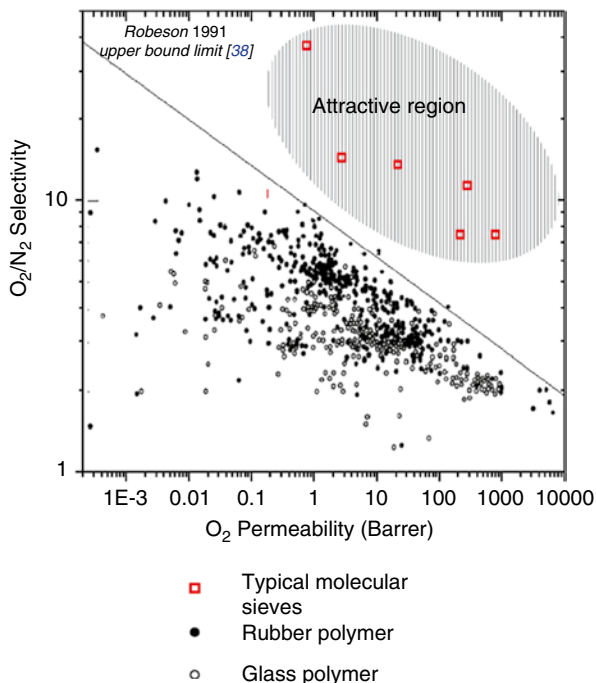


Fig. 3.58 Dicarboxylic acid linkers used in this work. *Left*, H₂ndc (ndc: 1,4-naphthalene dicarboxylate) and *right*, H₂BME-bdc (BME-bdc: 2,5-bis(2-methoxyethoxy)-1,4-benzene dicarboxylate)

Fig. 3.59 Relationship between the O₂/N₂ selectivity and O₂ permeability for polymeric membranes. (The dots indicates the performance of polymeric materials [3])



When the materials with separation properties near this limit were modified on the traditional structure–property relation, the points specific to the modified materials tracked along this line but did not exceed it. The inorganic materials have the properties lying far beyond the upper limit for the organic membranes, as shown by the square symbols in the desired region [294]. Although tremendous developments have occurred in tailoring polymer structures to enhance separation properties, further progress exceeding the trade-off line seems to present a challenge in the near future. The application of inorganic membranes is still hindered by the lack of technology to form continuous and defect free-membranes, the cost of membrane production, and handling problems (e.g., brittleness). Thus, a new approach is needed to provide an alternative membrane with separation properties well above the upper-bound limit between permeability and selectivity.

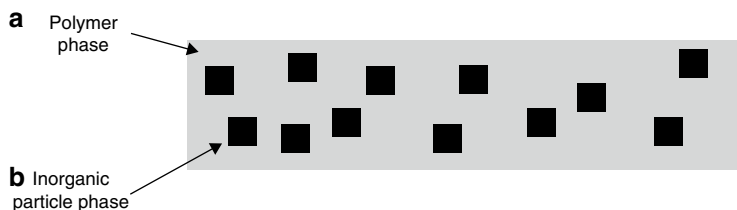


Fig. 3.60 Schematic of a mixed matrix membrane (MMM)

The inclusion of dispersed particles can have three possible effects on the permeability of gases: the discrete particles can act as molecular sieves, altering permeability in relation to molecular size, the particles can disrupt the polymeric matrix resulting in increased micro cavities and hence increase permeability, or they can act as a barrier to the gas transport and reduce permeability [19]. The mixed matrix membranes provide the opportunity to overcome the individual deficiencies of molecular sieves and polymers, and achieve gas separation performance well above famous Robeson's upper bound (again, see Fig. 3.57).

The schematic illustration of MMMs is shown in Fig. 3.60.

The bulk phase (phase A) is typically a polymer; the dispersed phase (phase B) represents the inorganic particles, which may be zeolite, carbon molecular sieves, or nano-size particles. Thus, MMMs have the potential to achieve higher selectivity, permeability, or both relative to the existing polymeric membranes, resulting from the addition of the inorganic particles with their superior inherent separation characteristics.

The review written by Chung et al. [294] gives an outline of the concept and the key advances in MMMs. The research conducted to date on MMMs has focused on the addition of porous inorganic filler to a polymer matrix. It is necessary that both materials should be selective for the same gas pairs. However, in most cases, the inorganic fillers have selectivity far superior to the neat polymer. Ideally, the incorporation of a small volume fraction of inorganic fillers into the polymer matrix can result in a significant increase in overall separation efficiency, as predicted by the so-called Maxwell model [295]. The Maxwell model equation for MMMs with dilute suspension of spherical particles can be written as follows:

$$P_{eff} = P_c \left[\left(P_d + 2P_c - 2\Phi_d (P_c - P_d) \right) / \left(P_d + 2P_c - \Phi_d (P_c - P_d) \right) \right]$$

where P_{eff} is the effective composite membrane permeability, Φ the volume fraction, P the single component permeability, and the subscripts d and c refer to the dispersed and continuous phase, respectively. To properly choose the dispersed and continuous phases, one must take into consideration the transport mechanisms and the gas component preferentially transporting through the membrane [294].

Funk and Lloyd [296] introduced the concept of zeolite-filled mixed matrix membranes, referred to as ZeoTIPS membranes, which were formed using the thermally induced phase separation (TIPS) process and consisted of zeolite particles supported in a microporous polymer matrix. On modeling, it was reported that the performance of these membranes could surpass Robeson's upper bound for gas separation polymers [3]. Paul and Kemps reported the delay in diffusion time lag effect for CO₂ and CH₄ when adding 5A zeolite into rubbery polymer PDMS [297]. On adding 5A zeolite into a polymer matrix, a very large increase in the diffusion time lag was observed but it had only minor effects on the steady-state permeation. Kulprathipanja et al. [298] reported that mixed matrix systems of polymer/adsorbent might yield superior separation performance to that of a pure polymeric system. They observed an enhanced O₂/N₂ selectivity from 3.0 to 4.3 when increasing silicate content in the cellulose acetate (CA) matrix. Kulprathipanja et al. [299] also observed that the calculated separation factor for CO₂/H₂ (50/50 mol%) was 5.15 ± 2.2 in a MMMs membrane in comparison with 0.77 ± 2.2 in a CA membrane, under similar conditions. This indicated that the presence of silicate in the membrane phase alternates the selectivity of H₂ over CO₂. MMMs comprising PDMS as continuous phase and zeolite (ZSM-5) as dispersed phase were prepared by Hussain and König [300] and used for the separation of CO₂ from gas mixtures. ZSM-5 incorporation in PDMS significantly increased the permeability of single gases and a similar effect was observed for gas mixtures. Membrane performance was evaluated using the Maxwell model and as a result an interphase gap between the filler and the polymeric phase was identified.

The gas separation performance of hollow fiber MMMs (PES-zeolite 4A) was enhanced through coating by silicon rubber solution, which could be due to sealing of the defect of the outermost skin of the membrane fiber [301]. Widjojo et al. [302] fabricated polyethersulfone (PES)-beta zeolite/PES-Al₂O₃ dual-layer mixed-matrix hollow-fiber membranes. The incorporation of 20 wt% beta zeolite in the outer selective layer and 60 wt% Al₂O₃ in the inner layer, coupled with spinning at high elongation draw ratios, yielded membranes with an O₂/N₂ selectivity of 6.89. Chaidou et al. [303] fabricated MMMs of polyimide (PI) with different types of zeolites via a solution-casting procedure. The effect of zeolite loading, pore size, and hydrophilicity/hydrophobicity of zeolite on gas separation properties of MMMs was studied. It was observed that the permeability of studied gases (He, H₂, CO₂, and N₂) for Matrimid-zeolite membranes increased with an increase in zeolite loading. The MMMs with zeolite ZSM-5 exhibited the highest permeabilities of all gases, for the same concentrations of zeolite, which could be due to the specific structure and properties of this particular zeolite. Boroglu and Gurkayank [304] fabricated new monomers having silica groups as an intermediate for the preparation of poly(imide-siloxane)-zeolite 4A and 13X MMMs. The addition of particles improved the thermal strength of the polymer to be sufficient for gas separation applications. Zeolites were well distributed throughout the membrane and the zeolites and polymers had good contact at the interface. The transport parameters for all the membranes were determined for N₂ and O₂. However, the permeability of all gases for the poly(imide siloxane)-zeolite 4A membrane decreased with an increase in zeolite loading.

Table 3.24 Averaged gas permeabilities ± 1 standard deviation (in Barrers) of pure PVAc and 15 % CuTPA PVAc MMMs (1 Barrer = $7.5 \times 10^{-8} \text{ m}^3(\text{STP}) \text{ m}^{-2} \text{ s}^{-1} \text{ Pa}^{-1}$)

Membrane	P_{He}	P_{O_2}	P_{N_2}	P_{CH_4}	P_{CO_2}
PVAc	15.1 ± 0.8	0.514 ± 0.034	0.0783 ± 0.0064	0.0697 ± 0.0034	2.44 ± 0.32
MMMs	18.0 ± 0.5	0.624 ± 0.026	0.0912 ± 0.0032	0.0806 ± 0.0035	3.26 ± 0.23

Interfacial void-free MMMs of polyimide (PI)/zeolite were developed by Karkhanechi et al. [305] using 13X and Linde type A nano-zeolites for gas separation. Fabrication of a void-free polymer-zeolite interface was verified by the decreasing permeability developed by the MMMs for the examined gases, in comparison to the pure PI membrane. The molecular sieving effect introduced by zeolite 13X improved the CO_2/N_2 and CO_2/CH_4 selectivity of the MMMs. The Koros group [306] synthesized a MOF of copper and terephthalic acid (CuTPA) and used it for MMMs (using polymer PVAc). The gas transport properties of these CuTPA MMMs showed improvements over the pure polymer transport properties. Table 3.24 summarizes the average pure gas permeabilities for pure PVAc and the MMMs.

Nik et al. [307] synthesized a glassy polyimide, 6FDA-ODA (diamine), and mixed it with several as-synthesized MOF fillers at 25 % content for CO_2/CH_4 gas separation MMMs. The gas separation properties improved. The data revealed that the presence of $-\text{NH}_2$ functional groups in the MOF structure could lead to creating a rigidified polymer at the interface of the filler and polymer matrix and therefore decrease the permeability while increasing the selectivity. Tanh Jeazet et al. [308] studied MOFs for MMMs including:

- $[\text{Cu}(\text{SiF}_6)(4,4'\text{-BIPY})_2]$.
- $[\text{Cu}_3(\text{BTC})_2(\text{H}_2\text{O})_3]$ (HKUST-1, Cu-BTC).
- $[\text{Cu}(\text{BDC})(\text{DMF})]$.
- $[\text{Zn}_4\text{O}(\text{BDC})_3]$ (MOF-5).
- $[\text{Zn}(2\text{-methylimidazolate})_2]$ (ZIF-8).
- $[\text{Zn}(\text{purinate})_2]$ (ZIF-20).
- $[\text{Zn}(2\text{-carboxyaldehyde imidazolate})_2]$ (ZIF-90).
- $\text{Mn}(\text{HCOO})_2$.
- $[\text{Al}(\text{BDC})(\mu\text{-OH})]$ (MIL-53(Al)).
- $[\text{Al}(\text{NH}_2\text{-BDC})(\mu\text{-OH})]$ ($\text{NH}_2\text{-MIL-53(Al)}$).
- $[\text{Cr}_3\text{O}(\text{BDC})_3(\text{F,OH})(\text{H}_2\text{O})_2]$ (MIL-101) (4,4'-BIPY = 4,4'-bipyridine,
- BTC = benzene-1,3,5-tricarboxylate,
- BDC = benzene-1,4-dicarboxylate, terephthalate).

MOF-polymer MMMs were investigated for the permeability of the single gases H_2 , N_2 , O_2 , CH_4 , and CO_2 and the gas mixtures O_2/N_2 , H_2/CH_4 , CO_2/CH_4 , H_2/CO_2 , CH_4/N_2 , and CO_2/N_2 . Results showed that MOF-MMMs had higher separation performance than pure polymer membranes for gas separation.

MOF crystals of $\text{Cu}_2(\text{BTC})_2$ (surface area $1,396 \text{ m}^2 \text{ g}^{-1}$) were mixed with polyimide (PI) to prepare hollow MMMs and the permeation of gases was studied [309]. The H_2 permeance and the selectivity of H_2 with respect to other gases such as N_2 , O_2 , CO_2 , and CH_4 both increased markedly with increased $\text{Cu}_2(\text{BTC})_2$ loading. At a loading of 6 wt% $\text{Cu}_2(\text{BTC})_2$, the permeance of H_2 increased by 45 %, and the ideal selectivity increased by a factor of 2–3 compared to the corresponding data for the pure PI. The influence of three different MOFs in MMMs for binary gas mixtures was reported by preparing dense and asymmetric Matrimid[®] membranes filled with $\text{Cu}_3(\text{BTC})_2$, ZIF-8, and MIL-53(Al). Dense membranes and asymmetric membranes for all three studied MOFs showed improvement in CO_2/CH_4 and CO_2/N_2 selectivity, and permeance, as compared to the unfilled reference membrane [310]. Li et al. [311] reported that a newly developed dual layer PES/P84 (copolyimide) hollow fiber with a PES-zeolite betamixed-matrix outer layer showed comparable permeance and selectivity of O_2/N_2 and CO_2/CH_4 in both single and mixed gas tests. Heating the membranes also improved the performances.

Li et al. [259] reported the first mixed matrix composite membrane made of commercially available poly(amide-b-ethylene oxide) (Pebax[®]1657, Arkema), mixed with the nano-sized zeolite imidazole framework ZIF-7. ZIF-7 was successfully deposited as a thin layer (less than $1 \mu\text{m}$) on a porous polyacrylonitrile (PAN) support. An intermediate gutter layer of PTMSP was applied to serve as a flat and smooth surface for coating to avoid polymer penetration into the porous support. The performance of the composite membrane was characterized by single gas permeation measurements of CO_2 , N_2 , and CH_4 . Both permeability (P_{CO_2} up to 145 Barrer) and gas selectivity (CO_2/N_2 up to 97 and CO_2/CH_4 up to 30) could be increased at low ZIF-loading. The CO_2/CH_4 selectivity could be further increased to 44 with a filler loading of 34 %, but the permeability was reduced compared to the pure Pebax[®] 1657 membrane.

Jiang et al. [312] reported that during the spinning of polymer-zeolite mixed matrix hollow fiber the particles located near the outer surface of the hollow fibers may form a defect free mixed-matrix structure with the surrounding polymer, which arises from the instantaneously solidification of the polymer phase. However, a continuous defect-free skin cannot be obtained because of the defects existing in the polymer matrix and the detachment of polymer chains from the particle surface during post treatment. More uniform and less defective mixed-matrix structures in the outer mixed-matrix layer of the dual-layer hollow fibers can be obtained by thermal treatment with a *p*-xylenediamine/methanol soaking method. Some fibers could obtain selectivity much higher than Knudsen diffusion even without silicon rubber coating, which indicates the significantly reduced amount of defects. Zeolite/carbon composite membranes represent another type of MMMS. A polyimide precursor containing MFI crystals was cast onto a stainless steel support and calcined at $580 \text{ }^\circ\text{C}$ in nitrogen. A medium O_2/N_2 selectivity of 4–6 with relatively high oxygen permeances of about $10^{-8} \text{ mol m}^{-2} \text{ s}^{-1} \text{ Pa}^{-1}$ was found [197].

3.4.1 Preparation of MMMs

Polymer-inorganic nanocomposite membranes present an interesting approach to improve the separation properties of polymer membranes because they possess the properties of both organic and inorganic membranes—good permeability, selectivity, mechanical strength, and thermal/chemical stability. The methods for the fabrication of mixed matrix membranes are very similar to ordinary polymer membrane fabrication. The most commonly used for the preparation of nanocomposite membranes can be divided into the following three types [313].

1. **Solution blending:** In this technique, the inorganic nanoparticles are mixed with the polymer solution and dispersed by stirring. The nanocomposite membrane is cast by removing the solvent through conventional means. The solution blending method is easy to operate and suitable for all kinds of inorganic materials, and the concentration of the polymer and inorganic components are easy to control; however, the inorganic ingredients are liable to aggregate in the membranes.
2. **In situ polymerization:** In this method, the nanoparticles are mixed well with organic monomers, and then the monomers are polymerized. There are some functional groups such as hydroxyl and carboxyl on the surface of inorganic particles, which can generate initiating radicals, cations or anions under high energy radiation, plasma or other circumstances to initiate the polymerization of the monomers on the surface. For instance, nanocomposite membranes of poly(methacrylic acid) (PMA)/TiO₂ were synthesized from TiO₂ nanopowder/methacrylic acid dispersions under microwave radiation [314]. In the in situ polymerization method, inorganic nanoparticles with functional groups can be connected with polymer chains by covalent bonds. However, it is still difficult to avoid the aggregation of inorganic nanoparticles in the final product (membrane).
3. **Sol–gel method:** In this method, organic monomers, oligomers, or polymers and inorganic precursors are mixed together in the solution. The inorganic precursors hydrolyze and condense into well-dispersed nanoparticles in the polymer matrix [313]. The advantages of this method include:
 - (a) The reaction conditions are moderate—usually room temperature and ambient pressure.
 - (b) The concentration of organic and inorganic components is easy to control in solution.
 - (c) The organic and inorganic ingredients are dispersed at the molecular or nanometer level in the membranes, and thus, membranes are homogeneous.

Iwata et al. [315] reported that by using the sol–gel method, a nanocomposite membrane of polyacrylonitrile (PAN) with hydrolysate of tetraethoxysilane (TEOS) as the inorganic phase showed a significant performance in O₂/N₂ separation. Ahmad et al. [316] studied the chemical, mechanical, and gas separation properties of PVA/TiO₂ nanocomposite membranes. The membrane was prepared using a polymer and TiO₂ (AEROXIDE hydrophilic fumed TiO₂P25) via solution blending (in water). It was reported that the addition of TiO₂ (up to 20 wt%) to PVA increased the

selectivity of gas pairs O_2/N_2 , H_2/N_2 , H_2/CO_2 , and CO_2/N_2 by 60 %, 55 %, 23 %, and 26 % respectively, with corresponding decreases in permeability. At higher loading of TiO_2 , a reverse trend was noticed. MOF materials are also used in making MMMs. MMMs fabricated from MOF-5 nanocrystals with a high surface area ($3,000\text{ m}^2/\text{g}$) and high thermal stability (up to $400\text{ }^\circ\text{C}$), along with Matrimid[®] were used for gas separation. Despite the high surface area of the MOF-5, no increase in ideal selectivity for any gas pairs was observed. However, up to a 120 % increase in permeability was achieved due to the porosity of the MOF-5 nanocrystals. Gas mixtures (CO_2/CH_4 , N_2/CH_4) showed a marked increase in selectivity for CH_4 due to the larger solubility of CO_2 and N_2 in the polymer matrix [317].

3.5 Other Materials

3.5.1 Metallic Membranes

Gas separation membranes based on Pd/Pt alloys can be used either independently or in conjunction with porous ceramic supports. Pd/Pt alloys have the ability to dissolve considerable amounts of hydrogen and to demonstrate increasing permeability. The major drawbacks to their industrial use are the high cost for Pd, the relatively low flux, and the irreversible change that takes place in the palladium lattice structure during cycling above and below a critical temperature, resulting in significant damage to the membrane.

Palladium thin films are known to selectively transmit hydrogen via an adsorption-desorption mechanism. Permeability of hydrogen as high as $10^{-6}\text{ mol m}^{-2}\text{ s}^{-1}\text{ Pa}^{-1}$ with H_2/N_2 permselectivity higher than 10,000 has been achieved [318]. As well, γ -alumina membranes modified by the deposition of metals such as Ru, Pd, Rh, and Pt possess hydrogen separation values that exceed limitation of Knudsen diffusion. Mixed proton- and electron-conducting materials consisting of barium cerate doped with rare-earth ions, that is, $BaCe_{1-x}M_xO_{3-\delta}$, where $M=Nd^{3+}$, La^{3+} , Y^{3+} , or Gd^{3+} , have been found to be of potential interest for hydrogen separation [319]. The presence of H_2S (low concentration) in the feed decreased the permeation of hydrogen through Pd and Pd–Cu alloy membranes by blocking H_2 dissociation sites. At high H_2S concentrations, a sulfur (due to decomposition of H_2S) surface layer did not allow H_2 to penetrate into the Pd–Cu surface [320].

If very pure hydrogen is required, dense metallic membranes may be a good option. Palladium and palladium alloys (practically the only types of hydrogen selective metallic membranes used) are extremely selective because only hydrogen can permeate through them [321]. Hydrogen transport through the membrane can best be described by the solution/diffusion mechanism. Hydrogen is adsorbed on one side of the membrane, splits into two atoms, diffuses through the metal matrix, and recombines and desorbs at the permeate side. To improve fluxes and reduce membrane costs (material cost of palladium is very high), usually thin layers deposited on a porous ceramic or metallic support are used. If palladium membranes are

exposed to hydrogen at lower temperatures, they can be seriously damaged, because hydrogen can become locked inside the palladium lattice. This will cause stresses in the membrane, increasing the likelihood of membrane failure. A solution to this problem is to dope the palladium with other elements such as silver or copper. Operating temperatures of today's palladium alloy membranes are in the range 300–600 °C. A major technical disadvantage of palladium membranes in most applications is their high sensitivity to chemicals such as sulfur, chlorine, and even CO. These chemicals can poison the membrane surface reducing the effective hydrogen fluxes by 20 to even 100 %. Although much attention is focused on development of palladium membranes, their commercial availability is still limited. Johnson Matthey produces palladium-silver alloy membranes up to 60 cm in size commercially for the production of ultra pure hydrogen in the electronics industry. However, there are some drawbacks to the material, i.e., its stability in the presence of high-temperature water vapor is questionable. Large-scale production of this type of material has long been considered a major challenge [282, 283].

3.5.2 Carbon-Based Membranes

Carbon-based membranes can be classified into three categories.

1. Carbon molecular sieve membranes (CMSMs) and adsorption selective carbon membranes (ASCMs).
2. Carbon nanotube (CNTs) membranes.
3. Graphene.

3.5.2.1 Carbon Molecular Sieve Membranes (CMSMs) and Adsorption Selective Carbon Membranes (ASCMs)

Depending on the separation mechanism, two types of carbon membranes can be distinguished: molecular sieve carbon membranes (MSCMs) and adsorption-selective carbon membranes (ASCMs). The separation of gas molecules by means of MSCM takes place via a molecular sieving mechanism. Since MSCMs have micropores with sizes close to the dimensions of permanent gases ($<4 \text{ \AA}$), the diffusivity of these gases through the membrane changes abruptly with the molecular size and shape. This allows the separation of gases with similar molecular sizes. These membranes have been demonstrated to be effective at separating gas mixtures, such as O_2/N_2 , CO_2/N_2 , and CO_2/CH_4 . Gas separation by MSCM is limited to gases with molecular sizes smaller than 4.0–4.5 \AA . However, MSCMs are not suitable to separate gas mixtures, such as *iso*-butane/*n*-butane or gas–vapor mixtures (i.e., air/hydrocarbons, H_2 /hydrocarbons, etc.) [322].

The separation of gas molecules by means of ASCM takes place as a consequence of their adsorption properties. The more strongly condensable components are preferentially adsorbed on the micropores of the membrane. This reduces the open porosity and consequently limits the diffusion in the micropores of the less adsorbable gases. As a consequence, the more strongly adsorbed components permeate preferentially through the ASCM membrane, being separated as the permeate stream (low-pressure side); whereas the less adsorbed components of the feed gas mixture are mainly recovered at the high-pressure side (retentate stream). Thus, ASCMs are effective at separating non-adsorbable or weakly adsorbable gases (i.e., He, H₂, air, O₂, N₂, CH₄, etc.) from adsorbable gases, such as hydrocarbons (C₂₊), NH₃, SO₂, H₂S, and CFCs. From a structural point of view, ASCMs are constituted by a carbon film with micropores slightly wider than those characteristic of CMSMs, probably in the range 5–7 Å.

Molecular sieving membranes are identified as promising, both in terms of separation properties (including achievable fluxes) and stabilities, but are not yet commercially available at a sufficiently large scale. The pore sizes are in the order of the size of H₂-molecules. Reported selectivities are in the range of 4–20. Adsorption selective carbon membranes separate non- (or weakly) adsorbable gases from adsorbable gases (such as H₂S, NH₃, and CFCs). The performance of these membranes will deteriorate severely if feed streams contain organic traces or other strongly adsorbing vapors. Carbon membranes can be used in non-oxidizing environments with temperatures in the range of 500–900 °C. A disadvantage of carbon membranes is that they are brittle and therefore difficult to package if the membrane surfaces become larger. Furthermore, the price of carbon membranes is still high and optimum manufacturing conditions still need to be determined.

The configuration of carbon membranes can be divided into two categories: supported and unsupported. Unsupported membranes have three different configurations: flat (film), hollow fiber, and capillary, while supported membranes consist of two configurations: flat and tube. Figure 3.61 shows the configurations of carbon membranes.

3.5.2.2 Carbon Molecular Sieve Membranes (CMSMs)

Carbon molecular sieve membranes have been seen as a very promising candidate for gas separations, both in terms of separation properties and stability. Carbon molecular sieves are porous solids that contain constricted apertures that approach the molecular dimensions of diffusing gas molecules. At this constriction the interaction energy between the molecule and the carbon comprises both dispersive and repulsive interactions. When the opening becomes sufficiently small relative to the size of the diffusing molecule, the repulsive forces dominate and the molecule requires activation energy to pass through the constrictions. In this region of activated diffusion, molecules with only slight differences in size can be effectively separated through molecular sieving [323]. The mechanism of gas permeation uptake through porous solid is thus closely related to the internal surface area and

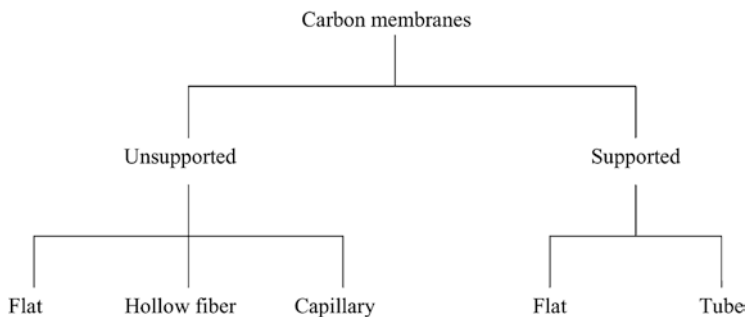


Fig. 3.61 Configurations of carbon membranes

dimensions of the pores and to the surface properties of the solid, rather than to the bulk properties of the solid (as in the case with polymers). CMSMs show excellent intrinsic performances for gas separation applications. This micro- to nanosize materials are obtained through the pyrolysis (at high temperature in an inert atmosphere) of polymeric precursors already processed in the form of membranes, and may be considered as just a type of “very high free-volume” material.

There are four different mechanisms for separation of a gas mixture through a porous membrane as discussed earlier (Chap. 2). The predominant transport mechanism of most carbon membranes is molecular sieving as shown in Fig. 3.60. The carbon membrane contains constrictions in the carbon matrix that approach the molecular dimensions of the absorbing species. In this manner, they are able to separate the gas molecules with similar size effectively. According to this mechanism, the separation is caused by passage of smaller molecules of a gas mixture through the pores while the larger molecules are obstructed. This mechanism exhibits high selectivity and permeability for the smaller components of a gas mixture. The carbon matrix is assumed to be impervious, and permeation through carbon membranes is attributed entirely to the pore system. The pore system consists of relatively wide openings with narrow constrictions. The openings contribute the major part of the pore volume and are thus responsible for the adsorption capacity, while the constrictions are responsible for the stereoselectivity of pore penetration by host molecules and for the kinetics of penetration. Hence, the diffusivity of gases in carbon molecular sieves changes abruptly depending on the size and shape of molecules because the carbon molecular sieve has pore size close to dimension of gas molecules (Fig. 3.62) [324].

The size of pores along the carbon fiber membrane can be controlled during the production process; it is possible to “tailor” the pore size distribution so that the diameter of virtually all pores will fall between the size of the large and small molecules of the gas mixture to be separated.

The fabrication of carbon membranes involves six important steps as shown in Fig. 3.63.

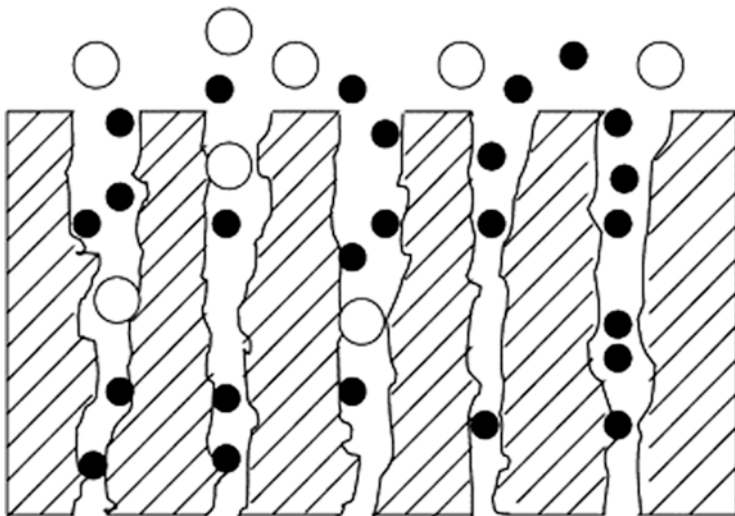


Fig. 3.62 Typical molecular sieving transport mechanism

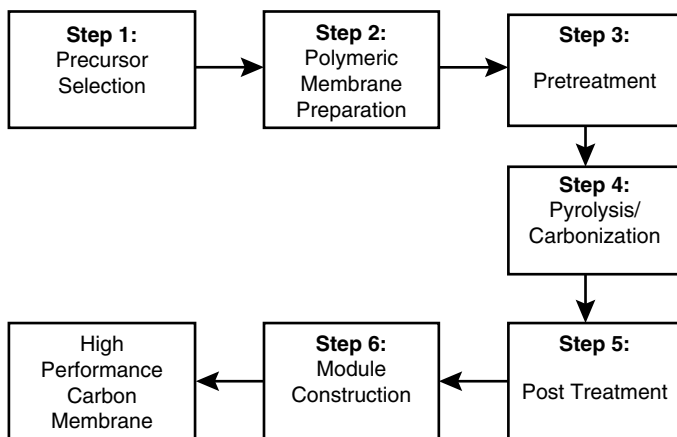


Fig. 3.63 Carbon membrane fabrication process [324]

At the same time, several other factors need to be considered, such as temperature and environment of carbonization, and polymeric precursors. The pyrolysis process is the most important step and can be regarded as the heart of the carbon membrane production process. During this stage, the pore structure of the carbon membrane is formed, and this determines the ability of a carbon membrane to separate gases.

The choice of the polymeric precursor is the first important factor. Pyrolysis of different precursors may produce different kinds of carbon membranes. Carbon membranes can be produced through the carbonization or pyrolysis process of suitable carbon containing materials such as resin, graphite, coal, pitch and plants, under inert atmosphere or in a vacuum. Lately, numerous synthetic precursors have been used to form carbon membranes, including polyimide and its derivatives, polyacrylonitrile (PAN), phenolic resin, polyfurfuryl alcohol (PFA), polyvinylidene chloride-acrylate terpolymer (PVDC-AC), phenol formaldehyde, and cellulose.

A polymeric membrane can be produced in two main configurations as precursor for carbon membranes, namely an unsupported membrane (flat, hollow fiber, capillary) and a supported membrane (flat, tube). For making the supported carbon membranes, various options are available for coating the supports with thin polymeric films, such as ultrasonic deposition, dip coating, vapor deposition, spin coating, and spray coating [325]. Because of the shrinkage of the polymer material during pyrolysis, the coating procedure has to be repeated until a defect-free carbon molecular sieve is obtained. The coating of the support surface with an intermediate layer reduces the number of defects existing on the original substrate.

Polymeric membranes are often subjected to pretreatments before they undergo a pyrolysis process. This step can ensure the stability of the polymeric precursor and the preservation of its structure during pyrolysis. In fact, carbon membranes of good quality, in terms of stability and separation performance, can be produced using specific pretreatments for a given precursor. Pretreatment methods can be divided into physical and chemical methods. Physical pretreatment consists of stretching or drawing hollow fiber membranes prior to pyrolysis. Chemical pretreatments involve some chemical reagents which are applied to the polymeric precursor.

Pyrolysis (sometimes referred to as carbonization) is a process in which a suitable carbon precursor is heated in a controlled atmosphere (vacuum or inert) to the pyrolysis temperature at a specific heating rate for a sufficiently long thermal soak time. During pyrolysis of a polymer, byproducts of different volatilities are produced resulting in a large weight loss. Depending on the polymer, typical volatile byproducts such as ammonia, hydrogen cyanide, methane, hydrogen, nitrogen, carbon monoxide, carbon dioxide and others may be produced. The polymer precursors are initially cross-linked or become cross-linked during pyrolysis. Pyrolysis creates an amorphous carbon material that exhibits a distribution of micropore dimensions with only short-range orders of specific pore sizes and also pores larger than the ultramicropores required to exhibit molecular sieving properties. One can determine which pyrolysis parameters are important and contribute most significantly to the structural changes of the material, where it would be possible to predict the trends of transport properties for a given carbon material more effectively.

Pyrolysis temperature was found to significantly change the structure and properties of carbon membranes based on PAN [326]. A similarly carbonization atmosphere was found to have a profound effect on the PAN-based carbon membranes [327]. As mentioned above, the MSCMs can separate gas components by means of their microporosity, which discriminates between molecules according to their size, shape and strength of interaction with the pore surfaces. Excellent performance with

respect to hydrogen permeability and selectivity in the separation of hydrogen from light hydrocarbons such as methane has been shown with MSCMs. MSCMs derived from the carbonization of cellulosic films were developed for the purpose of hydrogen recovery, by evaluating the effect of copper (II) nitrate addition to the cellulose precursor, carbonization temperature and environment on MSCMs performance [328]. The performance of MSCMs synthesized in this way was better than polymeric membranes for hydrogen/methane separation in terms of the Robeson trade-off curve, which plots membrane productivity (often represented by permeability against selectivity) [3].

Favvas et al. [329] prepared and characterized three different MSCMs from Matrimid® 5218 polyimide hollow fiber precursor. The formation of the selective layer on the fibers was independent from the initial orientation of the asymmetric polyimide precursor. The size of the pores was influenced by the temperature of the carbonization process whereas the pore volume was influenced by the pyrolysis environment conditions. Carbon dioxide seems to be a more effective oxidizing agent than water, one reason being the hydrophobicity of the carbon surface. Figure 3.64 shows schematically this oxidization process. The developed carbon fibers exhibited H_2 permeances varying from 20 to 52 GPU with a highest permselectivity coefficient of 137. Permeation rates of He, H_2 , Ar, CH_4 , CO_2 , CO, O_2 , and N_2 at various pressures were measured too. In most cases, permeation properties were independent of feed pressure indicating the absence of compaction. The size of pores was found to be mainly dependent of the carbonizing process rather than the pyrolytic environment, which does not play an important role.

Carbon hollow fiber membranes derived from a polymer blend of polyetherimide and polyvinylpyrrolidone (PVP) were prepared through stabilization under air atmosphere followed by carbonization under N_2 atmosphere by Salleh et al. [330]. The polymer blends with 6 wt% PVP showed the best composition in the preparation of PEI/PVP-based carbon hollow fiber membranes with CO_2/CH_4 and CO_2/N_2 selectivities of 55.53 and 41.5, respectively. These results (data) were superior in comparison with other published data as shown in Tables 3.25 and 3.26.

Yoshimune et al. [337] prepared MSCMs as hollow fibers using PPO and its functionalized derivatives (R-PPO) as a precursor, and gas transport properties were measured for He, H_2 , CO_2 , O_2 , and N_2 . PPO MSCMs exhibited higher performances than those polymeric precursors. The highest performance was attained by trimethylsilyl-PPO (TMSPPPO) MSCM pyrolyzed at 923 K, of which O_2 permeability was 125 Barrer and O_2/N_2 permselectivity was 10.0 at 298 K.

Amongst the polymer precursors applied for the preparation of carbon membranes, the most frequently used are polyfurfuryl alcohol (PFA), polyvinylidene chloride (PVDC), cellulose, phenolic resins, polyacrylonitrile (PAN), polyetherimides, and polyimides [331]. Polyimides are categorized as the most stable classes of polymer and can be used at temperatures higher than 573 K. They usually decompose before reaching their melting point. They are considered to be excellent precursors for glassy carbon as they do not go through a melting phase transition and thus do not lose their shape [331]. Matrimid®, Kapton®, and P84 polyimides are widely used for the preparation of CMS membranes.

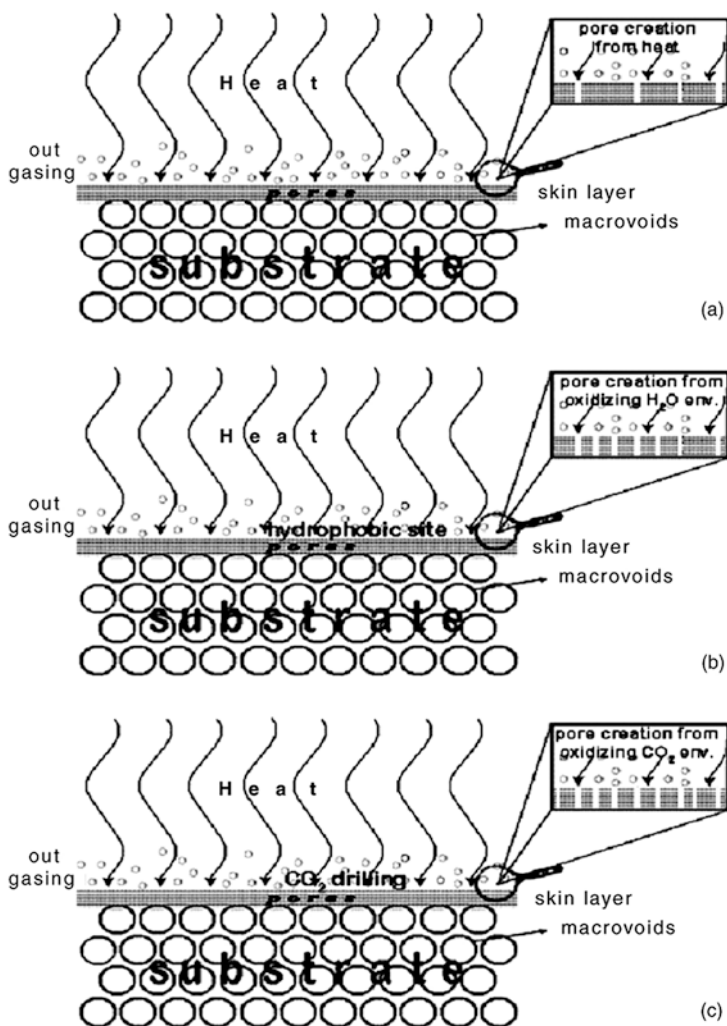


Fig. 3.64 Model of carbonization/activation process. (a) Carbonization in inert environment; (b) carbonization/activation in oxidizing H₂O environment; and (c) carbonization/activation in high oxidizing CO₂ environment [329]

Hattori and coworkers have prepared carbon films, including supported and unsupported, from Kapton-type polyimide [338, 339]. It was reported that the carbon molecular sieve film used for gas separation should be as thin as possible in order to enhance the separation efficiency; however, the thin film should be supported with a porous plate for handling convenience. The flat homogeneous carbon film prepared by pyrolysis at 800 °C had O₂/N₂ selectivities of 4.2.

Table 3.25 Permeation performance of the derived carbon membrane [330]

Membrane from (Precursor)	Configuration	Selectivity	
		CO ₂ /CH ₄	CO ₂ /N ₂
P84 copolyimide [331]	Hollow fiber	38.9	42.8
Matrimid [329]	Hollow fiber	20.86	23.6
PEI/PVP [332]	Flat sheet		13.70
PI/PVP [333]	Flat sheet		~40.00
PI/PVP [334]	Flat sheet		30 -38
PPO/PVP [335]	Tubular	~10.00	~20.00
PPESK/PVP [336]	Flat sheet		25-70

Table 3.26 Comparison of permeance on carbon hollow fiber

Precursor	Permeance (GPU)		
	N ₂	CO ₂	CH ₄
Matrimid [331]	0.270	6.300	0.300
P84 copolyimide [332]	0.006	0.276	0.007
PEI/PVP [329]	0.04	1.66	0.03

Rao and Sirkar [340–342] prepared nanoporous-supported carbon membranes by pyrolysis of the polyvinylidene chloride layer coated on a macroporous graphite disc support. By heat treatment at 800 °C for 3 h, the diameters of macropores were reduced to the order of a nanometer. These membranes were used to separate hydrogen–hydrocarbon mixtures and the results are discussed on the basis of the surface diffusion mechanism, in which selectivity depends on the adsorption of gas molecules on the pore wall. This transport mechanism differs from the molecular sieving mechanism; therefore, these membranes are called selective surface flow (SSFTM) membranes. They possess a thin layer (e.g., 2–5 μm) of nanoporous carbon (effective pore diameter in the range of 5–6 Å) supported on a mesoporous inert support, such as graphite or alumina (effective pore diameter in the range of 0.3–1.0 μm).

Centeno et al. [343] demonstrated that the gas separation performance of phenolic resin-based carbon membranes can be adjusted by pyrolysis processing variables (heat treatment temperature, heating rate, soaking time, and atmosphere). A large variety of carbon membranes for gas separation have been developed by simple carbonization of a phenolic resin film deposited on a ceramic tubular support. Thus, molecular sieve carbon membranes (MSCMs) with good capabilities towards the separation of O₂–N₂, CO₂–CH₄, CO₂–N₂, and olefin–paraffin mixtures, as well as adsorption-selective carbon membranes (ASCMS) effective in the recovery of hydrocarbons from hydrocarbon–N₂ mixtures, have been obtained.

A solution to overcome reproducibility problems of nanoporous carbon (NPC) membranes has been introduced by Acharya and Foley [344]. They used spray coating system for the production of thin layers of nanoporous carbon on the surface of

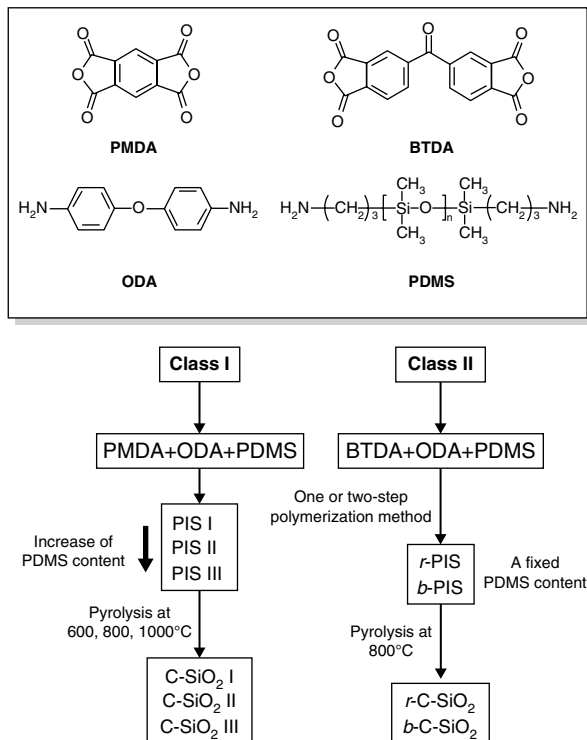
a porous stainless steel support. A solution of poly(furfuryl)alcohol (PFA) in acetone was sprayed onto the support in the form of a fine mist using an external mixer brush with nitrogen gas. The advantage of this technique is reproducibility, simplicity and good performance for O₂/N₂ separation. The resulting membranes were found to have oxygen over nitrogen selectivities up to 4 and oxygen fluxes on the order of 10⁻⁹ mol m⁻² s⁻¹ Pa⁻¹.

Favvas et al. [331] fabricated gas separation carbon hollow fiber membranes based on a 3,3',4,4'-benzophenone tetracarboxylic dianhydride and 80 % methylphenylene-diamine + 20 % methylene diamine co-polyimide precursor (BTDA-TDI/MDI, P84 Lenzing GmbH). Hollow fibers were initially prepared by the dry/wet phase inversion process in a spinning setup, while the spinning dope consisted of P84 as polymer and NMP as solvent. The developed polymer hollow fibers were further carbonized in nitrogen at temperatures up to 1,173 K. Permeability (Barrer) of He, H₂, CH₄, CO₂, O₂, and N₂ were measured at atmospheric pressure and temperatures of 313, 333, and 373 K and were found to be higher than those of the precursor. Moreover, the calculated permselectivity values were significantly improved. The developed carbon fibers exhibited rather low H₂ permeance values (8.2 GPU or 2.74 × 10⁻⁹ mol m⁻² s⁻¹ Pa⁻¹ with a highest H₂/CH₄ selectivity coefficient of 843 at 373 K).

Jones and Koros [323] prepared carbon membranes from the pyrolysis of several different hollow fiber polymeric materials, including cellulose acetate, polyaramides, and polyimides. Pyrolysis was done in a vacuum. The selectivities obtained with these membranes were much higher than those found with conventional polymeric materials, and the high selectivities were achieved without the loss of membrane productivity. Membranes were produced by two different temperature protocols, and were evaluated with mixed gas feeds at pressures ranging up to 200 psig (1.48 MPa). The lower temperature protocol yielded membranes with O₂/N₂ selectivities ranging from 8.5 to 11.5, and a higher temperature pyrolysis yielded membranes with selectivities ranging from 11.0 to 14.0. These membranes were found to be quite stable over time periods of several days with high-purity, dry feeds. Limited studies also showed that these membranes were highly effective for the separation of other mixed gas pairs, including CO₂/N₂, CO₂/CH₄, and H₂/CH₄.

Centeno et al. [345] described a method for the preparation of a composite carbon membrane from poly(vinylidene chloride-co-vinyl chloride) for gas separation. The membrane was formed by a thin microporous carbon layer (thickness, 0.8 μm) obtained by pyrolysis of a polymeric film supported over a macroporous carbon substrate (pore size, 1 μm; porosity, 30 %). In a few cases polymeric film was oxidized in presence of air (at 200 °C) before carbonization. An almost defect-free carbon membrane was obtained in only one casting step. This carbon film exhibited molecular sieving properties and allowed the separation of gases depending on their molecular sizes. Single gas permeation experiments with pure gases of different molecular size (He, CO₂, O₂, N₂, and CH₄) were performed at different temperatures between 25 °C and 150 °C. It was revealed that the microporous carbon layers had molecular sieving properties. The carbon membrane showed high selectivities for the separation of permanent gases like the O₂/N₂ system (selectivity ~ 14 at 25 °C).

Fig. 3.65 The overall scheme of the Park and Lee study [346]



Air preoxidation at 200 °C for 6 h improved the permselectivity but with a loss in gas permeance. It was also reported that the carbonization temperature had a marked effect on gas permeance.

Park and Lee [346] fabricated carbon–silica membranes, by pyrolysis of the imide siloxane copolymers as the precursor of C-SiO₂. This was the first reported case of a polymeric precursor containing two thermo-stable phases being used for the preparation of carbon membrane implanted SiO₂. Figure 3.65 shows the overall scheme of their study.

The change in morphology in polymeric nanomaterial (block or random copolymer consisting of two phases in nanoscale) was found to affect the permeation properties to a large extent. In the case of O₂/N₂ separation, the O₂/N₂ selectivity versus O₂ permeability for the C-SiO₂ membrane was higher than the values obtained with other gas separation membranes (Fig. 3.66). The authors concluded that the combination of two building blocks with different carbon densities on the nanoscale can provide a hint about a new type of template carbonization, which differs from the conventional method using thermally stable and thermally unstable phases.

Hosseini and Chung [347] studied H₂/CO₂ separation by using carbon membranes derived from a PBI/polyimide blend. The selectivity of H₂/CO₂ was increased as the PBI (polybenzimidazole) content in the blend increased due to the rigidity and high packing density of PBI. PBI/Matrimid (75/25 wt%) blend membranes

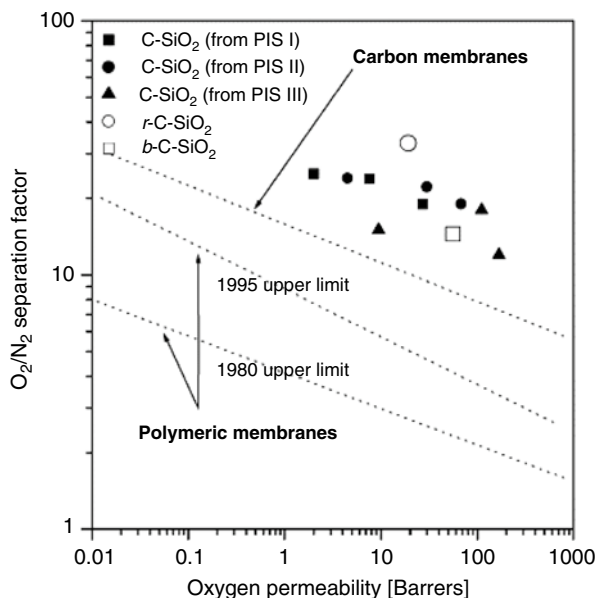


Fig. 3.66 O₂/N₂ selectivity vs. O₂ permeability (Barrer). (Filled square), (filled circle), (filled triangle): C-SiO₂ membrane derived from class I and (open circle), (open square): C-SiO₂ film derived from class II. 1 Barrer = 10⁻¹⁰ × cm³ (STP) cm cm⁻² s⁻¹ cmHg⁻¹

cross-linked with *p*-xylenediamine showed a H₂/CO₂ selectivity of 26 with H₂ flux of 3.6 Barrer. Fuertes [322] fabricated carbon membranes from deposition of a thin film of a phenolic resin on the inner surface of an alumina tube. After carbonization (under vacuum at 700 °C) and air oxidation (300–400 °C), carbon membrane was obtained. The prepared membrane showed high permeabilities and selectivities towards separation of gas mixtures formed by hydrocarbons and N₂. As an example, the values of permeability and selectivity (hydrocarbons/N₂) for the separation of a complex gas mixture formed by 16.3 % CH₄, 16.1 % C₂H₆, 16.2 % C₃H₈, 20 % C₃H₆, and 31.4 % N₂ are: CH₄, 320 Barrer ($\alpha=2.6$); C₂H₆, 1,104 Barrer ($\alpha=9.1$); C₃H₆, 2,930 Barrer ($\alpha=23.4$); C₃H₈, 2,850 Barrer ($\alpha=22.8$).

Polymeric precursor—poly(phthalazinone ether sulfone) (PPES)—was used as a precursor for the preparation of carbon membranes via stabilization and pyrolysis by Zhang et al. [348]. The evolution of functional groups of membrane was monitored by ATR-FTIR during the formation process of carbon membranes. It was noticed that PPES is a highly thermally stable polymer with the char yield of 38.2 wt% at 700 °C in nitrogen. The functional groups of PPES disappeared by forming graphite-like structures in the membrane matrix during pyrolysis. At the test condition of 0.1 MPa and 30 °C, the gas permeabilities of H₂, CO₂, O₂, and N₂ for carbon membranes prepared at the stabilization and pyrolytic temperature of 240 and 650 °C are 610.13, 439.9, 146.98, and 28.95 Barrer, together with the selectivities of gas pairs H₂/N₂, CO₂/N₂, and O₂/N₂ of 22.6, 16.3, and 5.5, respectively.

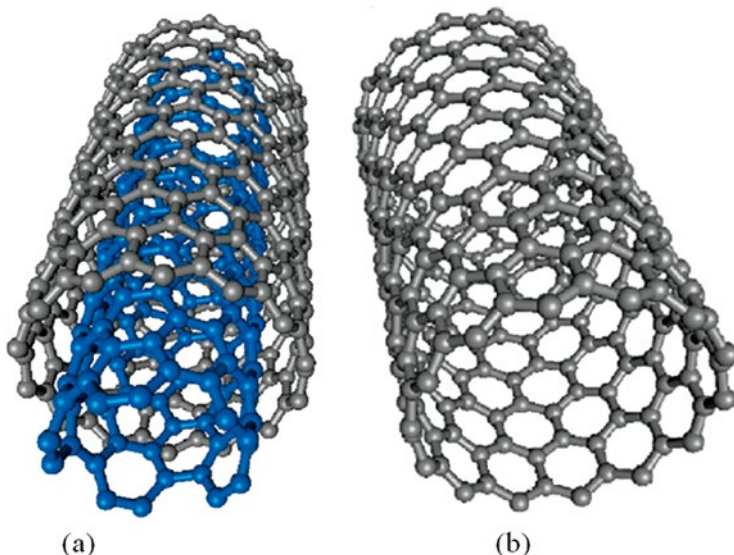


Fig. 3.67 (a) Structure of a multi-wall carbon nanotube (MWCNT) and (b) structure of a single-wall carbon nanotube (SWCNT) [353]

3.5.2.3 Carbon Nanotubes

Iijima in 1991 [349] reported the first detailed transmission electron microscope images of an arc-grown multiwalled carbon nanotube (MWCNT). The single walled carbon nanotubes (SWCNTs) were reported later [350]. Carbon nanotubes (CNTs) are allotropes of carbon with a cylindrical nanostructure. Nanotubes have been constructed with length to diameter ratios up to 132,000,000:1, significantly larger than for any other material [351, 352]. These cylindrical carbon molecules have unusual properties, which are valuable for nanotechnology, electronics, optics, and other fields of materials science and technology. Carbon nanotubes belong to a family of fullerenes. Nanotubes are categorized as single-walled nanotubes (SWNTs) and multi-walled nanotubes (MWNTs).

Most single-walled nanotubes (SWNT) have a diameter of close to 1 nm, with a tube length that can be many millions of times longer. The structure of a SWNT can be conceptualized by wrapping a one-atom-thick layer of graphite called graphene into a seamless cylinder (Fig. 3.67b). Multi-walled nanotubes (MWNT) consist of multiple rolled layers (concentric tubes) of graphene (Fig. 3.67a). Double-walled carbon nanotubes (DWNT) form a special class of nanotubes because their morphology and properties are similar to those of SWNT but their resistance to chemicals is significantly improved.

Individual nanotubes naturally align themselves into “ropes” held together by van der Waals forces. Other materials are also used as nanotubes composed of metal oxides, and their morphology is always very similar to carbon nanotubes.

All nanotubes have an extremely high aspect ratio in common, which makes them to molecular-level needles. Nanotubes are the strongest materials known, but the ultimate limits of their strength have yet to be reached experimentally [354]. The studies made by Sholl and Johnson [355] suggested that carbon nanotube membranes can have spectacularly high fluxes, must also high selectivity, and can be used in gas separation.

Carbon nanotubes represent a rare experimental realization of a nanofluidic channel, which has a molecularly smooth wall, and a nanometer-scale inner diameter. This unique combination of properties gives the carbon nanotube channel an ability to support enhanced transport of gases with flows often exceeding those of conventional channels by several order of magnitudes [356]. Noy [356] presented a simplified analytical model that uses classic theory formalism to describe gas transport in carbon nanotube channels and to highlight the role of surface defects and adsorbates in determining transport efficiency, including the possibility of gas molecule diffusion along the nanotube walls. They also mentioned that in all conditions the nanotube channel walls play a critical role in determining transport efficiency and that in some cases obtaining efficient transport has to involve optimization of flows from diffusion through the gas phase and along the nanotube surface.

In general, there are four routes for the preparation of membranes based on CNTs [357].

1. Deposition of carbonaceous materials inside preexisting ordered porous membranes, such as anodized alumina, also known as template-synthesized membranes.
2. Membranes based on the interstice between nanotubes in a vertical array of CNTs, subsequently referred to as the dense-array outer-wall CNT membranes.
3. Encapsulation of as-grown vertically aligned CNTs by a space-filling inert polymer or ceramic matrix followed by opening up to CNT tips using plasma chemistry, or open-ended CNT membranes.
4. Membranes composed of nanotubes as fillers in a polymer matrix, also known as mixed-matrix membranes.

In MMMs for gas separation, carbon nanotubes are among three emerging fillers for membranes (the two others are metal–organic frameworks and clay-layered silicate) [358]. The development of MMMs gas separation membranes started on the basis of simulations, proving the excellent factors of CNTs for gas separation. In MMMs for gas separation carbon nanotubes are among three emerging fillers for membranes (the two others are metal=organic frameworks and clay layered silicate) [358]. Arora and Sandler calculated the kinetic and ideal separation factors for a carbon nanotube membrane, and proved that for single wall carbon nanotubes, high permeance can be obtained along with good kinetic selectivities [359]. Chen and Sholl [360] made atomic calculations to predict the separation between CH_4 and H_2 for SWCNTs and found a remarkable selectivity for CH_4 .

Simulation predicting the diffusivity properties of simple gases in CNTs shows that these materials may be suitable filler in a polymer matrix to make MMMs. Atomistic simulations of diffusion of pure Ar and Ne through SWNTs were discussed by Ackerman et al. [361]. They also predicted the diffusion of these gases

through the zeolite silicate, a commonly used zeolite for industrial applications with pores of about the same size as the nanotubes (0.81 and 1.36 nm). Their results predicted that the self diffusivity of Ar in SWNTs was orders of magnitude larger than silicate. Theoretical work of Skoulidas et al. [362] has reported atomic simulation results for both self and transport diffusivities of light gases such as H₂ and CH₄ in carbon nanotubes and in zeolites. They reported transport rates in CNTs to be orders of magnitude faster than zeolites and the exceptionally high transport rates in nanotubes.

Kim et al. [363] tried to verify this hypothesis by developing and characterizing novel nanocomposite membranes based on carbon nanotubes dispersed inside a polymer (imide siloxane) matrix. It was observed that the permeability of He dropped with the addition of closed ended CNTs. This large drop in He permeability indicated that the copolymer adhered well to the CNTs and that the prepared CNT MMMs were defect free. The permeability of O₂, N₂, and CH₄ increased in proportion to the open-ended CNTs in the polymer matrix. The permeability of He, H₂, and CO₂ increased after the addition of 2 wt% CNTs. The increase in the diffusion coefficients for O₂, N₂, and CH₄ in MMMs based on open-ended CNTs indicated the presence of high diffusivity CNT tunnels within the poly(imide siloxane) matrix. This diffusion suggested that CNT is an attractive additive for universally enhancing the gas permeability of polymers.

Several articles are reported in literature for gas separation using CNT MMMs, for hydrogen/methane, carbon dioxide/methane, hydrogen/carbon dioxide, oxygen/nitrogen, and carbon dioxide/nitrogen separation [358]. Tseng et al. [364] introduced a new class of multi-wall carbon nanotubes (MWCNTs)/carbon nanocomposite thin films, which were prepared by incorporating (MWCNTs) into polyimide (PI) precursor solution. The carbon films were obtained in only one coating step by a spin-coating technique on a microporous alumina substrate and were carbonized at 773 K. The MWCNTs/carbon nanocomposite thin film exhibited the ideal carbon dioxide flux of 8,656.6 Barrer and the separation factor of CO₂/N₂ was 4.1 at room temperature and 1 atm. This result was 2–4 times of magnitude higher than that of pure carbon membrane prepared by the same procedure and conditions.

Kusworo et al. [365] synthesized a new type of MMM consisting of polyethersulfone (PES) and carbon nanotubes (CNTs) and applied for biogas purification application. PES chains were grafted on the carbon nanotube surface. The modified carbon nanotubes MMMs increase the mechanical properties and permeability of all gases. For PES-modified carbon nanotubes selectivity achieved for CO₂/CH₄ was 23.4.

3.5.2.4 Graphene Membranes

Graphene is a substance composed of pure carbon, with atoms arranged in a regular hexagonal pattern similar to graphite, but in a one-atom thick sheet. It is very light, with a square meter sheet weighing only 0.77 mg. It is an allotrope of carbon whose structure is a single planar sheet of sp²-bonded carbon atoms that are densely packed in a honey comb crystal lattice (Fig. 3.68) [366].

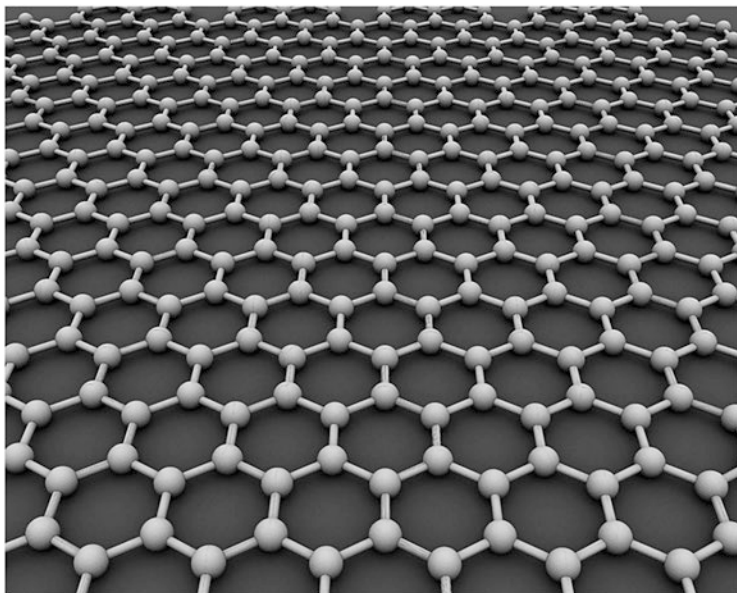


Fig. 3.68 Graphene is an atomic-scale honeycomb lattice made of carbon atoms

Graphene is most easily visualized as an atomic scale chicken wire made of carbon atoms and their bonds. In other words, graphene—a single layer of graphite—is the ultimate limit of a chemically stable and electrically conducting membrane one-atom in thickness [367]. The crystalline or “flake” form of graphite consists of many graphene sheets stacked together. The carbon-carbon bond length in graphene is about 0.142 nm. Graphene sheets stack to form graphite with an interplanar spacing of 0.335 nm. Graphene represents the first truly two-dimensional atomic crystal. It consists of a single layer of carbon atoms chemically bonded in a hexagonal “chicken wire” lattice. It has a unique atomic structure that gives it remarkable mechanical and thermal properties. Graphene is the basic structural element of some carbon allotropes including graphite, charcoal, carbon nanotubes and fullerene. It can also be considered as an indefinitely large aromatic molecule, the limiting case of the family of flat polycyclic aromatic hydrocarbons. Geim and Novoselov received the Noble Prize for groundbreaking experiments regarding this two-dimensional material [368].

Bunch et al. [369] demonstrated that a monolayer graphene membrane is impermeable to standard gases including helium. Bunch et al. measured both the elastic constant and the mass of a single layer of graphene by applying a pressure difference across the membrane. They claimed that this pressurized membrane is the world’s thinnest balloon and provides a unique separation barrier between two distinct regions that is only one atom thick. Bunch et al. also suggested that graphene drumheads offer the opportunity to probe the permeability of gases through atomic vacancies in a single layer of atoms. The authors reported that small molecules like

salts passed easily through a graphene membrane's tiny pores, while larger molecules were unable to penetrate. They suggested that the graphene has promising applications, such as membranes that filter microscopic contaminants from water, or that separate specific types of molecules from biological samples.

In the MIT news [370], Professor Rohit Karnik (mechanical engineering at MIT) suggested that a lot of chemical methods can be used to modify the pores in graphene membranes, thus creating a new technology for a new class of membranes. Karnik and O'Hern [370] observed the actual holes in the graphene membrane, looking at the material through a high powered electron microscope and found that the pores ranged in size from about 1 to 12 nm just wide enough to let some small molecules through the membrane.

Graphene can be prepared by simply heating and cooling down an SiC crystal [371]. In general, single layer or bilayer graphene forms on the Si face of crystal, whereas few-layer graphene grows on the C surface [372]. The results are highly dependent on the parameters used, like temperature, heating rate, or pressure. The other method is chemical vapor deposition, a well-known process in which a substrate is exposed to gaseous compounds. These compounds decompose on the surface in order to grow a thin film, where the by-products evaporate. Graphene can be grown by exposing a Ni film to a gas mixture of H₂, CH₄, and Ar at about 1,000 °C. The methane decomposes on the surface, so that the hydrogen evaporates. The carbon diffuses into the nickel. After cooling down in an Ar atmosphere, a graphene layer grows on the surface. The average number of layers depends on the Ni thickness and can be controlled in this way.

Porous graphene membranes have been suggested for the separation of hydrogen from methane, the separation of helium from other noble gases and methane, the selective passage of ions, the characterization of DNA, the filtration of water, and the separation of nitrogen from hydrogen. It was also reported that graphene pores are capable of separating fermionic He from bosonic He [373]. Surface adsorption effects have a significant influence on the gas permeability, especially at low temperatures [389]. Hauser and Schwerdtfeger [374] reported that nanoporous graphene membranes could be made CH₄ selective for gas purification by adjusting pore sizes in the graphene membrane.

Membranes act as selective barriers and play an important role in processes such as cellular compartmentalization and industrial-scale chemical and gas purification. The ideal membrane should be as thin as possible to maximize flux, mechanically robust to prevent fracture, and have well-defined pore sizes to increase selectivity. Graphene is an excellent starting point for developing size-selective membranes because of its atomic thickness, high mechanical strength, relative inertness and impermeability to all standard gases. However, pores that can exclude larger molecules but allow smaller molecules to pass through would have to be introduced into the material [375]. Koeing et al. [375] reported that ultraviolet-induced oxidative etching can create pores in micrometer-sized graphene membranes, and the resulting membranes can be used as molecular sieves. A pressurized blister test and mechanical resonance were used to measure the transport of a range of gases (H₂, CO₂, Ar, N₂, CH₄, and SF₆) through the pores. The experimentally measured leak

rate, separation factors and Raman spectrum agree well with models based on effusion through a small number of ångstrom-sized pores. Du et al. [373] showed, by molecular dynamics simulations, that the stronger adsorption of molecular nitrogen to graphene leads to a permeation ratio $N_2/H_2 > 1$ for graphene pores with sizes above 4.48 Å.

As the permeability of a membrane is inversely proportional to its thickness [376] the permeability of a graphene-based membrane can be enhanced tremendously because of its one-atom thickness. Unfortunately, the pristine graphene is impermeable to gases as small as helium. This is due to the electron density of its aromatic rings, which is enough to repel atoms and molecules trying to pass through the hollows; it is therefore necessary to destroy its aromatic structures for gas permeability. Fischbein and Drndic [377] sculpted closely spaced nanopores within suspended graphene using a focused electron beam of a transmission electron microscope. In addition, porous 2D sheets have been created by assembling molecular building blocks. Improvements in these techniques may be helpful for creating ordered subnanometer-sized pores within graphene which may then be used as a 2D molecular-sieve membrane [378]. Jiang et al. [379] used a porous graphene with nitrogen functionalization to separate H_2 and CH_4 .

Du et al. [373] presented porous graphene with various pore shapes for separation of hydrogen and nitrogen. The pore size and the functionalization of the pore introduced to graphene strongly affect the diffusion properties and the characteristics of the membrane. Blankenburg et al. [380] demonstrated that the porous graphene, which they fabricated, exhibits an extremely high selectivity in favor of H_2 and He among other atmospheric gases.

Qin et al. [378] proposed a new line defect-containing graphene as a gas filter for different gas species (He , H_2 , O_2 , N_2 , CO , CO_2 , and CH_4). They designed a new line defect consisting of a sequence of octagons and all-hydrogen passivated pores in graphene as a gas separation membrane using first-principles calculations. The all-hydrogen passivated pore produced a formidable barrier of 1.5 eV for CH_4 but an easily surmountable barrier of 0.12 eV for H_2 . Hence it exhibited extremely high separation capability in favor of H_2 among all studied species with selectivity on the order of 10^{22} for H_2/CH_4 . It was suggested by Qin et al. that such a line defect-containing a graphene-based membrane could play a great role on numerous clean energy applications.

Schrier [381] demonstrated that graphene could be permeable to gases and could be made selectively permeable by introduction of pores. Schrier proposed an economical means of separating He from the other noble gases and alkanes present in natural gases by using tailored graphene. Schrier and McLain [382] also demonstrated that isotope separation can be done by using graphene membranes. Jiang et al. [379] also investigated permeability and selectivity of graphene sheets with designed subnanometers pores using first principles density functional theory calculations. It was found that high selectivity on the order of 10^8 for H_2/CH_4 with a high H_2 permeance would be possible for a nitrogen-functionalized pore. Extremely high selectivity on the order of 10^{23} for H_2/CH_4 for an all-hydrogen passivated pore, whose small width (at 2.5 Å) presents a formidable barrier (1.6 eV) for CH_4 , would

be easily surmountable for H₂. These results suggest that these pores are far superior to traditional polymer and silica membranes, where bulk solubility and diffusivity dominate the transport of gas molecules through the material.

Junghwan et al. [383] studied the structural deformation of porous graphene (PG) under tensile stress and the diffusion properties of H₂, O₂, and CO₂ through PG under different strain conditions using the first-principles density functional theory. It was observed that the application of a tensile stress can significantly increase the diffusion rate of H₂, O₂, and CO₂ in PG by 7, 13, and 20 orders of magnitude, respectively. Thus, the diffusion rate of gases through PG can be controlled by applying tensile stress. This technique will lead to wide range of energy and environmental applications.

Lee and Aluru [384] observed that by introducing a water slab between a gas mixture and the graphene membrane, the gas mixture can be separated based on the water-solubility of the gas molecule. Lee and Aluru separated CO₂ from CO₂/O₂, CO₂/N₂, and CO₂/CH₄ mixtures by using this technique. The separation ratio followed the water solubility of gas molecules in the mixture. The separation of gas mixtures can be controlled and the selectivity ratio can be enhanced with the water slab. With a thicker water slab, higher selectivity can be obtained. Graphene may become an ideal material for next-generation membranes due to its atomistic thickness, remarkable mechanical strength, and potential for size selective transport through nanometer-scale holes in its lattice. In the near future, graphene membranes could take the place of polymeric membranes for gas separation.

3.6 Gas Separation Membrane Structures

Transport of small gas molecules through polymers occurs by diffusion through transient free-volume elements or through cavities by random thermally stimulated motion of the flexible chains. Cavity sizes and shapes in rigid microporous inorganic materials such as zeolite [385] and carbon molecular sieve materials [386] are uniform, but not in the amorphous polymers. The cavity radius (r) of the most selective polymer such as polyimides, polysulfones and polycarbonates, as measured by positron annihilation life time spectroscopy (PALS), is 0.3 nm or less with a broad distribution of cavity sizes, and gas permeability is rather low [387]. The most permeable polymer, poly(1-trimethylsilyl-1-propyne) (PTMSP) has a cavity size distribution centered at around $r=0.3$ nm and $r=0.6-0.7$ nm [124]. Thus, among known polymers, free volume element size and distribution play a key role in determining permeability and separation characteristics. However, the broad size range of free volume elements in such materials precludes the preparation of polymers having both high permeability and high selectivity.

Park et al. [388] demonstrated that free-volume structures in dense vitreous polymers that enable outstanding molecular and ionic transport and separation performance surpass the limits of conventional polymers. The unusual microstructure in these materials can be systematically tailored by thermally driven segment rearrangement.

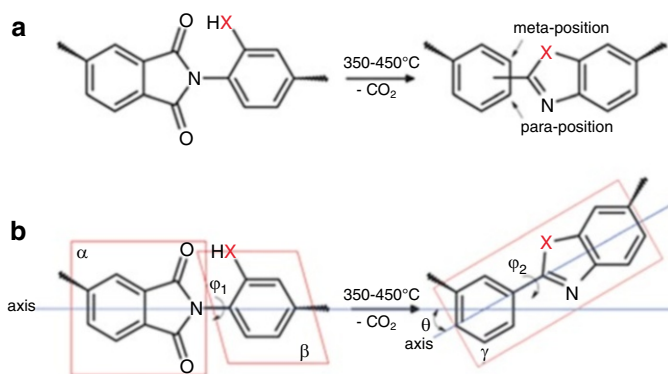


Fig. 3.69 Two major factors contributing to structural change during thermal chain rearrangement of polyimides containing ortho-positioned functional groups (X is O or S). **(a)** Change of chain conformation—polymer chains consisting of meta- and/or para-linked chain conformations can be created via rearrangement. **(b)** Spatial relocation due to chain rearrangement in confinement, which may lead to the generation of free-volume elements [α plane, phthalic imide ring; β plane, XH-containing phenylene ring; γ plane, newly created phenylene-heterocyclic ring (if X is O, benzoxazole-phenylene ring; if X is S, benzothiazole-phenylene ring); φ_1 and φ_2 , dihedral angle; θ , tilting angle after transformation]

Free volume topologies can be tailored by controlling the degree of rearrangement, flexibility of the original chain, and judicious inclusion of small templating molecules. Thus, this rational tailoring of free-volume element architecture provides a route for preparing high performance polymers for molecular-scale separation. For their demonstration, Park et al. prepared completely aromatic, insoluble, infusible polymers from highly soluble precursors of aromatic polyimides containing ortho-positioned functional groups (e.g., $-\text{OH}$ and $-\text{SH}$) by irreversible molecular rearrangement at about 350–450 °C (Fig. 3.69).

If managed properly, these changes in chain conformation and topology create well-connected, narrow size distribution of free volume elements (i.e., cavities) appropriate for molecular separation.

3.6.1 Homogeneous Dense Membranes or Symmetric Membranes

Symmetric membranes merely consist of a uniform structure (usually the cross-section of the membrane). Homogeneous and microporous are the two typical examples of symmetric membranes; in particular, a homogeneous membrane is referring to as a dense membrane, which has tremendous scientific value and are intensively used at the laboratory scale for the fundamental study of intrinsic membrane properties.

Non-porous or dense membranes provide high selectivity or separation of gases from their mixtures, but the rates of transport of gases are usually low. An important property of non-porous dense membranes is that even permeates of similar sizes may be separated if their solubility in the membrane differs significantly. Dense membranes can be prepared by melt extrusion, where a melt is envisioned as a solution in which the polymer is both a solute and solvent. In the solution-casting method, dense membranes are cast from polymer solution prepared by dissolution of a polymer in a solvent vehicle to form a sol. This is followed by complete evaporation of the solvent after casting.

3.6.2 *Asymmetric Membranes*

Asymmetric membranes are used primarily for pressure-driven membrane processes. In contrast to symmetric membranes, their structure consists of a very thin active skin layer on a highly porous substrate. The main purpose of this support layer is to provide the membrane with adequate mechanical strength and eliminate substantial structure resistance of gas transport through the polymer matrix. Phase inversion is mainly used to prepare asymmetric membranes.

In general, asymmetric membranes can be grouped into the following four basic structures [389]:

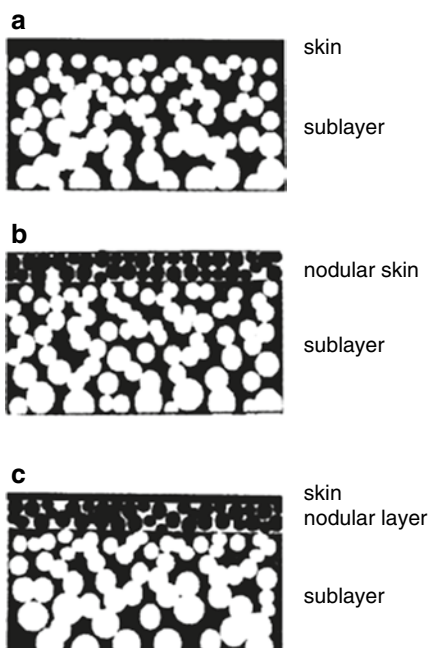
1. An integrally asymmetric membrane with a porous skin layer.
2. An integrally asymmetric membrane with a dense skin layer.
3. A thin-film porous composite membrane.
4. A thin-film dense composite membrane.

The membranes included in groups 1 and 2 are made of one material, whereas the membranes included in groups 3 and 4 are made of at least two different materials and consist of a thin top layer over a porous support or a backing material, which provides mechanical strength to the whole membrane while the membrane performance is controlled mainly by the top thin layer.

3.6.2.1 *Integrally Skinned Bilayer Membranes*

An integrally skinned asymmetric membrane consists of a relatively dense skin supported by a microporous sublayer as shown in Fig. 3.70a, b (bilayer). It is generally accepted that the bilayer membrane is formed by gelation and liquid–liquid demixing. When another layer, termed the nodular layer, is present between the skin and the sublayer, the membrane is called a trilayer membrane. A nodule denotes a fine spherical particle consisting of macromolecular aggregates. The skin layer itself consists of a closely packed array of nodules as shown in Fig. 3.70c. Most of integrally skinned asymmetric membranes have been prepared by an immersion precipitation process, which involves immersion of the polymer solution into a nonsolvent gelation bath.

Fig. 3.70 Schematic drawings of various membrane morphology. (a) Bilayer; (b) bilayer; and (c) trilayer



Both the thermodynamics and kinetics—but predominantly the kinetics—of the immersion process play important roles in determining the membrane morphology [390].

Loeb and Sourirajan (1960) invented the first integrally skinned membrane for desalination by phase inversion of cellulose acetate sols. In the integrally skinned membrane, the skin and the porous substrate are composed of the same material. Differences in density between the two layers are the result of interfacial forces and the fact that solvent loss occurs rapidly from the air-polymeric solution and polymeric solution-coagulation media interfaces from the solution interior [391].

Kesting [392] demonstrated that there are four superimposed tires of structure in integrally skinned phase inversion membrane:

1. **Macromolecules:** A macromolecule is a very large molecule commonly created by polymerization of smaller subunits. The individual constituent molecules of polymeric macromolecules are called monomers.
2. **Nodules:** these are the macromolecular aggregates consisting of several tens of individual macromolecules and approximately 200 Å in diameter.
3. **Nodule aggregates:** 400–1,000 Å in diameter spherical clumps of nodules.
4. **Supernodular aggregates:** aggregates of nodule aggregates which constitute the walls of 0.1–2 μm in diameter open cells in the membrane structure.

The skins of integrally skinned membranes consist of a single layer, one nodule aggregate thick of coalesced and compacted nodule aggregates. Pores in the various separation regimes (gas separation (GS), RO, UF, and MF) can be seen as more or

less static two-dimensional (or fractal) spaces that are bounded by progressively larger structural subelements and elements.

Two types of pore are found in the skins of GS membranes and these may account for the origin of dual mode sorption and the permeation of gases. The smaller pores, the Henry's mode sites, are the average interchain displacements between parallel chain segments within the nodule. The large pores, the Langmuir sorption sites, are the average displacements in the low density domain where nodules impinge on one another.

3.6.2.2 Integrally Skinned Trilayer Membranes

Figure 3.68c shows the structure of the integrally skinned trilayer membranes including

1. Skin
2. Nodular layer
3. Sublayer

To improve the permeation through a membrane is to reduce the thickness of the dense skin layer. To achieve this goal, integrally skinned asymmetric membranes [107, 390, 393] and multilayer composite membranes are most widely used [394]. As already mentioned, integrally skinned asymmetric membranes are made from one material and consist of a thin, essentially defect-free skin layer superimposed on a porous substrate; therefore, the gas permselectivity is determined by the intrinsic properties of the membrane material used. Multilayer composite membranes possess one or more selective layers on top of a microporous support layer, in which the selective layer and the support layer are made from different materials.

Figure 3.71 illustrates the schematic representation of an asymmetric bilayer and graded density skin asymmetric trilayer. The transition layer of the graded density skin asymmetric membrane corresponds to the nodular layer of the integrally skinned trilayer membrane.

Integrally skinned membranes can be formed by contacting the polymer solution with a non-solvent and forming the membrane in a one-step process. On contact with the non-solvent, mass transfer takes place between the non-solvent from the coagulation bath and the solvent in the nascent membrane resulting in micro-phase separation within the membrane. Depending on the pathway of phase separation, a dense layer, also called the skin layer, is believed to form on the surface of the membrane. The skin formation is hypothesized to occur when solvent outflow from the membrane exceeds the non-solvent inflow resulting in delayed demixing. This process increases the concentration of the polymer at the membrane-coagulant interface and forms the skin. An evaporative step can be included prior to the phase separation step to enhance skin formation by the evaporation of the volatile solvent from the nascent membrane, followed by a rapid phase separation of the underlying region to form a highly porous support [395]. Baker [396] predicted in 2002 that multilayer composite membranes will gradually displace simple Loeb-Sourirajan

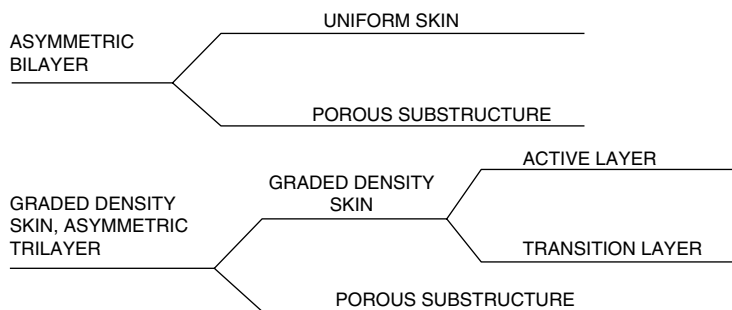


Fig. 3.71 Schematic representation of an asymmetric bilayer and graded density skin asymmetric trilayer membrane

membranes, which may be true for reverse osmosis (RO) and nanofiltration (NF) membranes but integrally skinned membranes are still dominant in manufacturing of other separation membranes. Even TFC RO and NF membranes use integrally skinned asymmetric membrane for the support layer.

Few patents are reported on integrally skinned membranes (trilayer)—mainly hollow fibers for gas separation [395, 397]. Fritzsche et al. [391] spun polysulfone hollow fiber membranes from propionic acid (*N*-methylpyrrolidone complex) and from a formylpiperidine/formamide mixture. The structure of these membranes was investigated as a function of progressive surface removal with oxygen plasma. A pure gas permeation rated was obtained on these samples. Li et al. [106] also studied integrally skinned hollow fibers with a defect free top layer for gas separation; however, not much research has been done so far on these membranes for gas separation.

3.6.2.3 Thin Film Composite Membranes (TFC)

Thin film, composite membranes consist of a thin polymer barrier formed on more porous support layers (almost always a different polymer from the surface layer). The skin layer determines the separation characteristics of the membrane; the porous backing serves only as a support for the selective layer and has no effect on membrane transport properties. In TFC membranes, it is possible to optimize the performance of the different materials independently (two steps). Composite membranes are less sensitive to the presence of humidity in the gas streams, avoiding the separate hydration step in their processing.

Thin-film composite membranes (TFC or TFM) are manufactured principally for use in water purification or water desalination systems. They also have use in chemical applications such as batteries and fuel cells. Essentially, TFC material is a molecular sieve constructed in the form of a film from two or more layered materials.

Thin film composite membranes are used:

- In water purification.
- As a chemical reaction buffer (batteries and fuel cells).
- In industrial gas separations.

Kusakabe et al. [398] coated the outer surface of a α -alumina tube with a γ -alumina film via the sol-gel process, then the tube was further coated with polycarbosilane (PC), which was cured at 473 K and pyrolyzed at 623–823 K. The composite membrane had 1–1.4 μm in thickness and had no pinholes larger than several nm. The permeation of H_2 and the separation factor of H_2 to N_2 were $5.5 \times 10^{-7} \text{ mol m}^{-2} \text{ s}^{-1} \text{ Pa}^{-1}$ and 7.2, respectively at 673 K.

Ren et al. [399] used poly(amide-6-b-ethylene oxide) (PEBA1657) copolymer to prepare a polyetherimide (PEI)/PEBA1657 (PEI as a support) composite membrane and ultra thin multilayer PEI/polydimethylsilicone (PDMS)/PEBA1657/PDMS composite membranes by dip-coating method for sour gas capturing. The gas permeation and transport characteristics of sour gases (CO_2 , H_2S and SO_2) were investigated and analyzed. With the increase of transmembrane pressure difference, the permeation of H_2S , CO_2 , and SO_2 increased due to a pressure-induced plasticization effect. The temperature dependency of H_2S permeance for PEI/PEBA1657 composite membranes changed from positive to negative when the transmembrane pressure difference increased from 3 to 7 atm. In the multilayer PEI/PDMS/PEBA1657/PDMS composite membrane, the transport resistance for CO_2 and H_2S was mainly from the PEBA1657 selective layer, and thus, the membranes had high permeances for CO_2 and H_2S and high selectivities for CO_2/N_2 and $\text{H}_2\text{S}/\text{N}_2$.

Jiang et al. [400] synthesized aqueous polyurethane dispersions (PUDs) with poly(dimethylsiloxane) (PDMS), or mixed PDMS/poly(ethylene glycol) (PDMS/PEG) as the soft segment and made thin film PUD-PVDF composite membranes for gas separation. PDMS/PEG-based PU was typically solubility-selective for condensable hydrocarbons, and nitrogen permeance was marginally enhanced in hydrocarbon–nitrogen mixtures. The copolymer membranes with both urethane and PEG segments could effectively tolerate the swelling caused by the condensable gases. The selectivities of propylene and propane to nitrogen were substantially improved, i.e., in a mixture of propylene (28 %) and nitrogen (72 %), the selectivity of propylene to nitrogen reached 29.2 with a propylene permeance of 34.4 GPU.

Gupta et al. [401] studied the gas separation on self-supported polyaniline films, and polyaniline nanomembranes with a selective layer thickness as thin as 300 nm supported on a porous polyvinylidene difluoride (PVDF). The selectivities, $\alpha_{A/B}$ (ideal) for the gas pairs H_2/N_2 , H_2/O_2 , H_2/CO_2 , CO_2/O_2 , CO_2/N_2 , and O_2/N_2 were 348, 69.5, 8.6, 8.1, 40.4, and 7.1, respectively, achieved for the self-supported undoped polyaniline films. The authors claimed that these values are considerably higher than reported by other researchers. The gas transport rates for various gases for the dense polyaniline nano-films supported on polyvinylidene difluoride were the order of 10^5 times higher than those reported for self-supported polyaniline membranes. The higher transport rates for various gases through the membranes may have been due to a higher free volume due to increased crystallinity of the polyaniline.

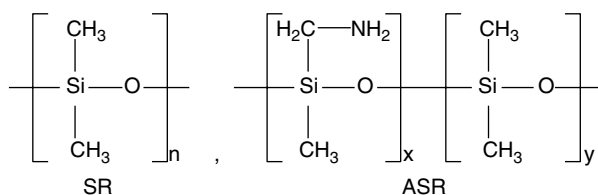


Fig. 3.72 Repeat unit structure of SR and ASR

Silicone rubber/poly(4-vinylpyridine)/polyetherimide (SR/P4VP/PEI) multilayer composite hollow fiber membranes were used for gas permeation performance (H_2 , CO_2 , O_2 , N_2 , CH_4) [394]. The PEI hollow fibers prepared from a PEI/PEG/NMP (23/0/77) spinning dope, after coating with 0.2 wt% P4VP and 3 wt% SR solutions, have gas permeances of $\text{H}_2=41$, $\text{CO}_2=7.4$, and $\text{O}_2=2.0$ GPU ($1 \text{ GPU} = 1 \times 10^{-6} \text{ cm}^3 \text{ (STP) cm}^{-2} \text{ s}^{-1} \text{ cmHg}^{-1}$) with selectivities of $\text{H}_2/\text{N}_2=117$, $\text{CO}_2/\text{CH}_4=62$, and $\text{O}_2/\text{N}_2=5.8$. Achalpurkar et al. [12] studied the gas permeation properties of dense and thin film composite membranes based on amine substituted silicon rubber (ASR) and unsubstituted silicon rubber (SR). Figure 3.72 shows the repeat unit structure of SR and ASR.

The ASR membrane exhibited higher CO_2 (15 %) as well as CH_4 (12 %) permeability as compared to the SR dense membrane, while the permeability for other gases (He , H_2 , N_2 , and O_2) were decreased up to 15 %. The permeance of TFC membranes based on different UF supports decreased in the order of decreasing porosity and increasing solution concentration (coating solution). The authors concluded that a careful variation of porosity (support material) and solution (coating solution) could lead to optimum combination of permeance and selectivity.

Monsanto-type silicon rubber-coated membranes are different from TFC membranes. High fluxes alone are not sufficient to make membrane gas separations competitive. Selectivity is also important. Membranes made from rubbery polymers, which usually are highly permeable, are not very selective. On the other hand glassy polymer membranes exhibit the opposite permeation characteristics. In order to take advantage of the high selectivities that glassy polymers afford, these materials have been spun into asymmetric hollow-fiber membranes, but such fibers normally contain surface pores or defects, which make the membranes nonselective, low-resistance channels for gas leakage. Because the permeabilities of glassy polymers are inherently low, a small number of surface pores in the skin of a glassy asymmetric fiber can significantly reduce its selectivity [402]. The Prism[®] gas separator developed by Monsanto [390, 403, 404], solved this problem by coating the skin of a glassy, asymmetric hollow fiber with an elastomer that serves to plug pores, thereby decreasing the effective permeability of these pores by four to five orders of magnitude. Although transport through pores that are coated and filled in this manner is still relatively nonselective, the volume of gas crossing the pores is greatly reduced by the coating process. Thus, the inherent selectivity of the glassy polymeric substrate can be approached. Unlike the TFC membranes in which the membrane properties are controlled by the top selective layer, the properties of

Monsanto's membrane are determined by the supporting membrane. In Monsanto's membrane, the silicon rubber layer does not function as a selective barrier but rather plugs the defects of the supporting membrane.

Reid et al. [405] studied the gas transport properties of surface treated poly (3-(2-acetoxyethyl)thiophene) (P3AcET). Hydrolysis of the ester group of P3AcET yields poly(3-(2-hydroxyethyl)thiophene) (P3HET) which is a highly permselective conducting polymer. Permeability coefficients were determined for as-cast P3AcET membranes ($P_{\text{CO}_2} = 1.42$, $P_{\text{O}_2} = 0.24$, $P_{\text{N}_2} = 0.05$, $P_{\text{CH}_4} = 0.08$ Barrers) and selectivity values were calculated ($\text{O}_2/\text{N}_2 = 5.1$, $\text{CO}_2/\text{CH}_4 = 18.5$). Formation of a thin selective P3HET surface layer resulted in an overall decrease in permeance accompanied by a dramatic increase in selectivity for both the base-treated ($\text{O}_2/\text{N}_2 = 12.9$, $\text{CO}_2/\text{CH}_4 = 20.0$) and acid-treated ($\text{O}_2/\text{N}_2 = 11.7$, $\text{CO}_2/\text{CH}_4 = 45.0$) composites.

3.7 Liquid Membranes for Gas Separation

A Liquid Membrane (LM) is just as it sounds—it is made of liquid. Because of the nature of a liquid, liquid membranes circumvent problems more conventional solid membranes encounter, but they have their own problems. One of the benefits of LMs is their high selectivity, and by using carriers, specific molecular recognition can be achieved. Despite high efficiency the lack of stability hampers LM's industrial applications.

Liquid membranes can be fashioned in two physical forms—immobilized on a solid support or as an emulsion, as shown in Fig. 3.70. Liquid membranes can perform in two modes: (1) with chemical carrier and (2) without chemical carrier. With a chemical carrier, diffusion of the permeant species is increased by diffusion of the reaction product. Without an active carrier, the liquid membrane relies on solubility differences and/or diffusion coefficient differences to separate components [406] (Fig. 3.73).

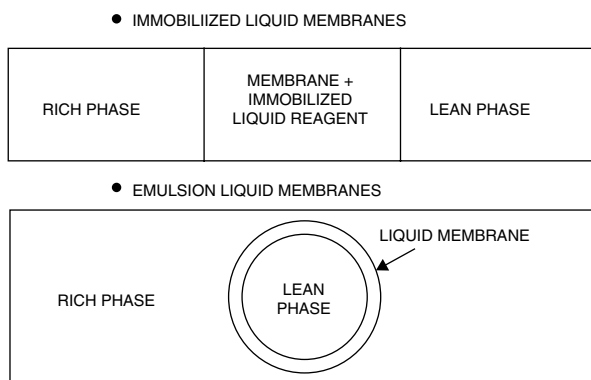


Fig. 3.73 The two forms of liquid membranes

There are two basic types of liquid membranes—emulsion liquid membrane (ELM) and immobilized liquid membrane (ILM), also called supported liquid membrane (SLM). It is necessary to stress that although supported liquid membrane and emulsion liquid membranes are conceptually similar—i.e., they employ liquid films as phase separators—the engineering aspects and applications of each are very different. Immobilized liquid membranes have been studied primarily for gas separations while emulsion liquid membranes have only been applied to liquid phase separations. ELMs remove the equilibrium limitation of solvent extractions by combining extraction and stripping in a single operation. ELMs have been successfully used to treat aqueous streams contaminated with heavy metals ions like Cu, Zn, Cd, Ni, Hg, Pb, and Cr.

3.7.1 Supported Liquid Membranes (SLM) or Immobilized Liquid Membranes (ILM)

Supported liquid membranes (SLMs) consist of an organic liquid immobilized in the pores of a support by means of capillary forces [407] and were reported for the first time in 1967 by Ward and Robb [408]. This first SLM consisted of an aqueous bicarbonate-carbonate solution fixed in a porous cellulose acetate film. Baker et al. [409] declared that supported liquid membranes (SLMs) are a possible solution to overcome low oxygen flux and selectivities.

In the early years, supported liquid membranes were called facilitated transport membranes. There are some disadvantages with supported liquid membranes: They degrade easily and have overly large membrane thicknesses, which influence the flux and selectivity of the membranes in a negative way. However, to eliminate this disadvantage, some developments have occurred. Lee et al. [410] developed SLM in which nanosized liquid domains were dispersed uniformly in the solid polymer matrix by using phase separation techniques to stabilize the supported liquid membrane. Ionic liquids were chosen as the liquid phase in the supported liquid membrane. In this system, the solvent was gradually evaporated under controlled conditions to induce the thermodynamically unstable state of the casting film. As a result, the ionic liquid domains were formed within the casting film and became bigger with decreasing solvent concentration in the cast film; the domain size can be controlled through determining the phase separation conditions in terms of the rate and time of solvent evaporation, temperature and quenching conditions. Several authors have reported a variety of active liquids that facilitate the transport of several gases. Cellulose acetate membrane used by Ward and Robb [408] for SLM was capable of separating CO₂ and O₂ with a selectivity of 4,100 using an aqueous bicarbonate-carbonate solution.

Chen et al. [411] developed a liquid membrane using hemoglobin as the carrier in a flat microporous sheet and obtained a maximum O₂ permeance of $1.4 \times 10^{-9} \text{ mol m}^{-2} \text{ s}^{-1} \text{ Pa}^{-1}$ at 720 Pa with a maximum O₂/N₂ selectivity of 18. Castro-Domínguez et al. [412] used perfluorotributylamine (PFTBA) supported on porous

alumina for the separation of O_2/N_2 and H_2/N_2 at 40 °C and 1 atm. The membrane had an average O_2/N_2 separation factor of about 60 with an O_2 permeance of $8 \times 10^{-10} \text{ mol m}^2 \text{ s}^{-1} \text{ Pa}^{-1}$, an average H_2/N_2 separation factor of 100, and a H_2 permeance of $1 \times 10^{-9} \text{ mol m}^2 \text{ s}^{-1} \text{ Pa}^{-1}$. The permeance of the perfluorocarbon membrane was correlated with the gas molecular size as $H_2 > O_2 > N_2$, suggesting that the liquid forms pockets for accommodating these gases. Although the PFTBA SLM presented an excellent separation performance, the poor stability of the membrane is a serious issue that requires significant improvements.

Deetz [413] studied the limitations of ILMs and recommended the following:

1. The stability of ILMs can be significantly improved by selecting a support with very small pore diameters.
2. Ultrathin liquid membranes can be fabricated down to 1 μm in thickness by forming in the skin layer of an porous asymmetric polymer membranes by the methods in which the liquid is selectively deposited in the skin rather than the backing support. The wide variety of pore sizes and membrane configurations available in asymmetric membranes allows for good flexibility in the design of an ultrathin liquid membrane system.

Deetz also describes the advantages of utilizing liquids as the membrane substrate rather than solids as follows:

1. *High selectivity.* The large differences in the gas/vapor solubilities of various liquid phases allow for the development of high selective membranes. It is possible to fabricate stable ILMs composed of homogeneous liquids with selectivity ratios greater than 100,000 to 1.
2. *High flux.* Because of their high gas diffusion coefficients (1,000 \times greater than in solids) and solubilities, liquid membranes are inherently more permeable. Homogeneous liquid membranes with permeabilities approaching those of microporous membranes (100,000 Barrer) are possible. The fabrication of ILMs in ultrathin form enhances the already high flux such that, in some cases, the boundary layer of gas passing over the membrane acts as a greater barrier than the membrane itself. In this case the design of a system in which the boundary layer thickness is minimized becomes the paramount concern.
3. *No pinhole problems.* When solids are cast very thin, pinhole problems frequently occur. The occurrence of pinholes results in the convective transfer of gases across the membrane and, thus, a reduction in selectivity.
4. *Short development time.* Due to the extensive database available on liquid systems, the performance of an ILM can be predicted or easily determined. No new materials need to be developed. Because of these factors the time required to develop a highly selective membrane can be short.

The most common mass transfer measurement made in liquid membrane research is flux. Several techniques have been reported for flux measurement. Ward [414] measured the pressure drop as a function of time across a liquid membrane and calculated a mass flux from the measurement. If the low pressure side of the membrane is swept by steam or an inert gas, the concentration of the permeant species

can be determined by a standard method such as chromatography. The mass or molar flux could be calculated by a material balance. To measure the flux directly, Donaldson and Quinn described a method based on radioisotope tracer technique [415]. Both sides of a permeation cell containing the liquid membrane was charged with an equal partial pressure of carbon dioxide. A small quantity $^{14}\text{CO}_2$ was introduced into the lower half of the cell and the rate of accumulation of $^{14}\text{CO}_2$ was measured by Geiger–Müller tube. This method does not create pH gradients across the membrane.

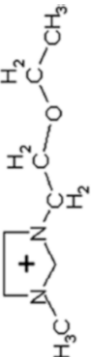
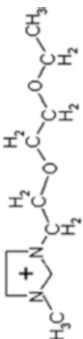
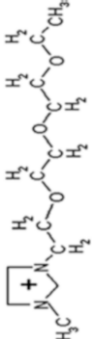
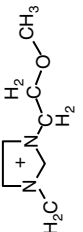
Since the major mechanism of transport in liquid membranes is diffusion for both of the transported species and the carrier complex, a knowledge of diffusion coefficients is essential for accurate description of the system performance. Many theoretical works for binary diffusion have been reported in the literature. Most theoretical developments for binary diffusion coefficients are based on modifications to the Stokes equation and are applicable to certain solvents and/or components [416, 417]. Reid et al. made a good description of predictive equations and their applicability and accuracy. In general, accuracy is decreased as the solutions become more non-ideal and/or the viscosity increases [418].

The supported ionic liquid membranes (SILMs), in which porous supports are filled with an ionic liquid (IL), have received significant attention during recent years. These membranes have been shown to be an attractive way for highly selective transport of organic compounds involved in the synthesis of pharmaceutical and fine chemicals. They can also be used for gas separation [419]. Seeberger et al. [420] showed the possibility of separating continuously gaseous compounds like CO_2 , H_2S , THT (tetrahydrothiophene), and SO_2 from N_2 or CH_4 with supported ionic liquid membranes. A polymer film as support was coated by ionic liquids and tested for continuous separation of CO_2 and sulfur compounds from different gas mixtures. The influence of support properties, ionic liquid and gas flow on the achievable degree of separation, i.e., permeabilities and selectivities, was studied. The results indicated that competitive selectivities and permeabilities can be achieved, as compared to industrial processes based on polymeric membranes.

Cserjési and Vass [421] introduced four types of novel ionic liquids named as VACEM type ionic liquids (Table 3.27) and impregnated them in a porous hydrophobic PVDF membrane. VACEM type ionic liquids, which were built up of a common hexafluorophosphate anion and different cations, were tailored in order to dissolve CO_2 . The permeability of H_2 , N_2 , and CO_2 was investigated under various gas phase pressures (2.2, 1.8, 1.4 bar) and temperatures (30, 40, 50 °C). It was observed that permeability of CO_2 was much higher than the permeability of the other two gases through the membranes prepared with VACEM type ionic liquids.

Gan et al. [422] studied the permeability of H_2 , O_2 , N_2 , CO , and CO_2 through SILMs supported on nanofiltration membranes, applying four types of ionic liquids—(C_4 -mim $[\text{NTf}_2]$, C_{10} -mim $[\text{NTf}_2]$, $\text{N}_{8881}[\text{NTf}_2]$, $\text{C}_8\text{P}_y[\text{NTf}_2]$)—with a common anion but different cations supported on nanofiltration membranes. The molecular structure of C_4 -mim $[\text{NTf}_2]$, C_{10} -mim $[\text{NTf}_2]$, $\text{N}_{8881}[\text{NTf}_2]$, and $\text{C}_8\text{P}_y[\text{NTf}_2]$ are given in Fig. 3.74.

Table 3.27 Names and structural formula of the VACEM type ionic liquid

Name		Cation	Anion
VACEM 42	1-(2-Etoxy-ethyl)-3-methylimidazolium hexafluorophosphate		PF ₆ ⁻
VACEM 44	1-[2-[2-(2-Etoxy)-ethoxy]-ethyl]-3-methylimidazolium hexafluorophosphate		PF ₆ ⁻
VACEM 47	1-[2-[2-[2-(2-Ethoxy)-ethoxy]-ethoxy]-ethoxy]-3-methylimidazolium hexafluorophosphate		PF ₆ ⁻
VACEM 58	1-(2-Methoxy-ethyl)-3-methylimidazolium hexafluorophosphate		PF ₆ ⁻

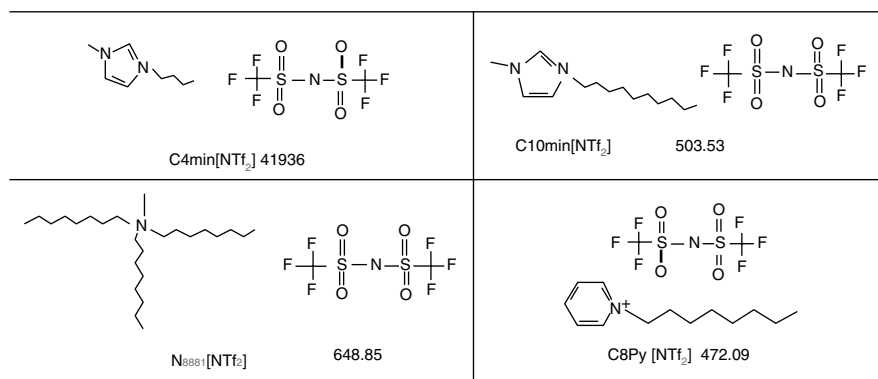


Fig. 3.74 The molecular structure of C₄-mim[NTf₂], C-mim[NTf₂], N₈₈₈₁[NTf₂], and C₈Py[NTf₂]

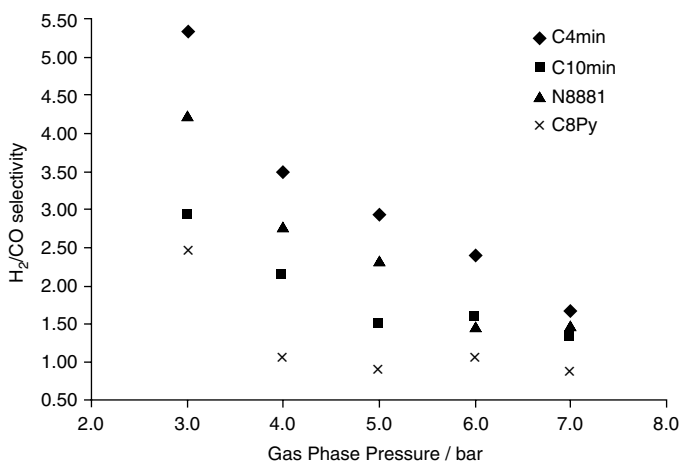


Fig. 3.75 Calculated H₂/CO selectivity based on single gas permeation measurements $T=20\text{ }^{\circ}\text{C}$

Figure 3.75 shows the calculated H₂/CO selectivity based on single gas permeation measurements at 20 °C.

N₈₈₈₁[NTf₂] had the best H₂/CO selectivity but offered a permeation rate far less than C₈Py[NTf₂], which had the best permeation performance but the worst selectivity. For all four ionic liquids, analysis of H₂/CO selectivity in single as well as binary gas feed systems established a trend of better H₂/CO selectivity associated with lower permeability at lower gas phase pressures, in contrast to lower selectivity associated with greater permeability at high pressures.

Neves et al. [423, 424] studied H₂, N₂, and CO₂ permeability and CO₂/H₂, CO₂/N₂, and H₂/N₂ ideal selectivity for (bmim)(PF₆), (omim)(PF₆), (hmim)(PF₆), and (bmim)(BF₄) IL based SILMs. All supported ionic liquid membranes (SILMs) had the highest permeability for CO₂ and the permeability was affected by the alkyl

chain length of the IL cation and by the anion. It was concluded that SILMs could be used in gas separation due to their adequate permeability and high selective values.

Cserjési et al. [425] prepared supported liquid membranes (SLMs) with 12 different types of ionic liquids: two well-known ILS—([bmim][BF₄]) and ([emim][CF₃SO₃])—and ten different types of commercially available novel ILS (Amoeng™ 100, Ecoeng™111P, Cyphos 102, Cyphos 103, Cyphos 104, Cyphos 106, Cyphos 166, Cyphos 163, Cyphos 169, and [Set₃][NTf₂]). The chemical structure, water content, purity, and the sources of the used ILS are given in Table 3.28. The supporting phase was hydrophobic porous PVDF flat sheet membrane.

Tables 3.29 and 3.30 contain the N₂, H₂, CH₄, and CO₂ permeabilities and the selectivities of the investigated SILMs.

All SILMs have the highest permeability values for CO₂ and the lowest for N₂ and the membrane permeabilities vary in the range of 37.5–210 × 10¹⁸ m² s⁻¹ Pa⁻¹ for N₂, 90–840 × 10¹⁸ m² s⁻¹ Pa⁻¹ for H₂, 45–847.5 × 10¹⁸ m² s⁻¹ Pa⁻¹ for CH₄, and 705–5,602.5 × 10¹⁸ m² s⁻¹ Pa⁻¹ for CO₂. Amoeng™ 100 has the lowest and [Set₃][NTf₂] the highest permeability for the four gases studied.

From Tables 3.29 and 3.30, it is clear that all of the SILMs are highly selective for CO₂ over the other three gases, selective for H₂ over N₂ and CH₄, and selective for CH₄ over N₂. However, there is a significant variance in the ideal selectivity results. There is a 500 % selectivity difference in CO₂/N₂, 260 % in CO₂/H₂, 406 % in CO₂/CH₄, 388 % in H₂/N₂, 187 % in H₂/CH₄, and 427% in CH₄/N₂. On comparing these preliminary selectivity results to the upper-bound values for the selectivity vs. permeability of polymer membranes for some common gas pairs (i.e., O₂/N₂, H₂/N₂, CO₂/CH₄) given by Robeson [426], most of these SILMs have better ideal-selection properties than the commonly used, industrial polymer membranes.

Hanioka et al. [427] demonstrated a support liquid membrane (SLM) based on task-specific ionic liquid to achieve the selective and facilitated CO₂ transport through the membrane. For this purpose three ionic liquids were synthesized:

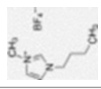

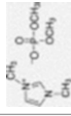

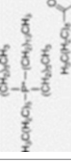
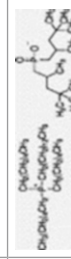
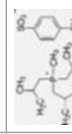
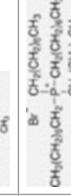
- 1-Butyl-3-methylimidazolium bis(trifluoromethylsulfonyl)imide [C₄mim][Tf₂N].
- N*-Aminopropyl-3-methylimidazolium bis(trifluoromethylsulfonyl)imide [C₃NH₂min][Tf₂N], and
- N*-Aminopropyl-3-methylimidazolium trifluoromethanesulfone [C₃NH₂min][CF₃SO₃].

Table 3.31 shows the molecular structures and abbreviations of the ionic liquids.

The porous hydrophilic polytetrafluoroethylene (PTFE) membrane was used as the support of the SLM.

Supported ionic liquid membranes (SILMs) have been used in gas separation of various gases, including CO₂/N₂, CO₂/CH₄, CO₂/H₂, CO/H₂, CO₂/He, and SO₂/CH₄. However, so far SILMs have not been used for industrial applications due to the membrane liquid loss under the high cross-membrane pressure difference (δp). It has been generally considered that the membrane liquid loss of SLMs is attributed to the high δp over the capillary force that the membrane can sustain. The maximum δp that a SLIM can resist is related to the maximum pore size of the membrane and the pore structure, the interfacial tension of membrane liquids, and the contact angle.

Table 3.28 The ionic liquids used in SILMs [425]

Short name	Name	Chemical structure	Water content (w/w, %)	Purity	Source
[bmim][BF ₄]	1-Butyl-3-methylimidazolium tetrafluoroborate		0.13	>97 %	Solvent Innovation GmbH, Cologne, Germany
Ammoeng™ 100			0.21	>95 %	
Ecoeng™ 111P	1,3-Dimethylimidazolium dimethylphosphate		0.78	>98 %	
Cyphos 102	Trihexyltetradecylphosphonium bromide		0.04	>85 %	
Cyphos 103	Trihexyltetradecylphosphonium decanoate		4.68	>95 %	IoLiTec GmbH & Co., KG, Germany
Cyphos 104	Trihexyltetradecylphosphonium bis(2,4,4-trimethylpentyl)phosphinate		0.07	>95 %	
Cyphos 106	Trisobutylmethylphosphonium tosylate		1.22	>95 %	
Cyphos 166	Tetraoctylphosphonium bromide		0.01	>95 %	

(continued)

Table 3.28 (continued)



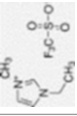
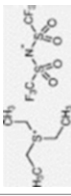
Short name	Name	Chemical structure	Water content (w/w, %)	Purity	Source
Cyphos 163	Tetrabutylphosphonium bromide		0.01	>95 %	
Cyphos 169	Ethyltributylphosphonium diethyl phosphate		0.01	>97 %	
[emim][CF ₃ SO ₃]	1-Ethyl-3-methylimidazolium triflate		0.83	>99 %	
[Set ₃][NTf ₂]	Triethylsulfonium bis(trifluoromethylsulfonyl) imide		0.32	>99 %	

Table 3.29 Permeability results of the SILMs [425]

SILMs	Permeability (barrer)			
	N ₂	H ₂	CH ₄	CO ₂
[bmim][BF ₄]	5.04	32.2	20.3	93.9
Ammeoeng TM 100	1.79	11.9	5.76	93.9
Ecoeng TM	11.6	19.9	15.6	127
Cyphos 102	15.3	92.6	76.5	637
Cyphos 103	11.3	86.6	65.1	487
Cyphos 104	20.3	124	113	642
[emim][CF ₃ SO ₃]	14.3	37.2	21.1	486
[Set ₃][NTf ₃]	28.4	112	81.2	747




Table 3.30 Selectivities results of the SILMs

SILMs	Selectivity					
	CO ₂ /N ₂	CO ₂ /H ₂	CO ₂ /CH ₄	H ₂ /N ₂	H ₂ /CH ₄	CH ₄ /N ₂
[bmim][BF ₄]	52.3	8.18	12.9	6.40	1.58	4.04
Ammeoeng TM 100	52.6	7.93	16.5	6.64	2.06	3.22
Ecoeng TM	10.9	6.38	8.12	1.71	1.27	1.35
Cyphos 102	41.5	6.87	8.32	6.03	1.21	4.99
Cyphos 103	43.1	5.62	7.49	7.67	1.33	5.76
Cyphos 104	31.6	5.17	5.66	6.11	1.10	5.58
[emim][CF ₃ SO ₃]	34.0	13.1	23.1	2.61	1.77	1.47
[Set ₃][NTf ₃]	36.2	6.67	9.290	3.93	1.38	2.85

Thus, several researchers have studied the stability of SILMs for gas separation. Zhao et al. [428] reported that the loss of the SILMs can be attributed to two reasons—membrane liquid loss from membrane compression and from the large pores. The latter can lead to SILM degradation, but the former does not lead to degradation owing to the decrease of membrane pore diameter under compression. Both the thickness and pore diameter of the SILM can be compressed due to δp , including the decrease in porosity. Luisa et al. [429] obtained the permeabilities of air, CO₂ and 10 vol% SO₂–air by using different SILMs. The permeability of air was one order of magnitude lower than CO₂ permeability and was also lower than the permeability of the mixture of air and 10 vol% SO₂.

Theoretically, SLM technology is one of the most efficient membrane-based methods of separation. It does not use pressure or voltage but is based on the difference of chemical energy as a driving force of the process; for example, the use of a simple H⁺ concentration difference. Coupled co- or counter-ion transport allows for an active transport of the targeted species from dilute solutions into more concentrated solutions and for collecting toxic or precious species in a small volume of the acceptor solution.

Table 3.31 Ionic liquid tested in the present study

Abbreviation	Molecular structure	Water content (%)	Viscosity (mPas)
[C ₃ NH ₂ mim][CF ₃ SO ₃]	 NH ₂ CF ₃ SO ₃ ⁻	1.4	3,760
[C ₃ NH ₂ mim][Tf ₂ N]	 [(CF ₃ SO ₂) ₂ N] ⁻	5.7	2,180
[C ₄ mim][Tf ₂ N]	 [(CF ₃ SO ₂) ₂ N] ⁻	1.8	70

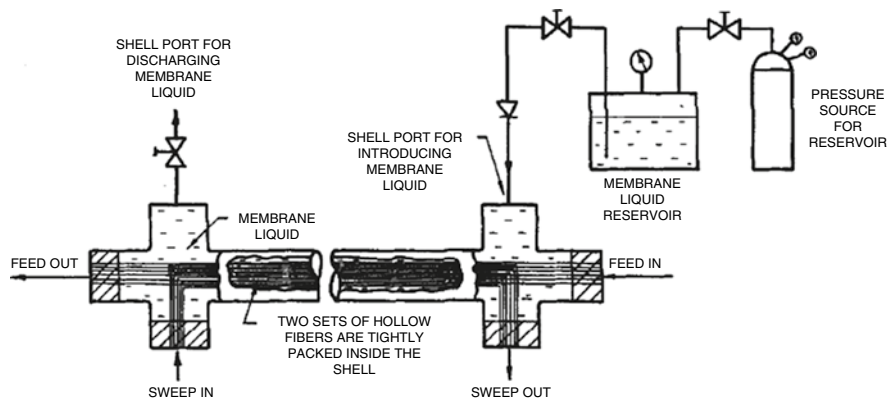


Fig. 3.76 HFCLM permeator with membrane liquid reservoir and pressure source

The primary drawback of supported liquid membrane is that over time the liquid carrier evaporates or is pushed out of membrane pores, resulting in a nonselective transport. Thick membranes could improve stability and allow a reasonable life time but with a sacrifice in gas flux. Room temperature ionic liquids with negligible vapor pressure may overcome the problem of volatility. Majumdar et al. [430] developed a new membrane separation technique for gas mixtures. In this technique feed and sweep gases flow through the lumen of two different sets of hydrophobic microporous hollow fibers while a liquid on the shell side acts as the membrane. This membrane was named the contained liquid membrane (CLM). The details are shown in Fig. 3.76.

The aqueous liquid membrane, generally maintained at a pressure higher than the feed gas and permeate gas pressures, prevents physical mixing of the feed gas or the sweep (permeate) gas. The aqueous liquid was introduced to the permeator shell side from a membrane liquid reservoir under pressure. There are two sets of hollow fibers, tightly packed together in the permeator shell, which provides a very high ratio of membrane surface area to volume. Experimental studies have been made with different CO/N₂ feed mixtures and a pure helium sweep stream, with special emphasis on model landfill gas purification. The experimental data showed good agreement with the theoretical predictions [430].

References

1. Sing KSW, Everett DH, Haul RAW, Moscou L, Pierotti RA, Rouquérol J, Siemieniowska T (1985) Reporting physisorption data for gas/solid systems with special reference to the determination of surface area and porosity. *Pure Appl Chem* 57:603–619
2. Rouquerol JJ, Avnir D, Fairbridge CW, Everett DH, Haynes JM, Pernicone N, Ramsay JDF, Sing KSW, Unger KK (1994) Recommendations for the characterization of porous solids (Technical Report). *Pure Appl Chem* 66:1739–1758

3. Robeson LM (1991) Correlation of separation factor versus permeability for polymeric membranes. *J Membr Sci* 62:165–185
4. Aoki T (1999) Macromolecular design of permselective membranes. *Prog Polym Sci* 24: 951–993
5. Schmeling N, Konietzny R, Sieffert D, Rölling P, Staudt C (2010) Functionalized copolyimide membranes for gaseous and liquid mixtures. *Beilstein J Org Chem* 6:789–800
6. Budd PM, McKeown NB (2010) High permeable polymers for gas separation membranes. *Polym Chem* 1:63–68
7. Powell CE, Qiao GG (2006) Polymeric CO₂/N₂ gas separation membranes for the capture of carbon dioxide from power plant flue gases. *J Membr Sci* 279:1–49
8. Gantzel PK, Merten U (1970) Gas separations with high flux cellulose acetate membranes. *Ind Eng Chem Process Des Dev* 9:331–332
9. Nunes SP, Pinemann K-V (2001) Membrane materials and membrane preparation. In: Nunes SP, Pinemann K-V (eds) *Membrane technology in chemical industry*. Wiley-VCH, Weinheim, FRG, pp 1–67
10. Bernardo P, Drioli E, Golemme G (2009) Membrane gas separation: a review/state of the art. *Ind Eng Chem Res* 48:4638–4663
11. Reddy BSR, Senthilkumar U (2003) Prospects of siloxane membrane technology for gas separation—a review. *J Sci Ind Res* 62:666–677
12. Achalpurkar MP, Kharul UK, Lohokare HR, Karadkar PB (2007) Gas permeation in amine functionalized silicon rubber membranes. *Sep Purif Technol* 57:304–313
13. Stern SA, Shah VM, Hardy BJ (1987) Structure-permeability relationships in silicone polymers. *J Polym Sci* 25:1263–1298
14. Furuzono T, Seki K, Kishida A, Ohshige T-A, Waki K, Maruyama I, Akashi M (1996) Novel functional polymers: poly(dimethylsiloxane)-polyamide multiblock copolymer. III. Synthesis and surface properties of disiloxane-aromatic polyamide multiblock copolymer. *J Appl Polym Sci* 59:1059–1065
15. Loeb S, Sourirajan S (1960) Sea water demineralization by means of a semipermeable membrane. *Sea Water Research Report* 60-60. UCLA, Department of Engineering
16. Dortmund D, Doshi K (1999) Recent developments in CO₂ removal membrane technology. UOP LLC, Des Plaines, IL
17. White L (2010) Evolution of natural gas treatment with membrane systems. In: Yampolskii Y, Freeman B (eds) *Membrane gas separation*. John Wiley & Sons, Ltd, Chichester, UK
18. Puleo AC, Paul DR, Kelley SS (1989) The effect of degree of acetylation on gas sorption and transport behaviour in cellulose acetate. *J Membr Sci* 47:301–332
19. Scholes CA, Stevens GW, Kentish SE (2012) Membrane gas separation applications in natural gas processing. *Fuel* 96:15–28
20. Minhas BS, Matsuura T, Sourirajan S (1987) Formation of asymmetric cellulose acetate membranes for the separation of carbon dioxide–methane gas mixtures. *Ind Eng Chem Res* 26: 2344–2348
21. Houde AY, Krishnakumar B, Charati SG, Stern SA (1996) Permeability of dense (homogeneous) cellulose acetate membranes to methane, carbon dioxide, and their mixtures at elevated pressures. *J Appl Polym Sci* 62:2181–2192
22. Donohue MD, Minhas BS, Lee SY (1989) Permeation behaviour of carbon dioxide–methane mixtures in cellulose acetate membranes. *J Membr Sci* 42:197–214
23. Houde AY, Stern SA (1997) Solubility and diffusivity of light gases in ethyl cellulose at elevated pressures: effects of ethoxy content. *J Membr Sci* 127:171–183
24. Park J, Steward MG (1968) Film-forming cellulose compounds. British Patent 1120373A, 17 June 1968
25. Cooley TE, Coady AB (1978) Removal of H₂S and/or CO₂ from a light hydrocarbon stream by use of gas permeable membrane. US Patent 4130403A, 19 Dec 1978
26. Sharma AK (1985) Fluorinated cellulose acetate polymers. US Patent 4549012A, 22 Oct 1985
27. Rahman SA, Ismail AF, Abdul-Rahman WAW (2001) Formation of cellulose acetate membrane for gas separation from binary dope system: effect of shear rate. Paper presented at

- Regional Symposium on Membrane Science and Technology, Puteri Pan Pacific Hotel, Johor Bharu, Malaysia, 21–25 Apr 2004
28. Vorotyntsev IV, Drozdov PN, Karyakin NV (2006) Ammonia permeability of a cellulose acetate membrane. *Inorg Mater* 42:231–235
 29. Tanioka A, Ishikawa K, Kakuta A, Kuramoto M, Ohno M (1984) Mixed gas separation by fine porous freeze-dried cellulose acetate membrane. *J Appl Polym Sci* 29:583–594
 30. Kim W, Lee JS, Bucknall DG, Koros WJ, Nair S (2013) Nanoporous layered silicate AMH-3/cellulose acetate nanocomposite membranes for gas separations. *J Membr Sci* 441:129–136
 31. Scholes CA, Kentish SE, Stevens GW (2008) Separation through polymeric membrane systems for flue gas applications. Recent patents on chemical engineering 1:52–66
 32. Ward WJ, Browall WR, Salemm RM (1976) Ultrathin silicon/polycarbonate membranes for gas separation processes. *J Membr Sci* 1:99–108
 33. Acharya NK, Yadav PK, Vijay YK (2004) Study of temperature dependent gas permeability of polycarbonate membrane. *Ind J Pure Appl Phys* 43:179–181
 34. Vijay YK, Acharya NK, Wate S, Avasthi DK (2004) Characterization of track etched membrane by gas separation. *Int J Hydrogen Energy* 29:515–519
 35. Fu YJ, Chen JT, Chen CC, Liao KS, Hu CC, Lee KR, Lai JY (2013) Characterization of morphology and gas separation performance of dry-cast polycarbonate membranes. *Polym Eng Sci* 53:1623–1630
 36. Hacarlioglu P, Toppare L, Yilmaz L (2003) Polycarbonate-polyppyrrrole mixed matrix gas separation membranes. *J Membr Sci* 225:51–62
 37. Sen D, Kalipecilar H, Yilmaz L (2006) Development of zeolite filled polycarbonate mixed matrix gas separation membranes. *Desalination* 200:222–224
 38. López-González M, Saiz E, Guzmán J, Riande E (2001) Experimental and simulation studies on the transport of gaseous diatomic molecules in polycarbonate membranes. *J Chem Phys* 115:6728–6736
 39. Yampol'skii YP, Bepalova NB, Finkel'shtein ES, Bondar VI, Papov AV (1994) Synthesis, gas permeability, and gas sorption properties of fluorine-containing norbornene polymers. *Macromolecules* 27:2872–2878
 40. Tetsuka H, Hagiwara M, Kaita S (2011) Addition-type poly(norbornene)s with siloxane substituents: synthesis, properties and nanoporous membrane. *Polym J* 43:97–100
 41. Tetsuka H, Isobe K, Hagiwara M (2009) Synthesis and properties of addition-type poly(norbornene)s with siloxane substituents. *Polym J* 41:643–649
 42. Dorkenoo KD, Pfromm PH, Rezac ME (1998) Gas transport properties of a series of high T_g polynorbornenes with aliphatic pendant groups. *Polym Sci B Polym Phys* 36:797–803
 43. Deniz S (2006) Effect of nonsolvent type on the surface morphology and preparation of microporous membranes from blends of poly(phenylene oxide) and poly(p-phenylene oxide sulfone) or polysulfone. *Desalination* 200:52–54
 44. Paul DR, Yampol'skii Y (eds) (1994) Polymer gas separation membranes. CRC Press, Boca Raton, FL
 45. Khulbe KC, Matsuura T, Lamarche G, Kim HJ (1997) The morphology characterization and performance of dense PPO membranes for gas separation. *J Membr Sci* 135:211–223
 46. Hamad F, Matsuura T (2005) Performance of gas separation membranes made from brominated high molecular weight poly(2,4-dimethyl-1,6-phenylene oxide). *J Membr Sci* 253:183–189
 47. Khulbe KC, Chowdhury G, Kruczek B, Vujosevic R, Matsuura T, Lamarche G (1997) Characterization of the PPO dense membrane prepared at different temperatures by ESR, atomic force microscope and gas permeation. *J Membr Sci* 126:115–122
 48. Hamad F, Khulbe KC, Matsuura T (2002) Characterization of gas separation membranes prepared from brominated poly(phenylene oxide) by infrared spectroscopy. *Desalination* 148:369–375
 49. Yu B, Cong H, Zhao X (2012) Hybrid brominated sulfonated poly(2,6-diphenyl-1,4-phenylene oxide) and SiO₂ nanocomposite membranes for CO₂/N₂ separation. *Prog Nat Sci Mater Int* 22:661–667

50. Langsam M (1996) Polyimides for gas separation. In: Ghosh MK, Mittal KL (eds) *Polyimides: fundamental and application*. Marcel Dekker, New York
51. Yoon JC, Park HB (2011) Gas separation properties of triptycene-based polyimide membranes. In: Escobar IC, Bruggen BV (eds) *Modern applications in membrane science and technology*. ACS symposium series, vol 1078. Oxford, Washington, DC; American Chemical Society, New York, pp 107–128
52. Kim KJ, Park SH, So WW, Ahn DJ, Moon SJ (2003) CO₂ separation performances of composite membranes of 6FDA-based polyimides with a polar group. *J Membr Sci* 211:41–49
53. Li DF, Chung TS, Wang R, Liu Y (2002) Fabrication of fluoropolyimide/polyethersulfone (PES) dual-layer asymmetric hollow fiber membranes for gas separation. *J Membr Sci* 198:211–223
54. Tin PS, Chung TS, Liu Y, Wang R, Liu SL, Pramoda KP (2003) Effects of cross-linking modification of Matrimid membranes. *J Membr Sci* 225:77–90
55. Kapantaidakis GC, Koops GH, Wessling M, Kaldis SP, Sakellaropoulos GP (2003) CO₂ plasticization of polyethersulfone/polyimide gas-separation membranes. *AIChE J* 49:1702–1711
56. Bos A, Punt I, Wessling M, Strathmann H (1998) Suppression of CO₂-plasticization by semi interpenetrating polymer network formation. *J Polym Sci B Polym Phys* 36:1547–1556
57. Faiz R, Li K (2012) Polymeric membranes for light olefin/paraffin separation. *Desalination* 287:82–97
58. Dong G, Li H, Chen V (2010) Factors affect defect-free Matrimid[®] hollow fiber gas separation performance in natural gas purification. *J Membr Sci* 353:17–27
59. Peng N, Chung TS (2008) The effects of spinneret dimension and hollow fiber dimension on gas separation performance of ultra-thin defect-free Torlon[®] hollow fiber membrane. *J Membr Sci* 310:455–465
60. Chung TS, Shao L, Tin PS (2006) Surface modification of polyimide membranes by diamines for H₂ and CO₂ separation. *Macromol Rapid Commun* 27:998–1003
61. Liu Y, Wang R, Chung TS (2001) Chemical cross-linking modification of polyimide films for gas separation. *J Membr Sci* 189:231–239
62. Wang L, Cao Y, Zhou M, Qiu X, Yuan Q (2009) Synthesis, characterization, and gas permeation properties of 6FDA-2,6-DAT/mPDA copolyimides. *Front Chem Chin* 4:215–221
63. Barsema JN, Kapantaidakis GC, van der Vegt NFA, Koops GH, Wessling M (2003) Preparation and characterization of highly selective dense and hollow fiber asymmetric membranes based on BTDA-TDI/MDI co-polyimide. *J Membr Sci* 216:195–205
64. Kneifel K, Peinemann KV (1992) Preparation of hollow fiber membranes from polyetherimide for gas separation. *J Membr Sci* 65:295–307
65. Wang D, Teo WK, Li K (2002) Permeation of H₂, N₂, CH₄, C₂H₆ and C₃H₈ through asymmetric poly(etherimide) hollow-fiber membrane. *J Appl Polym Sci* 86:698–702
66. Wang D, Li K, Teo WK (1998) Preparation and characterization of polyetherimide asymmetric hollow fiber membranes for gas separation. *J Membr Sci* 138:193–201
67. Wang D, Li K, Teo WK (2002) Preparation of asymmetric polyetherimide hollow fibre membrane with high gas selectivity. *J Membr Sci* 208:419–426
68. Pientka Z, Brožová L, Bleha M, Puri P (2003) Preparation and characterization of ultrathin polymeric films. *J Membr Sci* 214:157–161
69. Bruma M, Hamciuc E, Yampolskii Y, Alentiev A, Ronova IA, Rojkov EM (2004) Polyetherimides for gas separation membranes. *Mol Cryst Liq Cryst* 418:11–19
70. Squire EN (1988) Amorphous copolymers of perfluoro-2,2-dimethyl-1,3-dioxole. EP0645406 B1, 11 Apr 2001
71. Markel TC, Pinnau I, Prabhakar R, Freeman B (2006) Gas and transport properties of perfluoropolymers. In: Yampolskii Y, Pinnau I, Freeman B (eds) *Materials science of membrane for gas and vapor separation*. John Wiley & Sons, Chichester, UK
72. Pinnau I, Toy LG (1996) Gas and vapour transport properties of amorphous perfluorinated copolymer membranes based on 2,2-bistrifluoromethyl-4,5-difluoro-1,3-dioxole/tetrafluoroethylene. *J Membr Sci* 109:125–133
73. Alentiev AY, Yampolskii YP, Shantarovich VP, Nemser SM, Plate NA (1997) High transport parameters and free volume of perfluoroxole copolymers. *J Membr Sci* 126:123–132

74. Nemser SM, Roman IC (1991) Polymer of perfluoro-2,2-dimethyl-1,3-dioxole membranes. US Patent 5051114A, 24 Sept 1991
75. Masaru N, Isamu K, Kazuya O, Gen K, Masashi M, Shunichi S, Motoi K (1990) Novel fluorine-containing cyclic polymer. US Patent 4,897,457, 30 Jan 1990
76. Avery DL, Shanbhag PV (2002) Designed selectivity gas permeable membranes. US Patent 6406517B1, 18 June 2002
77. Tokarev A, Friess K, Machkova J, Sipek M, Yamapolskii Y (2006) Sorption and diffusion of organic vapors in amorphous Teflon AF2400. *J Polym Sci B Polym Phys* 44:832–844
78. Jansen JC, Macchione M, Drioli E (2005) High flux asymmetric gas separation membranes of modified poly(ether ether ketone) prepared by the dry phase inversion technique. *J Membr Sci* 255:167–180
79. Galland G, Lam TM (1993) Permeability and diffusion of gases in segmented polyurethanes: structure–properties relations. *J Appl Polym Sci* 50:1041–1058
80. Chen SH, Yu KC, Houg SL, Lai JY (2000) Gas transport properties of HTPB based polyurethane/cosalen membrane. *J Membr Sci* 173:99–106
81. Sadeghi M, Semsarzadeh MA, Barikani M, Chenar MP (2011) Gas separation properties of polyether-based polyurethane–silica nanocomposite membranes. *J Membr Sci* 376:188–195
82. Talakesh MM, Morteza S, Chenar MP, Afsaneh K (2012) Gas separation properties of poly(ethylene glycol)/poly(tetramethylene glycol) based polyurethane membranes. *J Membr Sci* 415–416:469–477
83. Liang W, Martin CR (1991) Gas transport in electronically conductive polymers. *Chem Mater* 3:390–391
84. Martin CR, Liang W, Menon V, Parthasarathy R, Parthasarathy A (1993) Electronically conductive polymers as chemically-selective layers in membrane-based separations. *Synth Met* 55–57:3766–3773
85. Anderson MR, Mattes BR, Reiss H, Kaner RB (1991) Conjugated polymer films for gas separations. *Science* 252:1412–1415
86. Sairam M, Nataraj SK, Aminabhavi TM, Roy M, Madhusoodana CD (2006) Polyaniline membranes for separation and purification of gases, liquids, and electrolyte solutions. *Sep Purif Rev* 35:249–283
87. Blinova NV, Frantisek S (2012) Functionalized polyaniline-based composite membranes with vastly improved performance for separation of carbon dioxide from methane. *J Membr Sci* 423–424:514–521
88. Kuwabata S, Martin CR (1994) Investigation of the gas-transport properties of polyaniline. *J Membr Sci* 91:1–12
89. Lee YM, Ha SY, Lee KY, Suh DH, Hong SY (1999) Gas separation through conductive polymer membranes. 2. Polyaniline membranes with high oxygen selectivity. *Ind Eng Chem Res* 38:1917–1924
90. Illing G, Hellgardt K, Wakeman RJ, Jungbauer A (2001) Preparation and characterisation of polyaniline based membranes for gas separation. *J Membr Sci* 184:69–78
91. Hasbullah H, Kumbharkar S, Ismail AF, Li K (2011) Preparation of polyaniline asymmetric hollow fiber membranes and investigations towards gas separation performance. *J Membr Sci* 366:116–124
92. Julian H, Wenten G (2012) Polysulfone membranes for CO₂/CH₄ separation: state of the art. *IOSR J Eng* 2:484–495
93. Dai Y, Guiver MD, Robertson GP, Kang YS, Lee KJ, Jho JY (2004) Preparation and characterization of polysulfones containing both hexafluoroisopropylidene and trimethylsilyl groups as gas separation membrane materials. *Macromolecules* 37:1403–1410
94. Dai Y, Guiver MD, Robertson GP, Kang YS, Lee KJ (2003) Enhancement in the gas permeabilities of novel polysulfones with pendant 4-trimethylsilyl- α -hydroxybenzyl substituents. *Macromolecules* 36:6807–6816
95. Mc Hattie JS, Koros WJ, Paul DR (1991) Gas transport properties of polysulphones: 1. Role of symmetry of methyl group placement on bisphenol rings. *Polymer* 32:840–850

96. Marchese J, Ochoa N, Pagliero C (1995) Preparation and gas separation performance of silicone-coated polysulfone membranes. *J Chem Technol Biotechnol* 63:329–336
97. Wang D, Teo WK, Li K (2002) Preparation and characterization of high-flux polysulfone hollow fiber gas separation membranes. *J Membr Sci* 204:247–256
98. Ahn J, Chung WJ, Pinnau I, Guiver MD (2008) Polysulfone/silica nanoparticle mixed-matrix membranes for gas. *J Membr Sci* 314:123–133
99. Weng TH, Tseng HH, Wey MY (2009) Preparation and characterization of multi-walled carbon nanotube/PBNPI nanocomposite membrane for H₂/CH₄ separation. *Int J Hydrogen Energy* 34:8707–8715
100. Mao Z, Jie X, Cao Y, Wang L, Li M, Yuan Q (2011) Preparation of dual-layer cellulose/polysulfone hollow fiber membrane and its performance for isopropanol dehydration and CO₂ separation. *Sep Puri Technol* 77:179–184
101. Arahman N, Arifin B, Mulyati S, Ohmukai Y, Matsuyama H (2012) Structure change of polyethersulfone hollow fiber membrane modified with pluronic F127, polyvinylpyrrolidone, and Tetronic 1307. *Mater Sci Appl* 3:72–77
102. Wang D, Li K, Teo WK (2000) Highly permeable polyethersulfone hollow fiber gas separation membranes prepared using water as non-solvent additive. *J Membr Sci* 176:147–158
103. Borneman Z, Vant's Hof JA, Smolders CA, Van vee HM (1986) Hollow fiber gas separation membranes: structure and properties. In: *Proceedings of the fourth BOC Priestley conference*. Royal Society of Chemistry, London, 16–18 Sept 1986
104. Vant's Hof JA (1988) Wet spinning of asymmetric hollow fiber membranes for gas separation. Ph.D. Thesis, Twente University, The Netherlands
105. Van't Hof JA, Reuvers AJ, Boon RM, Rolevink HHM, Smolders CA (1992) Preparation of asymmetric gas separation membranes with high selectivity by a dual-bath coagulation method. *J Membr Sci* 70:17–30
106. Li SG, Koops GH, Mulder MHV, Van den Boomgaard T, Smolders CA (1994) Wet spinning of integrally skinned hollow fiber membranes by a modified dual-bath coagulation method using a triple orifice spinneret. *J Membr Sci* 94:329–340
107. Kesting RE, Fritzsche AK, Murphy MK, Handermann AC, Cruse CA, Malon RF (1989) Process for forming asymmetric gas separation membranes having graded density skins. US Patent 4 871,494, 3 Oct 1989
108. Fritzsche AK, Cruse CA, Murphy MK, Kesting RE (1990) Polyethersulfone and polyphenylsulfone fiber trilayer membranes spun from Lewis acid:base complexes—structure determination by SEM, DSC and oxygen plasma ablation. *J Membr Sci* 54:29–50
109. Wang D (1995) Polyethersulfone hollow fiber gas separation membranes prepared from solvent systems containing nonsolvent additives. Ph.D. Thesis, National University of Singapore
110. Wang D, Li K, Teo WK (1996) Polyethersulfone hollow fiber gas separation membranes prepared from NMP/alcohol solvent systems. *J Membr Sci* 115:85–108
111. Kim DH, Ko YH, Kim TW, Park JS, Lee HK (2012) Separation of N₂/SF₆ binary mixtures using polyethersulfone (PESf) hollow fiber membrane. *Korean J Chem Eng* 29:1081–1085
112. Jiang L, Chung TS, Li DF, Cao C, Kulprathipanja S (2004) Fabrication of Matimid/polyethersulfone dual-layer hollow fiber membranes for gas separation. *J Membr Sci* 240:91–103
113. Ismail AF, Norida R, Rahman WAW, Matsuura T, Hashemifard SA (2011) Preparation and characterization of hyperthin-skinned and high performances asymmetric polyethersulfone membrane for gas separation. *Desalination* 273:93–104
114. Pesiri DR, Jorgensen B, Dye RC (2003) Thermal optimization of polybenzimidazole meniscus membranes for the separation of hydrogen, methane, carbon dioxide. *J Membr Sci* 218:11–18
115. Berchtold KA, Young JS, Dudeck KW (2006) High temperature separation membranes of hydrogen purification and carbon capture. LALP-06-043, Mar 2006
116. Choi S, Coronas J, Lai Z, Yust D, Onorato F, Tsapatsis M (2008) Fabrication and gas separation properties of polybenzimidazole (PBI)/nanoporous silicates hybrid membranes. *J Membr Sci* 316:145–152

117. Hosseini SS, Peng N, Chung TS (2010) Gas separation membranes developed through integration of polymer blending and dual-layer hollow fiber spinning process for hydrogen and natural gas hollow fiber spinning process for hydrogen and natural gas enrichments. *J Membr Sci* 349:156–166
118. Kumbharkar SC, Liu Y, Li K (2011) High performance polybenzimidazole based asymmetric hollow fiber membranes for H₂/CO₂ separation. *J Membr Sci* 375:231–240
119. Young JSY, Long GS, Espinoza BF (2006) Cross-linked polybenzimidazole membrane for gas separation. US Patent 20060021502A1, 2 Feb 2006
120. Kong J, Li K (2001) Preparation of PVDF hollow-fiber membranes via immersion precipitation. *J Appl Polym Sci* 81:1643–1653
121. Shen Y, Lua AC (2012) Preparation and characterization of mixed matrix membranes based on PVDF and three inorganic fillers (fumed nonporous silica, zeolite 4A and mesoporous MCM-41) for gas separation. *Chem Eng J* 192:201–210
122. Consolati G, Pegoraro M, Quasso F, Severini F (2001) Chlorinated PTMSP membranes: permeability, free volume and physical properties. *Polymer* 42:1265–1269
123. Masuda T, Isobe E, Higashimura T, Takada K (1983) Poly[1-(trimethylsilyl)-1-propyne]: a new high polymer synthesized with transition-metal catalysts and characterized by extremely high gas permeability. *J Am Chem Soc* 105:7473–7474
124. Nagai K, Masuda T, Nakagawa T, Freeman BD, Pinnau I (2001) Poly[1-(trimethylsilyl)-1-propyne] and related polymers: synthesis properties and functions. *Prog Polym Sci* 26:721–798
125. Ichiraku Y, Stern SA, Nakagawa T (1987) An investigation of the high gas permeability of poly(1-trimethylsilyl-1-propyne). *J Membr Sci* 34:5–18
126. Merkel TC, He Z, Pinnau I, Freeman BD, Meakin P, Hill AJ (2003) Effect of nanoparticles on gas sorption and transport in poly(1-trimethylsilyl-1-propyne). *Macromolecules* 36:6844–6855
127. Woo M, Choi J, Tsapatsis M (2008) Poly(1-trimethylsilyl-1-propyne)/MFI composite membranes for butane separation. *Microporous Mesoporous Mater* 110:330–338
128. Qiu J, Zheng JM, Peinemann KV (2006) Gas transport properties in a novel poly(trimethylsilylpropyne) composite membrane with nanosized organic filler trimethylsilylglucose. *Macromolecules* 39:4093–4100
129. Peter J, Peinemann KV (2009) Multilayer composite membrane for gas separation based on crosslinked PTMSP gutter layer and partially crosslinked Matrimid® 5218 selective layer. *J Membr Sci* 340:62–72
130. Vopiča O, De Angelis MG, Sarti GC (2014) Mixed gas sorption in glassy polymeric membranes: I. CO₂/CH₄ mixtures sorption in poly(1-trimethylsilyl-1-propyne) (PTMSP). *J Membr Sci* 449:97–108
131. Xiao S, Feng X, Huang RYM (2007) Trimesoyl chloride crosslinked membranes for CO₂/N₂ separation and pervaporation dehydration of isopropanol. *J Membr Sci* 306:36–46
132. Papanecia A, Valente AJM, Patachia S, Lobo VMM (2009) Poly (vinyl alcohol) (PVA)-based polymer membranes. Nova, NY
133. Zou J, Ho WSW (2006) CO₂-selective polymeric membranes containing amines in cross-linked poly(vinyl alcohol). *J Membr Sci* 286:310–332
134. Matsuyama H, Terada A, Nakagawara T, Kitamura Y, Teramoto Y (1999) Facilitated transport of CO₂ through polyethylenimine/poly(vinyl alcohol) blend membrane. *J Membr Sci* 163:221–227
135. Park YI, Lee KH (2001) Preparation of water-swollen hydrogel membranes for gas separation. *J Appl Polym Sci* 80:1785–1791
136. Jenkins AD, Kratochvíl P, Stepto RFT, Suter UW (1996) Glossary of basic terms in polymer science. *Pure Appl Chem* 68(12):2287–2311
137. Paul DR, Newman S (eds) (1978) *Polymer blends*. Academic, London
138. Schmidt JJ, Gardella JA Jr, Salvati L Jr (1989) Surface studies of polymer blends. 2. An ESCA and IR study of poly(methyl methacrylate)/poly(vinyl chloride) homopolymer blends. *Macromolecules* 22:4489–4495

139. Coleman MM, Painter PC (1976) Fourier transforms infrared studies of polymeric materials. *J Macromol Sci C* 16:197–313
140. Yoshino M, Ito K, Okamoto KI (2000) Effects of hard-segment polymers on CO₂/N₂ gas-separation properties of poly(ethyleneoxide)-segmented copolymers. *J Polym Sci B Polym Phys* 38:1707–1715
141. Zimmerman CM, Koros WJ (1999) Polypyrrolones for membrane gas separation. I. Structural comparison of gas transport and sorption properties. *J Polym Sci B Polym Phys* 37:1235–1249
142. Zimmerman CM, Koros WJ (1999) Polypyrrolones for membrane gas separation. II. Activation energies and heat of sorption. *J Polym Sci B Polym Phys* 37:1251–1265
143. Patil VE, van der Broeke LJP, Vercauteren FF, Keurentjes JTF (2006) Permeation of supercritical carbon dioxide through polymeric hollow fiber membranes. *J Membr Sci* 271:77–85
144. Wang M, Yang D, Wang Z, Wang J, Wang S (2010) Effects of pressure and temperature on fixed-site carrier membrane for CO₂ separation from natural gas. *Front Chem Eng Chin* 4:127–132
145. Semsarzadeh MA, Ghalei B (2012) Characterization and gas permeability of polyurethane and polyvinyl acetate blend membranes with polyethylene oxide-polypropylene oxide block copolymer. *J Membr Sci* 401–402:97–108
146. Car A, Stropnik C, Yave W, Peinemann KV (2008) PEG modified poly(amide-b-ethylene oxide) membranes for CO₂ separation. *J Membr Sci* 307:88–95
147. Yave W, Car A, Peinemann KV, Shaikh MQ, Rätzke K, Faupel F (2009) Gas permeability and free volume in poly(amide-b-ethylene oxide)/polyethylene glycol blend membranes. *J Membr Sci* 339:177–183
148. Yave W, Car A, Funari SS, Nunes SP, Peinemann KV (2010) CO₂-philic polymer membrane with extremely high separation performance. *Macromolecules* 43:326–333
149. Madaeni SS, Nooripour RM, Vatanpour V (2012) Preparation and characterization of polyimide and polyethersulfone blend membranes for gas separation. *Asia-Pacific J Chem Eng* 7:747–754
150. Kapantaidakis GC, Koops GH, Wessling M (2002) Preparation and characterization of gas separation hollow fiber membranes based on polyethersulfone-polyimide miscible blends. *Desalination* 145:353–357
151. Kapantaidakis GC, Koops GH (2002) High flux polyethersulfone-polyimide blend hollow fiber membrane for gas separation. *J Membr Sci* 204:153–171
152. Kapantaidakis GC, Koops GH, Wessling M (2002) Effect of spinning conditions on the structure and the gas permeation properties of high flux polyethersulfone-polyimide blend hollow fibers. *Desalination* 144:121–125
153. Koros WJ, Woods DG (2001) Elevated temperature application of polymer hollow-fiber membranes. *J Membr Sci* 181:157–166
154. Seo Y, Kim S, Hong SU (2006) Highly selective polymeric membranes for gas separation. *Polymer* 47:4501–4504
155. Okamoto K, Tanaka K, Muraoka M, Kita H, Maruyama Y (1992) Gas permeability and permselectivity of fluorinated polybenzoxazoles. *J Polym Sci B* 30:1215–1221
156. McKeown NB (1998) Phthalocyanine materials: synthesis, structure and function. CUP, Cambridge, UK
157. Ilinitch OM, Fenelonov VB, Lapkin AA, Okkel LG, Terskikh VV, Zamaraev KI (1999) Intrinsic microporosity and gas transport in polyphenylene oxide polymers. *Microporous Mesoporous Mater* 31:97–110
158. McKeown NB, Budd PM (2009) Polymers of intrinsic microporosity. In: *Encyclopedia of polymer science and technology*. John Wiley & Sons, NY
159. McKeown NB, Budd PM, Msayib KJ, Ghanem BS, Kingston HJ, Tattershall CE, Makhseed S, Reynolds KJ, Fritsch D (2005) Polymers of intrinsic microporosity (PIMs): bridging the void between microporous and polymeric materials. *Chem Eur J* 11:2610–2620
160. McKeown NB (2012) Review article: Polymers of intrinsic microporosity. *ISRN Mater Sci*. Article ID 513986, 16p

161. Makhseed S, McKeown NB, Msayib K, Bumajdad A (2005) Inducing solid-state isolation of the phthalocyanine macro-cycle by its incorporation within rigid, randomly shaped oligomers. *J Mater Chem* 5:1865–1870
162. Msayib K, Makhseed S, McKeown NB (2001) Synthetic strategies towards macrodiscotic materials. Can a new dimension be added to liquid crystal polymers? *J Mater Chem* 11:2784–2789
163. Du NY, Song J, Robertson GP, Pinnau I, Guiver M (2008) Linear high molecular weight ladder polymer via fast polycondensation of 5,5',6,6'-tetrahydroxy-3,3,3',3'-tetramethylspirobisindane with 1,4-dicyanotetrafluoroben-zene. *Macromol Rapid Commun* 29:783–788
164. Du NY, Cin MMD, Pinnau I, Nicalek A, Robertson GP, Guiver MD (2011) Azide-based cross-linking of polymers of intrinsic microporosity (PIMs) for condensable gas separation. *Macromol Rapid Commun* 32:631–636
165. Du N, Park HB, Robertson GP, Dal-Cin MM, Visser T, Scoles L, Guiver MD (2011) Polymer nanosieve membranes for CO₂-capture applications. *Nat Mater* 10:372–375
166. Koros WJ, Mahajan R (2000) Pushing the limits on possibilities for large scale gas separation: which strategies? *J Membr Sci* 175:181–196
167. Roualdes S, Lee AVD, Berjoan R, Sanchez J, Durand J (1999) Gas separation properties of organosilicon plasma polymerized membranes. *AIChE J* 45:1566–1575
168. Won J, Kim MH, Kang YS, Park HC, Kim UY, Choi SC, Koh SK (2000) Surface modification of polyimide and polysulfone membranes by ion beam for gas separation. *J Appl Polym Sci* 75:1554–1560
169. Maya EM, Munoz DM, de la Campa JG, de Abajo J, Lozano AE (2006) Thermal effect on polyethyleneoxide-containing copolyimide membranes for CO₂/N₂ separation. *Desalination* 199:188–190
170. Li Y, Cao C, Chung TS, Pramoda KP (2004) Fabrication of dual-layer polyethersulfone (PES) hollow fiber membranes with an ultrathin dense-selective layer for gas separation. *J Membr Sci* 245:53–60
171. Castro-Domínguez B, Leelachaikul P, Takagaki A, Sugawara T, Kikuchi R, Oyama ST (2013) Perfluorocarbon-based supported liquid membranes for O₂/N₂ separation. *Sep Purif Technol* 116:19–24
172. McLeay EE, Jansen JC, Kapteijn F (2006) Zeolite based films, membranes and membrane reactors: progress and prospects. *Microporous Mesoporous Mater* 90:198–220
173. Barrer RM (1939) Activated diffusion in membranes. *Trans Faraday Soc* 35:644–656
174. Van Den Broeke LJP, Bakker WJW, Kapteijn F, Moulijn JA (1999) Binary permeation through a silicalite-1 membrane. *AIChE J* 45:976–985
175. Petersa TA, Fontalvoa J, Vorstmana MAG, Benesa NE, van Damb RA, Vroonb ZAEP, van Soest-Vercammenc ELJ, Keurentjesa JTF (2005) Hollow fibre microporous silica membranes for gas separation and pervaporation: synthesis, performance and stability. *J Membr Sci* 248:73–80
176. Uhlhorn RJR, Keizer K, Burggraaf AJ (1992) Gas transport and separation with ceramic membranes. Part II. Synthesis and separation properties of microporous membranes. *J Membr Sci* 66:271–287
177. de Lange RSA, Hekkink JHA, Keizer K, Burggraaf AJ (1995) Formation and characterization of supported microporous ceramic membranes prepared by sol-gel modification techniques. *J Membr Sci* 99:57–75
178. de Vos RM, Verweij H (1998) Improved performance of silica membranes for gas separation. *J Membr Sci* 143:37–51
179. Pohl PI, Heffelfinger GS (1999) Massively parallel molecular dynamics simulation of gas permeation across porous silica membrane. *J Membr Sci* 155:1–7
180. Zhang K, Sunarso J, Shao Z, Zhou W, Sun C, Wang S, Liu S (2011) Research progress and materials selection guidelines on mixed conducting perovskite-type ceramic membranes for oxygen production. *RSC Adv* 1:1661–1676

181. Kharton VV, Yaremchenko AA, Kovalevsky AV, Viskup AP, Naumovich EN, Kerko PF (1999) Perovskite-type oxides for high-temperature oxygen separation membranes. *J Membr Sci* 163:307–317
182. Ayral A, Julbe A, Roualdes S, Rouessac V, Durand J, Sala B (2006) Silica membranes-basic principles. *Period Polytech Ser Chem Eng* 50:67–79
183. Ramsay JDF (1999) Characterization of the pore structure of membranes. *MRS Bull* 24: 36–40
184. Topuz B, Gifcioglu M (2006) Permeation of pure gases through silica membranes with controlled pore size. *Desalination* 200:80–82
185. Shelekhin AB, Dixon AG, Ma YH (1992) Adsorption, permeation, and diffusion of gases in microporous glass membranes. *J Membr Sci* 75:233–244
186. Naskar MK, Kundu D, Chatterjee M (2009) Silicate-1 zeolite membranes on unmodified and modified surfaces of ceramic supports: a comparative study. *Bull Mater Sci* 32:537–541
187. Marković A, Stoltenberg D, Enke D, Schlünder E-U, Seidel-Morgenstern A (2009) Gas permeation through porous glass membranes. Part 1. Mesoporous glasses—Effect of pore diameter and surface properties. *J Membr Sci* 336:17–31
188. Structure-zeolites. www.ch.ic.ac.uk/vchemlib/course/zeolite/structure.html
189. Nomura M, Yamaguchi T, Nakao S (1997) Silicalite membranes modified by counterdiffusion CVD technique. *Ind Eng Chem Res* 36:4217–4223
190. Zeolite—Wikipedia, the free encyclopedia. International Zeolite Association, database of zeolite structures
191. Zeolite—Wikipedia, the free encyclopedia. Webmineral Zeolites, Dana Classification
192. Caro J, Noack M, Kolsch P, Schafer R (2000) Zeolite membranes—state of their development and perspective. *Microporous Mesoporous Mater* 38:3–24
193. Worathanakul P, Kongkachuichay P (2008) New SUZ-4 zeolite membrane from sol-gel technique. *World Acad Sci Technol* 2:11–21
194. Wong WC, Au LTY, Ariso CT, Yeung KL (2001) Effects of synthesis parameters on the zeolite membrane growth. *J Membr Sci* 191:143–146
195. Horri K, Tanaka K, Kita K, Okamoto K (1994) In: *Proceedings of the 26th autumn meeting of Soc. Chem. Eng., Japan*, p 99
196. Bernal MP, Xometritakis G, Tsapatsis M (2001) Tubular MFI zeolite membranes made by secondary (seeded) growth. *Catal Today* 67:101–107
197. Caro J, Noack M (2008) Zeolite membranes—recent developments and progress. *Microporous Mesoporous Mater* 115:215–233
198. Tompsett GA, Conner WC, Yngvesson KS (2006) Microwave synthesis of nanoporous materials. *Chem Phys Chem* 7:296–319
199. Li Y, Yang W (2008) Microwave synthesis of zeolite membranes: a review. *J Membr Sci* 316:3–17
200. Cundy CS (1998) Microwave techniques in the synthesis and modification of zeolite catalyst. A review. *Collect Czech Chem Commun* 63:1699–1723
201. Li Y, Chen H, Liu J, Yang W (2006) Microwave synthesis of LTA zeolite membranes without seeding. *J Membr Sci* 277:230–239
202. Choi J, Jeong HK, Snyder MA, Stoeger JA, Masel RI, Tsapatsis M (2009) Grain boundary defect elimination in a zeolite membrane by rapid thermal processing. *Science* 325:590–593
203. Varoon K, Zhang X, Elyassi B, Brewer DD, Gette M, Kumar S, Lee A, Maheshwari S, Mittal A, Sung CY, Cococcioni M, Francis LF, McCormick AV, Mkhoyan A, Tsapatsis M (2011) Dispersible exfoliated zeolite nanosheets and their application as a selective membrane. *Science* 334:72–75
204. Liu L, Cheng M, Ma D, Hu G, Pan X, Bao X (2006) Synthesis, characterization, and catalytic properties of MWW zeolite with variable Si/Al ratios. *Microporous Mesoporous Mater* 94: 304–312
205. Huang A, Wang N, Caro J (2012) Stepwise synthesis of sandwich-structured composite zeolite membranes with enhanced separation selectivity. *Chem Commun* 48:3542–3544

206. Cheng ZL, Liu Z, Wan HL (2005) Microwave-heating synthesis and gas separation performance of NaA zeolite membrane. *Chin J Chem* 23:28–31
207. Yuwen L, Zhu M, Su H, You X, Deng C, Lv X (2011) Effects of synthesis parameters on hydrothermal synthesis of NaA zeolite. *Adv Mater Res* 148:1444–1448
208. Xu X, Yang W, Liu J, Lin L, Strohn N, Brunner H (2000) Synthesis and gas permeation properties of an NaA zeolite membrane. *Chem Commun* :603–604
209. Aoki K, Kusakabe K, Morooka S (1998) Gas permeation properties of A-type zeolite membrane formed on porous substrate by hydrothermal synthesis. *J Membr Sci* 141:197–205
210. Chen X, Yang W, Liu J, Xu X, Huang A, Lin L (2002) Synthesis of NaA zeolite membrane with high performance. *J Mater Sci Lett* 21:1023–1025
211. Dey KP, Kundu D, Chatterjee M, Naskar MK (2013) Preparation of NaA zeolite membranes using poly(ethyleneimine) as buffer layer, and study of their permeation behavior. *J Am Chem Soc* 96:68–72
212. Gies H (1986) Studies on clathrates. VI: Crystal structure of decadodecasil 3R the missing link between zeolites and clathrasils. *Z Kristallogr* 175:93–104
213. Nakayama K, Suzuki K, Yoshida M, Tomita T (2006) Method of preparing DDR type zeolite membrane, DDR type zeolite membrane, and composite DDR type zeolite membrane, and method for preparation thereof. US Patent 7014680B2, 21 Mar 2006
214. van den Bergh J, Zhu W, Kapteijn F, Moulijn JA, Yajima K, Nakayama K, Tomita T, Yoshida S (2007) Natural gas purification with a DDR zeolite membrane: permeation modeling with Maxwell–Stefan equations. *Stud Surf Sci Catal* 170:1021–1027
215. van den Bergh J, Zhu W, Gascon J, Moulijn JA, Kapteijn F (2008) Separation and permeation characteristics of a DDR zeolite membrane. *J Membr Sci* 316:35–45
216. Tomita T, Nakayama K, Sakai H (2004) Gas separation characteristics of DDR type zeolite membrane. *Microporous Mesoporous Mater* 68:71–75
217. Kanezashi M, O'Brien-Abraham J, Lin YS (2008) Gas permeation through DDR-type zeolite membranes at high temperatures. *AIChE J* 54:1478–1486
218. Xiao J, Wei J (1992) Diffusion mechanism of hydrocarbons in zeolites. 1. Theory. *Chem Eng Sci* 47:1123–1141
219. Himeno S, Tomita T, Suzuki K, Nakayama K, Yajima K, Yoshida S (2007) Synthesis and permeation of a DDR-type zeolite membrane for separation of CO₂/CH₄ gaseous mixtures. *Ind Eng Chem Res* 46:6989–6997
220. Himeno S, Takeya K, Fujita S (2010) Development of biogas separation process using DDR-type zeolite membrane. *Kagaku Kogaku Ronbun* 36:545–551
221. Hong M, Li S, Falconer JL, Noble RD (2008) Hydrogen purification using a SAPO-34 membrane. *J Membr Sci* 307:277–283
222. Li S, Falconer JL, Noble RD (2006) Improved SAPO-34 membranes for CO₂/CH₄ separations. *Adv Mater* 18:2601–2603
223. Li S, Martinek JG, Falconer JL, Noble RD, Gardner TQ (2005) High-pressure CO₂/CH₄ separation using SAPO-34 membranes. *Ind Eng Chem Res* 44:3220–3228
224. Poshusta JC, Tuan VA, Pape EA, Noble RD, Falconer JL (2000) Separation of light gas mixtures using SAPO-34 membranes. *AIChE J* 46:779–789
225. Zhou R, Ping EW, Funke HH, Falconer JL, Noble RD (2013) Improving SAPO-34 membrane synthesis. *J Membr Sci* 444:384–393
226. Li S, Carreon MA, Zhang Y, Funke HH (2010) Scale-up of SAPO-34 membranes for CO₂/CH₄ separation. *J Membr Sci* 352:7–13
227. Ping WE, Zhou R, Funke HH, Falconer JL, Noble RD (2012) Seeded-gel synthesis of SAPO-34 single channel and monolith membranes, for CO₂/CH₄ separations. *J Membr Sci* 415–416:770–775
228. Poshusta JC, Noble RD, Falconer JL (2001) Characterization of SAPO-34 membranes by water adsorption. *J Membr Sci* 186:25–40
229. Carreon ML, Li S, Carreon MA (2012) AIPO-18 membranes for CO₂/CH₄ separation. *Chem Commun* 48:2310–2312

230. Wikipedia, the free encyclopedia. ZSM-5. <http://en.wikipedia.org/wiki/ZSM-5>. Accessed
231. Poshusta JC, Noble RD, Falconer JL (1999) Temperature and pressure effects on CO₂ and CH₄ permeation through MFI zeolite membranes. *J Membr Sci* 160:115–123
232. Takata Y, Tsuru T, Yoshioka T, Asaeda M (2002) Gas permeation properties of MFI zeolite membranes prepared by the secondary growth of colloidal silicate and application to the methylation of toluene. *Microporous Mesoporous Mater* 54:257–268
233. Kwon WT, Kim SR, Kim EB, Bae SY, Kim Y (2011) H₂/CO₂ gas separation characteristics of zeolite membrane at high temperature. *Adv Mater Res* 26–28:267–270
234. Welk ME, Nenoff TM (2004) H₂ separation through zeolite thin film membranes. *Prep Pap Am Chem Soc Div Fuel Chem* 40:889–890
235. Richter H, Voigt I, Fischer G, Puhlfürß P (2003) Preparation of zeolite membranes on the inner surface of ceramic tubes and capillaries. *Sep Purif Technol* 32:133–138
236. Aoki K, Tuan VA, Falconer JL, Noble RD (2000) Gas permeation properties of ion-exchanged ZSM-5 zeolite membranes. *Microporous Mesoporous Mater* 39:485–492
237. Tuan VA, Noble RD, Falconer JL (2000) Boron-substituted ZSM-5 membranes: preparation and separation performance. *AIChE J* 46:1201–1208
238. Wang H, Lin YS (2012) Synthesis and modification of ZSM-5/silicate bilayer membrane with improved hydrogen separation performance. *J Membr Sci* 396:128–137
239. Cheng Y, Li JS, Wang LJ, Sun XY, Liu XD (2006) Synthesis and characterization of Ce-ZSM-5 zeolite membranes. *Sep Purif Technol* 51:210–218
240. Hasegawa Y, Tanaka T, Watanabe K, Jeong BH, Kusakabe K, Morooka S (2002) Separation of CO₂/CH₄ and CO₂/N₂ systems using ion-exchanged FAU-type zeolite membranes with different Si/Al ratios. *Korean J Chem Eng* 19:309–313
241. Gu X, Dong J, Nenoff TM (2005) Synthesis of defect-free FAU-type zeolite membranes and separation for dry and moist CO₂/N₂ mixtures. *Ind Eng Chem Res* 44:937–944
242. Kumar P, Sung CY, Muraza O, Cococcioni M, Hashimi SA (2011) H₂S adsorption by Ag and Cu ion exchanged faujasite. *Microporous Mesoporous Mater* 156:127–133
243. Julbe A, Motuzas J, Cazeville F, Volle G, Guizard C (2003) Synthesis of sodalite/ α -Al₂O₃ composite membranes by microwave heating. *Sep Purif Technol* 32:139–149
244. Xu X, Bao Y, Song C, Yang W, Liu J, Lin L (2004) Microwave-assisted hydrothermal synthesis of hydroxyl-sodalite zeolite membrane. *Microporous Mesoporous Mater* 75:173–181
245. Cui Y, Kita H, Okamoto KI (2004) Preparation and gas separation performance of zeolite T membrane. *J Mater Chem* 14:924–952
246. Chen X, Wang J, Yin D, Yang J, Lu J, Zhang Y, Chen Z (2013) High performance zeolite T membrane for dehydration of organics by a new varying temperature hot-dip coating method. *AIChE J* 59:936–947
247. Barrer RM, Villger H (1969) The crystal structure of the synthetic zeolite L. *Z Kristallogr Bd* 128:352–370
248. Tsapatsis M, Lovallo M, Okubo T, Davis ME, Sadakata M (1995) Characterization of zeolite L nanoclusters. *Chem Mater* 7:1734–1741
249. Yin X, Wang X, Chu N, Yang J, Lu J, Zhang Y, Yin D (2010) Zeolite L/carbon nanocomposite membrane on the porous alumina tubes and their gas separation properties. *J Membr Sci* 348:181–189
250. Corma A, Rey F, Rius J, Sabater MJ, Valencia S (2004) Supramolecular self-assembled molecules as organic directing agent for synthesis of zeolites. *Nature* 431:287–290
251. Casado-Coterillo C, Sato J, Jimare MT, Valencia S, Corma A (2012) Preparation and characterization of ITQ-29/polysulfone mixed-matrix-membranes for gas separation: effect of zeolite composition crystal size. *Chem Eng Sci* 73:116–122
252. Tiscornia I, Valencia S, Corma A, Téllez C, Coronas J, Santamaría J (2008) Preparation of ITQ-29 (Al-free zeolite A) membranes. *Microporous Mesoporous Mater* 110:303–309
253. Huang A, Caro J (2010) Steam-stable hydrophobic ITQ-29 molecular sieve membrane with H₂ selectivity prepared by secondary growth using Krytox 222 as SDA. *Chem Commun* 46:7748–7750

254. Moscoso JG, Lewis GJ, Miller MA, Jan DY, Patton RL, Rohde LM (2003) UZM-5, UZM-5P and UZM-6: crystalline aluminosilicate zeolite and processes using the same. US Patent 6613302 B1, 2 Sept 2003
255. Blackwell CS, Broach RW, Gatter MG, Holmgren JS, Jan DY, Lewis GJ, Mezza BJ, Mezza TM, Miller MA, Moscoso JG, Patton RL, Rohde LM, Schoonover MW, Sinkler W, Wilson BA, Wilson ST (2003) Open-framework materials synthesized in the TMA+TEA+Mixed-Template system: the new low Si/Al ratio zeolites UZM-4 and UZM5. *Angew Chem Int Ed* 42:1737–1740
256. Liu C, Moscoso JG, Wilson ST (2012) Microporous UZM-5 inorganic zeolite membranes for gas, vapor, and liquid separations. US Patent 20120240763 A1, 27 Sept 2012
257. Maghsoodloord H, Mirfendereski SY, Mohammadi T, Pak A (2011) Effects of gel parameters on the synthesis and characteristics of W-type zeolite nanoparticles. *Clay Clay Miner* 59:328–335
258. Mohammadi T, Maghsoodloord H (2012) Synthesis and characterization of ceramic membranes (W-Type) zeolite membrane. *Int J Appl Ceram Technol* 1:1–11
259. Li T, Pan Y, Peinemann KV, Lai Z (2013) Carbon dioxide selective mixed matrix composite membrane containing ZIF-7 nano-fillers. *J Membr Sci* 425–426:235–242
260. Bae TH, Lee JS, Qiu W, Koros WJ, Jones CW, Nair S (2010) A high performance gas-separation containing submicrometer-sized metal-organic framework crystals. *Angew Chem Int Ed* 49:9863–9866
261. Bux H, Liang F, Li Y, Cravillon J, Wiebcke M, Caro J (2009) Zeolitic imidazolate membrane with molecular sieving properties by microwave-assisted solvothermal synthesis. *J Am Chem Soc* 131:1600–1601
262. Li YS, Liang FY, Bux H, Feldhoff A, Yand WS, Caro J (2010) Molecular sieve membrane: supported metal-organic framework with high hydrogen selectivity. *Angew Chem Int Ed* 49:548–551
263. Liu Y, Hu E, Khan EA, Lai Z (2010) Synthesis of ZIF-69 membranes and separation of CO₂/CO mixture. *J Membr Sci* 153:36–40
264. Venna SR, Carreon MA (2010) Highly permeable zeolite imidazolate framework-8 membranes for CO₂/CH₄ separation. *J Am Chem Soc* 132:76–78
265. Sandström L, Sjöberg E, Hedlund J (2011) Very high flux MFI membrane for CO₂ separation. *J Membr Sci* 380:232–240
266. Nair S, Lai Z, Nikolakis V, Xomeritakis G, Bonilla G, Tsapatsis M (2001) Separation of close-boiling hydrocarbon mixtures by MFI and FAU membranes made by secondary growth. *Microporous Mesoporous Mater* 48:219–228
267. Bétard A, Bux HG, Henke S, Zacher D, Caro J, Fischer RA (2012) Fabrication of a CO₂-selective membrane by step-wise liquid-phase deposition of an alkylether functionalized pillared-layer metal-organic framework [Cu₂L₂P]*n* on a macroporous support. *Microporous Mesoporous Mater* 150:76–82
268. Bennett TD, Goodwin AL, Dove MT, Keen DA, Tucker MG, Barney ER, Soper AK, Bithell EG, Tan JC, Cheetham AK (2010) Structure and properties of an amorphous metal-organic framework. *Phys Rev Lett* 104:115503–115506
269. Ranjan R, Tsapatsis M (2009) Microporous metal organic framework membrane on porous support using the seeded growth method. *Chem Mater* 21:4920–4924
270. Bohrman JA, Carreon MA (2012) Synthesis of CO₂/CH₄ separation performance of Bio-MOF-1 membranes. *Chem Commun* 48:5130–5132
271. An J, Rosi NL (2010) Tuning MOF CO₂ adsorption properties via cation exchange. *J Am Chem Soc* 132:5578–5579
272. An J, Shade CM, Chengelis-Czegan DA, Petoud S, Rosi NL (2011) Zinc-adeninate metal-organic framework for aqueous encapsulation and sensitization of near-infrared and visible emitting lanthanide cations. *J Am Chem Soc* 133:1220–1223
273. Xomeritakis G, Naik S, Braunbarth CM, Cornelius CJ, Pardey R, Brinker CJ (2003) Organic-templated silica membranes. I. Gas and vapor transport properties. *J Membr Sci* 215:225–233

274. Li Y, Chung TS (2008) Exploratory development of dual-layer carbon-zeolite nanocomposite hollow fiber membrane with high performance for oxygen enrichment and natural gas separation. *Microporous Mesoporous Mater* 113:315–324
275. Alfaro S, Valenzuela A (2006) Zeolite membrane prepared by the dry gel method for gas separation. *Adv Mater Technol Mater Proc J* 8:63–66
276. Kuznicki SM (1990) Preparation of small-pored crystalline titanium molecular sieve zeolites. US Patent 4938939 A, 3 July 1990
277. Stoeger JA, Veziri CM, Palomino M, Corma A, Kanellopoulos NK, Tsapatsis MN, Karanikolos G (2012) On stability and performance of highly c-oriented $\text{AlPO}_4\text{-5}$ and CoAPO-5 membranes. *Microporous Mesoporous Mater* 147:286–294
278. Nagase T, Kiyozumi Y, Hasegawa Y, Inoue T, Ikeda T (2007) Dehydration of concentrated acetic acid solutions by pervaporation using novel MER zeolite membranes. *Chem Lett* 36:594–595
279. Hasegawa Y, Nagase T, Kiyozumi Y, Mizukami F (2010) Preparation, characterization, and dehydration performance of MER-type zeolite membranes. *Sep Purif Technol* 73:25–31
280. Kim SJ, Yang S, Reddy GK, Smirniotis P, Dong J (2013) Zeolite membrane reactor for high-temperature water-gas shift reaction: effects of membrane properties and operating conditions. *Energy Fuel* 27:4471–4480
281. Yang S, Lin X, Lewis W, Suyetin M, Bichoutskaia E, Parker JE, Tang CC, Allan DR, Rizkallah PJ, Hubberstey P, Champness NR, Thomas KM, Blake AJ, Schröder M (2012) A partially interpenetrated metal-organic framework for selective hysteretic sorption of carbon dioxide. *Nat Mater* 11:710–716
282. Radnedge S (2012) New holey material soaks up CO_2 /News/gasworld. 18 June 2012
283. <http://www.gasworld.com/news/regions/west-europe/new-hole-y-mat>
284. Shah M, McCarthy MC, Sachdeva S, Lee AK, Jeong HK (2012) Current status of metal-organic framework membranes for gas separations: promises and challenges. *Ind Eng Chem Res* 51:2179–2199
285. Rowsell JLC, Yaghi OM (2004) Metal-organic frameworks: a new class of porous materials. *Microporous Mesoporous Mater* 73:3–14
286. Yoo Y, Lai Z, Jeong HK (2009) Fabrication of MOF-5 membranes using microwave-induced rapid seeding and solvothermal secondary growth. *Microporous Mesoporous Mater* 123:100–106
287. Liu Y, Ng Z, Khan AE, Jeong HK, Ching CB, Lai Z (2009) Synthesis of continuous MOF-5 membranes on porous α -alumina substrates. *Microporous Mesoporous Mater* 118:296–301
288. Klinowski J, Paz FAA, Silva P, Rocha J (2011) Microwave-assisted synthesis of metal-organic frameworks. *Dalton Trans* 40:321–330
289. Hu Y, Dong X, Nan J, Jin W, Ren X, Xu N, Lee YM (2011) Metal-organic framework membranes fabricated *via* reactive seeding. *Chem Commun* 47:737–739
290. Schoedel A, Scherb C, Bein T (2010) Oriented nanoscale films of metal-organic frameworks by temperature gel-layer synthesis. *Angew Chem Int Ed* 49:7225–7228
291. Lu H, Zhu S (2013) Interfacial synthesis of free standing metal-organic framework-membranes. *Eur J Inorg Chem* 2013:1294–1300
292. Ben T, Lu C, Pei C, Xu S, Qiu S (2012) Polymer-supported and free-standing metal-organic framework membrane. *Chem Eur J* 18:10250–10253
293. Ai X, Hu X (2003) Study on organic-inorganic hybrid membranes. *Huxue Jinzhan* 16:83–89
294. Chung TS, Jiang LY, Kulprathipanja S (2007) Mixed matrix membranes (MMMs) comprising organic polymers with dispersed inorganic fillers for gas separation. *Prog Polym Sci* 32:483–507
295. Bouma RHB, Checchetti A, Chidichimo G, Drioli E (1997) Permeation through a heterogeneous membrane: the effect of the dispersed phase. *J Membr Sci* 128:141–149
296. Funk CV, Lloyd DRE (2008) Zeolite-filled microporous mixed matrix (ZeoTIPS) membranes: prediction of gas separation performance. *J Membr Sci* 313:224–231

297. Paul DR, Kems DR (1973) The diffusion time lag in polymer membranes containing adsorptive fillers. *J Polym Sci Polym Phys* 41:79–93
298. Kulprathipanja S, Neuzil RW, Li NN (1988) Separation of fluids by means of mixed matrix membranes. US Patent 4740219, 26 Apr 1988
299. Kulprathipanja S, Neuzil RW, Li NN (1992) Separation of gases by means of mixed matrix membranes. US Patent 5127925, 7 July 1992
300. Hussain M, König A (2012) Mixed-matrix membranes for gas separation, polydimethylsiloxane filled with zeolite. *Chem Eng Technol* 35:561–569
301. Ismail AF, Kusworo TD, Mustafa A (2008) Enhanced gas permeation of polyethersulfone mixed matrix hollow fiber membranes using novel Dynasylan Ameo silane agent. *J Membr Sci* 319:306–312
302. Widjojo N, Chung TS, Kulprathipanja S (2008) The fabrication of hollow fiber membranes with double-layer mixed-matrix materials for gas separation. *J Membr Sci* 325:326–335
303. Chaidou CI, Pantoleontos G, Koutsonikolas DE, Kaldis SP, Sakellaropoulos GP (2012) Gas separation properties of polyimide-zeolite mixed matrix membrane. *Sep Purif Technol* 47:950–962
304. Boroglu MS, Gurkaynak MA (2011) Fabrication and characterization of silica modified polyimide-zeolite mixed matrix membranes for gas separation properties. *Polym Bull* 66:463–478
305. Karkhanechi H, Kazemian H, Nazockdast H, Mozdianfard MR, Bidoki SM (2012) Fabrication of homogeneous polymer-zeolite nanocomposites as mixed-matrix membranes for gas separation. *Chem Eng Technol* 35:885–888
306. Adams R, Carson C, Ward J, Tannenbaum R, Koros W (2010) Metal organic framework mixed matrix membranes for gas separation. *Microporous Mesoporous Mater* 131:13–20
307. Nik OG, Chen XY, Kaliaguine S (2012) Functionalized metal organic framework-polyimide mixed matrix membranes for CO₂/CH₄ separation. *J Membr Sci* 413–414:48–61
308. Tanh Jeazet HB, Staudt C, Janiak C (2012) Metal-organic frameworks in mixed-matrix membranes for gas separation. *Dalton Trans* 41:14003–14027
309. Hu J, Cai H, Ren H, Wei Y, Xu Z, Liu H, Hu Y (2010) Mixed-matrix membrane hollow fibers of Cu₂(BTC)₂ MOF and polyimide for gas separation and adsorption. *Ind Eng Chem Res* 49:12605–12612
310. Basu S, Cano-Odena A, Vankelecom IFJ (2011) MOF-containing mixed-matrix membranes for CO₂/CH₄ and CO₂/N₂ binary gas mixture separations. *Sep Purif Technol* 81:31–40
311. Li Y, Chung TS, Huang Z, Kulprathipanja S (2008) Dual-layer polyethersulfone (PES)/BTDA-TDI/MDI co-polyimide (P84) hollow fiber membrane with submicron PES-zeolite beta mixed matrix dense-selective layer for gas separation. *J Membr Sci* 277:28–37
312. Jiang LY, Chung TS, Kulprathipanja S (2006) Fabrication of mixed matrix hollow fibers with intimate polymer-zeolite interface for gas separation. *AIChE J* 52:2898–2908
313. Cong H, Radosz M, Towler BF, Shen Y (2007) Polymer-inorganic membrane for gas separation. *Sep Purif Technol* 55:281–291
314. Liu H (1997) Synthesis of TiO₂ nanopowder enwrapped by organic membrane with microwave induced plasma method. *Huaxue Tongbao* 10:44–46
315. Iwata M, Adahi T, Tomidokoro M, Ohta M, Kobayashi T (2003) Hybrid sol-gel membranes of polyacrylonitrile-tetraethoxysilane composites for gas perm selectivity. *J Appl Polym Sci* 88:1752–1759
316. Ahmad J, Deshmukh K, Hägg MB (2013) Influence of TiO₂ on the chemical, mechanical, and gas separation properties of polyvinyl alcohol-titanium dioxide (PVA-TiO₂) nanocomposite membrane. *Int J Polym Anal Charact* 18:287–296
317. Perez EV, Balkus KJ, Ferraris JP, Musselman IH (2009) Mixed-matrix membranes containing MOF-5 for gas separation. *J Membr Sci* 328:165–173
318. Morooka S, Kusakabe K (1999) Ceramics: getting into the 2000s, Part D. In: *Advances in science and technology* (Faenza, Italy), vol 16, pp 389–400

319. Gopalan S (2002) Using ceramic mixed ionic and electronic conductors for gas separation. *JOM* 54:26–29
320. Kulprathipanja A, Alptekin GO, Falconer JL, Way JD (2005) Pd and Pd-Cu membranes: inhibition of H₂ Permeation by H₂S. *J Membr Sci* 254:49–62
321. Kluiters SCA (2004) Status review on membrane system for hydrogen preparation. Intermediate Report EU Project MIGREYD NNES-2001-670, ECNC-04-102
322. Fuertes AB (2000) Adsorption-selective carbon membranes for gas separation. *J Membr Sci* 177:9–16
323. Jones CW, Koros WJ (1994) Carbon molecular sieve gas separation membranes. Part I. Preparation and characterization based on polyimide precursors. *Carbon* 32:1419–1425
324. Ismail AF, David LIB (2001) A review of the latest development of carbon membranes for gas separation. *J Membr Sci* 193:1–18
325. Sauf SM, Ismail AF (2004) Fabrication of carbon membranes for gas separation—a review. *Carbon* 42:241–259
326. Saufi SM, Ismail AF (2002) Development and characterization of polyacrylonitrile (PAN) based carbon hollow fiber membrane. *Songklanakarin J Sci Technol* 24:843–854
327. Song C, Wang T, Qiu Y, Qiu J, Cheng H (2009) Effect of carbonization atmosphere on the structure changes of PAN carbon membranes. *J Porous Mater* 16:197–203
328. Grainger D, Hägg MB (2008) The recovery of carbon molecular sieve membranes of hydrogen transmitted in natural gas networks. *Int J Hydrogen Energy* 33:2379–2388
329. Favas EP, Kapantaidakis GC, Nolan JW, Mitropoulos AC, Kanellopoulos NK (2007) Preparation, characterization and gas permeation properties of carbon hollow fiber membranes based on Matrimid® 5218 precursor. *J Mater Process Technol* 186:102–110
330. Salleh WNW, Ismail AF (2011) Fabrication and characterization of PEI/PVP-based carbon hollow fiber membranes for CO₂/CH₄ and CO₂/N₂ separation. *AIChE J* 58:3167–3175
331. Favvas EP, Kouvelos EP, Romanos GE, Pillatos GL, Mitropoulos AC, Kanellopoulos NK (2008) Characterization of highly selective microporous carbon hollow fiber membranes prepared from commercial co-polyimide. *J Porous Mater* 15:625–613
332. Rao PS, Wey MY, Tseng HH, Kumjar IA, Weng TH (2008) A comparison of carbon/nanotube molecular sieve membranes with polymer blend carbon molecular sieve membranes for the gas permeation application. *Microporous Mesoporous Mater* 113:499–510
333. Kim YK, Park HB, Lee YM (2004) Carbon molecular sieve membranes derived from thermally labile polymer containing blend polymers and their gas separation properties. *J Membr Sci* 343:9–17
334. Kim YK, Park HB, Lee YM (2005) Gas separation properties of carbon molecular sieve membranes derived from polyimide/polyvinylpyrrolidone blends: effect of the molecular weight of polyvinylpyrrolidone. *J Membr Sci* 251:159–167
335. Lee HJ, Suda H, Haraya K, Moon SH (2007) Gas permeation properties of carbon molecular sieving membranes derived from the polymer blend of polyphenylene oxide (PPO)/polyvinylpyrrolidone (PVP). *J Membr Sci* 296:139–146
336. Zhang B, Wang T, Wu Y, Liu Q, Liu S, Qiu J (2008) Preparation and gas permeation of composite carbon membranes from poly(phthalazinone ether sulfone ketone). *Sep Purif Technol* 60:259–263
337. Yoshimune M, Fujiwara I, Suda H, Haraya K (2005) Novel carbon molecular sieve membranes derived from poly (phenylene oxide) and its derivatives for gas separation. *Chem Lett* 34:958–959
338. Hatori H, Yamada Y, Shiraishi M (1992) Preparation of macroporous carbon films from polyimide by phase inversion method. *Carbon* 30:303–304
339. Hatori H, Shiraishi M, Nakata H, Yoshitomi S (1992) Carbon molecular sieve films from polyimide. *Carbon* 30:305–306
340. Rao MB, Sirkar S (1993) Nanoporous carbon membranes for separation of gas mixtures by selective surface flow. *J Membr Sci* 85:253–254
341. Rao MB, Sirkar S (1996) Performance and pore characterization of nanoporous carbon membrane for gas separation. *J Membr Sci* 110:109–118

342. Rao MB, Sirkar S (1993) Nanoporous carbon membrane for gas separation. *Gas Sep Purif* 7:279–284
343. Centeno TA, Vilas JL, Fuertes AB (2004) Effect of phenolic resin pyrolysis conditions on carbon membrane performance for gas separation. *J Membr Sci* 228:45–54
344. Acharya M, Foley HC (1991) Spray-coating of nanoporous carbon membranes for air separation. *J Membr Sci* 161:1–5
345. Centeno TA, Fuertes AB (2000) Carbon molecular sieve gas separation membranes based on poly(vinylidene chloride-co-vinyl chloride). *Carbon* 38:1067–1073
346. Park HB, Lee YM (2003) Pyrolytic carbon-silica membrane: a promising membrane for improved gas separation. *J Membr Sci* 213:263–272
347. Hosseini SS, Chung TS (2009) Carbon membranes from blends of PBI and polyimides for N_2/CH_4 and CO_2/CH_4 separation and hydrogen purification. *J Membr Sci* 328:174–185
348. Zhang B, Shen G, Wu Y, Wang T, Qiu J, Xu T, Fu C (2009) Preparation and characterization of carbon membranes derived from poly(phthalazinone ether) for gas separation. *Ind Eng Chem Res* 48:2886–2890
349. Iijima S (1991) Helical microtubules of graphitic carbon. *Nature* 354:56–58
350. Iijima S, Ichihashi T (1993) Single-shell carbon nanotubes of 1-nm diameter. *Nature* 663:603–605
351. Cho SJ, Shrestha SP, Lee SB, Boo JH (2014) Electrical characteristics of carbon nanotubes by plasma and microwave surface treatments. *Bull Korean Chem Soc* 35(3):905–907
352. Wang X, Li Q, Xie J, Jin Z, Wang J, Li Y, Jiang K, Fan S (2009) Fabrication of ultralong and electrically uniform single-walled carbon nanotubes on clean substrates. *Nano Lett* 9: 3137–3141
353. Zhao YL, Stoddart JF (2009) Noncovalent functionalization of single-walled carbon nanotubes. *Acc Chem Res* 42:1161–1171
354. Bernhole J, Brenner D, Buongiorno Nardelli M, Meunier V, Roland C (2002) Mechanical and electrical properties of nanotubes. *Annu Rev Mater Sci* 32:347–375
355. Sholl DS, Johnson JK (2006) Making high-flux membranes with carbon nanotubes. *Science* 312:1003–1004
356. Noy A (2013) Kinetic model of gas transport in carbon nanotube channels. *J Phys Chem C* 117:7656–7660
357. Majumder M, Ajayan PM (2010) Carbon nanotube membranes: a new frontier in membrane science. In: Drioli E, Giorno L (eds) *Comprehensive membrane science and engineering*. Elsevier Science, Amsterdam
358. Bruggen BV (2012) The separation power of nanotubes in membranes: a review. *ISRN Nanotechnol* 2012:1–17
359. Arora G, Sandler SI (2006) Air separation by single wall carbon nanotubes: mass transport and kinetic selectivity. *J Chem Phys* 124:084702
360. Chen H, Sholl DS (2006) Prediction of selectivity and flux for CH_4/H_2 separations using single walled carbon nanotubes as membranes. *J Membr Sci* 269:152–162
361. Ackerman DM, Skoulidas AI, Sholl DS, Johnson JK (2003) Diffusivities of Ar and Ne in carbon nanotubes. *Mol Simulat* 29:677–684
362. Skoulidas AI, Ackerman DM, Johnson JK, Sholl DS (2002) Rapid transport of gases in carbon nanotubes. *Phys Rev Lett* 89:185901/1–4
363. Kim S, Pechar TW, Marand E (2006) Poly(imide siloxane) and carbon nanotube mixed matrix membranes for gas separation. *Desalination* 192:330–339
364. Tseng HH, Kumar IA, Weng TH, Lu CY, Wey MY (2009) Preparation and characterization of carbon molecular sieve membranes for gas separation—the effect of incorporated multi-wall carbon nanotubes. *Desalination* 240:40–45
365. Kusworo TD, Ismail AF, Widiyasa IN, Johari S, Sunarso S (2010) CO_2 removal from biogas using carbon nanotubes mixed matrix membranes. *Int J Sci Eng* 1:1–6
366. Geim AK, Novoselov KS (2007) The rise of graphene. *Nat Mater* 6:183–191
367. Meyer JC, Geim AK, Katsnelson MI, Novoselov KS, Booth TJ, Roth S (2007) The structure of suspended graphene sheets. *Nature* 446:60–63

368. Noble Foundation announcement (2010) On line at: http://www.nobelprize.org/nobel_prizes/physics/laureates/2010/press.html
369. Bunch JS, Verbridge SS, Alden JS, van der Zande AM, Parpia JM, Craighead HG, McEuen PL (2008) Impermeable atomic membranes from graphene sheets. *Nano Lett* 8:2458–2462
370. Jennifer C (2012) MIT news, tiny pores in graphene could give rise to membranes: new membranes may filter ware or separate biological samples. MIT News Office, 23 Oct 2012. <http://newsoffice.mit.edu/2012/graphene=pores-and-membrans-1023>
371. Forbeaux I, Themlin J-M, Debever J-M (1998) Heteroepitaxial graphite on 6H-SiC(0001): interface formation through conduction-band electronic structure. *Phys Rev B* 58: 16396–16406
372. Cambaz ZG, Yushin G, Osswald S, Mochalin V, Gogotsi Y (2008) Noncatalytic synthesis of carbon nanotubes, graphene and graphite on SiC. *Carbon* 48:841–849
373. Du H, Li J, Zhang J, Su G, Li X, Zhao Y (2011) Separation of hydrogen and nitrogen gases with porous graphene membrane. *J Phys Chem C* 115:23261–23266
374. Hauser AW, Schwerdtfeger P (2012) Methane-selective nanoporous graphene membranes for gas purification. *Phys Chem Chem Phys* 14:13292–13298
375. Koeing SP, Wang L, Pellegrino J, Bunch S (2012) Selective molecular sieving through porous graphene. *Nat Nanotechnol* 7:728–732
376. Oyama ST, Lee D, Hacıoğlu P, Saraf RF (2004) Theory of hydrogen permeability in non-porous silica membranes. *J Membr Sci* 244:45–53
377. Ying J, Peng C, Lei F, Huiqian L, Huan Y, Cong R, Lei S, Changzhi G, Hai-Hu W (2008) Critical fields and anisotropy of NdFeAsO_{0.82}F_{0.18} single crystals. *Appl Phys Lett* 93:032503
378. Qin X, Meng Q, Feng Y, Gao Y (2013) Graphene with line defect as a membrane for gas separation: design via a first-principles modeling. *Surf Sci* 607:153–158
379. Jiang DE, Cooper VR, Dai S (2009) Porous graphene as the ultimate membrane for gas separation. *Nano Lett* 9:4019–4024
380. Blankenburg S, Bieri M, Fasel R, Mullen K, Pignedoli CA, Passerone D (2010) Graphene as an atmospheric nanofilter. *Small* 6:2266–2271
381. Schrier J (2010) Helium separation using porous graphene membranes. *J Phys Chem Lett* 1:2284–2287
382. Schrier J, McClain J (2012) Thermally-driven isotope separation across nanoporous graphene. *Chem Phys Lett* 521:118–124
383. Jungthawan S, Reunchan P, Limpijumnog S (2013) Theoretical study of strained porous structures and their gas separation properties. *Carbon* 54:359–364
384. Lee J, Aluru NR (2013) Water-solubility-driven separation of gases using graphene membrane. *J Membr Sci* 428:546–553
385. Lai Z, Bonilla G, Diaz I, Nery JG, Sujaoti K, Amat MA, Kokkoli E, Terasaki O, Thompson RW, Tsapatsis M, Vlachos DG (2003) Microstructural optimization of a zeolite membrane for organic vapor separation. *Science* 300:456–460
386. Park HB, Lee YM (2005) Fabrications and characterization of nanoporous carbon/silica membrane. *Adv Mater* 17:477–483
387. Yampolskii Y, Pinnau I, Freeman B (eds) (2006) *Materials science of membrane for gas and vapor separation*. John Wiley & Sons, Chichester, UK
388. Park HB, Jung CH, Lee YM, Hill AJ, Pas SJ, Mudie ST, Wagner EV, Freeman BD, Cookson DJ (2007) Polymers with cavities tuned for fast selective transport of small molecules and ions. *Science* 318:254–258
389. Khayet M, Matsuura T (2011) *Membrane distillation, principles and applications*. Elsevier, Amsterdam
390. Henis JMS, Tripodi MK (1980) Multicomponent membranes for gas separation. US Patent 4230463A, 28 Oct 1980
391. Fritzsche AK, Cruse CA, Kesting RE, Murphy MK (1990) Hollow fiber membranes spun from lewis acid:base complexes. I. Structure determination by oxygen plasma ablation. *J Appl Polym Sci* 40:19–40

392. Kesting RE (1990) The four tires of structure in integrally skinned phase inversion membranes and their relevance to the various separation regimes. *J Appl Polym Sci* 41: 2739–2752
393. Chung TS, Teoh SK, Hu X (1997) Formation of ultrathin high-performance hollow fiber membranes. *J Membr Sci* 133:161–175
394. Shieh JJ, Chung TS, Wang R, Srinivasan MP, Paul DR (2001) Gas separation performance of poly(4-vinylpyridine)/polyetherimide composite hollow fibers. *J Membr Sci* 182:111–123
395. Husain S (2013) Methods of preparing a crosslinked fiber membrane. US Patent 20130239805 A1, 19 Sept 2013
396. Baker WR (2002) Future directions of membrane gas separation technology. *Ind Eng Chem Res* 41:1393–1411
397. Kesting RE, Cruse CA, Fritzsche AK, Malon RF, Murphy MK, Handermann AC (1992) Asymmetric gas separation membranes having graded density skins. EP0257012 B1, 7 Oct 1992
398. Kusakabe K, Li ZY, Maeda H, Morooka S (1995) Preparation of supported composite membrane by pyrolysis of polycarbosilane for gas separation at high temperature. *J Membr Sci* 103:175–180
399. Ren X, Ren J, Deng M (2012) Poly(amide-6-b-ethylene oxide) membranes for sour gas separation. *Sep Purif Technol* 89:1–8
400. Jiang X, Ding J, Kumar A (2008) Polyurethane-poly(vinylidene fluoride) (PU-PVDF) thin film composite membranes for gas separation. *J Membr Sci* 323:371–378
401. Gupta Y, Hellgardt K, Wakeman RJ (2006) Enhanced permeability of polyaniline based nano membranes for gas separation. *J Membr Sci* 282:60–70
402. Lopez JL, Matson SL, Marchese J, Quinn JA (1986) Diffusion through composite membranes: a two dimensional analysis. *J Membr Sci* 27:301–325
403. Henis JMS, Tripodi MK (1980) A novel approach to gas separations using composite hollow fiber membranes. *Sep Sci Technol* 15:1059–1068
404. Henis JMS, Tripodi MK (1981) Composite hollow fiber membranes for gas separation: the resistance model approach. *J Membr Sci* 8:233–246
405. Reid BD, Ebron VHM, Musselman IH, Ferraris JP, Balkus JKJ (2002) Enhanced gas selectivity in thin film composite membranes of poly(3-(2-acetoxyethyl)thiophene). *J Membr Sci* 195:181–192
406. Way JD, Noble RD, Flynn TM, Sloan ED (1982) Liquid membrane transport: a survey. *J Membr Sci* 12:239–259
407. Kocherginsky NM, Yang Q, Seelam L (2007) Recent advances in supported liquid membrane technology. *Sep Purif Technol* 53:171–177
408. Ward WJ, Robb WL (1967) Carbon dioxide-oxygen separation: facilitated transport of carbon dioxide across a liquid film. *Science* 156:1481–1484
409. Baker RW, Roman I, Lonsdale HK (1987) Liquid membranes for the production of oxygen enriched air. *J Membr Sci* 31:15–29
410. Lee SH, Kim BS, Lee EW, Park YI, Lee JM (2006) The removal of acid gases from crude natural gas by using novel supported liquid membranes. *Desalination* 200:21–22
411. Chen XS, Nishide H, Tsuchida E (1996) Analysis of facilitated oxygen transport through in a liquid membrane of hemoglobin. *Bull Chem Soc Jpn* 69:255–259
412. Castro-Domínguez B, Leelachaikul P, Takagaki A, Sugawara T, Oyama ST (2013) Perfluorocarbon-based supported liquid membrane for O₂/N₂. *Sep Purif Technol* 118:19–24
413. Deetz DW (1987) Stabilized ultrathin liquid membranes for gas separation. In: Noble RD, Way JD (eds) *Liquid membranes*, ACS symposium series. American Chemical Society, Washington, DC
414. Ward WJ (1970) Analytical and experimental studies of facilitated transport. *AIChE J* 16:405–410
415. Donaldson TL, Quinn JA (1975) Carbon dioxide transport through enzymatically active synthetic membranes. *Chem Eng Sci* 30:103–115

416. Ghai RK, Ertl H, Dullien FAL (1973) Liquid diffusion of nonelectrolytes, Part I. *AIChE J* 19:881–900
417. Ghai RK, Ertl H, Dullien FAL (1974) Liquid diffusion of nonelectrolytes, Part II. *AIChE J* 20:1–20
418. Reid RC, Prausnitz JM, Sherwood TK (1977) *The properties of gases and liquids*. McGraw-Hill, New York
419. Cserjési P, Nemestóthy N, Vass A, Csanádi Z, Bélafi-Bako K (2009) Study on gas separation by supported liquid membranes applying novel ionic liquids. *Desalination* 246:370–374
420. Seeberger A, Kern C, Uerdingen M, Jess A (2007) Gas separation by supported ionic liquid membranes. In: DGMK-conference, opportunities and challenges at the interface between petrochemistry and refinery, 10–12 Oct 2007, Hamburg, Germany
421. Cserjési P, Nemestóthy N, Vass A, Csanádi Z, Bélafi-Bakó K (2009) Study on gas separation by supported liquid membranes applying novel ionic liquids. *Desalination* 245:743–747
422. Gan Q, Rooney D, Xue M, Thompson G, Zou Y (2006) An experimental study of gas transport and separation properties of ionic liquids supported on nanofiltration membranes. *J Membr Sci* 280:948–956
423. Neves L, Nemestóthy N, Alves VD, Cserjési P, Bélafi-Bakó K, Coelho I (2009) Separation of bio-hydrogen by supported ionic liquid membranes. *Desalination* 240:311–315
424. Neves L, Dabek W, Coelho IM, Crespo JG (2006) Design of new selective Nafion membranes using room temperature ionic liquids. *Desalination* 199:525–526
425. Cserjési P, Nemestóthy N, Bélafi-Bakó K (2010) Gas separation properties of supported liquid membranes prepared with unconventional ionic liquids. *J Membr Sci* 349:6–11
426. Robeson LM (2008) The upper bound revisited. *J Membr Sci* 320:390–400
427. Hanioka S, Maruyama T, Sotani T, Teramoto M, Matsuyama H, Nakashima K, Hanaki M, Kuboto F, Goto M (2008) CO₂ separation facilitated by task-specific ionic liquids using a supported liquid membrane. *J Membr Sci* 314:1–4
428. Zhao W, He G, Nie F, Zhang L, Feng H, Liu H (2012) Membrane liquid loss mechanism of supported ionic liquid membrane for gas separation. *J Membr Sci* 411–412:73–80
429. Luis P, Neves LA, Afonso CAM, Coelho IM, Crespo JG, Garea A, Irabien A (2009) Facilitated transport of CO₂ and SO₂ through supported ionic liquid membranes (SILMs). *Desalination* 245:485–493
430. Majumdar S, Guha AK, Sirkar KK (1998) A new liquid membrane technique for gas separation. *AIChE J* 34:1135–1245